Okinawa Institute of Science and Technology

Graduate University

Thesis submitted for the degree

Doctor of Philosophy

Synthesis and Reactivity of Transition Metal Complexes Supported by Non-Phosphine Ligands in Metal-Ligand Cooperation and Fluoroalkyl Incorporation

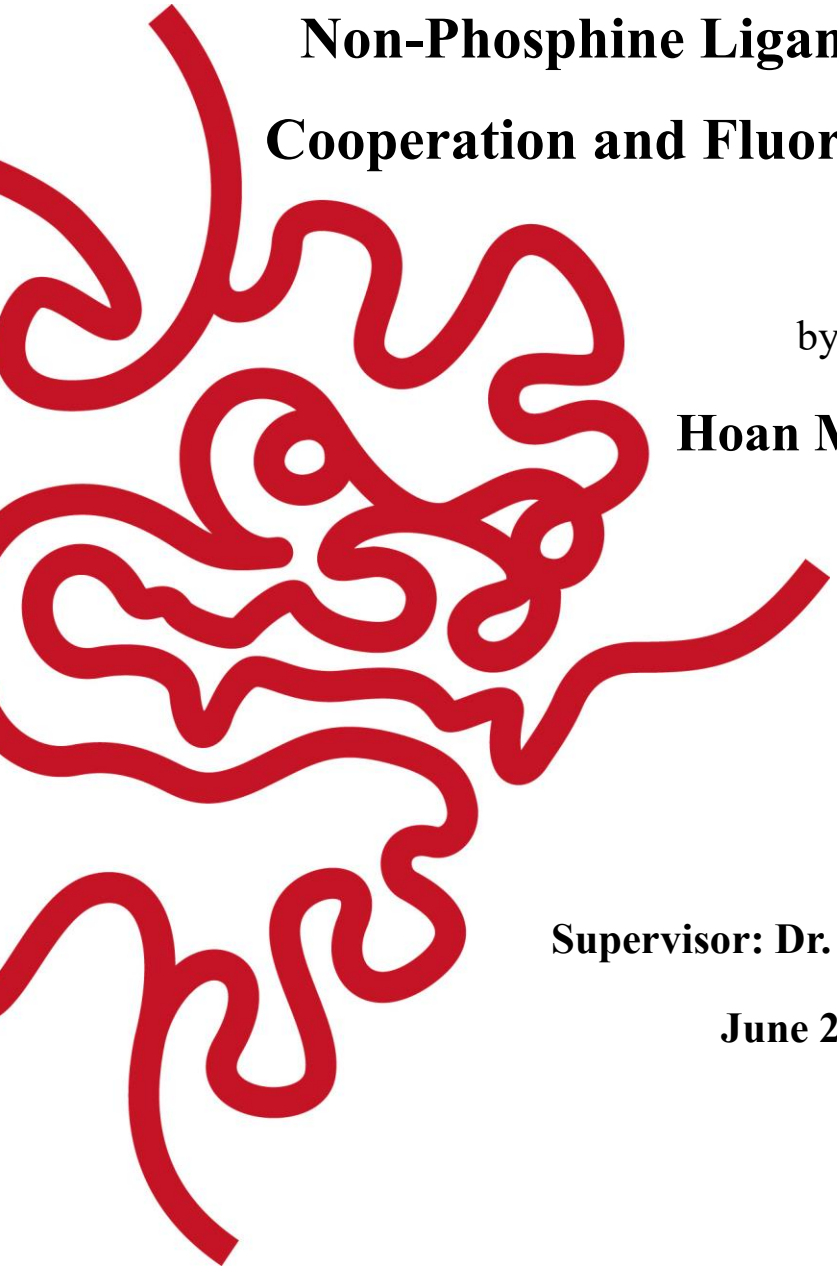

by

Hoan M. Dinh

Supervisor: Dr. Julia R. Khusnutdinova

June 2024

Declaration of Original and Sole Authorship

I, Hoan M. Dinh, declare that this thesis entitled *Synthesis and Reactivity of Transition Metal Complexes Supported by Non-Phosphine Ligands in Metal-Ligand Cooperation and Fluoroalkyl Incorporation* and the data presented in it are original and my own work.

I confirm that:

- This work was done solely while a candidate for the research degree at the Okinawa Institute of Science and Technology Graduate University, Japan.
- No part of this work has previously been submitted for a degree at this or any other university.
- References to the work of others have been clearly attributed. Quotations from the work of others have been clearly indicated and attributed to them.
- In cases where others have contributed to part of this work, such contribution has been clearly acknowledged and distinguished from my own work.
- None of this work has been previously published elsewhere, with the exception of the following:

  Dinh, M. H.; He, Y.-T.; Fayzullin, R. R.; Vasylevskyi, S.; Khaskin, E.; Khusnutdinova, J. R. "Synthesis of Aryl-Manganese(III) Fluoride Complexes via α-Fluorine Elimination from CF_3 and Difluorocarbene Generation" *Eur. J. Inorg. Chem.* **2023**, *26* (32), e202300460.

  Declaration of contribution: I (Hoan M. Dinh) synthesized and characterized the Mn^{III} complexes, performing the difluorocarbene trapping experiment and reactivity of Mn^{III} dibromo complex in difluorocarbenation reaction.

  Dinh, M. H.; Govindarajan, R.; Deolka, S.; Fayzullin, R. R.; Vasylevskyi, S.; Khaskin, E.; Khusnutdinova, J. R. "Photoinduced Perfluoroalkylation Mediated by Cobalt Complexes Supported by Naphthyridine Ligands" *Organometallics*, **2023**, 42, 2632-2643.

  Declaration of contribution: I (Hoan M. Dinh) synthesized and characterized all complexes, performed the reactivity and catalytic activity of cobalt complexes in photo-induced perfluoroethylation, as well as conducted the computational calculations.

  Dinh, M. H.; Gridneva, T.; Karimata, A.; Garcia-Roca, A.; Pruchyathamkorn, J.; Patil, P. H.; Petrov, A.; Sarbajna, A.; Lapointe, S.; Khaskin, E.; Fayzullin, R. R.; Khusnutdinova, J. R. "Single and Double Deprotonation/Dearomatization of N,S-Donor Pyridinophane Ligand in Ruthenium complexes" *Dalton Trans.* **2022**, *51*, 14734-14746.

  Declaration of contribution: I (Hoan M. Dinh) synthesized and characterized the Ru(II) complexes and performed the deprotonation experiments and reactivity tests of the deprotonated complexes.

  Sarbajna, A.; He, Y.-T.; **Dinh, M. H.**; Gladkovskaya, O.; Rahaman, S. M. W.; Karimata, A.; Khaskin, E.; Lapointe, S.; Fayzullin, R. R.; Khusnutdinova, J. R. "Aryl–X Bond-Forming Reductive Elimination from High-Valent Mn–Aryl Complexes" *Organometallics* **2019**, *38*, 4409-4419.

Declaration of contribution: I (Hoan M. Dinh) optimized the synthesis of the complexes, performed characterization and magnetic measurements in solution and mechanistic studies.

Sarbajna, A.; Patil, P. H.; **Dinh, M. H.**; Gladkovskaya, O.; Fayzullin, R. R.; Lapointe, S.; Khaskin, E.; Khusnutdinova, J. R. "Facile and Reversible Double Dearomatization of Pyridines in Non-Phosphine Mn^{I} Complexes with N,S-Donor Pyridinophane Ligand" *Chem. Commun.* **2019**, *55*, 3282-3285.

Declaration of contribution: I (Hoan M. Dinh) synthesized the first Mn^{I} complex and explored the double deprotonation in this complex, as well as conducted the reactivity tests of the double deprotonated complexes.

- Authorization for the reuse of the work that includes co-author's contribution has been signed.

Date: 2024/06/04

Signature:

Abstract

The thesis describes the synthesis and reactivity of metal complexes supported by non-phosphine ligands in metal-ligand cooperation and fluoroalkyl incorporation. The first chapter introduces the literature review on metal-ligand cooperation as a tool for bond activation and catalysis, and the synthesis of manganese(I) and ruthenium(II) complexes supported by non-phosphine N,S-donor macrocyclic pyridinophane ligands. These complexes undergo a facile, reversible single and double dearomatization in pyridine rings in the presence of the base. In the second chapter, we continue utilizing the macrocyclic pyridinophane scaffolds for the synthesis of high-valent manganese(III) complexes via oxidative addition of aryl bromide to manganese(I) precursor and study Ar-Br reductive elimination via one-electron oxidation. We also present the new synthetic route to cyclometalated high-valent manganese(III) fluoro complexes using a trifluoromethylating reagent via transmetalation followed by α-fluorine elimination, resulting in the release of a difluorocarbene. That facile generation of a difluorocarbene could be utilized in difluorocarbenation of alkenes and alkynes using Zn trifluoromethyl reagent at lower temperatures and shorter time as compared to a manganese-free reaction. The third chapter includes literature review on radical fluoroalkylation mediated by first-row transition metal complex, then focusing on the synthesis of cobalt perfluoroethyl complexes supported by simple N-donor naphthyridine ligands. These complexes showed Co-C_2F_5 bond homolysis under visible-light irradiation and could be utilized as catalysts for light-induced C-H bond perfluoroalkylation in arenes using Togni reagent.

Acknowledgments

Before any word, I would like to express my deepest gratitude to my supervisor, Professor ***Julia R. Khusnutdinova***, for her unwavering guidance and support throughout my Ph.D. journey. You have always been welcoming, spending countless hours with me to answer my myriad questions, even when they seemed nonsensical, and offering a wealth of suggestions to help me navigate through my projects whenever I encounter obstacles. I started on my Ph.D. with no background in organometallic chemistry and no confidence, but thanks to your support, I am now confident enough to say to myself "Ah, I can do science". I am so lucky to have had you as my supervisor at the beginning of my adventure in science.

Second, I extend my gratitude to the entire Khusnutdinova Group, both present and past, for making this journey as pleasant as possible. Thank you, ***Eugene*** for your endless patience in teaching me essential laboratory skills, ranging from the most basic in organic synthesis to more complex tasks, such as using the XRD instrument. ***Tomas***, thank you for generously sharing your extensive knowledge of organic chemistry with me and for always being ready to answer any chemistry questions I have. And, of course, thank you for sharing your food to ensure that I never went hungry during my late-night stay at the lab. ***Ayumu***, thank you for the many discussions we had during lunchtime and for introducing and bringing me closer to Okinawan culture. ***Govind*** and ***Dilip***, thank you for always being there to help whenever I needed it. ***Sebastien***, thank you for bringing laughter into the lab and for behaving like a big brother to me. ***Aleria***, thank you for being a good friend and labmate since I started working in the lab, and for treating me to your delicious homemade Spanish food, even if it was only for a short time during your stay in Okinawa. ***Pradnya***, ***Yutao***, ***Abir, Olga, Jiratheep, Andrey, Wahidur, Pavan***, ***Tatiana***, ***Aleksandr***, ***Aleksei***, ***Daria***, ***Valerya***, ***Janet***, ***Mitsuyuki***, ***Thomas***, and ***Shubham***, thank you for being amazing colleagues and assisting me during my studies. ***Robert*** and ***Serhii***, thank you for being an amazing crystallographer. ***Chinen***-san, thank you for helping me with administrative documents.

List of Abbreviations

°	Degrees
°C	Degrees Celsius
$^{13}C\{^{1}H\}$ NMR	Carbon nuclei NMR with proton decoupling (spectroscopy)
$^{19}F\{^{1}H\}$ NMR	Fluorine nuclei NMR with proton decoupling (spectroscopy)
^{1}H NMR	Proton nuclei NMR (spectroscopy)
$^{31}P\{^{1}H\}$ NMR	Phosphorus nuclei NMR with proton decoupling (spectroscopy)
Å	Ångström
ATR	Attenuated-total-reflectance (spectroscopy)
bpy	2,2'-bipyridine
CV	Cyclic voltammetry (electrochemistry)
d	Doublet (Spectroscopy)
DCM	Dichloromethane
dd	doublet of doublets (spectroscopy)
DEPT-135 NMR	Distortionless Enhancement by Polarization Transfer (Spectroscopy)
DFT	Density functional theory
$E_{1/2}$	Half-wave potential
eq or equiv.	Equivalent or equivalents
ESI-HRMS	Electron-spray ionization high resolution mass spectrometry
Et	Ethyl group
FT-IR	Fourier-transformed Infrared (spectroscopy)
GC	Glassy carbon disk electrode (electrochemistry)
GC-MS	Gas-chromatography coupled with mass-spectrometry (spectrometry)
^{i}Pr	isopropyl group
J_{XY}	Coupling constant between X and Y nuclei (spectroscopy)
K	Kelvins
m	Multiplet (Spectroscopy)
M	Molar concentration or molarity
Me	Methyl group
MLC	Metal-ligand cooperation
NMR	Nuclear Magnetic Resonance (spectroscopy)
OMe	Methoxy group
Ph	Phenyl group

q	Quadruplet (Spectroscopy)
RT	Room temperature
s	Singlet (Spectroscopy)
S	Spin
^{t}Bu	tert-butyl group
THF	Tetrahydrofuran
tt	triplet of triplets (spectroscopy)
UV-vis	Ultraviolet-visible (Spectroscopy)
v	virtual (spectroscopy)
V or mV	Volts or millivolts (electrochemistry)
δ	Chemical shift (spectroscopy)
ΔE_p	Peak potential separation (electrochemistry)
ε	molar absorptivity (spectroscopy)
λ_{max}	Wavelength at maximum absorption (spectroscopy)
μ_{eff}	effective moment (spectroscopy)

Table of Contents

List of Figures

List of Tables

List of Schemes

Chapter 1. Introduction

1.1. Metal-ligand cooperation by aromatization/dearomatization

Homogeneous transition metal-catalyzed reactions have emerged as powerful tools in the contemporary manufacture of diverse chemical products over the past several decades.[1-4] The catalytic processes enable the production of a vast array of commodity chemicals and high-value pharmaceuticals with remarkable efficiency and selectivity, thereby minimizing energy consumption and waste generation.[2] The development of well-defined transition metal catalysts has expanded the scope with improved activity due to the ability of transition metals to participate in various reaction types, such as oxidative addition, reductive elimination, and β-hydride elimination.[5-6] In many classical examples of homogeneous catalysis, such transformations occur at the metal center, while the ligands act as "spectators" only to provide electronic and steric effects and remain structurally unchanged over the course of the reaction.

However, in both chemical and biological processes, certain types of catalysis involve ligands and metal centers collaborating to activate bonds, resulting in the chemical modification of both the ligand and the metal center. For example, in [FeFe], [NiFe], and [Fe]-only hydrogenases, H_2 activation occurs through the synergistic action of the ligand and the metal, causing H_2 to undergo heterolytic splitting across the metal–ligand bond without changing the metal's oxidation state.[7-9] The identification of such systems has led to the development of innovative approaches to ligand design and has expanded the range of catalytic reactions.

There are several different approaches in which metal-ligand cooperation has been demonstrated for bond activation: (1) a ligand can act as a Lewis base to accept a proton, together with the metal center cleaving H-X bond (H-X; X = H, OH, OR, NH_2, C..); (2) a ligand can act as a Lewis acid to accept electron from the substrate, while the metal center plays a role as a Lewis base to cooperatively cleave a substrate bond; (3) a polydentate ligand containing aromatic framework which can undergo dearomatization/aromatization by deprotonation to promote bond activation; (4) a redox non-innocent ligand can act as an electron donor/acceptor to maintain the oxidation state in the metal center during a catalytic cycle or act as a radical source to activate bond.[10]

Since the first introduction in the 1970s by Shaw[11] and van Koten[12-13], pincer ligands and their corresponding complexes have been widely utilized in bond activation and catalysis. Lutidine and picoline-based ligand are a type of pincer ligand which contains a CH_2 group adjacent to the aromatic ring that is acidic and can be deprotonated in the presence of a strong base. Although the deprotonation occurs in the remote CH_2 group, the electronic redistribution leads to the dearomatization of the pyridine ring converting it into an anionic amide-donor type ligand. The dearomatized complex can then activate bonds (H-X; X = H, OH, OR, NH_2, C..), and rearomatization in the ligand, while the oxidation state of the metal center remains unchanged.

Scheme 1.1. Metal-ligand cooperation via aromatization/dearomatization

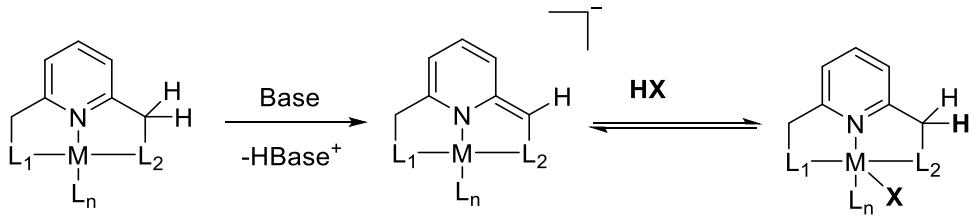

In 2006, Milstein and coworkers reported the metal-ligand cooperation via aromatization/dearomatization in Ir^{I} complex supported by PNP pincer ligand.[14] Reaction of Ir^{I} complex **1.1** with KO^{t}Bu in THF at room temperature led to the formation of dearomatized **1.2**. ^{1}H NMR spectrum of **1.2** showed an up-field shift of three protons in the dearomatized pyridine ring. According to the XRD analysis, the C6-C7 bond distance is shortened to 1.350 Å, which is consistent with typical double C-C bond (ca. 1.34 Å).[14] Additionally, the C7-P2 bond was slightly shortened compared to the C1-P1 bond, suggesting the minor contribution of phosphor-ylide resonance structure.[14]

Scheme 1.2. Deprotonation leading to the dearomatization in PNP pincer Ir^{I} complex **1.2.**

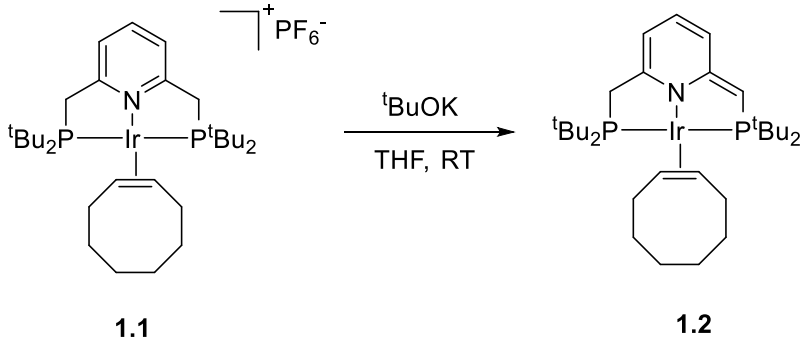

1.1 **1.2**

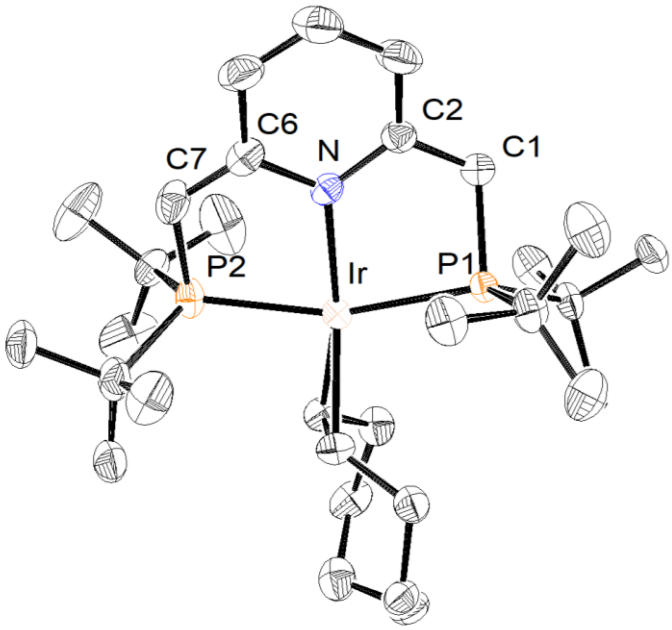

Figure 1.1. ORTEP of **1.2** at 50 % probability level according to single-crystal X-ray diffraction. Hydrogen atoms are omitted for clarity. Selected bond distances (Å): C1–C2 1.506, C6–C7 1.351, C1–P1 1.830, C7–P2 1.784, Ir–N 2.089.

The treatment of dearomatized complex **1.2** with benzene led to the C(sp^2)-H activation of benzene and the re-aromatization of the pyridine ring, resulting in the formation of the phenyl iridium(I) complex **1.3**.[14] The reaction of **1.3** with dihydrogen yields the *trans*-dihydride complex **1.4** as a product. Notably, no evidence of a *cis*-dihydride complex was observed, indicating that the mechanism of H_2 activation does not involve oxidative addition at the iridium center. The reaction of deuterium (D_2) with **1.3** surprisingly led to the formation of an H-Ir^{III}-D complex, with one deuterium atom incorporating into the ligand arm. This suggests that while a two-electron oxidation process occurs at the iridium center post-reaction, H_2 activation likely takes place at the Ir^{III} center via the dearomatized Ir^{III} complex **1.5**. To validate this hypothesis, the authors independently synthesized the dearomatized Ir^{III} complex **1.5** at low temperature and demonstrated its reaction with H_2 to yield the expected *trans*-dihydride Ir^{III} complex **1.4**.[14]

Scheme 1.3. H_2 activation mediated by Ir^{I} complex **1.3**.

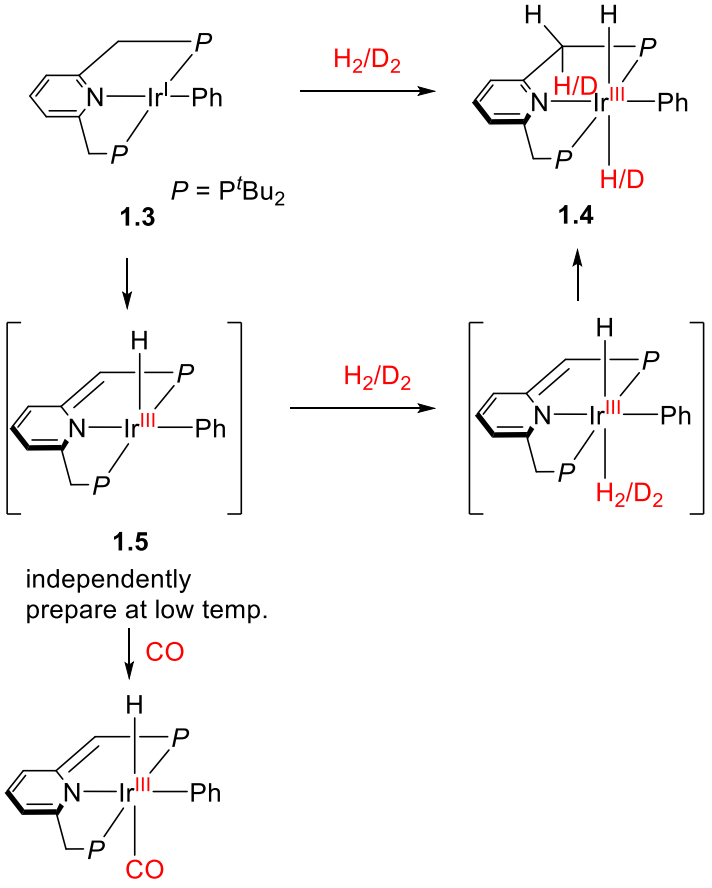

Ruthenium is one of the transition metals which has shown great reactivity for bond activation/catalysis via metal-ligand cooperation concept.[15-19] Below are some examples of application of metal-ligand cooperation via aromatization/dearomatization in bond activation and catalysis mediated by ruthenium complexes.

In 2006, the Milstein group demonstrated the formation of dearomatized PNP and PNN pincer complex **1.8** and **1.9** by deprotonation of the precursors **1.6** and **1.7**, respectively.[20] Notably, the deprotonation of PNN complex **1.7** resulted in the selective formation of a P-arm deprotonated complex **1.9**. Treatment of complexes **1.8** and **1.9** with dihydrogen led to the formation of *trans*-hydride complexes **1.10** and **1.11** in a reversible fashion, which was confirmed by ^{1}H NMR spectroscopy. Both complexes have shown a catalytic activity for ester hydrogenation, however, the dearomatized PNN complex **1.9** is more active.[20] The reverse reaction, alcohol dehydrogenation, could be catalyzed by complex **1.6** and **1.7** in the

presence of the base, or by dearomatized complex **1.9** with the absence of the base.[21] Complex **1.9** was also demonstrated as a good catalyst for amide synthesis by acceptorless dehydrogenative coupling of alcohols and amines.[22] In both these reactions, the reversible H_2 activation was suggested as one of the key steps to produce or consume hydrogen.[20, 22]

Scheme 1.4. H_2 activation mediated by dearomatized ruthenium complexes **1.8** and **1.9** and the catalytic activity of these complexes in ester hydrogenation and acceptorless dehydrogenative reactions.

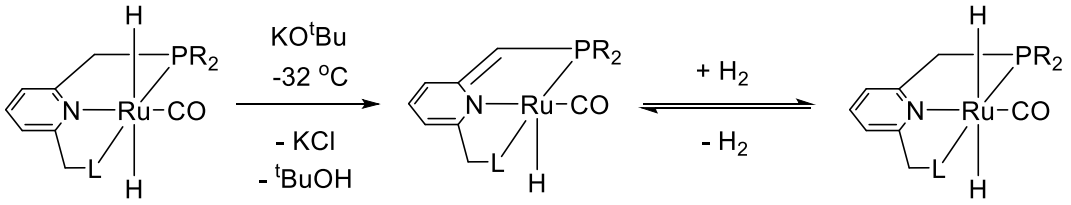

1.6: R = ^{i}Pr, L = P^{i}Pr$_2$
1.7: R = ^{t}Bu, L = NEt$_2$

1.8: R = ^{i}Pr, L = P^{i}Pr$_2$
1.9: R = ^{t}Bu, L = NEt$_2$

1.10: R = ^{i}Pr, L = P^{i}Pr$_2$
1.11: R = ^{t}Bu, L = NEt$_2$

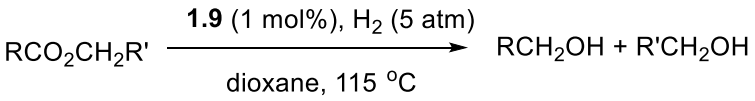

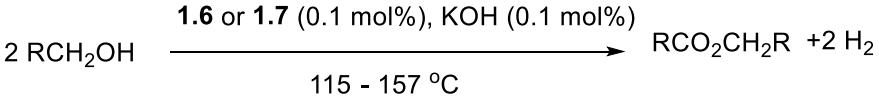

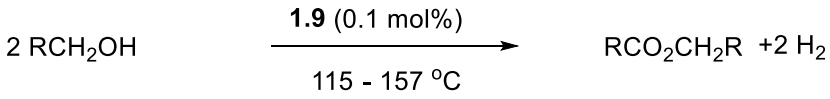

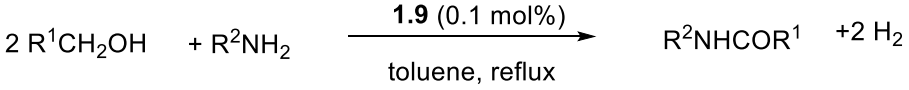

In 2011, Milstein and coworkers used the bipyridyl-PNN Ru dearomatized pincer complexes **1.12** to catalyze the hydrogenation of organic carbonates, carbamate esters[23] and urea derivates[24] to yield methanol, alcohols and amines. In 2015, this group demonstrated the one-pot two-step methanol generation by catalyst **1.12** via in situ CO_2 capturing and hydrogenation.[25] In particular, CO_2 was first captured by aminoalcohol at low pressure (1-3 atm) in the presence of Cs_2CO_3 and the in situ formed oxazolidinone was hydrogenated by complex **1.12** to generate methanol.

Scheme 1.5. Hydrogenation of esters, organic carbonates, carbamates, and urea by complexes **1.12.**

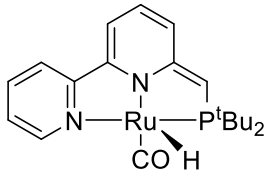

1.12

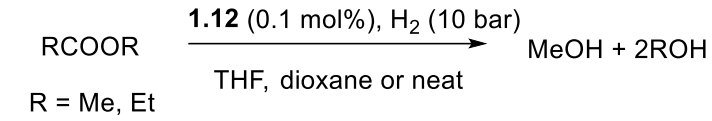

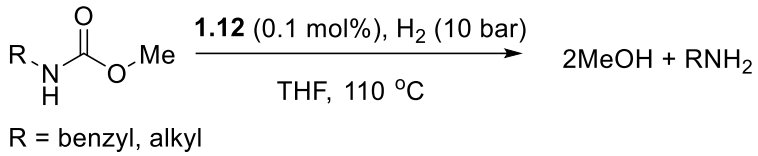

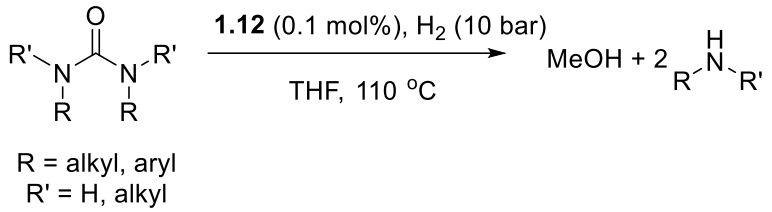

In order to understand the mechanism of alcohol dehydrogenation catalyzed by pincer ruthenium complexes, Milstein and coworkers reported the alcohol activation by dearomatized (PNP)Ru complex.[26] Treating complex **1.13** with excess amount of benzyl alcohol or ethanol led to the reversible formation of alkoxo complex **1.14**. Warming up the reaction mixture to -30 °C, the alkoxo complex disappeared and underwent alcohol dehydrogenation to generate dihydride complex **1.15** and complex **1.16**, resulting from new Ru-O bond formation and C-C coupling with the ligand P-arm. No free aldehyde was observed under these conditions. In addition, complex **1.13** reacted with aldehydes even at -70 °C to yield complex **1.16.** Warming up the reaction to –50 °C led to the aldehyde elimination to give an equilibrium mixture of **1.16**, **1.13** and aldehyde. In addition, facile alcohol dehydrogenation occurs even at -30 °C, suggesting that dehydrogenation mechanism did not likely involve β-hydride elimination mechanism, since coordinative unsaturation is not favored at this temperature.[26]

Scheme 1.6. Alcohol and aldehyde activation with dearomatized PNP Ru complex **1.13**.

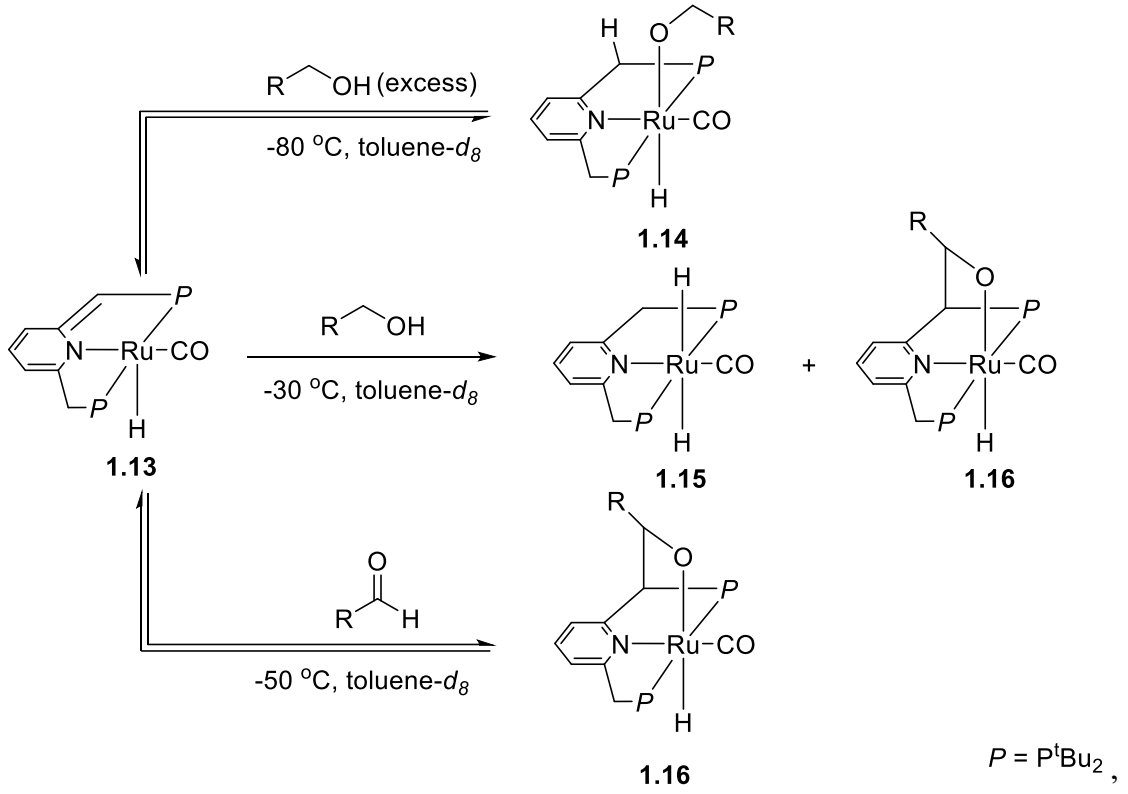

In 2013, the Sanford group reported a study of carbonyl compound activation using dearomatized (PNN)Ru complex **1.9**.[27] The treatment of **1.9** with benzaldehyde at low temperature generated a P-arm adduct **1.17a'** as a kinetic product. Upon raising the temperature of the reaction to room temperature, the aldehyde group migrated to the N-arm, yielding **1.17a** as a mixture of diastereomers. Similarly, reactions of **1.9** with formate esters and ketones at room temperature resulted in the formation of N-arm products 1.17b, 1.17c, and **1.17d**. With the exception of benzaldehyde, the reaction of **1.9** with carbonyl compounds was found to be reversible, and **1.9** could be regenerated by removing volatiles under vacuum conditions. The equilibrium constants (K_{eq}) of the reaction are sensitive to both steric and electronic properties of carbonyl compounds.[27] No reaction was observed when treating **1.9** with N,N-dimethyl formamide and methyl acetate, while only trace amount of product was obtained with acetone.

Scheme 1.7. Ketone activation mediated by dearomatized PNN Ru^{II} complex **1.9**.

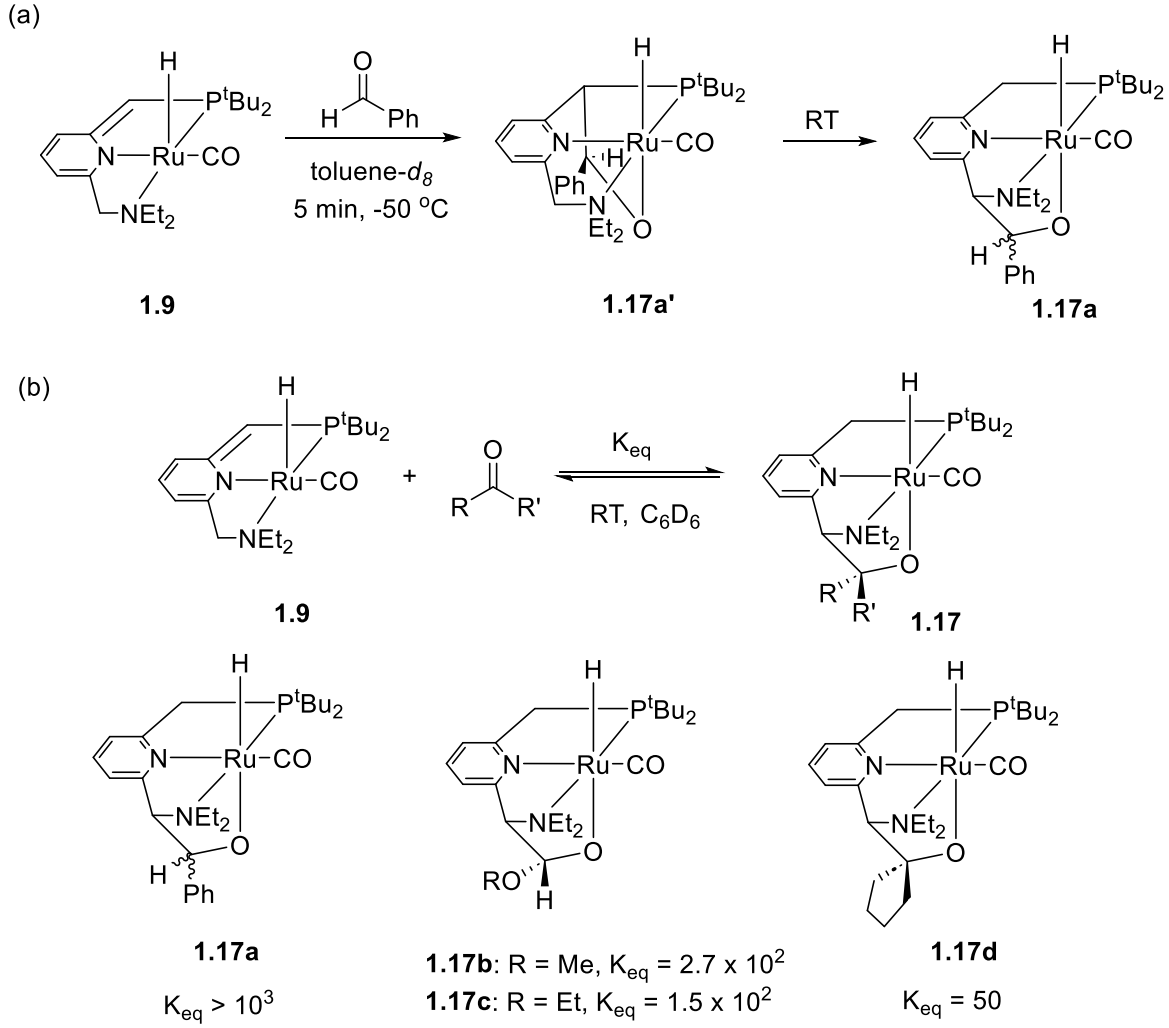

In 2012, the Milstein group reported a new mode of CO_2 activation via metal-ligand cooperation by aromatization/dearomatization.[28] Reaction of CO_2 with dearomatized PNP pincer Ru complex **1.13** at room temperature resulted in the coordination of CO_2 via both Ru-O bond formation at the metal center and C-C bond formation at the methylene arm, leading to the aromatization of the Ru complex **1.18**. Later, Sanford group reported the CO_2 activation in dearomatized PNN pincer Ru complex.[29] At room temperature, CO_2 reacts reversibly in 5 min with the dearomatized PNN pincer Ru complex **1.9** to form C-C bond at P-arm. Interestingly, after prolonging the reaction overnight or heating at 70 °C for 15 min, a second product **1.20** was obtained, where CO_2 binds to the N-arm.

Scheme 1.8. CO_2 activation by dearomatized pincer Ru complexes via aromatization/dearomatization.

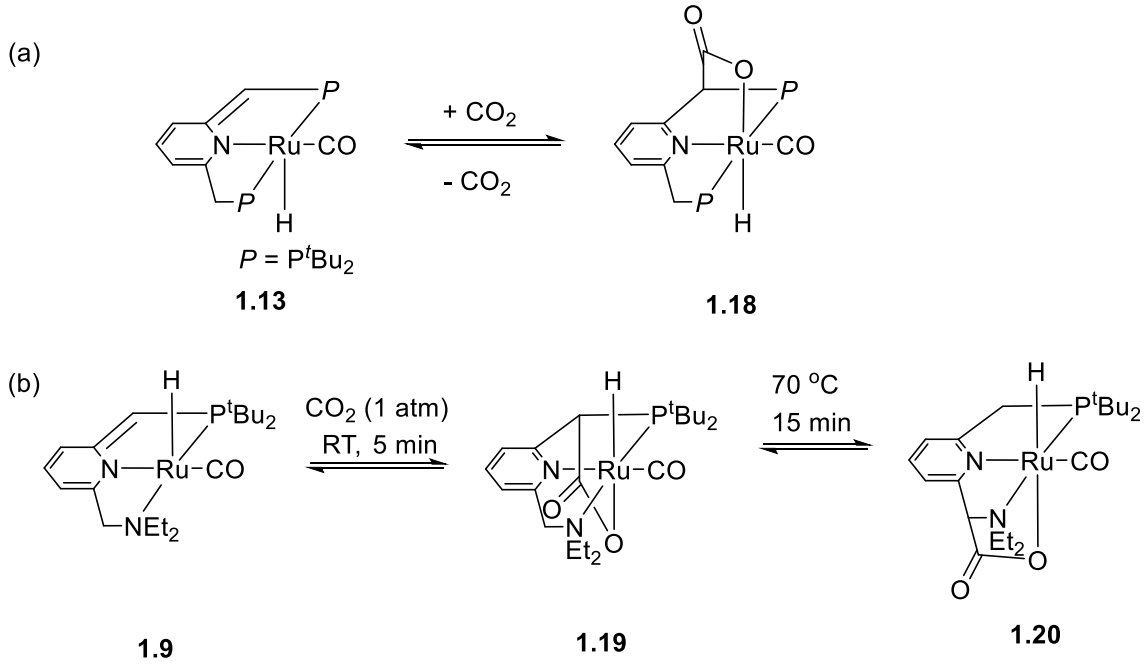

In 2014, Milstein and coworkers reported the boron-hydrogen activation via aromatization/dearomatization metal-ligand cooperation. Treating the dearomatized PNP ruthenium complex **1.13** with cathecholborane or pinacolborane at room temperature led to the formation of a mixture of rearomatized dihydride complex **1.15** and dearomatized complex **1.21** where the boryl group bound to the dearomatized methine arm, while heating the reaction to 60 °C resulted in the complete conversion of **1.21.** Based on DFT calculations, the mechanism of B-H activation was proposed through an unobserved intermediate **1.22**, followed by a H_2 elimination to generate complex **1.21** as a product.[30]

Scheme 1.9. Boron-hydrogen activation mediated by dearomatized PNP pincer ruthenium complex.

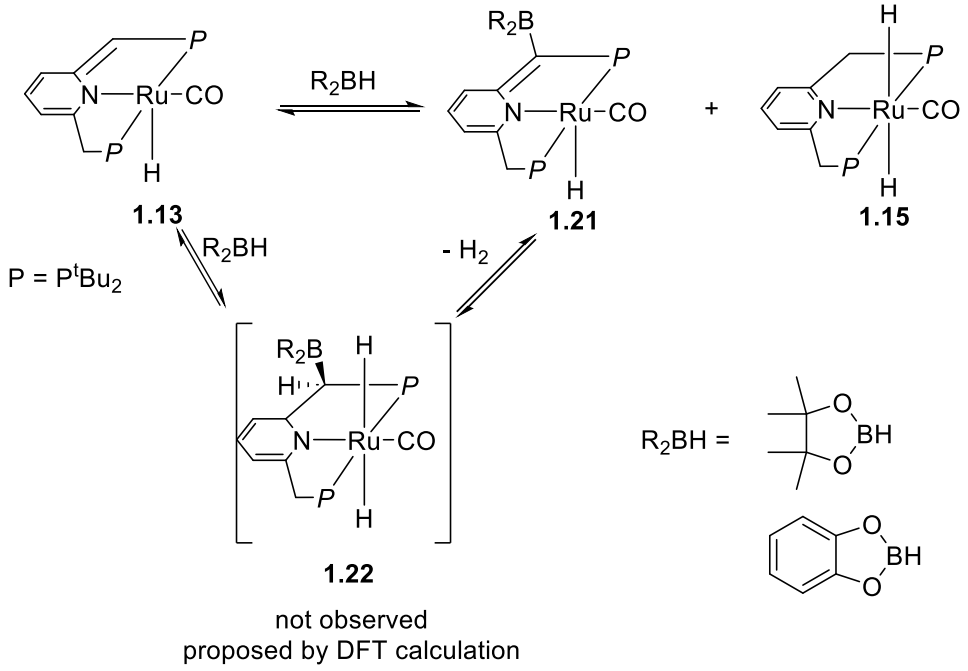

Similarly, the dearomatized PNN ruthenium complex **1.9** reacted with pinacol borane at room temperature to give the borylation product **1.23** at the methine P-arm. Treatment of the

complex **1.9** with 1.05 equiv of less-bulky cathecholborane led to the formation of σ-boryl complex **1.24** where the boryl group bound to the metal center. [30]

The author demonstrated the catalytic activity of complex **1.9** and **1.13** in dehydrogenative coupling of boranes, however, diborane product was obtained in low yields. Complex **1.9** could play a role as a catalyst for C-H borylation of benzene and toluene, however, the detailed mechanism of this reaction was not reported.[30]

Scheme 1.10. Boron-hydrogen activation mediated by dearomatized PNN pincer ruthenium complex **1.9**.

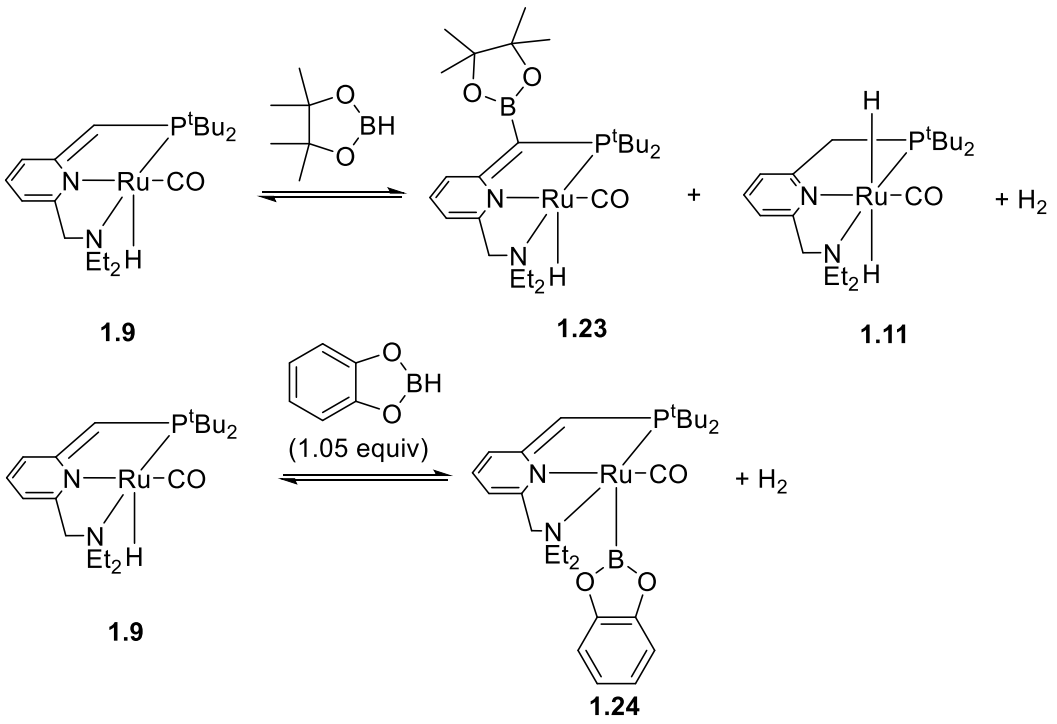

The scarcity, high cost, and toxicity associated with precious second and third-row transition metals have led to a growing interest in replacing "traditional" precious metal complexes with more economical, environmentally friendly, earth-abundant first-row transition metal complexes. Manganese complexes, particularly those in the Mn^I oxidation state, have become the focus of recent research. One notable advantage of Mn^I complexes is their diamagnetic characteristics, which, combined with the metal-ligand cooperation via aromatization/dearomatization, typically does not result in a change in the metal center's oxidation state throughout catalytic cycle. As a result, these complexes provide valuable insights to understand the detail of mechanism by using NMR spectroscopy.

For example, in 2016, Milstein and coworkers reported the first example of dehydrogenative coupling of amine and alcohol to form imines catalyzed by pincer manganese(I) complexes.[31] In detail, reaction of alcohol and amine with the presence of 3 mol% of complex **1.25** in benzene at 135 °C for 60 h produced imine with the liberation of H_2. Notably, the presence of the base is not required for the reaction. An in-depth mechanistic study based on NMR monitoring and intermediate isolation was carried out. First, dearomatized complex **1.25** reacted with alcohol to form an alkoxo Mn complex **1.26** in an equilibrium fashion. The complex **1.26** was independently synthesized by reacting **1.25** with 3 equiv. of alcohol, which was confirmed by NMR spectroscopy and XRD analysis, to confirm the O-H bond activation by metal-ligand cooperation.[31] Thus, the mechanism was proposed to proceed through the formation of an intermediate **1.27**, followed by direct β-hydride elimination of the alkoxy ligand to release aldehyde and form hydride complex **1.28**, which was confirmed

by NMR and XRD analysis. The aldehyde then reacts with amine to form hemiacetal, followed by a release of water to yield the imine product, whereas hydride complex **1.28** undergoes dehydrogenation to form back **1.25** with the release of H_2.[31]

Scheme 1.11. Imine formation via acceptorless dehydrogenative coupling catalyzed by Mn^I complex **1.25** and the proposed mechanism.

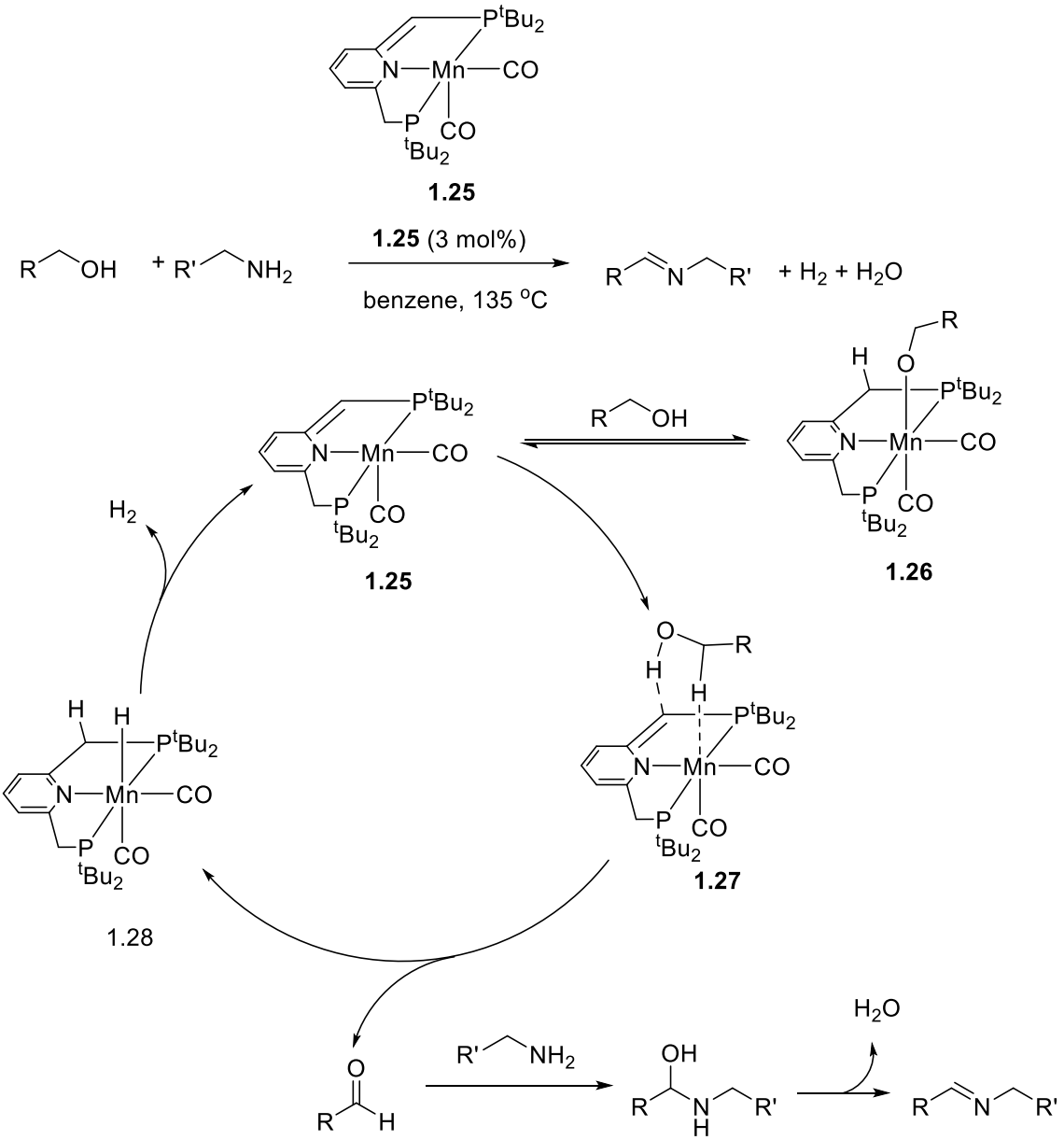

In 2018, the Milstein group reported a protocol for deoxygenative hydrogenation of amide to amine catalyzed by Mn^I complex **1.29**.[32] In detail, the reaction operated in the presence of 5 mol% complex **1.29**, 6 mol% of KO^{t}Bu as a base and 1.5 equiv of $B(C_6F_5)_3$ in m-xylene at 150 °C under 50 bar H_2 for 72 hours. (**Scheme 1.12a**)[32] In the same year, the same group reported the usage of bpy-based pincer (PNN)Mn^I complex **1.30** as a catalyst for the acceptorless dehydrogenative cross-coupling of primary alcohols to form a cross-ester. (**Scheme 1.12b**)[33] One year later, Milstein and coworkers demonstrated complex **1.30** as a first example of earth-abundant metal catalyst for hydrogenation of carbamates and urea. **(Scheme 1.12c)**[34] In both these reactions, the mechanistic investigation based on experimental studies was carried out, suggesting that the reversible H_2 activation via

manganese(I) hydride intermediate was suggested as one of the key steps to produce or consume hydrogen.[32-34]

Scheme 1.12. Catalytic activity of pincer Mn^I complexes **1.29** and **1.30**.

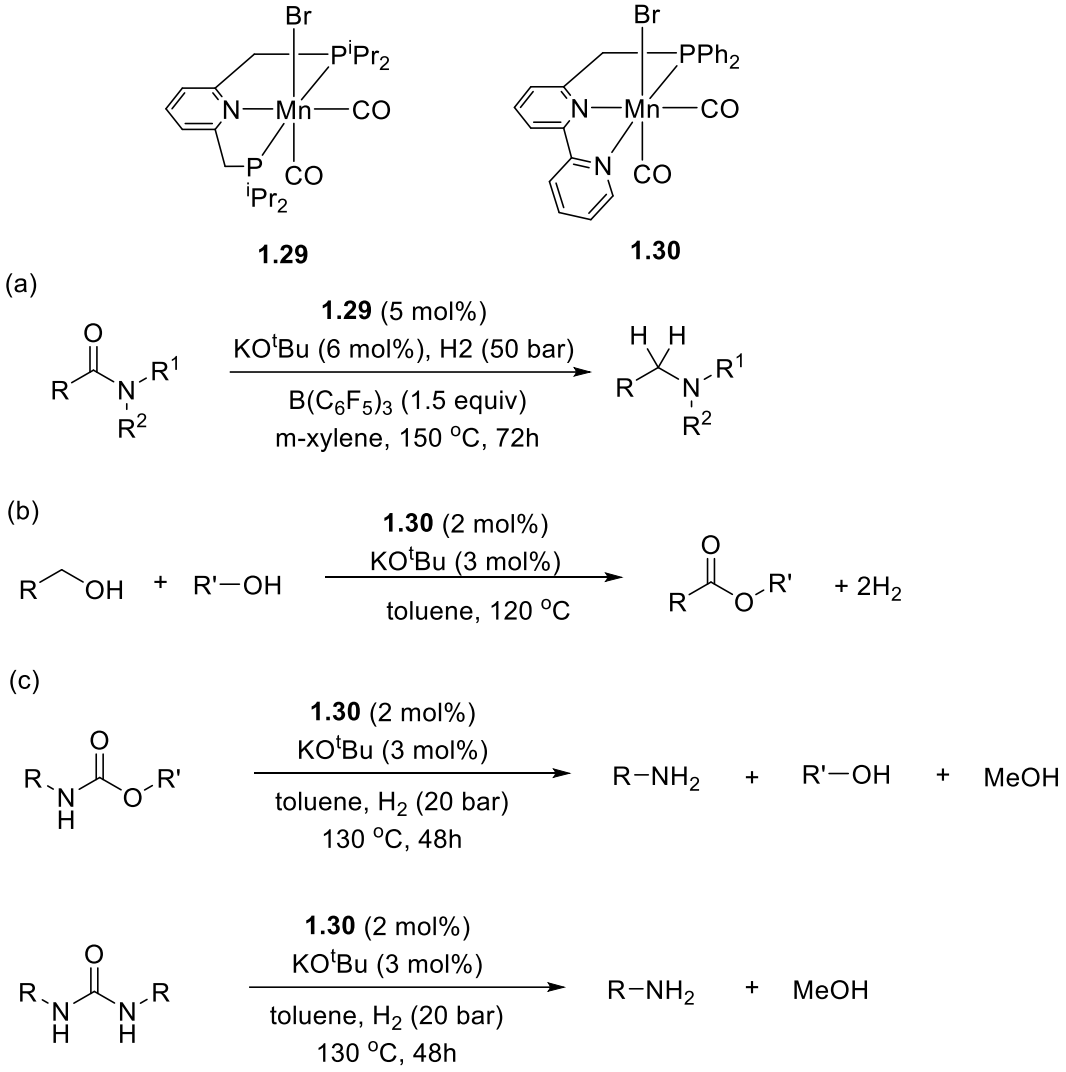

In 2019, Milstein and coworkers reported the study of reactivity of Mn^I complex in CO_2 activation.[35] Reaction of dearomatized PNN pincer Mn^I complex **1.31** with CO_2 resulted in the formation of 1,3 CO_2 addition product **1.32** along with the Mn-O bond formation at the metal center and C-C bond formation at P-arm. On the other hand, reaction of complex **1.31** with dihydrogen led to the formation of Mn^I hydride complex **1.33** with the aromatized PNN pincer ligand. Treatment of Mn^I hydride complex **1.33** with 1 bar of CO_2 immediately led to the formation of **1.34**, where CO_2 inserted to the hydride ligand. The authors also reported the hydrogenation of CO_2 catalyzed by 10 mol% of **1.31**, however, only low yield of formate was obtained.[35]

Scheme 1.13. Reactivity of dearomatized PNN Mn^{I} complex **1.31** with H_2 and CO_2.

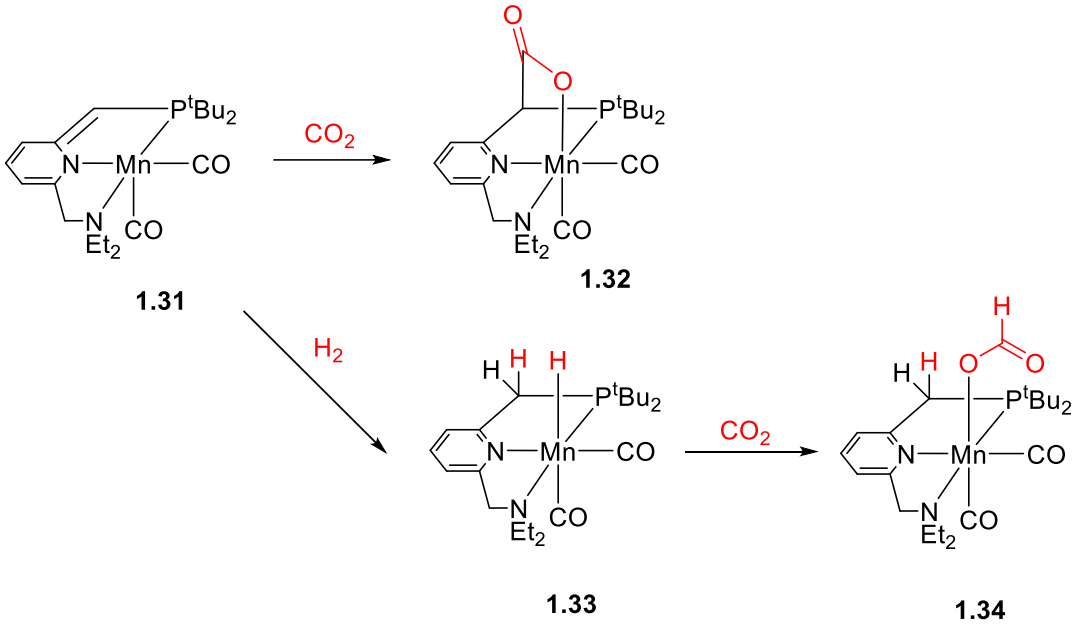

1.2. Small molecule activation and catalysis mediated by non-phosphine metal complexes

The majority of well-known effective homogeneous catalysts contain phosphine in their ligand framework, providing these complexes with remarkable stability. However, the presence of phosphine causes the ligand to be highly susceptible to air and moisture instability, in addition to contributing to the high cost and complexity of synthesis. Therefore, the substitution of phosphines with alternative "soft" donors, such as sulfides, may yield ligand types that are potentially more air-stable and less expensive, while maintaining similar reactivity patterns. For example, Gusev and coworkers reported the use of catalytically active Ru complexes featuring an SNS ligand.[36] With a minimal amount of catalyst (substrate/catalyst ratio up to 80000), the (SNS)Ru complex **1.35** exhibited excellent catalytic activity in the hydrogenation of ketones, aldehydes, imines, and esters under mild conditions. Additionally, this complex **1.35** was identified as a catalyst for the acceptorless dehydrogenative coupling of alcohols, a reverse reaction of ester hydrogenation.[36]

In 2018, the Vries group demonstrated the utility of an air-stable NNS pincer-based [Ru(NNS)(PPh_3)Cl_2] (NNS = 2-(methylthio)-N-(pyridine-2-yl-methyl)ethan-1-amine) complex **1.36** as a catalyst for ester hydrogenation.[37] The catalyst was employed at a 0.05 mol% loading, with a 0.25 mol% KO^{t}Bu base, under mild conditions (40 °C, 30 bar H_2), resulting in a 92% yield of ester. Additionally, the authors reported that changing the alkyl group in the sulfur arms from methyl to tert-butyl, or switching the solvent from toluene to methanol, led to a change in reaction selectivity from ester hydrogenation to olefin reduction.[37]

Scheme 1.14. Ester hydrogenation catalyzed by non-phosphine pincer-based Ru complexes.

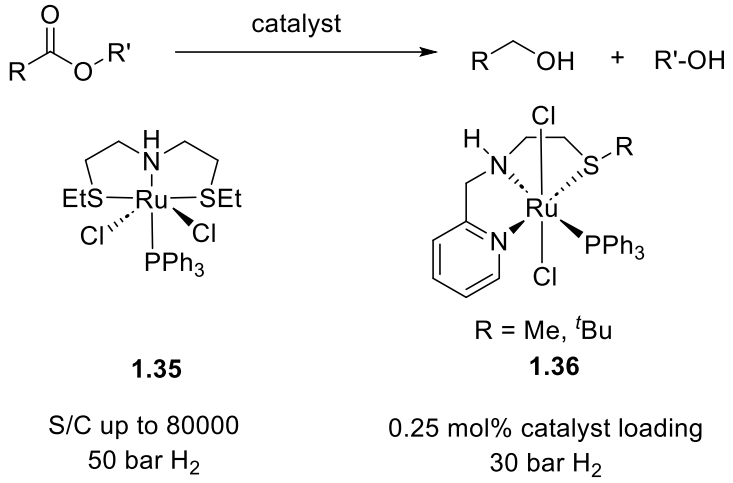

In 2018, Balaraman and coworkers reported the synthesis of pyrroles, pyridines and pyrazine via acceptorless dehydrogenative coupling of aminoalcohols with alcohol catalyzed with the presence of phosphine-free SNS pincer dimeric Co^{II} complex **1.37** as catalyst.(**Scheme 1.15**)[38] The reaction was carried out by heating a mixture of secondary alcohols and β- or γ-aminoalcohols in m-xylene at reflux condition for 24 hours in the presence of 2 mol% catalyst loading of **1.37** and an equivalent amount of KO^tBu as a base to yield pyrroles or pyridines, respectively. In addition, reaction of β-aminoalcohol with a stoichiometric amount of KO^tBu in the presence of **1.37** as a catalyst led to the formation of pyrazine in gram scale.[38]

In 2019, the Srimani group published a study that focused on the utilization of phosphine-free NNS pincer Mn^I complexes as catalysts for the N-alkylation reaction via the "borrowing hydrogen" coupling of amine and alcohol. (**Scheme 1.16**)[39] By utilizing 0.5 mol% of complex **1.38** in the presence of KO^tBu as a base, the desired amine products were obtained in 52- 90% yields.[39] Furthermore, the reaction between amines and alcohols could yield imines as the primary products when the base was changed from KO^tBu to KOH. Notably, this transformation was found to be applicable in the synthesis of 2,3-dihydro-1H-perimidine derivatives, achieving an 84% yield. In a separate report, Srimani and coworkers used the same complex (**1.38**) as a catalyst for synthesis of quinazoline and 2-amino quinazoline via acceptoerless dehydrogenative annulation of nitrile and 2-aminobenzyl alcohol.[40] The authors also demonstrated one-pot synthesis approach for 2-alkylaminoquinolines via two steps: (1) dehydrogenative annulation of dehydrogenative annulation and (2) dehydrogenative coupling of 2-amino quinazoline and primary alcohol by only **1.38** presented as a catalyst.[40]

Scheme 1.15. Synthesis of pyrroles, pyridines via acceptorless dehydrogenative annulation of alcohols with aminoalcohols catalyzed by dimeric complex **1.37**

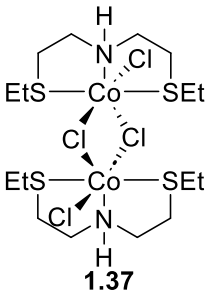

1.37

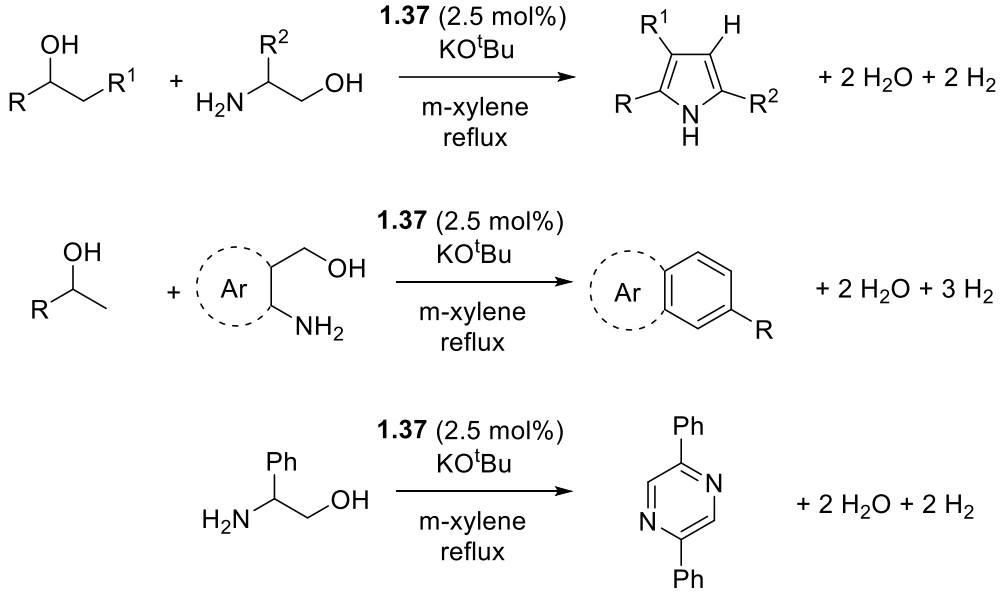

Scheme 1.16. Hydrogen auto-transfer coupling of amine and alcohol catalyzed by phosphine-free NNS pincer-based Mn^I complex **1.38**.

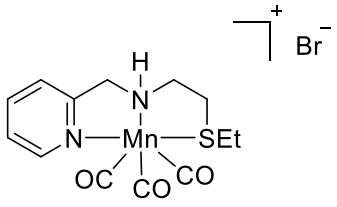

1.38

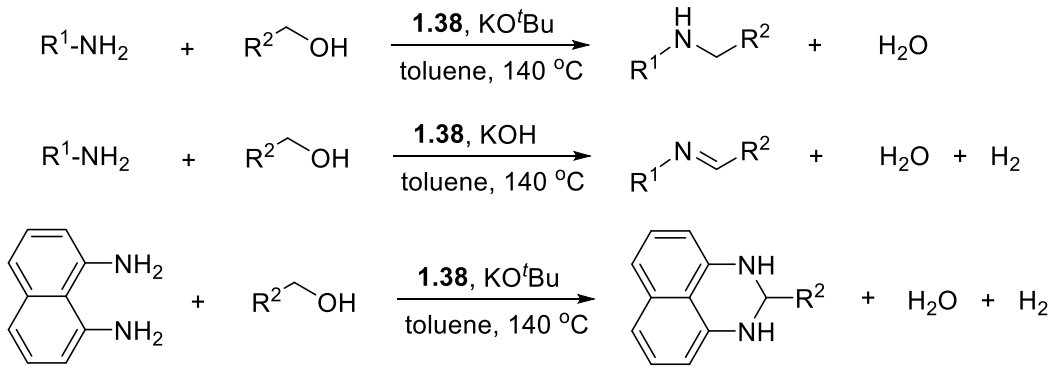

Chapter 2. Single and Double Dearomatization in Non-Phosphine Complexes Supported by N,S-Donor Pyridinophane Ligand

The content described in this chapter is reported in the two following publications:[41-42]

1. Sarbajna, A.; Patil, P. H.; Dinh, M. H.; Gladkovskaya, O.; Fayzullin, R. R.; Lapointe, S.; Khaskin, E.; Khusnutdinova, J. R. "Facile and Reversible Double Dearomatization of Pyridines in Non-Phosphine Mn^{I} Complexes with N,S-Donor Pyridinophane Ligand" *Chem. Commun.* **2019**, *55*, 3282-3285. Copyright **2019** Royal Society of Chemistry.

Declaration of contribution: Prof. Julia R. Khusnutdinova guided the project. Dr. Abir Sarbajna and Dr. Pradnya H. Patil performed the characterization of all complexes in this study and studied the reversible dearomatization transformation. I (Hoan M. Dinh) synthesized the first Mn^{I} complex and explored the double deprotonation in this complex, as well as conducted the reactivity tests of the double deprotonated complexes. Dr. Olga Gladkovskaya helped with ligand synthesis. Dr. Sebastien Lapointe and Dr. Eugene Khaskin performed X-ray data collection. Dr. Robert R. Fayzullin finalized X-ray structural measurement to publication level.

The figure **2.1**-**2.3** and scheme **2.3**-**2.5** in this chapter are from this publication.[42]

2. Dinh, M. H.; Gridneva, T.; Karimata, A.; Garcia-Roca, A.; Pruchyathamkorn, J.; Patil, P. H.; Petrov, A.; Sarbajna, A.; Lapointe, S.; Khaskin, E.; Fayzullin, R. R.; Khusnutdinova, J. R. "Single and Double Deprotonation/Dearomatization of N,S-donor Pyridinophane Ligand in Ruthenium Complexes" *Dalton Trans.* **2022**, *51*, 14734-14746. Copyright **2022** Royal Society of Chemistry.

Declaration of Contribution: Prof. Julia R. Khusnutdinova guided the project and performed DFT calculations. I (Hoan M. Dinh) synthesized and characterized the Ru(II) complexes and performed the deprotonation experiments and reactivity tests of the deprotonated complexes. Ms. Tatiana Gridneva, Dr. Ayumu Karimata, Dr. Aleria Garcia-Roca, Mr. Jiratheep Pruchyathamkorn, Dr. Pradnya H. Patil, Mr. Andrey Petrov and Dr. Abir Sarbajna were involved in the synthesis and characterization of the complexes. Dr. Sebastien Lapointe and Dr. Eugene Khaskin helped with the crystal mounting. Dr. Robert R. Fayzullin finalized X-ray structural measurement to publication level.

The scheme **2.4**-**2.7,** figure **2.4**-**2.9** and table **2.1**-**2.2** in this chapter are from this publication.[41]

2.1. Introduction

As discussed in chapter 1, the development of a new class of N,S-donor ligands has emerged recently as cheaper, less toxic alternatives for phosphine-based ligands to stabilize transition metal complex and also show comparable reactivity in hydrogenation, and acceptorless dehydrogenative coupling reaction. However, research on the deprotonation reactivity of sulfur-based ligands, crucial to understand the mechanism, have been relatively scarce. For example, the Milstein group investigated the deprotonation of a PNS pincer ligand in Ru complex **2.1**, which resulted in the dimerization of Ru complex and eventually to an irreversible cleavage of the ligand framework to form **2.2**. (**Scheme 2.16**)[43] On the other hand, dearomatized Rh complex supported by sulfoxide-based NNS pincer ligands exhibited no reprotonation even in the presence of excess protic solvent.[44]

Scheme 2.1. Deprotonation of pincer (PNS)Ru complex **2.1**.

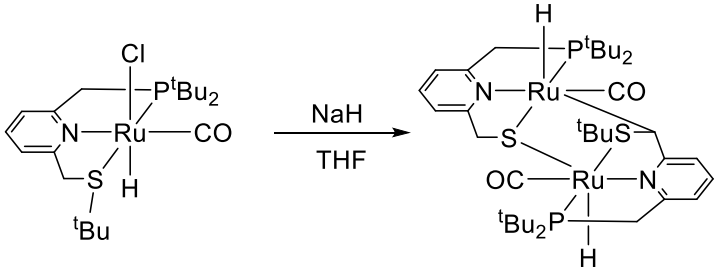

2.1 **2.2**

Our research group has been interested in the investigation of tetradentate macrocyclic pyridinophane N2Y2-type ligands, which consist of two pyridine fragments linked by four methylene bridges to two donor atoms, typically nitrogen or sulfur (**Scheme 2.2**). When compared to tridentate pincer ligands, these N2Y2 ligands may be viewed as two pincer fragments linked together via coordinating heteroatoms, with two isolated pyridine donors. This class of ligands exhibits a unique coordination behavior, capable of binding to a metal center in either a κ^2 (bidentate), κ^3 (tridentate), or κ^4 (tetradentate) mode, depending on the nature of the metal center, therefore showing coordinating properties different from the classical pincer motifs.[45-46] The κ^4 coordination mode is particularly known for its ability to stabilize uncommon oxidation states or other reactive species that may not be attainable using alternative ligand frameworks.[47-49] In another variation of this ligand, one of the pyridine rings may be replaced with a phenyl or substituted phenyl ring, which then may be cyclometalated serving as an anionic aryl ligand (**Scheme 2.2**).

Scheme 2.2. N2Y2-and NY2C-Pyridinophane ligand structure and their coordination modes in metal complexes.

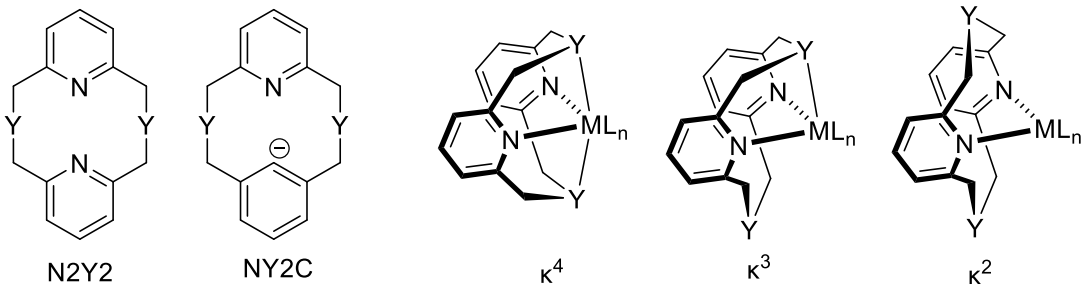

In this study, we utilize the macrocyclic structure and high stability of the pyridinophane **N2S2** ligand (N2S2 = 2,11-dithia[3.3](2,6)pyridinophane to stabilize the Mn^{I} and Ru^{II} complexes and investigate their reactivity for deprotonation in the presence of base, which gives us access to the structural analysis of the deprotonation of N,S-donor ligand.

2.2. Result and Discussion

2.2.1 Synthesis and reactivity of manganese(I) complexes

2.2.1.1. Complex synthesis

Our first efforts to obtain metal complexes supported by **N2S2** ligand were focused on using Mn^{I} precursor. $Mn(CO)_5Br$ was reacted with 1 equivalent of the ligand in a toluene/methanol mixture at 80 ºC for 24 hours to produce the yellow-colored compound **2.3**. Complex **2.3** was isolated in 95% yield and characterized by NMR, UV-vis, IR spectroscopy and elemental analysis. The NMR spectrum was consistent with a C_{2v}-symmetrical structure in solution, showing two doublets at 4.79 and 4.90 ppm that correspond to the geminally coupled CH_2 group of **N2S2**. The *para*-protons and two equivalent *meta*-protons of pyridine appeared as a triplet at 7.74 and a doublet at 7.47 ppm, respectively. The stretching bands of carbonyl ligands in the solid-state FT-IR spectrum appear at 1934 and 1866 cm^{-1}. The X-ray structure shows a distorted octahedral Mn center with the **N2S2** ligand bound in a *syn*-boat-boat conformation.

Scheme 2.3. Synthesis scheme of complex **2.3**.

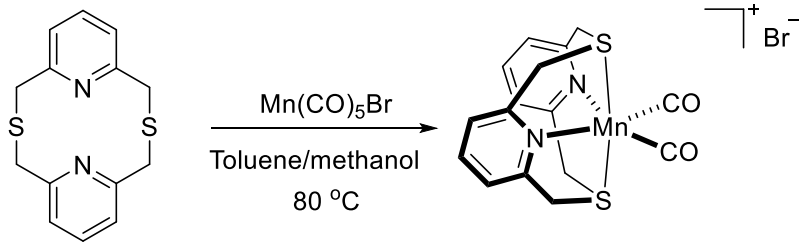

N2S2 **2.3**

95 %

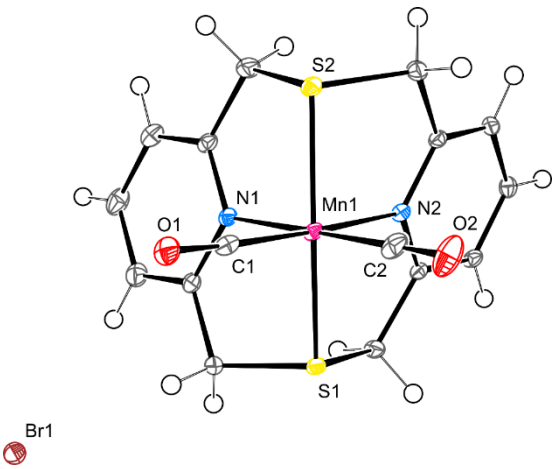

Figure 2.1. ORTEP at 50 % probability anisotropic displacement ellipsoids of non-hydrogen atoms for compound **2.3**. Selected interatomic distances [Å]: Mn1–S1 2.2712(5), Mn1–S2 2.2609(5), Mn1–N1 2.0582(15), Mn1–N2 2.0572(14), Mn1–C1 1.7897(18), Mn1–C2 1.797(2).

2.2.1.2. Deprotonation of Mn^{I} complexes

Treating complex **2.3** with 2.2 equivalents of KO^{t}Bu in THF led to the formation of an orange solution within a few seconds. Orange single crystals were generated by diffusing pentane to the THF solution at -30 °C. SC-XRD data confirmed the doubly deprotonated structure of **2.3b**. According to XRD, the bond distance of C11-C12 and C26-C27 are significantly shortened to 1.384(4) and 1.367(4) Å, respectively, which is consistent with a typical double C-C bond length (ca 1.34 Å), whereas the bonds C16-C17 and C21-C22 are of 1.499(4) and 1.508(4) Å, suggesting that the deprotonation occurred at C11 and C27 centers. The positions of the hydrogen atom H11 and H27 of the deprotonated arms were determined by difference Fourier maps. On the other hand, the sulfur-carbon bonds S1-C11 and S2-C27 (1.737(3) and 1.752(3) Å) in the deprotonated arms are significantly shorter compared to the S1-C21 and S2-C17 bonds in the non-deprotonated arms (1.820(3) and 1.825(3) Å). The shortening in sulfur-carbon bonds ($\Delta \approx 0.08$ Å) is less significant compared to the carbon-carbon bonds ($\Delta \approx 0.13$ Å), suggesting the sulfur ylide resonance structure has much less contribution compared to the dearomatized pyridine ring resonance.

^{1}H NMR spectrum of complex **2.3b** in THF-d_8 is consistent with double deprotonation: two equivalent CH groups appear as a singlet at 3.38 ppm, whereas the two protons on the non-deprotonated CH_2 groups appear as two geminally coupled doublets at 3.44 ppm. In addition, the ^{1}H NMR spectrum showed an upfield-shifted of the pyridine protons which appear as a doublet of doublets at 6.13 ppm for the proton in the *para*-position and two doublets at 5.74 and 5.37 ppm for the two *meta*-protons.

Scheme 2.4. Double deprotonation/dearomatization of complex **2.3**.

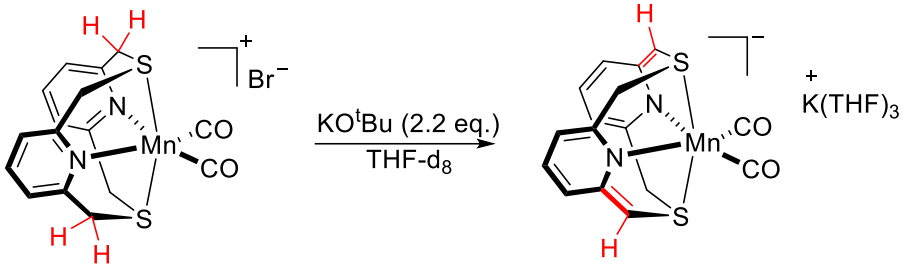

2.3 **2.3b**

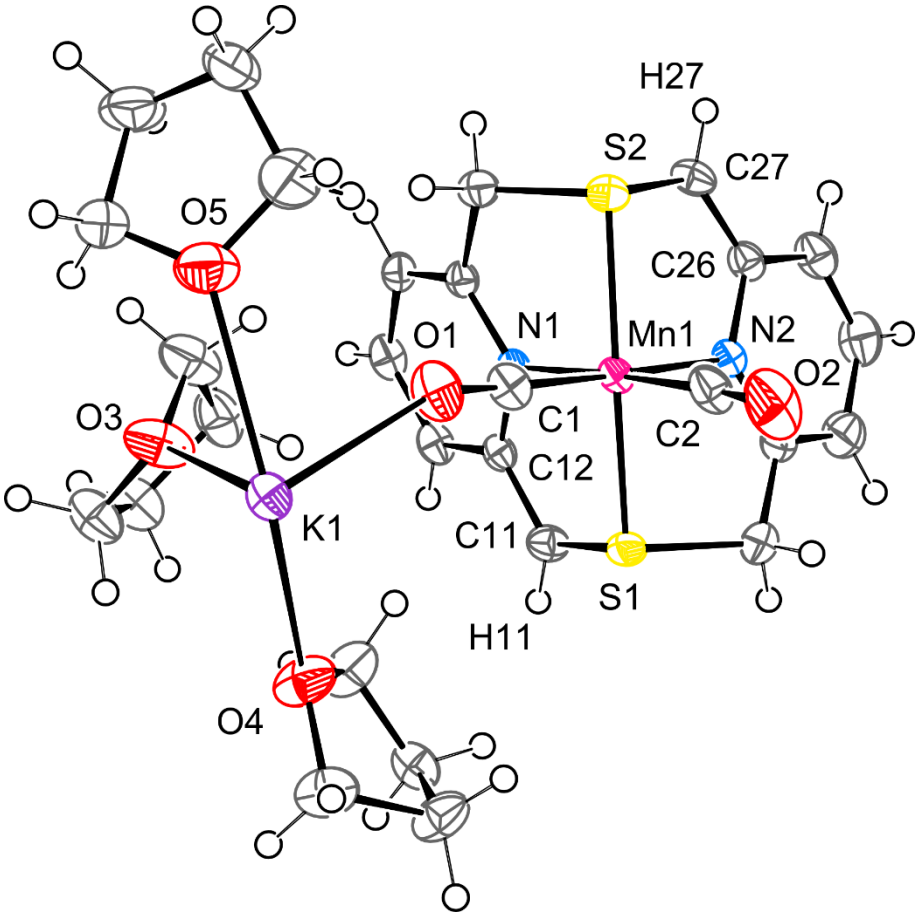

Figure 2.2. ORTEP at 50 % probability anisotropic displacement ellipsoids of non-hydrogen atoms for compound **2.3b**. Minor disordered components of THF ligands are omitted for clarity. Selected interatomic distances [Å]: Mn1–S1 2.2756(8), Mn1–S2 2.2867(7), Mn1–N1 2.044(2), Mn1–N2 2.049(2), Mn1–C1 1.767(3), Mn1–C2 1.779(3), C11–C12 1.384(4), C26–C27 1.367(4), C16–C17 1.499(4), C21–C22 1.508(4), S1–C11 1.737(3), S1–C21 1.820(3), S2–C17 1.825(3), S2–C27 1.752(3).

After having a full characterization of complex **2.3b**, we next examined if the deprotonation was reversible. Addition of 2.5 equivalent of HBr in diethyl ether to the in situ generated **2.3b** led to the formation of **2.3**, which was confirmed by XRD and other spectroscopies.

After observing the double dearomatization in complex **2.3**, we next examine if we can find the monodeprotonated Mn^{I} complexes. Treating **2.3** with 1.2 – 1.8 equiv. of KO^{t}Bu did not lead to the formation of monodeprotonated complexes. Instead, incomplete conversion of doubly deprotonated complex **2.3b** was observed in all cases. We then reacted doubly dearomatized complex **2.3b** with 1 equiv. of HBr, interestingly, a neutral monodeprotonated compound **2.3a** was yielded, which was confirmed by NMR spectroscopies and XRD analysis. ^{1}H NMR spectrum of **2.3a** showed six sets of doublets for the three non-deprotonated methylene groups and one singlet for dearomatized CH group at 3.54 ppm. The aromatic region in ^{1}H NMR displays one triplet and two doublets at 7.55 – 7.32 ppm, whereas the dearomatized pyridine appeared as three upfield-shifted peaks at 6.27 – 5.63 ppm. DEPT-135 NMR analysis showed the carbon peak of deprotonated CH arm at 54.6 ppm, whereas the non-deprotonated CH_2 arms appeared reversed in phase at 60.1, 52.2 and 47.5 ppm.

XRD analysis confirmed the neutral structure of **2.3a** without counteranions. The structure is CH_2/CH disordered (**Figure 2.3**) into two components with the same occupancies. The apparent geometry of the ligand seems to be an average of two configurations, with either the C11 or C27 arm being deprotonated. The overall lengths of the C11–C12 and C26–C27

bonds are approximately 1.44 Å, shorter than those of C16–C17 and C21–C22 (around 1.50 Å). Similarly, the sulfur–carbon bonds S1–C11 and S2–C27 (about 1.78 Å) in the deprotonated segments are shorter than those of S1–C21 and S2–C17 (approximately 1.82 Å).

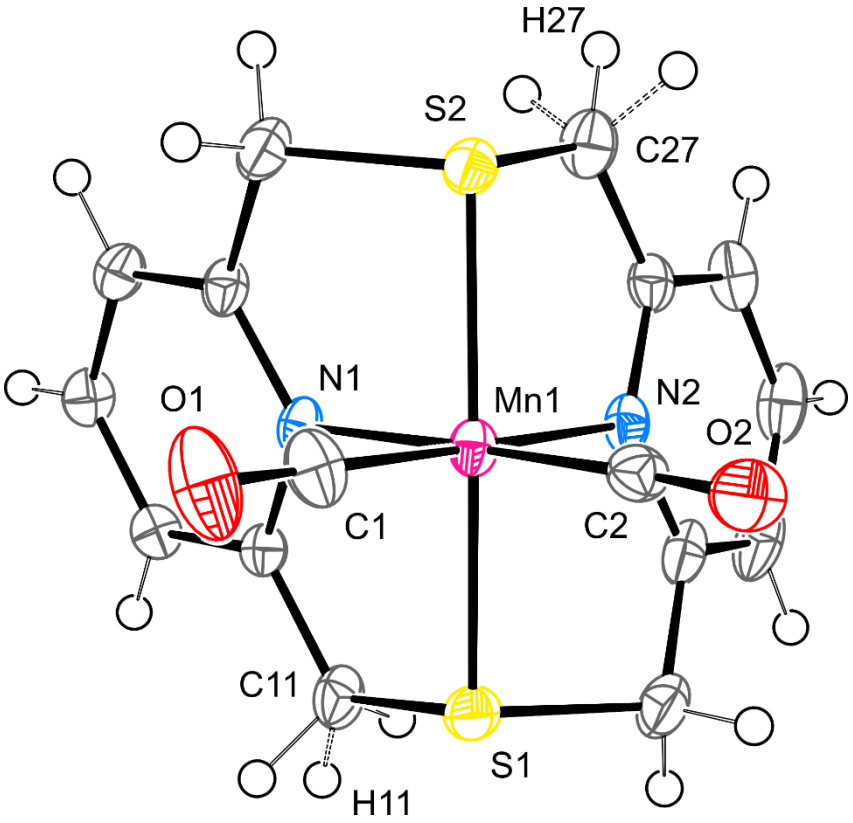

Figure 2.3. ORTEP at 50 % probability anisotropic displacement ellipsoids of non-hydrogen atoms for compound **2.3a**. Minor disordered component is shown by dash lines. Selected interatomic distances [Å]: Mn1–S1 2.2726(9), Mn1–S2 2.2866(9), Mn1–N1 2.051(2), Mn1–N2 2.056(2), Mn1–C1 1.782(3), Mn1–C2 1.784(3), C11–C12 1.444(4), C26–C27 1.441(4), C16–C17 1.507(4), C21–C22 1.494(5), S1–C11 1.784(3), S1–C21 1.816(3), S2–C17 1.823(3), S2–C27 1.784(3). The geometry is averaged over two forms with either C11 or C27 arm being deprotonated.

Singly deprotonated **2.3a** could be deprotonated by one equiv. of KO^{t}Bu to form doubly deprotonated **2.3b**. In addition, complex **2.3a** could be protonated by reacting with one equiv. of HBr to form back the non-aromatized complex **2.3**.

Interestingly, treating doubly deprotonated complex **2.3b** with one equiv. of H_2O as a weakly acidic proton donor led to the clean formation of monodeprotonated **2.3a**. Even after a presence of >10 equiv. of water, only **2.3a** is yielded. The formation of **2.3a** from **2.3b** could also be proceeded in a weakly basic media by using one equiv. of aqueous ammonia solution.

Scheme 2.5. Interconversions between **2.3**, **2.3a** and **2.3b**.

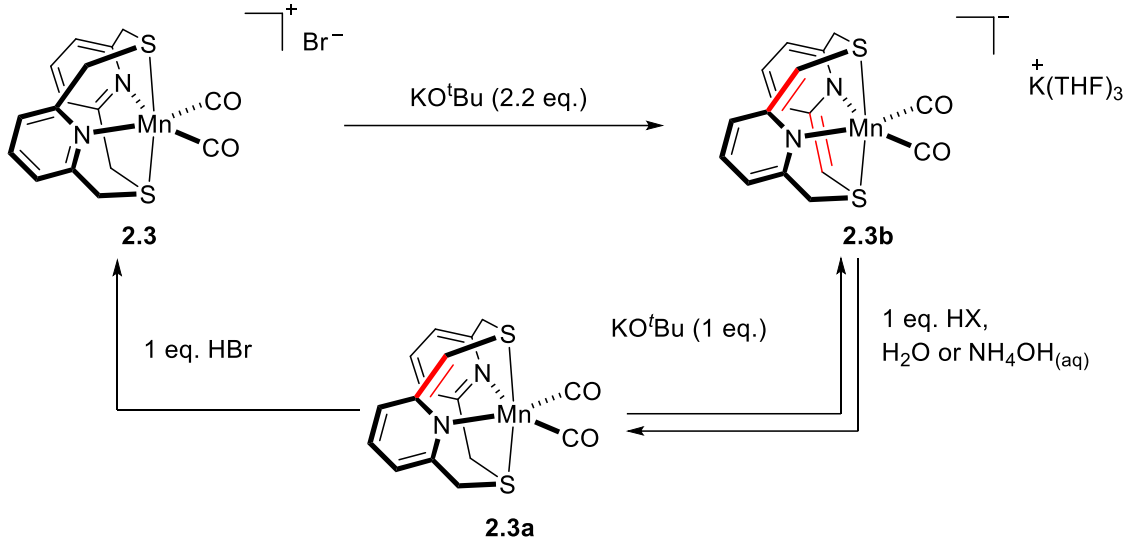

After fully characterizing singly and doubly dearomatized complexes, we next examined the reactivity of these complexes in small molecule activation and catalysis. Reaction of doubly deprotonated **2.3b** with CO_2 led to the formation of unidentified insoluble products. The complex **2.3b** showed no catalytic reactivity in hydrogenation of CO_2 or ketone under a range of conditions. We reasoned that the lack of reactivity in complex **2.3b** is likely due to the presence of strongly bound carbonyl ligands and the system is needed to have more labile ligands to create a vacant site to enable metal-ligand cooperation reactivity. At the same time, carbonyl ligand is required for stabilization of Mn^I and our attempts to replace it with another ligand under UV light irradiation were unsuccessful.

As an alternative way to circumvent this problem, we have decided to switch our attention to another metal commonly used to study metal-ligand cooperation pincer-like complexes – ruthenium. Ruthenium(II) complexes feature a d^6 configuration and they can be conveniently obtained using a variety of precursors containing non-carbonyl ligands. The initial expectation behind this choice was that the presence of Ru^{II} may enable greater stoichiometric or even catalytic reactivity, allow for stabilization of reactive species, such as hydrides, and potentially allow for the synthesis of precursors containing more labile and easily replaced ligands. The final results showed that the reactivity of Ru complexes is further complicated by unexpected ligand rearrangement.

2.2.2 Synthesis and reactivity of Ru^{II} complexes

2.2.2.1. Ru^{II} complexes preparation and characterization

As previously discussed, Mn^I complexes supported by non-phosphine **N2S2** ligand showed a facile, stable single and double dearomatization in the presence of a base. However, no metal-ligand cooperation reactivity was observed, likely due to the lack of labile coordination ligands. Ruthenium, on the other hand, has proved to have a great reactivity in metal-ligand cooperation reactivity, also, has a range of common precursors containing labile ligands. Therefore, we next targeted ruthenium complexes containing our N,S-donor **N2S2** ligand, with the aim to study both metal-ligand cooperation and find the reactivity of the deprotonated complexes.

We examined the reactivity of the **N2S2** ligand with a range of common ruthenium precursors which allowed us to obtain dicationic and monocationic (**N2S2**)Ru complexes. First, the $[RuCl_2(p\text{-cymene})]_2$ dimer was pre-treated with silver triflate in acetonitrile

solution followed by the addition of the **N2S2** ligand, which yielded the dicationic bis-acetonitrile complex **2.4** (**Scheme 2.6**). Complex **2.4** was isolated in 64% yield and characterized by NMR, UV-vis, IR spectroscopy and elemental analysis. The ^{1}H NMR spectrum was consistent with a C_{2v}-symmetrical structure in solution, showing two doublets at 4.76 and 4.74 ppm that correspond to the geminally coupled CH_2 groups of N2S2. The *para*-protons and two equivalent *meta*-protons of pyridine appeared as a triplet at 7.60 and a doublet at 7.38 ppm, respectively. The uncoordinated triflate counteranion appears at −79.25 ppm in the ^{19}F NMR spectrum, ruling out the interaction with the ruthenium center. Crystals were obtained by diethyl ether diffusion into an acetonitrile solution and analyzed by single-crystal X-ray diffraction (SC-XRD), showing the expected κ^4-coordination geometry.

Scheme 2.6. Synthesis of Ru complexes

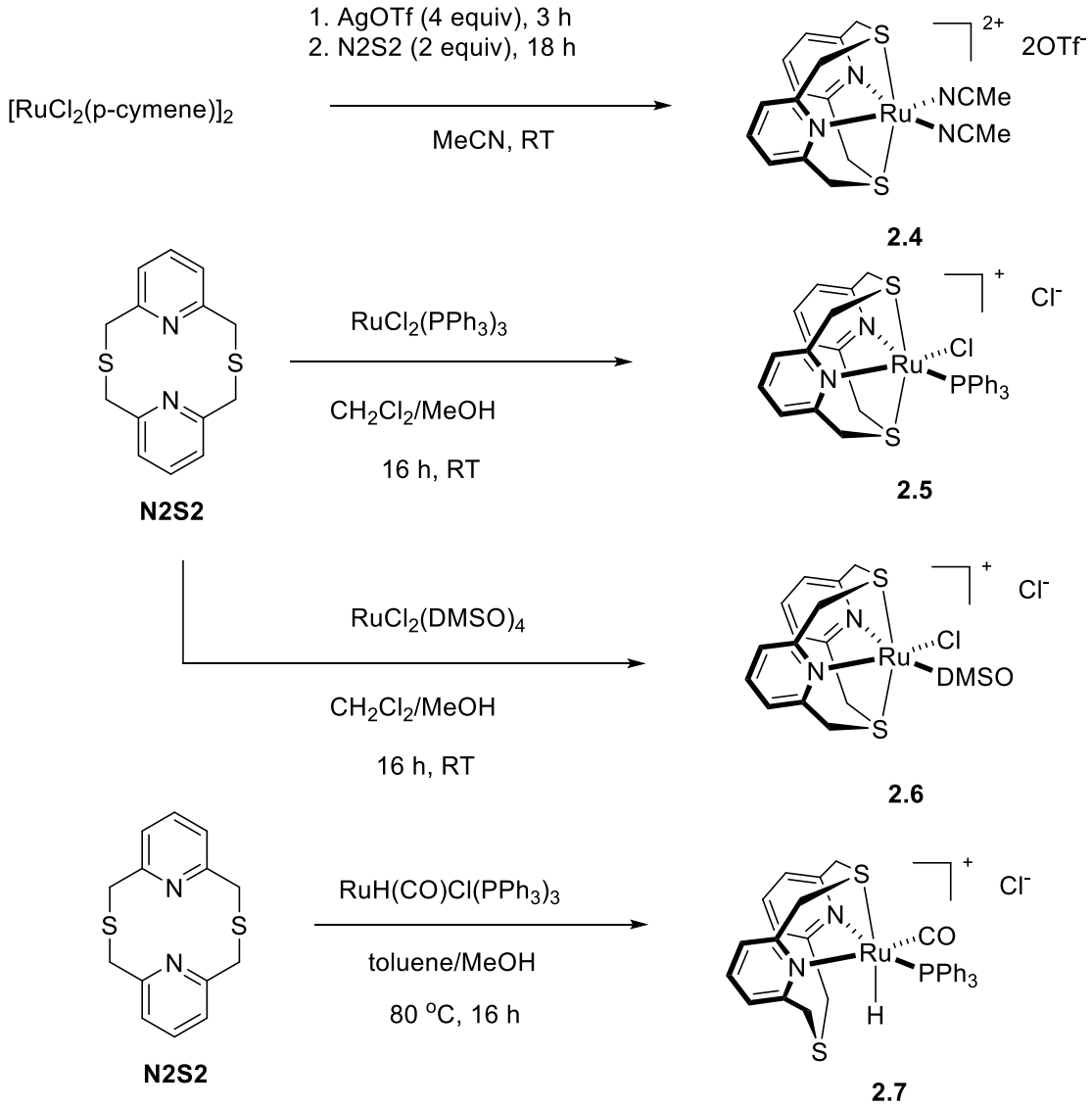

Next, the monocationic chloro-complexes **2.5** and **2.6** were obtained by the reaction of **N2S2** with $RuCl_2(PPh_3)_3$ or $RuCl_2(DMSO)_4$, respectively (**Scheme 2.6**). Treating **N2S2** ligand with 1 equiv. of $RuCl_2(PPh_3)_3$ precursor in DCM at room temperature in 16 hours led to the formation of complex **2.5**. Complex **2.5** was isolated as a yellow powder in 70% yield and characterized by XRD, NMR, ESI-HRMS, UV-vis and IR spectroscopy. According to SC-XRD, the N2S2 bound to ruthenium in a κ^4 fashion. The PPh_3 and coordinated chloro

ligands bound to ruthenium in the trans-position compared to N-donor pyridines, whereas one uncoordinated chloride plays as a counteranion. The $^{31}P\{^{1}H\}$ NMR spectrum shows the signal of the coordinated phosphine in **2.5** at 46.28 ppm.

Similarly, reaction of **N2S2** ligand with 1 equiv. of $RuCl_2(DMSO)_4$ in DCM/methanol mixture at room temperature resulted in the formation of complex **2.6**. The complex **2.6** was isolated as crystalline solids in 84% yield. According to SC-XRD, DMSO and Cl ligand bind to the ruthenium center in the trans position compared to N-donor pyridines and one uncoordinated Cl^- appears as a counteranion. In ^{1}H NMR spectrum of **2.6** in chloroform-d_3, the two para-protons and four meta-protons of pyridines appeared as a triplet at 7.50 and 7.35 ppm and a doublet at 7.53 and 7.43 ppm, respectively; whereas the CH_2 protons appeared as four sets of geminally-coupled doublet at 5.67, 5.64, 4.74 and 4.69 ppm. The Ru-bound DMSO of **2.6** appears as a singlet at 3.48 ppm in the ^{1}H NMR spectrum.

In an attempt to obtain a ruthenium hydride complex, we reacted a common hydride precursor, $RuHCl(CO)(PPh_3)_3$, with **N2S2** ligand in a mixture of toluene and methanol. However, even after heating at 80 ^{o}C for 16 hours, the **N2S2** binds to the ruthenium center in a κ^3-fashion resulting the formation of **2.7**, where one of the S-donor in the ligand remained unattached, which was confirmed XRD. According to SC-XRD, the hydride is present in a *trans*-position to the coordinated S atom, while CO and PPh_3 are located in *trans*-positions to pyridines, and one chloride is present as a counteranion (**Figure 2.6**). The ^{1}H NMR spectrum showed highly unsymmetrical structures of **2.7** with 8 geminally-coupled doublets of CH2 protons at 6.46, 5.96, 5.89, 4.32, 3.94, 3.39 and 3.15 ppm, and the hydride proton appears as doublet at -6.68 ppm due to phosphorus splitting. The $^{31}P\{^{1}H\}$ NMR spectrum of 4 shows one singlet at 62.90 ppm corresponding to the coordinated PPh_3. The IR spectrum shows the CO stretching frequency at 1934 cm^{-1}.

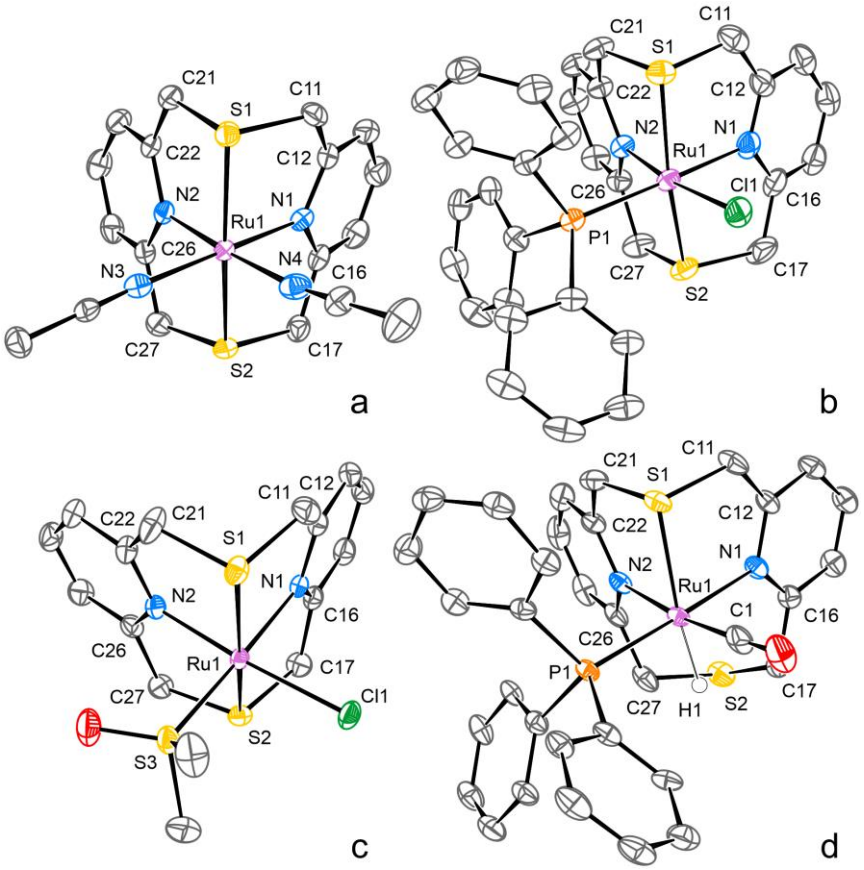

Figure 2.4. ORTEP of cationic parts of complexes **2.4** (a), **2.5** (b), **2.6** (c) and **2.7** (d) at 50 % (b, d), 70 % (a) or 80 % (c) probability level according to SC-XRD. Hydrogen atoms, except for [Ru]H1, are omitted for clarity. In the case of **2.5**, one of two symmetry independent molecules is shown. Selected interatomic distances [Å]: Ru1–S1 2.3226(12), Ru1–S2 2.3144(12), Ru1–N1 2.045(4), Ru1–N2 2.046(4), Ru1–N3 2.054(4), Ru1–N4 2.040(4) for **2.4**; Ru1–Cl1 2.4315(7), Ru1–S1 2.3228(8), Ru1–S2 2.3186(8), Ru1–P1 2.3070(7), Ru1–N1 2.122(3), Ru1–N2 2.042(2) for **2.5**; Ru1–Cl1 2.4293(3), Ru1–S1 2.3190(3), Ru1–S2 2.3173(3), Ru1–S3 2.2521(3), Ru1–N1 2.0856(10), Ru1–N2 2.0495(10) for **2.6**; Ru1–S1 2.3840(15), Ru1–P1 2.2994(14), Ru1–N1 2.219(5), Ru1–N2 2.223(5), Ru1–C1 1.851(7), Ru1–H1 1.60(3) for **2.7**.

2.2.2.2. Deprotonation of ruthenium complex

a. Deprotonation of 2.4

Based on our previous studies of single and double dearomatization of Mn complexes with the **N2S2** ligand, we expected similar reactivity in (**N2S2**)Ru complexes upon treatment with variable amounts of base.

First, treatment of complex **2.4** with 2.2 equiv. of KO^{t}Bu in toluene-d_8 gave a poorly soluble doubly deprotonated product **2.4b** (**Scheme 2.7**). Filtration of the toluene solution and crystallization at -20 °C yielded orange single crystals of **2.4b**. XRD of **2.4b** confirmed the double deprotonated structure in the **N2S2** ligand. The bond length of C16-C17 and C21-C22 are significantly shortened (1.387(3) and 1.382(3) Å, respectively), which is close agreement with a typical C-C double bond (ca 1.34 Å), suggesting that the deprotonation has occurred in C16 and C21 centers. The position of the hydrogen atom H17 and H21 were determined by difference Fourier maps. On the other hand, the C11-C12 and C26-C27 bond distances are 1.501(3) Å and 1.502(3) Å, respectively, which is consistent with the typical Csp2-Csp3 bond. In addition, the methine C–S distances at the deprotonated arms are also considerably shorter, 1.730(2) Å and 1.733(2) Å, as compared to the methylene C–S distances of 1.839(2) Å and 1.847(2) Å.

The double deprotonation in **2.4b** was also confirmed by ^{1}H NMR spectroscopy. The ^{1}H NMR of **2.4b** in toluene-d_8 shows a significant upfield shift of the *para*- and *meta*-protons in the pyridines which appear at 6.13 ppm as a doublet of doublets and 5.74 and 5.37 ppm as a doublet, respectively. The two equivalent CH protons of the deprotonated arms appear as a singlet at 4.18 ppm, whereas the remaining CH_2 groups appear as two geminally coupled doublets at 3.89 and 3.73 ppm.

Interestingly, the doubly deprotonated **2.4b** was moderately stable in acetonitrile-d_3: treating of **2.4** with 2.2 equiv. of KOtBu in CD_3CN led to the formation of **2.4b** with 80% NMR yield, which was proved by ^{1}H NMR. ^{1}H NMR spectrum of **2.4b** in CD_3CN showed a doublet of doublets at 6.28 ppm and two doublets at 5.85 and 5.53 ppm, however, the peaks of CH/CH_2 disappeared due to H/D exchange with the deuterated solvent.

The compound **2.4b** was slowly decomposed in room temperature in acetonitrile-d_3 or toluene-d_8: when **2.4b** was generated by deprotonation of **2.4** with 2 equiv. of KO^{t}Bu, only about half of the initially formed complex remained in solution after 10 min at RT, forming an insoluble precipitate.

Next, we attempted to generate monodeprotonated species by reacting **2.4** with 1.1 equiv. of KO^{t}Bu in toluene-d_8, however, only **2.4b** was found in the solution, along with a poorly soluble precipitate which might contain monodeprotonated product. Interestingly, monodeprotonated product **2.4a** was formed by reacting **2.4** with 1.1 equiv. of KO^{t}Bu in acetonitrile-d_3 giving in 90% yield, which was confirmed by ^{1}H NMR. The dearomatized pyridine peaks are upfield shifted and appear as a doublet of doublets at 6.37 ppm and two doublets at 5.92 and 5.75 ppm, whereas the aromatic pyridine protons appear in the 7.24-7.53 range. In CD_3CN solution, the methylene and methine groups undergo slow H/D exchange.

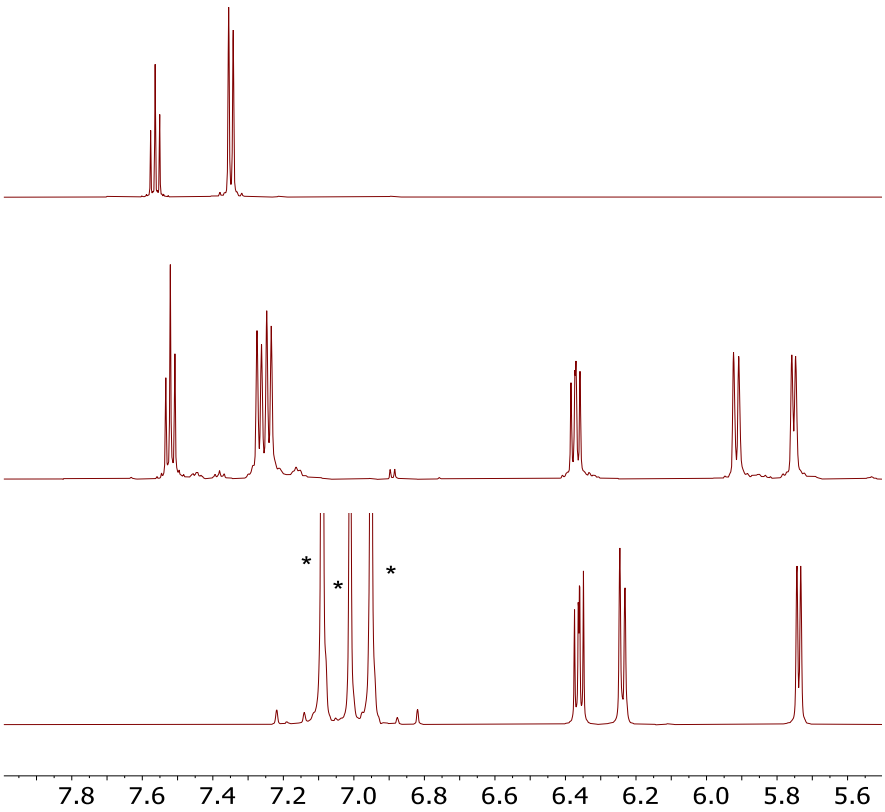

Figure 2.5. Pyridine peaks in ^{1}H NMR spectra of **2.4** (top; in CD_3CN), **2.4a** (middle; in CD_3CN) and **2.4b** (bottom; in toluene-d_8). Peaks of residual toluene are marked with an asterisk.

Next, we examined if the deprotonated complexes **2.4a** and **2.4b** can be re-protonated. Treating complex **2.4a** and **2.4b** with HBF_4 resulted in the full recovery of $[(\mathbf{N2S2})Ru(MeCN)_2]^{2+}$, proving that the deprotonation in complex **2.4** is reversible.

Unfortunately, an attempt to get single crystals of **2.4a** was not successful. Therefore, we tested the reactivity of monocationic complex **2.5-2.7** with the base as an alternative route to get monodeprotonated species. We expected that single deprotonation of these complexes would lead to the formation of neutral species, thereby improving the solubility and stability in nonpolar solvents.

Scheme 2.7. Deprotonation of **2.4**-**2.7**.

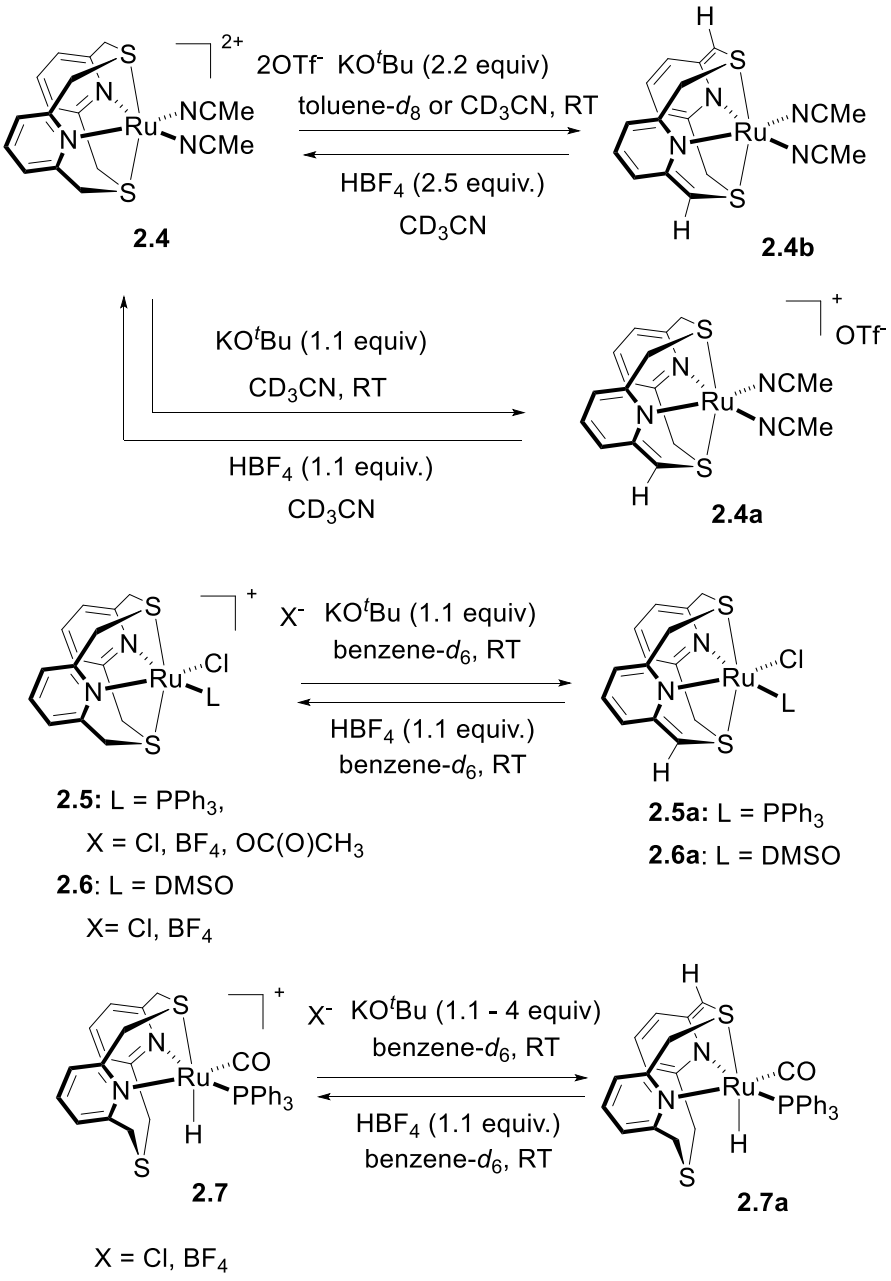

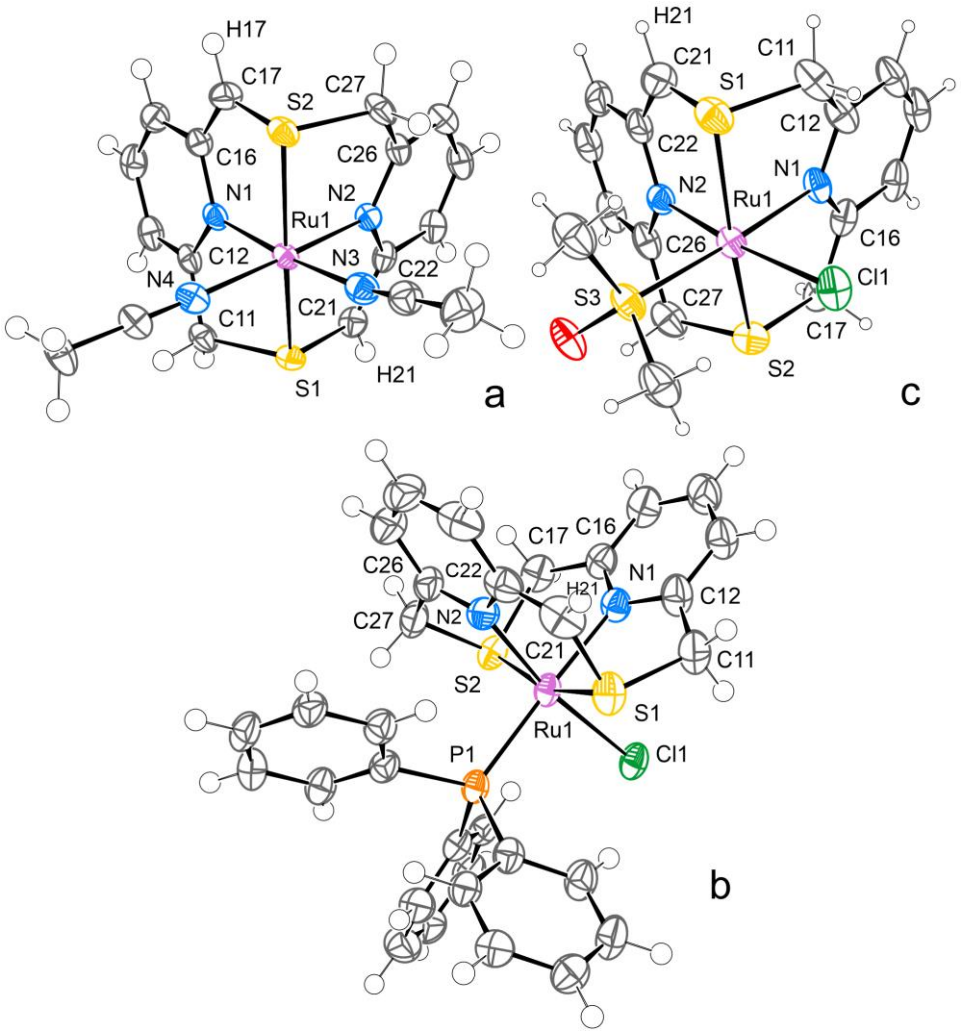

Figure 2.6. ORTEP of complexes **2.4b** (a), **2.5a** (b) and **2.6a** (c) at 70 % (a, b) or 30 % (c) probability level according to SC-XRD. In the case of **2.4b**, one of two symmetrical independent molecules is shown. The minor disorder component for **2.6a** and solvent molecules are omitted for clarity. Selected interatomic distances [Å]: Ru1–S1 2.3441(5), Ru1–S2 2.3280(5), Ru1–N1 2.0416(18), Ru1–N2 2.0425(17), Ru1–N3 2.0473(19), Ru1–N4 2.0461(19) for **2.4b**; Ru1–Cl1 2.4548(6), Ru1–S1 2.3229(7), Ru1–S2 2.3196(7), Ru1–P1 2.2950(7), Ru1–N1 2.099(2), Ru1–N2 2.052(2) for **2.5a**; Ru1–Cl1 2.442(2), Ru1–S1 2.329(3), Ru1–S2 2.316(2), Ru1–S3 2.235(5), Ru1–N1 2.104(7), Ru1–N2 2.061(7) for **2.6a**.

b. Deprotonation of monocationic complexes 2.5-2.7

Treating monocationic phosphine complex **2.5** with 1.1 equivalent of KO^{t}Bu in benzene-d_6 for 20 min resulted in a formation of a new singly deprotonated complex **2.5a** with 88% yield. Orange single crystals were obtained by vapor diffusion of pentane into a benzene solution. According to SC-XRD, **2.5a** is a neutral complex with Cl and PPh_3 bound to ruthenium center. The single deprotonation structure of the **N2S2** with one CH and three CH_2 arms as confirmed by X-ray and NMR. The SC-XRD structure reveals one shortened C21-C22 bond (1.368(4) Å), whereas the other C11–C12, C16–C17 and C26–C27 bond distances are 1.501(4) Å, 1.504(4) Å and 1.500(4) Å, respectively. Similar to the double deprotonated **2.4b**, the methine C-S bond in the deprotonated arm is shortened to 1.744(3) Å, while the methylene C-S bond distances in the non-deprotonated arms are 1.852(3), 1.829(3) and 1.828(3) Å.

The singly deprotonated structure of **2.5a** was also confirmed by NMR spectroscopy. The deprotonated methine group shows a singlet peak at 3.86 ppm that corresponded to the ^{13}C signal at 65.0 ppm as confirmed by HMQC and DEPT spectroscopy, while the non-

deprotonated CH_2 protons appear as a set of six geminally-coupled doublets at 4.81, 4.02, 3.82, 3.23, 2.96 and 2.76 ppm. The protons of the dearomatized ring are upfielded shifted, showing as a doublet of doublets at 6.04 ppm and two doublets at 5.92 and 5.06 ppm corresponding to a proton in para- and meta-position, respectively. For comparison, the protons of the aromatic pyridine ring appear as a triplet at 6.33 ppm and two doublets at 6.29 and 6.06 ppm.

Similarly, the monocationic DMSO-coordinated complex **2.6** reacted with 1.1 equiv. of KO^{t}Bu in benzene-d_6 for 20 min to give a monodeprotonated complex **2.6a** in 57% yield, which was also characterized by NMR and SC-XRD. SC-XRD confirmed that **2.6a** is a neutral complex with S-coordinated DMSO and Cl bound to the metal center. The C21-C22 and S1-C21 bonds distance are shortened (1.406(17) and 1.681(15) Å, respectively), indicating that the deprotonation occurred in C21 position. According to ^{1}H NMR spectroscopy, the deprotonated methine proton appears at a singlet at 3.86 ppm and the proton in methylene groups appear a six set of doublets at 4.75, 4.61, 3.74, 3.20 and 3.08 ppm.

Both complexes **2.5a** and **2.6a** are unstable in the presence of an excess amount of base: reaction of **2.5** or **2.6** with 2 equiv. of KO^{t}Bu led to the formation of unidentified products.

Treating hydride complex **2.7** with 1.1 equiv. of KO^{t}Bu in benzene-d_6 also yielded a singly deprotonated complex **2.7a** selectively, while the Ru-H remained intact, which was proved by ^{1}H NMR spectroscopy. The Ru-H hydride peak appears as a doublet at -6.55 ppm, the deprotonated CH peak appears as a singlet at 3.81 ppm, while the non-deprotonated methylene protons appear at a six set of geminally-coupled doublet. In contrast to monodeprotonated **2.5a** and **2.6a**, complex **2.7**a showed noticeable stability in the presence of an excess of base (up to 4 equiv.) with the yield ranging from 96 – 99%.

Table 2.1. Selected bond distance (Å) for complexes **2.4**-**2.7** and their deprotonated species according to SC-XRD data[a]

Complex	S1–C11	S1–C21	S2–C17	S2–C27	C11–C12	C16–C17	C21–C22	C26–C27
2.4	1.825(5)	1.822(5)	1.810(5)	1.823(5)	1.494(6)	1.496(6)	1.499(6)	1.494(6)
2.4b[b]	1.847(2)	1.733(2)	1.730(2)	1.839(2)	1.501(3)	1.387(3)	1.382(3)	1.502(3)
2.5[b]	1.821(4)	1.817(3)	1.818(4)	1.812(3)	1.501(5)	1.497(5)	1.497(4)	1.503(4)
2.5a	1.852(3)	1.744(3)	1.829(3)	1.828(3)	1.501(4)	1.504(4)	1.368(4)	1.500(4)
2.6	1.8158(13)	1.8198(13)	1.8140(12)	1.8181(12)	1.4964(17)	1.4990(16)	1.5017(17)	1.4998(16)
2.6a	1.832(11)	1.681(15)	1.837(11)	1.795(12)	1.456(17)	1.459(16)	1.406(17)	1.471(16)
2.7	1.791(7)	1.791(7)	1.834(8)	1.829(7)	1.504(9)	1.497(9)	1.508(9)	1.498(10)

[a] Atom numbering corresponds to that of **Figures 2.5** and **2.6**. [b] There are two complexes in the asymmetric cell, data are tabulated for the first complex

Unfortunately, we could not obtain single crystal of **2.7a**. To prove the structure of **2.7**a, we calculated the Gibbs free energy of several possible isomers of **2.7a** by DFT calculations, and the structure **2.7a-A** with the deprotonated CH_2S coordinated to the ruthenium center, while the **2.7a-C** and **2.7a-D** with the deprotonation in the dangling S-arm are highly unstable.

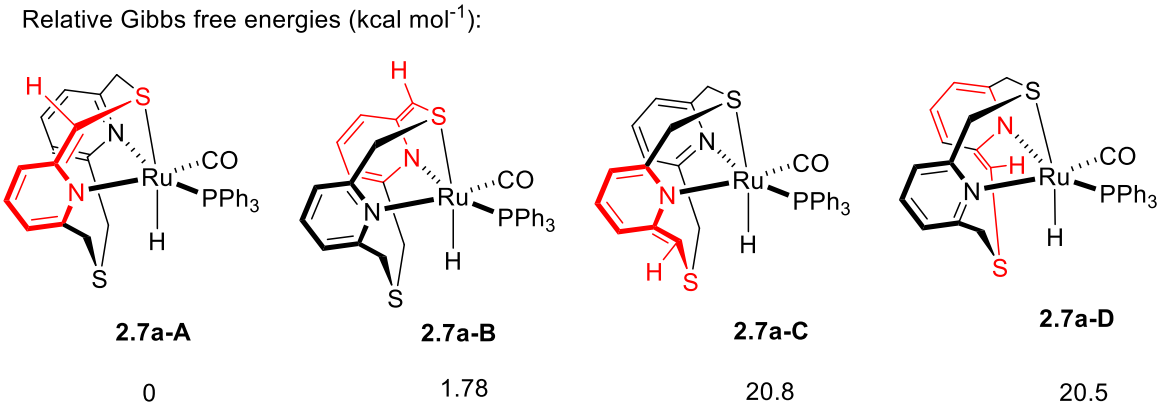

Figure 2.7. Relative Gibbs free energies (kcal mol^{-1}) for DFT-optimized isomers of **2.7a** (M06/SDD(Ru), 6-311+g(d,p); SMD solvation in benzene).

Similar with complex **2.4a**, the singly deprotonated complex **2.5a** and **2.6a** could be reprotonated by reacting with HBF_4 to form back the $[(\mathbf{N2S2})RuCl(L)]^+$ core (L = PPh_3 or DMSO). At the same time, treating complex **2.5a** or **2.6a** with MeOH did not result in the formation of the reprotonation products and the deprotonated complexes remained unreacted. On the other hand, treatment of singly deprotonated complexes **2.7a** with 1.1 equiv. of HBF_4 resulted in the recovery of the hydride complex $[(\kappa^3\text{-}\mathbf{N2S2})RuH(CO)(PPh_3)]$ with no effect of the strong acid to the hydride ligand.

c. Reactivity of deprotonated complexes

To our disappointment, both complexes **2.4b** and **2.5a** showed no reactivity towards H_2 or terminal alkyne activation. Treatment of these complexes with CO_2 and CS_2 resulted in a complex mixture of insoluble products. We then examined the reactivity of these deprotonated complexes as catalysts for hydrogenation or transfer hydrogenation, however, complex **2.4-2.7** were inactive in hydrogenation or transfer hydrogenation of acetophenone in the presence of base. Complex **2.4b** showed no reactivity in nitrile hydration of acetonitrile, dehydrogenation of benzyl alcohol, and hydrogenation of benzonitrile or benzyl benzoate.

The observed lack of catalytic activity could be due to the presence of strongly coordinating ligands and potential decomposition of the sulfur-containing ligand framework which was reported earlier by Milstein and coworkers in ruthenium complexes supported by PNS pincer ligands. [43] As expected, prolonging the deprotonation of **2.5** with excess (3.6 equiv.) of KO^{t}Bu or NaH in THF or benzene led to the formation of a mixture of products, from which a rearrangement product **2.8** was isolated and crystallized.

Scheme 2.8. Formation of **2.8**.

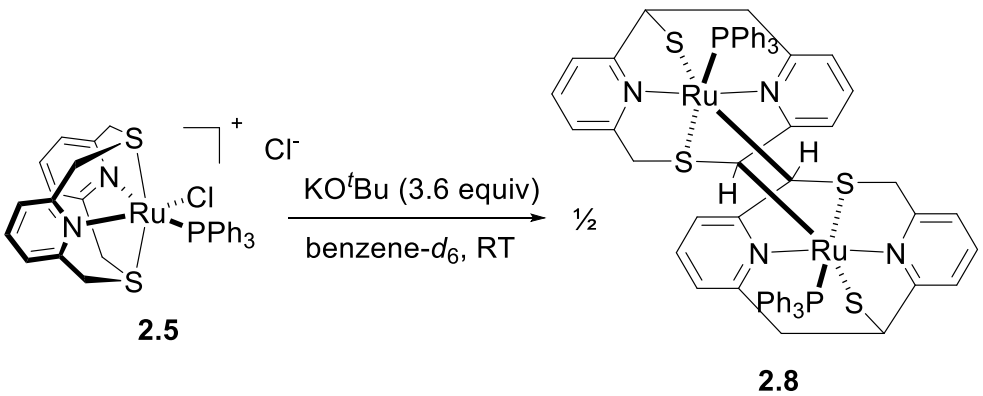

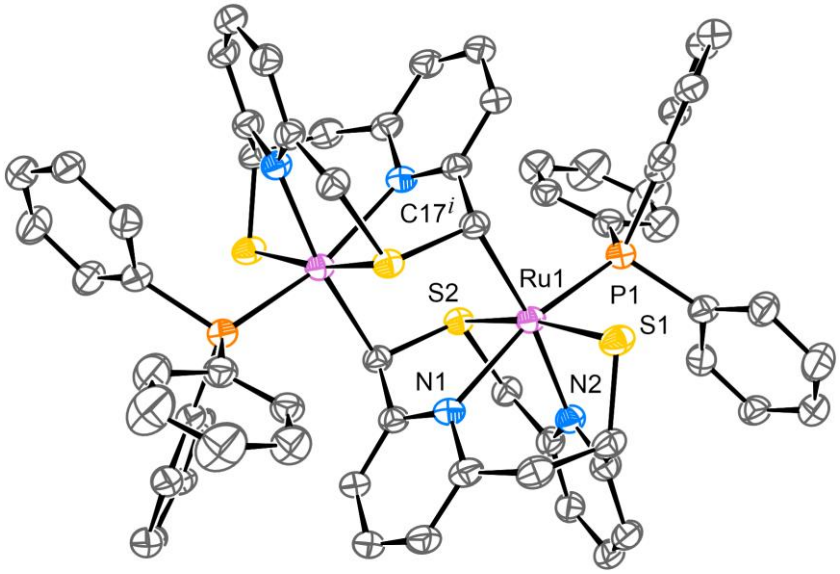

Figure 2.8. ORTEP for **2.8** at 30 % probability level according to SC-XRD. Hydrogen atoms and minor disorder components are omitted for clarity. Selected interatomic distances [Å]: Ru1–S1 2.3758(9), Ru1–S2 2.2996(8), Ru1–P1 2.2713(10), Ru1–N1 2.297(3), Ru1–N2 2.080(3), Ru1–C17^i 2.194(3) (symmetry code *i*: 5/3–*x*, 4/3–*y*, 4/3–*z*).

According to SC-XRD, complex **2.8** is a centrosymmetric binuclear complex, where the N2S2 ligand undergoes macrocycle ring rearrangement via 1,2-migration of a picolyl CH_2 carbon from sulfur to the CH arm (**Figure 2.8**). The sulfur atom serves as an anionic donor for the ruthenium center and the pyridine ring is re-aromatized. In addition, each ruthenium atom is also coordinated to the remaining deprotonated CH arm of the counterpart ligand with the Ru-C bond distance of 2.194(3) Å, leading to the re-aromatization of the second pyridine ring. In the ^{1}H NMR spectrum of **2.8** in THF-d_8, the methylene CH_2 protons appear as four sets of doublets at 3.94, 3.49, 3.08 and 2.41 ppm, corresponding to the carbon methylene peaks at 59.93 and 58.87 ppm, based on DEPT and HMQC NMR analyses. The two CH groups appear as two singlets at 3.47 and 3.58 ppm, showing correlation to the ^{13}C peaks at 64.35 and 63.48 ppm.

The formation of complex **2.8** suggests that the inherent reactivity of the sulfide-containing pincer structure could be a contributing factor to the observed absence of catalytic activity and irreversible ligand decomposition in the presence of a base. This is similar to the dimerization in (PNS)Ru complex **2.1** by deprotonation leading to the catalytic deactivation reported by the Milstein group.[43] Notably, the picolyl arm migration within a pincer-like structure has been reported in other pincer-type ligands. For instance, Khaskin and coworkers showed the migration of a picolyl arm in a functionalized PNP pincer ligand, resulting in the chelate ring expansion and ultimately leading to the loss of catalytic function.[50] Hence, the pincer ligand framework, traditionally perceived as highly stable due to robust chelation, may undergo significant rearrangements under basic conditions, thereby altering the coordination environment of the metal and consequently affecting catalytic or stoichiometric reactivity.

2.2.2.3. DFT calculations

To get more insight into how the ligand framework changes during single and double deprotonation and dearomatization, we carried out DFT calculations to compare the structure of complex **2.4**, **2.4a** and **2.4b**. The geometries of these complexes were optimized using M06 functional and SDD (for Ru)/6-311+g(d,p) (for all other elements) basis set, SMD model was used to account for the solvation in toluene.

To explain why the double deprotonation occurred at two methylene group in the opposite sites of the **N2S2** ligand framework, we calculated three possible isomers of complex **2.4b**: the experimentally observed **2.4b** and the alternative isomers **2.4b-A** and **2.4b-B** where deprotonation occurs at the methylene sites adjacent to the same pyridine rings or to the same S-atom, respectively. As expected, both alternative isomers were significantly less stable than **2.4b** (figure 6), consistent with the experiment that **2.4b** was the only species observed in SC-XRD and NMR spectroscopies.

Relative Gibbs free energies (kcal mol^{-1}):

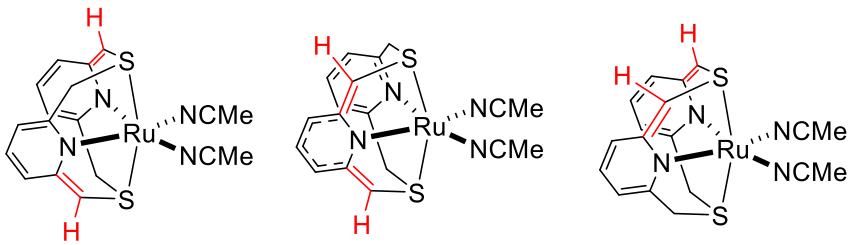

Figure 2.9. Relative Gibbs free energies (kcal mol^{-1}) for DFT-optimized isomers of **2.4b** (M06/SDD(Ru), 6-311+g(d,p); SMD solvation in toluene).

Next, we calculated the Wiberg bond indices (WBI) and partial atomic charges (Truhlar's Charge Model 5, CM5) for DFT solution-optimized structures for the non-deprotonated complex **2.4**, singly deprotonated complex **2.4a**, and doubly deprotonated complex **2.4b** (**Table 2.2**). The Wiberg bond indices of C-C bond between the methylene group and pyridine *o*-carbon in complex **2.4** and in non-dearomatized ring in singly deprotonated **2.4b** are WBI ~1.0 corresponding to a single bond character, whereas the bond index in this bond in the dearomatized site in singly deprotonated **2.4b** and doubly deprotonated 1a increases to WBI ~1.4, suggesting a double bond character. The dearomatized system of the pyridine ring is characterized by changing of the bond indices indicating single and double bond character and consistent with deprotonation-induced dearomatization of the pyridine ring. In the singly dearomatized **2.4a**, alternating single/double bond system only occurs at the pyridine ring attached to the deprotonated methine group, while no significant changes were observed at the non-dearomatized ring proving by the analogous bond indices to that in **2.4**.

According to CM5 charges analysis in doubly deprotonated **2.4b**, the negative charge accumulation is mostly observed at the methine carbons and the N-atoms of dearomatized pyridine ring, and to a much lesser extent at the meta-carbons. In the singly deprotonated **2.4a**, the charge distribution in the aromatic pyridine ring matches up to that in non-deprotonated **2.4**, whereas the negative charge accumulation was only observed in the dearomatized pyridine ring, in a way similar to that in doubly deprotonated **2.4b.**

Overall. The WBI and CM5 charge analysis of the macrocyclic **N2S2** pyridinophane ligand indicates that during the deprotonation of one or two methylene arms, the pyridine binding to the methine arms undergoes partial dearomatization, and the N-atom of the dearomatized pyridine takes on the characteristics of the amide donor, which is similar to how the dearomatization in PNP-type pincer ligands.[51]

Table 2.2. Selected Wiberg bond indices and Partial Atomic Charges (Turhlar's CM5 Model) for optimized structures of **2.4** (cationic part), **2.4a** (cationic part) and **2.4b**.

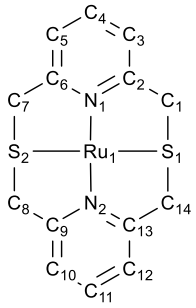

2.41

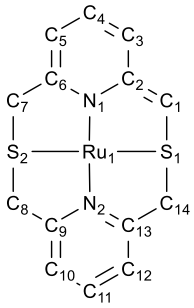

2.41a

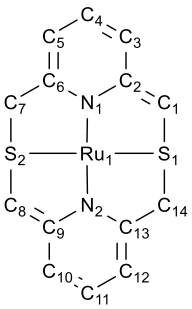

2.41b

Bond	Wiberg bond index			Atom	CM5 charge		
	2.4	**2.4a**	**2.4b**		**2.4**	**2.4a**	**2.4b**
N1-C2	1.29	1.16	1.16	Ru1	0.83	0.83	0.83
N1-C6	1.30	1.25	1.27	N1	-0.38	-0.42	-0.41
N2-C9	1.29	1.31	1.16	N2	-0.38	-0.37	-0.41
N2-C13	1.30	1.28	1.27	S1	0.05	0.00	-0.04
S1-C1	0.98	1.09	1.08	S2	0.05	0.01	-0.04
S1-C14	0.98	0.89	0.90	C1	-0.11	-0.20	-0.21
S2-C7	0.98	0.97	0.90	C2	0.13	0.10	0.10
S2-C8	0.98	0.98	1.08	C3	-0.06	-0.10	-0.11
C1-C2	1.03	1.44	1.43	C4	-0.03	-0.07	-0.09
C2-C3	1.42	1.19	1.19	C5	-0.06	-0.13	-0.14
C3-C4	1.41	1.61	1.59	C6	0.13	0.10	0.11
C4-C5	1.42	1.26	1.28	C7	-0.11	-0.12	-0.14
C5-C6	1.41	1.49	1.46	C8	-0.11	-0.12	-0.21
C6-C7	1.03	1.03	1.03	C9	0.13	0.13	0.10
C8-C9	1.03	1.02	1.43	C10	-0.06	-0.08	-0.11
C9-C10	1.42	1.40	1.19	C11	-0.03	-0.05	-0.09
C10-C11	1.41	1.43	1.59	C12	-0.06	-0.07	-0.14
C11-C12	1.42	1.41	1.28	C13	0.13	0.13	0.11
C12-C13	1.41	1.41	1.46	C14	-0.11	-0.14	-0.14
C13-C14	1.03	1.04	1.03				
Ru1-N1	0.44	0.48	0.47				
Ru1-N2	0.44	0.44	0.47				
Ru1-S1	0.49	0.50	0.47				
Ru1-S2	0.49	0.45	0.47				

2.3. Conclusion

In conclusion, we reported the synthesis and characterization of manganese(I) and a series of monocationic and dicationic ruthenium(II) complexes supported by an N,S-donor pyridinophane ligand. Under the presence of the base, the manganese(I) and ruthenium(II) complexes undergo single or double deprotonation of the CH_2S arms, leading to the single or double dearomatization of pyridine rings. We also demonstrated that the dearomatization in both Mn^{I} and Ru^{II} complexes are reversible in the presence of suitable Brönsted acid/base.

In contrast with previous reports of deprotonated ruthenium complexes supported by N,P-donor pincer ligand, the deprotonated (**N2S2**)Ru complexes exhibit lower stability, which is one of the main reasons that hinders their application in selective bond activation. One of the decomposition products was isolated and identified as the consequence of macrocyclic ring rearrangement, resulting in the decreased macrocycle size and forcing sulfur into the exocyclic position.

2.4. Experimental section

Below experimental data is reported in the following publications:

1. Sarbajna, A.; Patil, P. H.; Dinh, M. H.; Gladkovskaya, O.; Fayzullin, R. R.; Lapointe, S.; Khaskin, E.; Khusnutdinova, J. R., Facile and Reversible Double Dearomatization of Pyridines in Non-Phosphine Mn^{I} Complexes with N,S-Donor Pyridinophane Ligand. *Chem. Commun.* **2019**, *55*, 3282-3285.

2. Dinh, M. H.; Gridneva, T.; Karimata, A.; Garcia-Roca, A.; Pruchyathamkorn, J.; Patil, P. H.; Petrov, A.; Sarbajna, A.; Lapointe, S.; Khaskin, E.; Fayzullin, R. R.; Khusnutdinova, J. R. "Single and Double Deprotonation/Dearomatization of N,S-Donor Pyridinophane Ligand in Ruthenium Complexes" *Dalton Trans.* **2022**, *51*, 14734-14746.

General considerations

Solvent and reagents: Unless otherwise indicated, all solvents and reagents were used as received without further purification. Non-deuterated solvents were taken from a solvent purification system (MBRAUN SPS). Anhydrous deuterated solvents were purchased from Eurisotop and stored over 4 Å molecular sieves. **N2S2** ligand was synthesized according to the literature procedure.[52]

Nuclear Magnetic Resonance (NMR) spectroscopic analyses: NMR spectra were measured on JEOL ECZ400S 400MHz, JEOL ECZ600R 600 MHz, Bruker Avance II 400 MHz and Bruker Avance III 500 MHz. The following abbreviations are used for describing NMR spectra: s (singlet), d (doublet), t (triplet), vt (virtue triplet), q (quartet), dd (doublet of doublets), m (multiplet), quat (quaternary carbon). Residual solvent peaks or internal standard was used as a reference for chemical shifts in ^{1}H NMR spectra.

Solid-state FT-IR spectra were measured using Agilent Cary 630 with ATR module in an argon-filled glovebox. The following abbreviations are used for describing FT-IR spectra: s (strong), m (medium), w (weak), br (broad).

Electrospray Ionization Mass Spectrometry (ESI-MS) measurements were performed on a Thermo Scientific ETD apparatus using MeOH or MeCN as a solvent for injection.

Elemental analyses were performed using an Exeter Analytical CE440 instrument.

UV-vis spectra were recorded on an Agilent Cary 60 spectrophotometer.

The X-ray diffraction data for the single crystals **2.3-2.7**, **2.3a**, **2.3b**, **2.4b**, **2.5a** and **2.6a** were collected on a Rigaku XtaLab PRO instrument.

Computational details: All calculations were performed using density functional theory (DFT) as implemented in the Gaussian 16 suite of programs.[53] Geometry optimizations and frequency analyses were carried out without symmetry restrictions; ground states corresponded to the absence of imaginary frequencies. The initial atomic coordinates were taken from the crystal structures determined by SC XRD. Gibbs free energies are reported as the 'Sum of electronic and thermal free energies'. The results reported in Tables XX and XX are reported for geometries optimized using M06 functional[54] and SDD (for Ru)[55] /6-311+g(d,p) (for other elements)[56-63] basis set taking into account solvent effect via SMD

model.[64] This method was found to provide good match to the structural parameters from SC XRD data for complex **2.4b** and was previously used for computational analysis of dearomatized pincer Ru complexes.[65]

Synthesis of $[Mn(CO)_2(N2S2)]Br$ 2.3

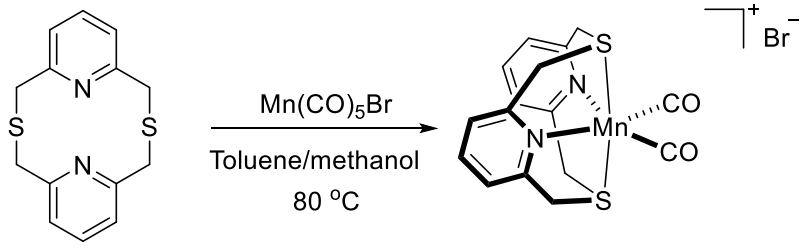

N2S2 **2.3**

95 %

206.0 mg (0.751 mmol) of N2S2 ligand and 200.2 mg (0.729 mmol, 0.97 equiv.) of $Mn(CO)_5Br$ were combined in a flame dried Schlenk flask inside a glove box and 10 mL toluene was added to give a yellow suspension. Subsequently, 1 mL methanol was added to the reaction mixture to yield a clear solution. The flask was taken outside the glove box and heated at 80 °C for 24 hours and then cooled inside the glove box to room temperature. The solution was then filtered through a celite pad. The filtrate obtained was evaporated under reduced pressure to yield a yellow solid which was washed thrice with copious amounts of diethyl ether (~15 mL) and then dried to produce **2.3**. Yellow crystals were grown by vapor diffusion of ether into a 1:1 dichloromethane and methanol mixture of the complex. Yield: 330 mg (95 %).

^{1}H NMR (400 MHz, 25 °C, DMSO-d_6): δ 7.74 (t, $^3J_{HH}$ = 7.8 Hz, *p*-$\boldsymbol{H}_{Py}$, 2H), 7.47 (d, $^3J_{HH}$ = 7.8 Hz, *m*-$\boldsymbol{H}_{Py}$, 4H), 4.90 (d, $^2J_{HH}$ = 18.0 Hz, Py-C$\boldsymbol{H}_2$-N, 4H), 4.79 (d, $^2J_{HH}$ = 18.0 Hz, Py-C$\boldsymbol{H}_2$-N, 4H).

^{13}C NMR (151 MHz, 25 °C, DMSO-d_6): δ 225.6 (***C***O), 159.0 (quat. $\boldsymbol{C}_{Py}$), 137.2 (*p*-$\boldsymbol{C}_{Py}$), 121.4 (*m*-$\boldsymbol{C}_{Py}$), 49.1 (Py-***C***H_2-N).

Anal. Calcd. for $Mn_1C_{16}H_{14}N_2S_2O_2Br_1$: C, 41.30; H, 3.03; N, 6.02. Found: C, 41.41; H, 3.03; N, 6.03.

UV-vis, λ, nm (ε, M^{-1} cm^{-1}), CH_2Cl_2:MeOH (1:1): 225 (27900), 259 (17900), sh 282 (7960), 342 (7560), sh 366 (7160).

FT-IR (ATR, solid): υ 2935 (m), 2880 (m), 1935 (s), 1864 (s), 1593 (m), 1567 (m), 1457 (s), 1426 (m), 1398 (br), 1384 (br), 1156 (br), 905 (w), 858 (s), 778 (s), 668 (s) cm^{-1}.

ESI-HRMS (*m/z*): calculated for $[C_{16}H_{14}MnN_2O_2S_2]^+$, ($[M\text{-}Br]^+$, *z* = 1): 384.9872; Found: 384.9868.

Synthesis of 2.3b from 2.3

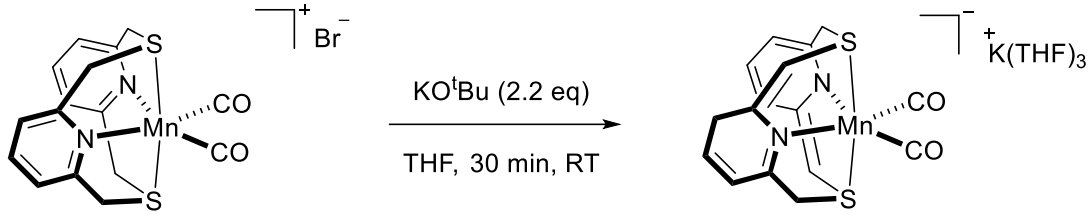

2.3 **2.3b**

42.0 mg (0.090 mmol) of **2.3** was weighed out in a scintillation vial inside a glove box and 5 mL THF was added to give a yellow suspension. 22.1 mg (0.198 mmol, 2.2 equiv.) of KO^{t}Bu was weighed out in another vial and added in one portion to the yellow suspension. The solution immediately turned into a deep orange color and was stirred for 30 minutes. After 30 minutes, the solution was filtered through a layer of celite and a clear orange solution was obtained that was characterized as **2.3b**. *A THF solution of the compound is stable at -30 °C for about 2 days but if solvent is evaporated, the orange solid starts to decompose immediately and turns black within minutes. Hence, isolated yield of the compound could not be calculated, however, NMR shows complete conversion. All subsequent yields were based upon the parent compound used in the reaction.* Yellow crystals were grown by vapor diffusion of pentane into a THF-d_8 solution of **2.3b** at -30 °C overnight.

^{1}H NMR (600 MHz, -30 °C, THF-d_8): 6.13 (dd, $^3J_{HH}$ = 7.1, 8.1 Hz, *p*-***H***$_{Py}$, 2H), 5.74 (d, $^3J_{HH}$ = 8.3 Hz, *m*-***H***$_{Py}$, 2H), 5.37 (d, $^3J_{HH}$ = 6.5 Hz, *m*-***H***$_{Py}$, 2H), 3.44 (2 doublets, $^2J_{HH}$ = 14.7 Hz, Py-C***H***$_2$-N, 4H), 3.38 (s, Py-C***H***-N, 2H). *tert*-Butanol is a by-product of the reaction giving a singlet at δ 1.13 (C***H***$_3$, *t*Bu) and a broad peak at δ 10.6 (br s, OH). ^{13}C NMR (151 MHz, -30 °C, THF-d_8): δ230.5 (***C***O), 166.2 (quat. ***C***$_{Py}$), 156.9 (quat. ***C***$_{Py}$), 129.6 (*p*-***C***$_{Py}$), 109.6 (*m*-***C***$_{Py}$), 99.6 (*m*-***C***$_{Py}$), 63.8 (Py-***C***H-N), 60.0 (Py-***C***H$_2$-N). *tert*-Butanol is a by-product of the reaction giving two peaks in ^{13}C NMR at δ 66.6 (***C***(CH$_3$)-OH), 33.7 (C(***C***H$_3$)-OH).

UV-vis, λ, nm (ε, M^{-1} cm^{-1}), THF: 211 (43200), 294 (28200), 322 (25800), 438 (4480), sh 493 (1790).

FT-IR (ATR, solid): υ 3795 (w), 3693 (w), 3052 (m), 2951 (w), 2880 (m), 2234 (m), 2090 (m), 1889 (s), 1801 (s), 1597 (s), 1517 (s), 1475 (s), 1418 (s), 1383 (s), 1286(s), 1247 (s), 1158 (s), 1095 (m), 1023 (s), 969 (s), 872 (s), 833 (s), 746 (s), 720 (s), 679 (s) cm^{-1}.

ESI-MS could not be determined accurately due to high air and moisture sensitivity of **2.3b**.

Synthesis of 2.3 from 2.3b

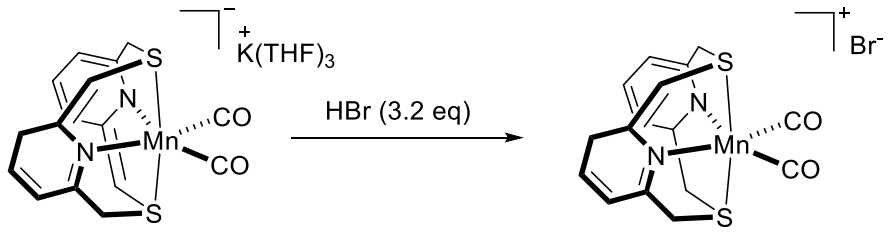

2.3b **2.3**

Compound **2.3b** was prepared from 42.0 mg (0.090 mmol) of **[1]Br** and 22.1 mg (0.198 mmol, 2.2 equiv.) of KO^{t}Bu in THF. To the orange solution, 680 µL of 33% HBr in acetic acid (0.225 mmol, 3.2 equivalents) was added using a microsyringe. The solution upon complete addition of acid turned yellowish in color. The solution was then evaporated to give a yellow solid identified as **2.3**. Crystals of **2.3** could be re-grown from vapor diffusion of hexane into the dichloromethane solution of the yellow compound. Yield: 36 mg (86%). NMR is identical to the complex obtained as described above from N2S2 and $Mn(CO)_5Br$.

Synthesis of 2.3a from 2.3b using aq. ammonia

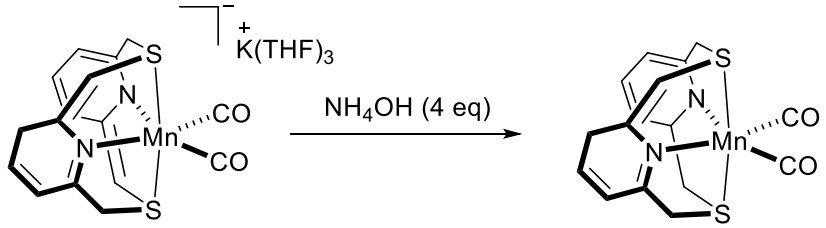

2.3b **2.3a**

Compound **2.3b** was prepared from 42.0 mg (0.090 mmol) of **2.3** and 30.4 mg (0.271 mmol, 3 equiv.) of KO^{t}Bu in THF. To the yellowish orange solution, aqueous ammonia (28%) (15 µL, 0.36 mmol, 4 equiv.) was added using a microsyringe. The solution immediately turned reddish. The solution was stirred for 15 minutes and filtered through a plug of celite, and the filtrate was evaporated to dryness to yield a red solid **2.3a** which was confirmed by NMR.

^{1}H NMR (600 MHz, -30 °C, THF-d_8): δ 7.55 (vt, $^3J_{HH}$ = 7.5 Hz, *p*-***H***$_{Py}$, 1H), 7.41 (d, $^3J_{HH}$ = 7.6 Hz, *m*-***H***$_{Py}$, 1H), 7.32 (d, $^3J_{HH}$ = 7.2 Hz, *m*-***H***$_{Py}$, 1H), 6.27 (dd, $^3J_{HH}$ = 8.7 Hz, 6.5 Hz, *p*-***H***$_{Py}$, 1H), 5.84 (d, $^3J_{HH}$ = 8.7 Hz, *m*-***H***$_{Py}$, 1H), 5.63 (d, $^3J_{HH}$ = 6.5 Hz, *m*-***H***$_{Py}$, 1H), 4.67 (d, $^2J_{HH}$ = 16.8 Hz, Py-C***H***$_2$-N, 1H), 4.28 (d, $^2J_{HH}$ = 16.8 Hz, Py-C***H***$_2$-N, 1H), 4.23 (d, $^2J_{HH}$ = 16.8 Hz, Py-C***H***$_2$-N, 1H), 4.17 (d, $^2J_{HH}$ = 16.8 Hz, Py-C***H***$_2$-N, 1H), 4.05 (d, $^2J_{HH}$ = 16.8 Hz, Py-C***H***$_2$-N, 1H), 3.84 (d, $^2J_{HH}$ = 16.8 Hz, Py-C***H***$_2$-N, 1H), 3.54 (s, Py-C***H***-N,1H). ^{13}C NMR (151 MHz, -30 °C, THF-d_8): δ 228.7 (CO), 228.1 (CO), 166.5 (quat. ***C***$_{Py}$), 162.6 (quat. ***C***$_{Py}$), 160.5 (quat. ***C***$_{Py}$), 152.9 (quat. ***C***$_{Py}$), 135.9 (*p*-***C***$_{Py}$), 130.6 (*p*-***C***$_{Py}$), 123.4 (*m*-***C***$_{Py}$), 120.8 (*m*-***C***$_{Py}$), 111.3 (*m*-***C***$_{Py}$), 100.6 (*m*-***C***$_{Py}$), 64.6 (Py-***C***H-N-), 60.1 (Py-***C***H$_2$-N), 52.2 (Py-***C***H$_2$-N), 47.5 (Py-***C***H$_2$-N).

UV-vis, λ, nm (ε, M^{-1} cm^{-1}), THF: 214 (7860), 261 (244), 329 (3400), sh 368 (120), 436 (50) sh 498 (20).

FT-IR (ATR, solid): υ3844 (w), 3759 (w), 3676 (w), 3055 (m), 2913 (br), 2235 (m), 2081 (br), 1914 (s), 1834 (s), 1605 (s), 1517 (s), 1476 (s), 1403 (s), 1293 (s), 1253 (s), 1169 (s), 1107 (s), 1046 (s), 1023 (s), 976 (s), 909 (m), 866 (s), 841 (s), 779 (m), 742 (s), 723 (s), 669 (s) cm^{-1}.

Synthesis of 2.3a from 2.3b using H_2O

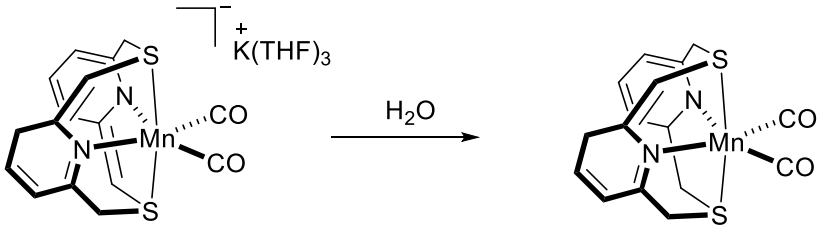

2.3b **2.3a**

Compound **2.3b** was prepared from 42.0 mg (0.090 mmol) of **2.3** and 30.4 mg (0.271 mmol, 3 equiv.) of KO^{t}Bu in THF. To the yellowish orange solution, 1.6 µL of deionized H_2O (0.090 mmol, 1 equiv.) was added using a microsyringe. The solution immediately turned reddish. The solution was stirred for 15 minutes and filtered through a plug of celite and the filtrate was evaporated to dryness to yield a red solid **2.3a** which was confirmed by NMR.

Stability of 2.3a in the presence of excess of water

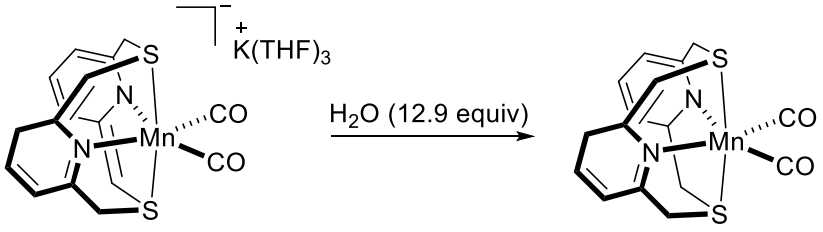

2.3b **2.3a**

Compound **2.3b** was prepared from 20.0 mg (0.043 mmol) of **2.3** and 14.5 mg (0.129 mmol, 3.0 equiv.) of KO^{t}Bu in THF. To the yellowish orange solution, 10 µL of degassed D_2O (0.55 mmol, 13 equiv.) was added using a microsyringe. The solution immediately turned reddish. The solution was stirred for 15 minutes and filtered through a plug of celite and the filtrate was directly used for the NMR characterization.

Synthesis of complex 2.4, [Ru(N2S2)(MeCN)$_2$](OTf)$_2$

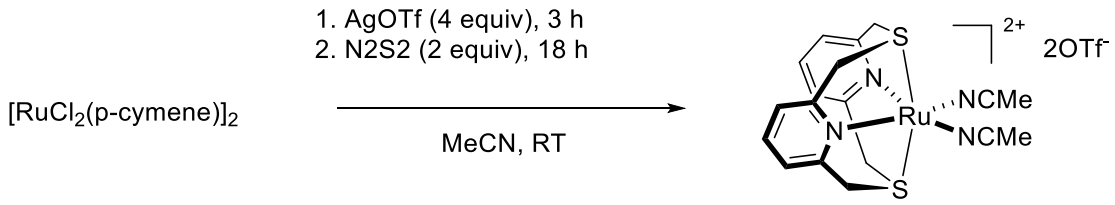

2.4

In a glove box, 155 mg (0.253 mmol) of dichloro(p-cymene)ruthenium(II) dimer was dissolved in 12 mL of acetonitrile. To the red solution, 260 mg (1.012 mmol, 4 equiv.) of AgOTf was added and the mixture was stirred in the dark for 3 hours. The AgCl precipitation was then filtered off, and 136 mg (0.495 mmol, 2 equiv.) of **N2S2** ligand was added. The resulting solution was stirred for 18 hours. The mixture was filtered through celite to remove the remaining AgCl precipitation to give a yellowish-orange solution. The obtained solution was subsequently evaporated to give a yellowish-orange solid, which was washed thrice with a copious amount of ether and pentane and then dried to produce 1. Yellowish orange crystals were grown by vapor diffusion of diethyl ether to the saturated acetonitrile solution of **2.4**. Yield: 244 mg (0.323 mmol - 64%).

^{1}H NMR (600 MHz, 23 °C, CD_3CN): δ 7.60 (t, $^{3}J_{HH}$ = 7.9 Hz, *p*-***H***$_{Py}$, 2H), 7.38 (d, $^{3}J_{HH}$ = 7.9 Hz, *m*-***H***$_{Py}$, 4H), 4.76, 4.74 (ABq, J_{AB} = 18 Hz, Py–C***H***$_2$–S, 8H), 2.35 (s, NC–C***H***$_3$, 6H).

^{13}C{^{1}H} NMR (151 MHz, 23 °C, CD_3CN): δ 162.29 (quat. ***C***$_{Py}$), 137.35 (p-***C***$_{Py}$), 130.28 (SO_3–***C***F_3), 123.05 (m-***C***$_{Py}$), 48.43 (Py–***C***H_2–S), 4.74 (NC–***C***H_3).

^{19}F NMR (376 MHz, 23 °C, CD_3CN): δ –79.25 (SO_3–C***F***$_3$).

EA Found (Calculated) $C_{20}H_{20}N_4O_6F_6RuS_4$: C 31.78 (31.79), H 2.67 (2.67), N 7.41 (8.00).

ESI-HRMS (*m/z*): calculated for $[C_{18}H_{20}N_4RuS_2]^{2+}$: 230.0082; Found: 230.0086.

FT-IR (ATR, solid): 2980 (br), 2915 (br), 1602 (m), 1596 (br), 1463 (m), 1406 (m), 1257 (s), 1222 (m), 1148 (s), 1027 (s), 915 (m), 856 (m), 775 (m), 750 (m). UV-Vis (CH_3CN), λ, nm (ε, M^{-1} cm^{-1}): 344 (8670), 250 (9723), 213 (21954).

Synthesis of complex 2.5, [Ru(N2S2)(PPh$_3$)Cl]Cl

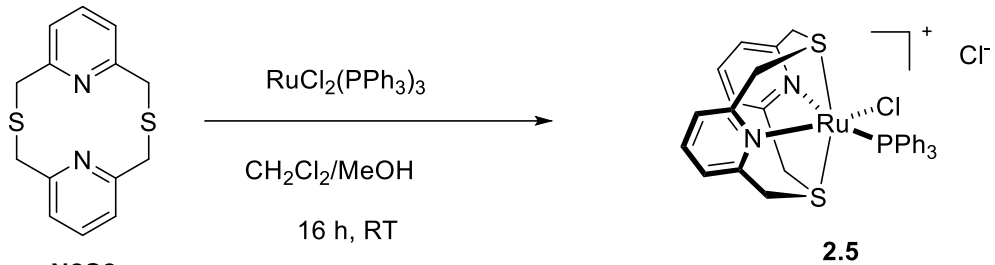

N2S2 **2.5**

In a glove box, 174.2 mg (0.182 mmol) of dichlorotris(triphenylphosphine)ruthenium(II) and 51.6 mg (0.188 mmol, 1.0 equiv.) of **N2S2** ligand were dissolved in 5.0 mL of dichloromethane in a 20 mL vial to give a dark red solution. The reaction mixture was stirred at room temperature for 19 hours, during which time the solution color gradually changed to yellow. The obtained solution was subsequently evaporated at reduced pressure to give a yellow solid, which was washed with ether (3 × 5 mL) and a 1:1 dichloromethane and ether mixture (3 × 5 mL) and then dried to produce **2.5.** Yellow needle crystals were grown by vapor diffusion of diethyl ether into the dichloromethane solution of the complex. Yield: 109 mg (0.154 mmol - 85%).

^{1}H NMR (600 MHz, 23 °C, CD_2Cl_2): δ 7.54-7.12 (m, ***H***$_{PPh3}$ and ***H***$_{Py}$, 21H), 5.29 (d, $^{2}J_{HH}$ = 17.1 Hz, Py–C***H***$_2$–S, 2H), 5.10 (d, $^{2}J_{HH}$ = 17.9 Hz, Py–C***H***$_2$–S, 2H), 4.82 (d, $^{2}J_{HH}$ = 17.0 Hz, Py–C***H***$_2$–S, 2H), 3.37 (d, $^{2}J_{HH}$ = 17.5 Hz, Py–C***H***$_2$–S, 2H).

^{13}C{^{1}H} NMR (151 MHz, 23 °C, CD_2Cl_2): δ 161.22 (quat. ***C***$_{Py}$), 159.02 (quat. ***C***$_{Py}$) 136.59 (p-***C***$_{Py}$), 134.29 (d, $^{1}J_{PC}$ = 47.0 Hz, quat. ***C***P), 133.84 (m-***C***$_{Py}$), 133.61 (d, $^{2}J_{PC}$ = 10.3 Hz, o-***C***P), 130.59 (m-***C***$_{Py}$), 128.74 (d, $^{3}J_{PC}$ = 9.4 Hz, m-***C***P), 122.18 (d, $^{2}J_{PC}$ = 25.3 Hz, p-***C***P), 50.34 (Py–***C***H_2–S), 48.98 (Py–***C***H_2–S).

^{31}P{^{1}H} NMR (162 MHz, 23 °C, CD_2Cl_2): δ 46.28 (***P***Ph_3).

EA Found (Calculated) $C_{75}H_{60}Cl_6N_4P_2Ru_2S_4$ (2 $Ru(N_2S_2)(PPh_3)Cl)Cl{\cdot}1$ CH_2Cl_2): C 51.24 (51.97), H 3.90 (4.03), N 3.74 (3.73).

ESI-HRMS (*m/z*): Found (Calcd): $C_{32}H_{29}N_2ClPRuS_2^{+}$: 673.0231 (673.0236).

FT-IR (ATR, solid) : 3057 (m), 2924 (m), 2858 (m), 1595 (m), 1590 (m), 1457 (m), 1431 (m), 1185 (m), 1155 (m), 1091 (s), 910 (m), 856 (m), 776 (m), 747 (s), 694 (s).

UV-Vis (CH_2Cl_2), λ, nm (ε, M^{-1} cm^{-1}): 379 (5843).

Synthesis of complex 2.6, [Ru(N2S2)(DMSO)Cl]Cl

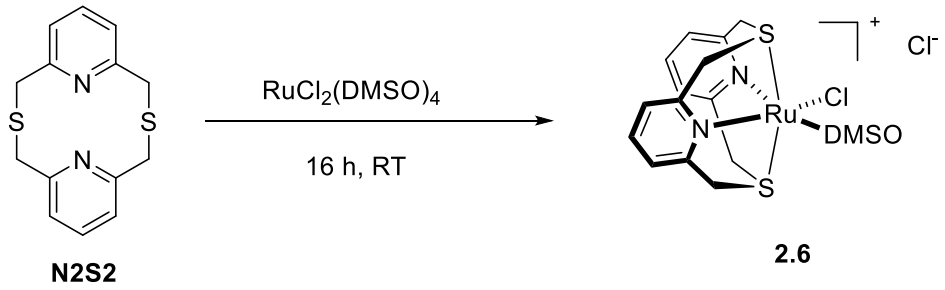

N2S2 **2.6**

In a glove box, 87.7 mg (0.182 mmol) of dichlorotetrakis(dimethylsulfoxide)ruthenium(II) and 50.0 mg (0.182 mmol, 1.0 equiv.) of **N2S2** ligand were dissolved in a 5.0 mL mixture of 2:1 dichloromethane and methanol in a 20 mL vial to give a yellow solution. The reaction mixture was stirred at room temperature for 16 hours. Yellow needle crystals were grown by vapor diffusion of diethyl ether into the obtained solution of complex to produce **2.6**. Yield: 67.0 mg (0.128 mmol - 70%).

^{1}H NMR (600 MHz, 23 °C, $CDCl_3$): δ 7.53 (d, $^{3}J_{HH}$ = 7.0 Hz, m-***H***$_{Py}$, 2H), 7.50 (t, $^{3}J_{HH}$ = 7.4 Hz, p-***H***$_{Py}$, 1H), 7.43 (d, $^{3}J_{HH}$ = 7.5 Hz, m-***H***$_{Py}$, 1H), 7.35 (t, $^{3}J_{HH}$ = 7.8 Hz, p-***H***$_{Py}$, 1H), 5.67 (d, $^{2}J_{HH}$ = 17.8 Hz, Py–C***H***$_2$–S, 2H), 5.64 (d, $^{2}J_{HH}$ = 17.4, Py–C***H***$_2$–S, 2H), 4.74 (d, $^{2}J_{HH}$ = 17.6 Hz, Py–C***H***$_2$–S, 2H), 4.69 (d, $^{2}J_{HH}$ = 17.8 Hz, 2H), 3.48 (s, (C***H***$_3$)$_2$SO, 6H).

^{13}C{^{1}H} NMR (151 MHz, 23 °C, CD_3Cl): δ 161.18 (quat. ***C***$_{Py}$), 159.31 (quat. ***C***$_{Py}$), 137.30 (p-***C***$_{Py}$), 135.88 (p-***C***$_{Py}$), 122.69 (m-***C***$_{Py}$), 122.45 (m-***C***$_{Py}$), 49.05 ((***C***H$_3$)$_2$SO), 48.35 (Py–***C***H$_2$–S), 48.24 (Py–***C***H$_2$–S).

EA Found (Calculated) $C_{16}H_{20}Cl_2N_2ORuS_3$ C 35.7 (35.34), H 3.92 (3.36), N 4.92 (4.89).

ESI-HRMS (*m/z*): Found (Calcd): $C_{16}H_{20}ClN_2ORuS_3^+$: 488.9461 (488.9464).

FT-IR (ATR, solid): 3214 (br), 2871 (br), 1596 (m), 1591 (m), 1459 (s), 1396 (m), 1161 (s), 1083 (s), 1012 (s), 908 (s), 855 (m), 779 (s), 718 (m), 684 (m).

UV-Vis (CH_3OH), λ, nm (ε, M^{-1} cm^{-1}): 335 (4253), 256 (7404).

Synthesis of complex 2.7, [Ru(N2S2)H(CO)(PPh$_3$)]Cl

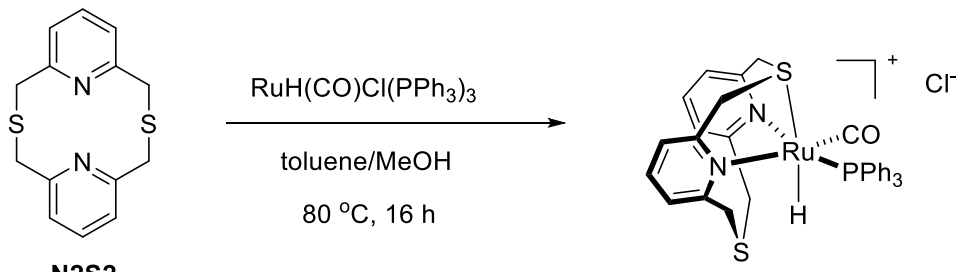

N2S2 **2.7**

In a glove box, 102.0 mg (0.372 mmol) of **N2S2** ligand and 354.0 mg (0.372 mmol, 1 equiv.) of $RuHCl(CO)(PPh_3)_3$ were dissolved in a mixture containing 6 mL toluene and 3 mL of methanol. The mixture was then transferred into flame dried Schlenk flask. The flask was taken outside the glove box and heated at 80 °C overnight to give a clear yellow solution. The solution was then evaporated under reduced pressure inside the glove box to yield a yellow solid, which was washed thrice with a copious amount of diethyl ether and pentane and then dried to produce **2.7**. Yellow crystals were grown by vapor diffusion of diethyl ether into a concentrated solution of **2.7** in dichloromethane. Yield: 246.4 mg (0.351 mmol - 94%).

^{1}H NMR (600 MHz, 23 °C, CD_2Cl_2): δ 7.58-6.88 (m, $\boldsymbol{H}_{PPh3}$ and $\boldsymbol{H}_{Py}$, 21H), 6.46 (d, $^{2}J_{HH}$ = 13.5 Hz, Py–C$\boldsymbol{H}_2$–S, 1H), 5.96 (d, $^{2}J_{HH}$ = 17.5 Hz, Py–C$\boldsymbol{H}_2$–S, 1H), 5.89 (d, $^{2}J_{HH}$ = 17.8 Hz, Py–C$\boldsymbol{H}_2$–S, 1H), 5.60 (d, $^{2}J_{HH}$ = 13.6 Hz, Py–C$\boldsymbol{H}_2$–S, 1H), 4.32 (d, $^{2}J_{HH}$ = 17.1 Hz, Py–C$\boldsymbol{H}_2$–S, 1H), 3.94 (d, $^{2}J_{HH}$ = 14.1 Hz, Py–C$\boldsymbol{H}_2$–S, 1H), 3.39 (d, $^{2}J_{HH}$ = 17.3 Hz, 1H), 3.15 (d, $^{2}J_{HH}$ = 14.1 Hz, 1H), –6.68 (d, $^{2}J_{PH}$ = 28.9 Hz, Ru-***H***, 1H).

^{13}C{^{1}H} NMR (151 MHz, 23 °C, CD_2Cl_2): δ 204.07 (d, $^{2}J_{PC}$ = 18.2 Hz, Ru–***C***O), 164.29 (quat. $\boldsymbol{C}_{Py}$), 163.32 (quat. $\boldsymbol{C}_{Py}$), 161.47 (quat. $\boldsymbol{C}_{Py}$), 160.23 (quat. $\boldsymbol{C}_{Py}$), 139.31 (d, $^{1}J_{PC}$ = 25.1 Hz, quat. ***C***P), 133.64 (d, $^{2}J_{PC}$ = 10.4 Hz, o-***C***P), 131.04 (p-***C***P), 128.88 (d, $^{3}J_{PC}$ = 10.4 Hz, m-***C***P), 124.51 (p-$\boldsymbol{C}_{Py}$), 124.34 (p-$\boldsymbol{C}_{Py}$), 123.77 (m-$\boldsymbol{C}_{Py}$), 123.64 (m-$\boldsymbol{C}_{Py}$), 46.18 (Py–***C***H_2–S), 44.07 (Py–***C***H_2–S), 43.73 (Py–***C***H_2–S), 42.28 (Py–***C***H_2–S).

^{31}P{^{1}H} NMR (243 MHz, 23 °C, CD_2Cl_2): δ 62.90 (***P***Ph_3).

EA Found (Calculated) $C_{33}H_{30}ClN_2OPRuS_2$: C 51.14 (50.97), H 3.91 (3.85), N 3.53 (3.50).

ESI-HRMS (*m/z*): Found (Calcd): $C_{33}H_{30}N_2OPRuS_2^+$: 667.0580 (667.0575).

FT-IR (ATR, solid) : 3043 (br), 2876 (br), 2173 (br), 1934 (s), 1598 (m), 1594 (m), 1480 (m), 1455 (m), 1432 (m), 1398 (m), 1311 (m), 1157 (s), 1091 (s), 998 (m), 852 (s), 788 (m), 745 (s), 724 (m), 693 (s).

UV-Vis (CH_2Cl_2), λ, nm (ε, M^{-1} cm^{-1}) : 382 (843).

Formation of 2.4a in acetonitrile-*d*$_3$

In a glove box, 10.0 mg (0.013 mmol) of complex **2.4** was weighed in a 20 mL vial equipped with a stirring bar. The complex was dissolved in 1 mL of acetonitrile-d_3, and 1.6 mg (1.1 equiv.) of KO^{t}Bu was added. The reaction mixture was stirred for 3 min and then filtered through celite to give a solution of **2.4a**. The solution of **2.4a** was directly characterized by NMR.

^{1}H NMR (CD_3CN, –30 °C, 600 MHz): δ 7.53 (t, $^{3}J_{HH}$ = 7.7 Hz, p-$\boldsymbol{H}_{Py}$, 1H), 7.26 (m, m-$\boldsymbol{H}_{Py}$, 2H), 6.37 (dd, $^{3}J_{HH}$ = 9.0 Hz, 6.5 Hz, p-$\boldsymbol{H}_{Py}$, 1H), 5.92 (d, m-$\boldsymbol{H}_{Py}$, $^{3}J_{HH}$ = 8.9 Hz, 1H), 5.75 (d, $^{3}J_{HH}$ = 6.5 Hz, m-$\boldsymbol{H}_{Py}$, 1H).

^{13}C{^{1}H} NMR (CD_3CN, –30 °C, 151 MHz): δ 167.87 (quat. $\boldsymbol{C}_{Py}$), 163.05 (quat. $\boldsymbol{C}_{Py}$), 162.95 (quat. $\boldsymbol{C}_{Py}$), 154.95 (quat. $\boldsymbol{C}_{Py}$), 135.87 (p-$\boldsymbol{C}_{Py}$), 130.71 (p-$\boldsymbol{C}_{Py}$), 123.75 (m-$\boldsymbol{C}_{Py}$), 120.90 (m-$\boldsymbol{C}_{Py}$), 111.18 (m-$\boldsymbol{C}_{Py}$), 101.80 (m-$\boldsymbol{C}_{Py}$), 61.70 (Py–***C***H–S), 58.48 (Py–***C***H_2–S), 49.32 (Py–***C***H_2–S), 45.53 (Py–***C***H_2–S).

Yield determination of 2.4a

In a glove box, 10.0 mg (0.013 mmol) of complex **1** was weighed in a 20-mL vial equipped with a stir bar. The complex was dissolved in 1.5 mL of acetonitrile-d_3 and 1.6 mg (0.014 mmol, 1.1 equiv.) of KO^{t}Bu were added. 1.8 μL (0.013 mmol, 1 equiv.) of mesitylene was added to the solution by microsyringe as an internal standard. The reaction mixture was stirred for 3 min. After the reaction, the solution was taken out to analyze by ^{1}H NMR spectroscopy. The yield of **2.4a** was determined by the peak of complex **2.4a** at 6.37 ppm against the internal standard peak at 6.80 ppm. Yield: 98%.

Protonation of 2.4a by HBF_4

Complex **2.4a** was prepared in-situ from 10.0 mg (0.0132 mmol) of 1 with 1.6 mg (0.0145 mmol) of KO^{t}Bu in acetonitrile-d_3 in 3 min. To the orange solution of **2.4a**, 2.0 μL (0.015 mmol – 1.1 equiv.) of tetrafluoroboric acid diethyl ether complex (HBF_4.Et_2O) was added by micro syringe, and the solution color immediately changed to yellow. The solution was identified as **2.4** by ^{1}H NMR spectroscopy.

Formation of 2.4b in toluene-d_8

In a glove box, 15.0 mg (0.020 mmol) of complex **2.4** was weighed in a 20 mL vial equipped with a stirrer bar. The complex was dissolved in 1.5 mL of toluene-d_8, and 4.5 mg (0.040 mmol, 2.0 equiv.) of KO^{t}Bu were added. The reaction mixture was stirred for 3 min. The crude was filtered using an HPLC filter, leaving a brown solid in the filter, and the filtrate is collected in a second vial to give **2.4b**. The solution of **2.4b** was directly characterized by NMR spectroscopy. The orange crystals of **2.4b** were grown by cooling a saturated toluene solution at –20 °C.

^{1}H NMR (C_7D_8, –30 °C, 600 MHz): δ 6.38 (dd, $^3J_{HH}$= 8.6, 6.6 Hz, ***p*-H**$_{Py}$, 2H), 6.26 (d, $^3J_{HH}$ = 8.7 Hz, m-***H***$_{Py}$, 2H), 5.76 (d, $^3J_{HH}$ = 6.5 Hz, m-***H***$_{Py}$, 2H), 4.18 (s, Py–C***H***–S, 2H), 3.89 (d, $^2J_{HH}$ = 14.5 Hz, Py–C***H***$_2$–S, 2H), 3.73 (d, $^2J_{HH}$ = 14.5 Hz, Py–C***H***$_2$–S, 2H), 0.41 (s, NC–C***H***$_3$, 6H).

^{13}C{^{1}H} NMR (C_7D_8, –30 °C, 151 MHz): δ 168.49 (quat. ***C***$_{Py}$), 156.68 (quat. ***C***$_{Py}$), 129.70 (p-***C***$_{Py}$), 110.58 (*m*-***C***$_{Py}$), 101.67 (m-***C***$_{Py}$), 61.43(Py–***C***H–S), 58.23 (Py–***C***H$_2$–S), 1.55 (NC–***C***H$_3$), 1.38 (NC–***C***H$_3$).

Yield determination of 2.4b, general procedure

In a glovebox, the mixture of **2.4** and KO^{t}Bu was added to toluene-d_8. After stirring, the reaction mixture was filtered through a syringe filter to get a clear yellow solution of **2.4b**. 4.0 µL (0.029 mmol) of mesitylene was added to the solution as an internal standard. The solution was taken out to analyze by ^{1}H NMR spectroscopy. The yield of **2.4b** was determined by the peak of **2.4b** at 4.18 ppm against the internal standard peak at 6.66 ppm. Using 0.5 equiv. to 2 equiv. of base in all cases produced similar yields of **2.4b**, 17-21%, limited by the solubility of **2.4b** in toluene. When the formed precipitate was collected and dissolved in a more polar solvent such as CD_3CN, its ^{1}H NMR also corresponded to **2.4b** showing that low solubility was the main factor responsible for limited yield determined in non-polar solvents.

Formation of 2.4b in acetonitrile-d_3

In a glove box, 10.0 mg (0.013 mmol) of complex **2.4** was weighed in a 20 mL vial equipped with a stir bar. The complex was dissolved in 1.5 mL of acetonitrile-d_3, and 3.2 mg (0.029 mmol, 2.2 equiv.) of KO^{t}Bu was added. The reaction mixture was stirred for 3 min and then filtered through celite to give a solution of **2.4b**. 1.8 µL of mesitylene (0.013 mmol, 1 equiv.) was added to the solution as an internal standard. The obtained solution was characterized by ^{1}H NMR spectroscopy. The yield of **2.4b** was determined by the peak of **2.4b** at 4.18 ppm against the internal standard peak at 6.66 ppm. Yield: 80%.

^{1}H NMR (CD_3CN, –30 °C, 600 MHz): δ 6.28 (dd, $^3J_{HH}$ = 8.7 Hz, $^3J_{HH}$ = 6.6 Hz, p-***H***$_{Py}$, 2H), 5.85 (d, $^3J_{HH}$ = 8.7 Hz, m-***H***$_{Py}$, 2H), 5.53 (d, $^3J_{HH}$ = 6.5 Hz, m-***H***$_{Py}$, 2H).

Protonation of 2.4b by HBF_4: Complex **2.4b** was prepared in-situ from 10.0 mg (0.0132 mmol) of **1** with 3.7 mg (0.0331 mmol – 2.5 equiv.) of KO^{t}Bu in acetonitrile-d_3 in 3 min. To the red solution of **2.4b**, 4.5 µL (0.033 mmol – 2.5 equiv.) of tetrafluoroboric acid diethyl ether complex ($HBF_4.Et_2O$) was added by micro syringe, and the solution color immediately changed to yellow. The formation of [(**N2S2**)Ru(MeCN)$_2$]$^{2+}$ was established by a comparison of the ^{1}H NMR spectrum with complex **2.4**.

Formation of 2.5a in benzene-d_6

In a glove box, 10.0 mg (0.014 mmol) of **2.5** was added to 1 mL of benzene-d_6. To the mixture, 3.0 mg (0.025 mmol, 1.8 equiv.) of KO^{t}Bu was added to the mixture. The solution

gradually became orange-red and was stirred for 20 min. After 20 minutes, the solution was filtered through a layer of celite and a clear orange solution was obtained that was characterized as **2.5a**. Orange crystals were grown by vapor diffusion of pentane to the benzene solution of **2.5a**.

^{1}H NMR (600 MHz, 23 °C, C_6D_6): δ 8.02 (t, $^{3}J_{HH}$ = 8.6 Hz, o-$\boldsymbol{H}_{PPh3}$, 6H), 7.12 (t, $^{3}J_{HH}$ = 6.8 Hz, p-$\boldsymbol{H}_{PPh3}$, 6H), 7.04 (t, $^{3}J_{HH}$ = 7.3 Hz, m-$\boldsymbol{H}_{PPh3}$, 3H), 6.33 (t, $^{3}J_{HH}$ = 7.6 Hz, p-$\boldsymbol{H}_{Py}$, 1H), 6.29 (d, $^{3}J_{HH}$ = 7.6 Hz, m-$\boldsymbol{H}_{Py}$, 1H), 6.06 (d, $^{3}J_{HH}$ = 7.6 Hz, m-$\boldsymbol{H}_{Py}$, 1H), 6.04 (dd, $^{3}J_{HH}$ = 9.0 Hz, p-$\boldsymbol{H}_{Py}$, 1H), 5.92 (d, $^{3}J_{HH}$ = 8.7 Hz, m-$\boldsymbol{H}_{Py}$, 1H), 5.06 (d, $^{3}J_{HH}$ = 6.6 Hz, m-$\boldsymbol{H}_{Py}$, 1H), 4.81 (d, $^{2}J_{HH}$ = 14.7 Hz, Py–C$\boldsymbol{H}_2$–S, 1H), 4.02 (d, $^{2}J_{HH}$ = 17.9 Hz, Py–C$\boldsymbol{H}_2$–S, 1H), 3.86 (s, Py–C$\boldsymbol{H}$–S, 1H), 3.82 (d, $^{2}J_{HH}$ = 14.8 Hz, Py–C$\boldsymbol{H}_2$–S, 1H), 3.23 (d, $^{2}J_{HH}$ = 16.5 Hz, Py–C$\boldsymbol{H}_2$–S, 1H), 2.96 (d, $^{2}J_{HH}$ = 15.9 Hz, Py–C$\boldsymbol{H}_2$–S, 1H), 2.76 (d, $^{2}J_{HH}$ = 15.9 Hz, Py–C$\boldsymbol{H}_2$–S, 1H).

^{13}C{^{1}H} NMR (151 MHz, 23 °C, C_6D_6): δ 167.51 (quat. $\boldsymbol{C}_{Py}$), 162.35 (quat. $\boldsymbol{C}_{Py}$), 157.94 (quat. $\boldsymbol{C}_{Py}$), 153.68 (quat. $\boldsymbol{C}_{Py}$), 136.02 (d, $^{1}J_{PC}$ = 40.9 Hz, quat. $\boldsymbol{C}_{PPh3}$), 134.57 (d, $^{2}J_{PC}$ = 10.1 Hz, o-$\boldsymbol{C}_{PPh3}$), 133.47 (o-$\boldsymbol{C}_{Py}$), 129.28 (m-$\boldsymbol{C}_{PPh3}$), 128.35 (p-$\boldsymbol{C}_{PPh3}$), 122.37 (m-$\boldsymbol{C}_{Py}$), 118.32 (m-$\boldsymbol{C}_{Py}$), 110.85 (m-$\boldsymbol{C}_{Py}$), 99.75 (m-$\boldsymbol{C}_{Py}$), 65.03 (Py–$\boldsymbol{C}$H–S), 61.20 (Py–$\boldsymbol{C}$H$_2$–S), 51.62 (Py–$\boldsymbol{C}$H$_2$–S), 48.68 (Py–$\boldsymbol{C}$H$_2$–S); (the signal of dearomatized ortho-C_{Py} peak overlaps with benzene-d_6 peak and cannot be clearly detected).

^{31}P{^{1}H} NMR (243 MHz, 23 °C, C_6D_6): δ 52.37 (s, $\boldsymbol{P}$Ph$_3$).

A similar procedure was used to determine the yield of **2.5a** in benzene-d_6 in the presence of mesitylene as an internal standard. The yield of **2.5a** in the presence of 0.9-1.4 equiv. of KO^{t}Bu was found to be identical, 88%, after 60 min at RT. The yield of **2.5a** was determined by the peak of complex **2.5a** at 4.81 ppm against the internal standard peak at 6.73 ppm.

Using over 2 equiv. of base leads to decomposition, accelerated by an excess base. When 2 equiv. of KO^{t}Bu are used, initially formed **2.5a** (36% after 20 min) decomposes after 60 min, while using 3 equiv. and more leads to no detectable **2.5a** and the formation of a mixture of products.

Protonation of 2.5a by HBF$_4$

Complex **2.5a** was prepared in-situ from 10.0 mg (0.0141 mmol) of **2** with 1.7 mg (0.0155 mmol) of KO^{t}Bu in benzene-d_6 in 1 hour. To the orange solution of **2.5a**, 2.1 μL (0.016 mmol – 1.1 equiv.) of tetrafluoroboric acid diethyl ether complex (HBF$_4$.Et$_2$O) was added by micro syringe, and the yellow precipitate was immediately formed. The benzene solvent was evaporated under vacuum to give a yellow powder, which was identified as **2.5[BF$_4$]** by NMR spectroscopy (with dichloromethane-d_2 as NMR solvent).

Protonation of 2.5a by acetic acid:

Complex **2.5a** was prepared in-situ from 10.0 mg (0.0141 mmol) of **2** with 1.7 mg (0.0155 mmol) of KO^{t}Bu in benzene-d_6 in 1 hour. To the orange solution of **2.5a**, 0.9 μL (0.016 mmol – 1.1 equiv.) of acetic acid was added via microsyringe, and the yellow precipitate was immediately formed. The benzene solvent was evaporated under vacuum to give a yellow powder, which was identified as **2.5[OC(O)CH3]** by ^{1}H NMR spectroscopy (with dichloromethane-d_2 as NMR solvent).

Formation of 3a in benzene-d_6

In a glove box, 10.0 mg (0.019 mmol) of **3** was added to 0.7 mL of benzene-d_6. To the mixture, 2.4 mg (0.021 mmol, 1.1 equiv.) of KO^{t}Bu was added to the mixture. The mixture gradually became orange and was allowed to stir for 1 hour. After 1 hour, the solution was filtered through a layer of celite, and a clear orange solution was obtained that was

characterized as **3a**. Orange crystals were grown by vapor diffusion of pentane to the benzene solution of **3a**.

^{1}H NMR (600 MHz, C_6D_6, 23 °C) δ 6.31 (t, $^3J_{HH}$ = 7.7 Hz, p-***H***$_{Py}$, 1H), 6.21-6.20 (m, m- and p-***H***$_{Py}$, 2H), 6.04 (d, $^3J_{HH}$ = 8.8 Hz, m-***H***$_{Py}$, 1H), 5.89 (d, $^3J_{HH}$ = 7.7 Hz, m-***H***$_{Py}$, 1H), 5.46 (d, $^3J_{HH}$ = 6.7 Hz, m-***H***$_{Py}$, 1H), 4.75 (d, $^2J_{HH}$ = 15.8 Hz, Py–C***H***$_2$–S, 1H), 4.61 (d, $^2J_{HH}$ = 14.8 Hz, Py–C***H***$_2$–S, 1H), 3.86 (s, Py–C***H***–S, 1H), 3.74 (d, $^2J_{HH}$ = 14.8 Hz, Py–C***H***$_2$–S, 1H), 3.64 (d, $^2J_{HH}$ = 17.9 Hz, Py–C***H***$_2$–S, 1H), 3.33 (s, (C***H***$_3$)$_2$SO, 3H), 3.20 (d, $^2J_{HH}$ = 15.7 Hz, Py–C***H***$_2$–S 1H), 3.08 (d, $^2J_{HH}$ = 17.9 Hz, Py–C***H***$_2$–S, 1H), 2.50 (s, (C***H***$_3$)$_2$SO, 3H).

Yield determination of 2.6a

In a glovebox, 5.0 mg (0.01 mmol) of **2.6** was combined with 2 mL of benzene-d_6; KO^{t}Bu (1.1 or 2.0 equiv) was then added. 1.3 μL (0.01 mmol, 1 equiv.) of mesitylene was added to the solution as an internal standard. The solution was placed into an NMR tube and analyzed by ^{1}H NMR spectroscopy. The yield of **2.6a** was determined by the peak of complex **2.6a** at 5.46 ppm against the internal standard peak at 6.72 ppm. When 1.1 equiv. of KO^{t}Bu was used, the yield **of 2.6a** was 29% after 20 min and further increased to 55% after 60 min. When 2.0 equiv. of KO^{t}Bu was used, no detectable **2.6a** was present and an intractable mixture of products formed.

Protonation of 2.6a by HBF_4

Complex **2.6a** was prepared in-situ from 10.0 mg (0.0141 mmol) of **2.6** with 2.4 mg (0.021 mmol) of KO^{t}Bu in benzene-d_6 in 60 min. To the orange solution of **2.6a**, 2.9 μL (0.021 mmol – 1.1 equiv.) of tetrafluoroboric acid diethyl ether complex (HBF_4.Et_2O) was added by micro syringe, and the yellow precipitate was immediately formed. The benzene solvent was evaporated under vacuum to give a yellow powder, which was identified as **2.6[BF_4]** by NMR spectroscopy (with dichloromethane-d_2 as NMR solvent).

Deprotonation of complex 2.7

In a glove box, 14.0 mg (0.020 mmol) of **2.7** was added to 0.7 mL of benzene-d_6. To the mixture, 2.5 mg (0.022 mmol, 1.1 equiv.) of KO^{t}Bu was added. The mixture gradually became red and was allowed to stir for 1 hour. After 1 hour, the solution was filtered through celite and a clear red solution of **2.7a** was obtained that was characterized by NMR spectroscopy.

^{1}H NMR (600 MHz, 23 °C, C_6D_6): δ 7.82 (t, $^3J_{HH}$ = 9.6 Hz, o-***H***$_{PPh3}$, 6H), 7.06 (t, $^3J_{HH}$ = 6.9 Hz, p-***H***$_{PPh3}$, 6H), 7.02 (d, $^3J_{HH}$ = 6.9 Hz, m-***H***$_{PPh3}$, 3H), 6.67 (d, $^2J_{HH}$ = 13.7 Hz, Py–C***H***$_2$–S, 1H), 6.46 (d, $^2J_{HH}$ = 8.2 Hz, p-***H***$_{Py}$, 1H), 6.36 (d, $^3J_{HH}$ = 5.5 Hz, m-***H***$_{Py}$, 1H), 6.05 (vt, $^3J_{HH}$= 8.7 Hz, 6.6 Hz p-***H***$_{Py}$, 1H), 5.92 (d, $^3J_{HH}$ = 9.6 Hz, m-***H***$_{Py}$, 1H), 5.70 (d, $^2J_{HH}$ = 13.7 Hz, Py–C***H***$_2$–S, 1H), 4.98 (d, $^3J_{HH}$ = 6.9 Hz, m-***H***$_{Py}$, 1H), 3.90 (d, $^2J_{HH}$ = 13.7 Hz, Py–C***H***$_2$–S, 1H), 3.81 (s, Py–C***H***–S, 1H), 3.74 (d, $^2J_{HH}$ = 13.7 Hz, Py–C***H***$_2$–S, 1H), 3.46 (d, $^2J_{HH}$ = 13.7 Hz, Py–C***H***$_2$–S, 1H), 2.61 (d, $^2J_{HH}$ = 13.7 Hz, Py–C***H***$_2$–S, 1H), –6.55 (d, $^2J_{PH}$ = 28.8 Hz, Ru–***H***, 1H).

^{13}C{^{1}H} NMR (151 MHz, 23 °C, C_6D_6): δ 206.58 (d, $^2J_{PC}$ = 18.6 Hz, Ru-***C***O), 170.78 (quat. ***C***$_{Py}$), 165.65 (quat. ***C***$_{Py}$), 164.60 (quat. ***C***$_{Py}$), 158.80 (quat. ***C***$_{Py}$), 135.62 (m-***C***$_{Py}$), 135.24 (d, $^1J_{PC}$ = 47.7 Hz, quat. ***C***$_{PPh3}$), 134.14 (d, $^2J_{PC}$ = 10.5 Hz, o-***C***$_{PPh3}$), 132.00 (p-***C***$_{Py}$), 129.77 (m-***C***$_{PPh3}$), 128.35 (p-***C***$_{PPh3}$), 123.53 (p-***C***$_{Py}$), 122.78 (m-***C***$_{Py}$), 113.50 (m-***C***$_{Py}$), 102.82 (m-***C***$_{Py}$), 59.69 (Py–***C***H–S), 58.54 (Py–***C***H_2–S), 53.32 (Py–***C***H_2–S), 43.61 (Py–***C***H_2–S), 43.25 (Py–***C***H_2–S).

^{31}P{^{1}H} NMR (162 MHz, 23 °C, C_6D_6): δ 67.86 (***P***Ph_3).

Yield determination of 2.7a: In a glovebox, 5.0 mg (0.007 mmol) of **2.7** was combined with 2 mL of benzene-d_6; KO^{t}Bu was then added (1.1, 2.0, 3.0 or 4.0 equiv.). 1.0 µL (0.01 mmol, 1 equiv.) of mesitylene was added to the solution as an internal standard. After 60 minutes, the solution was taken out for analysis by ^{1}H NMR spectroscopy. The yield of **2.7a** was determined by the peak of complex **2.7a** at 4.98 ppm against the internal standard peak at 6.73 ppm. The yields varied in the range of 96-99% when 1.1, 2.0, and 3.0 equiv. of KO^{t}Bu were used. In the presence of 4.0 equiv. of KO^{t}Bu, a slightly diminished yield of 77% was obtained after 60 min.

Protonation of 2.7a by HBF_4

Complex **2.7a** was prepared in-situ from 10.0 mg (0.0142 mmol) of **2.7** with 1.8 mg (0.0157 mmol) of KO^{t}Bu in benzene-d_6 in 30 min. To the orange solution of **2.7a**, 2.1 µL (0.016 mmol – 1.1 equiv.) of tetrafluoroboric acid diethyl ether complex ($HBF_4.Et_2O$) was added by micro syringe, and the yellow precipitate was immediately formed. The benzene solvent was evaporated under vacuum to give a yellow powder, which was identified as **2.7[BF$_4$]** by NMR spectroscopy (with dichloromethane-d_2 as NMR solvent).

Formation of complex 2.8

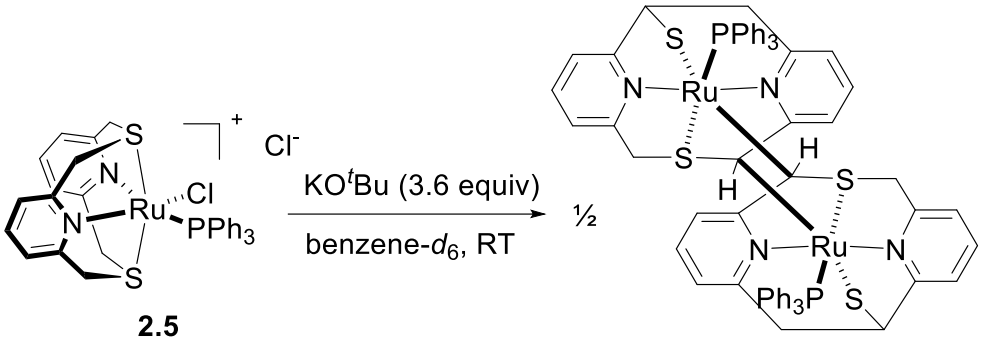

2.5 **2.8**

In a glove box, 50.0 mg (0.070 mmol) of **2.5** was dissolved in THF. To the mixture, 25 mg (0.023 mmol, 3.2 equiv.) of potassium tert-butoxide was added. The mixture was stirred at room temperature for 1.5 hours. During this time, the solution became dark brown. The solution was then concentrated under vacuum. 2 mL of benzene was added to dissolve the solid and the obtained solution was filtered through Celite and left for crystallization by vapor diffusion of pentane. Complex **2.8** was obtained as red crystals in very low yield, *ca.* 5–10 mg, as a part of a more complex mixture of unidentified products that could be isolated.

^{1}H NMR (600 MHz, 23 °C, THF-d_8): δ 7.50 (t, $^3J_{HH}$ = 8.6 Hz, o-***H***$_{PPh3}$, 12H), 7.16 (t, $^3J_{HH}$ = 7.2 Hz, p-***H***$_{PPh3}$, 6H), 7.10 (t, $^3J_{HH}$ = 7.6 Hz, m-***H***$_{PPh3}$, 12H), 6.34-6.29 (m, p-***H***$_{Py}$, 2H), 5.96-5.93 (m, p-***H***$_{Py}$ & m-***H***$_{Py}$, 4H), 5.73 (d, $^3J_{HH}$ = 8.3 Hz, m-***H***$_{Py}$, 2H), 5.56 (d, $^3J_{HH}$ = 6.2 Hz, m-***H***$_{Py}$, 2H), 4.95 (d, $^3J_{HH}$ = 6.2 Hz, m-***H***$_{Py}$, 2H), 3.94 (d, $^2J_{HH}$ = 14.5 Hz, Py–C***H***$_2$–S, 2H), 3.49 (d, $^2J_{HH}$ = 13.8 Hz, Py–C***H***$_2$–S, 2H), 3.47 (s, Py-C***H***(Ru)-S, 2H), 3.08 (d, $^2J_{HH}$ = 14.5 Hz, Py–C***H***$_2$–CH, 2H), 2.41 (d, $^2J_{HH}$ = 14.5 Hz, P–C***H***$_2$–CH, 2H); (proton peak of Py–C***H***(CH$_2$)–S overlaps with THF).

^{13}C{^{1}H} NMR (600 MHz, 23 °C, THF-d_8): δ 168.78 (quat. ***C***$_{Py}$), 166.20 (quat. ***C***$_{Py}$), 159.50 (quat. ***C***$_{Py}$), 157.97 (quat. ***C***$_{Py}$), 138.13 (d, $^1J_{CP}$ = 36.1 Hz, quat. ***C***$_{PPh3}$), 135.31 (d, $^2J_{CP}$ = 10.1 Hz, o-C$_{PPh3}$), 130.72 (p-***C***$_{Py}$), 128.90 (p-***C***$_{PPh3}$), 128.14 (p-***C***$_{Py}$), 127.78 (d, $^3J_{CP}$ = 10.1 Hz, m-***C***$_{PPh3}$), 109.54 (m-***C***$_{Py}$), 108.81 (m-***C***$_{Py}$), 101.14 (m-***C***$_{Py}$), 100.78 (m-***C***$_{Py}$), 64.35 (Py–***C***H(CH$_2$)–S), 63.48 (Py–***C***H(Ru)–S), 60.30 (Py–***C***H$_2$–S), 59.36 (Py–***C***H$_2$–CH).

Chapter 3. Mn^{III} N3C-Pyridinophane Complexes and Their Reactivity in C-Halide and C-C Bond Formation

The content described in this chapter is reported in the two following publications:[66-67]

1. Sarbajna, A.; He, Y.-T.; Dinh, M. H.; Gladkovskaya, O.; Rahaman, S. M. W.; Karimata, A.; Khaskin, E.; Lapointe, S.; Fayzullin, R. R.; Khusnutdinova, J. R. "Aryl–X Bond-Forming Reductive Elimination from High-Valent Mn–Aryl Complexes" *Organometallics* **2019**, *38*, 4409-4419. Copyright 2019 American Chemical Society.

Declaration of Contribution: Prof. Julia R. Khusnutdinova guided the project. I (Hoan M. Dinh) optimized the synthesis of the complexes, performed characterization and magnetic measurements in solution and mechanistic studies. Dr. Sarbajna and Dr. He studied C-X elimination and initial mechanistic studies. Dr. Gladkovskaya, Dr. Rahaman and Dr. Karimata participated in synthesis of ligands and PPMS measurements in solid state. Dr. Lapointe and Dr. Khaskin performed X-ray data collection that was then refined by Dr. Fayzullin.

The scheme **3.11** – **3.12** and figure **3.1** – **3.4** in this chapter are from this publication.[67]

2. Dinh, M. H.; He, Y.-T.; Fayzullin, R. R.; Vasylevskyi, S.; Khaskin, E.; Khusnutdinova, J. R. "Synthesis of Aryl-Manganese(III) Fluoride Complexes via α-Fluorine Elimination from CF_3 and Difluorocarbene Generation" *Eur. J. Inorg. Chem.* **2023***, 26* (32)*,* e202300460.

Declaration of Contribution: Prof. Julia R. Khusnutdinova guided the project. I (Hoan M. Dinh) synthesized and characterized the second complex, conducted the difluorocarbene trap experiment and studied the reactivity of manganese(III) dibromide complex in difluorocyclopropanation and difluorocyclopropenation. Dr. Yu-Tao He synthesized and characterized the first complex. Dr. Eugene Khaskin and Dr. Serhii Vasylevskyi performed X-ray data collection. Dr. Robert R. finalized X-ray structural measurement to publication level.

The Scheme **3.13** – **3.16**, Figure **3.5** – **3.6** and Table **3.1** – **3.3** in this chapter are from this publication.[66]

3.1. Introduction

The results described in Chapter 2 indicated that the presence of sulfur in a pyridinophane macrocycle might have imposed limitations to the complex stability under forcing conditions, although the ability of the N2S2 ligand to strongly chelate to a metal center was crucial to enable characterization and structural and spectroscopic comparison of deprotonate species.

To overcome the problems associated with low stability of **N2S2** ligand scaffold, another pyridinophane ligand motif was then examined in manganese complexes, an N3C-type pyridinophane, which cyclometalates to a metal center coordinating with one aryl group and three N-donors. The presence of cyclometalated aryl was further expected to assist in stabilization of organomanganese derivatives in higher oxidation states and provided a convenient handle to study elementary reaction steps at high-valent paramagnetic Mn center, such as oxidative addition, reductive elimination, and α-fluorine elimination.

3.1.1 Oxidative addition and reductive elimination in first-row transition metal complexes

Oxidative addition and reductive elimination stand as key elemental steps in numerous transitional-metal-mediated catalytic processes including C-C coupling and C-H bond functionalization.[5-6, 68] Due to the propensity of second and third-row transition metals, such as Pt, Pd, Ir, Rh, to participate in two-electron oxidative addition and reductive elimination steps, precious metals have been playing a major role in catalytic reactions that involve these steps. [69-72] By contrast, first-row metals that tend to participate in one-electron oxidation or reduction events have rarely been studied in these transformations, and mechanistic studies of the oxidative addition and reductive elimination are often based on using diamagnetic precious metal complexes as model systems.[73-81] However, due to the scarcity, high cost, and toxicity of the precious metals, the urge to find alternative catalysts based on cheap, non-toxic first-row transition metals that can provide similar or better reactivity has intensified. In terms of that, manganese complexes have recently gained a lot of attention as a catalyst for C-H bond functionalization and C-C coupling reaction.[82-89]

While the majority of C-H functionalization reactions catalyzed by manganese complexes are proposed to be carried out via Mn^{I} intermediate with no change in the oxidation state[89-90], some studies proposed the involvement of Ar–Mn^{III} or Ar–Mn^{IV} species, however, no experimental evidence was reported.[82, 91-94] However, compared with second and third-row transition metals, the investigation of fundamental reactivity such as oxidative addition and reductive elimination from manganese complexes, or first-row transition metal complexes in general, is still a challenge due to their low stability, paramagnetism, and multiple available oxidation states.[95-96] The studies of two-electron aryl-X oxidative addition and reductive elimination at iron[97-100] and cobalt[101-102] are scarce, while there is no report so far for manganese.

One common approach to studying mechanisms in first-row transition metals is to utilize the macrocyclic aryl-X or aryl-H substrate model in order to stabilize reactive species. For example, in 2010, Ribas and coworkers reported the synthesis of aryl-Cu^{III}-X complexes supported by triazamacrocyclic ligands **L3.1**.[103] The Cu-Cl and Cu-Br complex was prepared via disproportionation of Cu^{II} salts to afford 0.5 equiv. of $Cu^{I}X$ (X = Cl, Br) and the protonated ligand. The complex is stable under heating conditions. Interestingly, in the presence of Bronsted acid CF_3SO_2H, the complex undergoes reductive elimination to form protonated aryl-X product **L3.2H**$^{+}$ and Cu^{I} species. Interestingly, the protonated ligand **L3.2H**$^{+}$ undergoes reversible oxidative addition with Cu^{I} precursor $[Cu(MeCN)_4]OTf$ in the presence of Proton Sponge® as a base to form back Cu^{III} complex **3.1 (Scheme 3.1).**

Scheme 3.1. Synthesis of Cu^{III} complex **3.1**. and reversible reductive elimination/oxidative addition promoted by Bronsted acid.

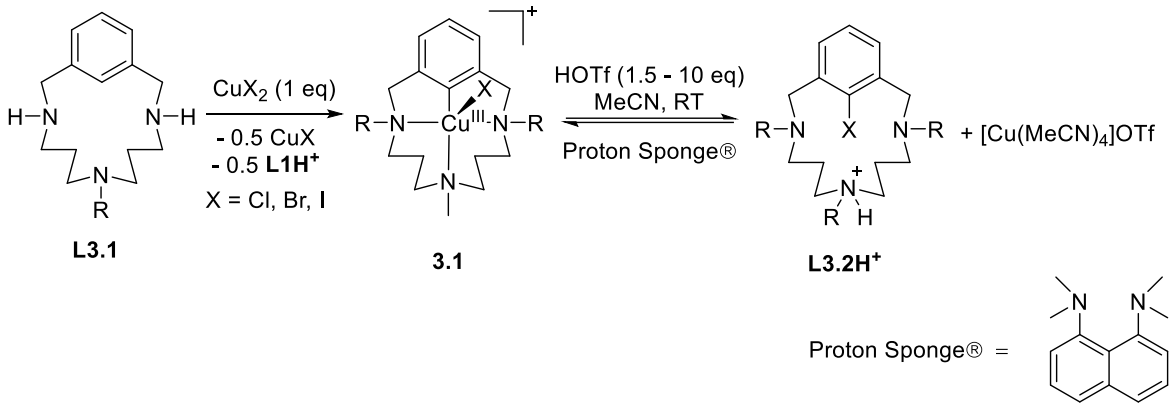

Scheme 3.2. Synthesis of Ni^{II} complex **3.2** and C-CF_3 bond formation via reductive elimination.

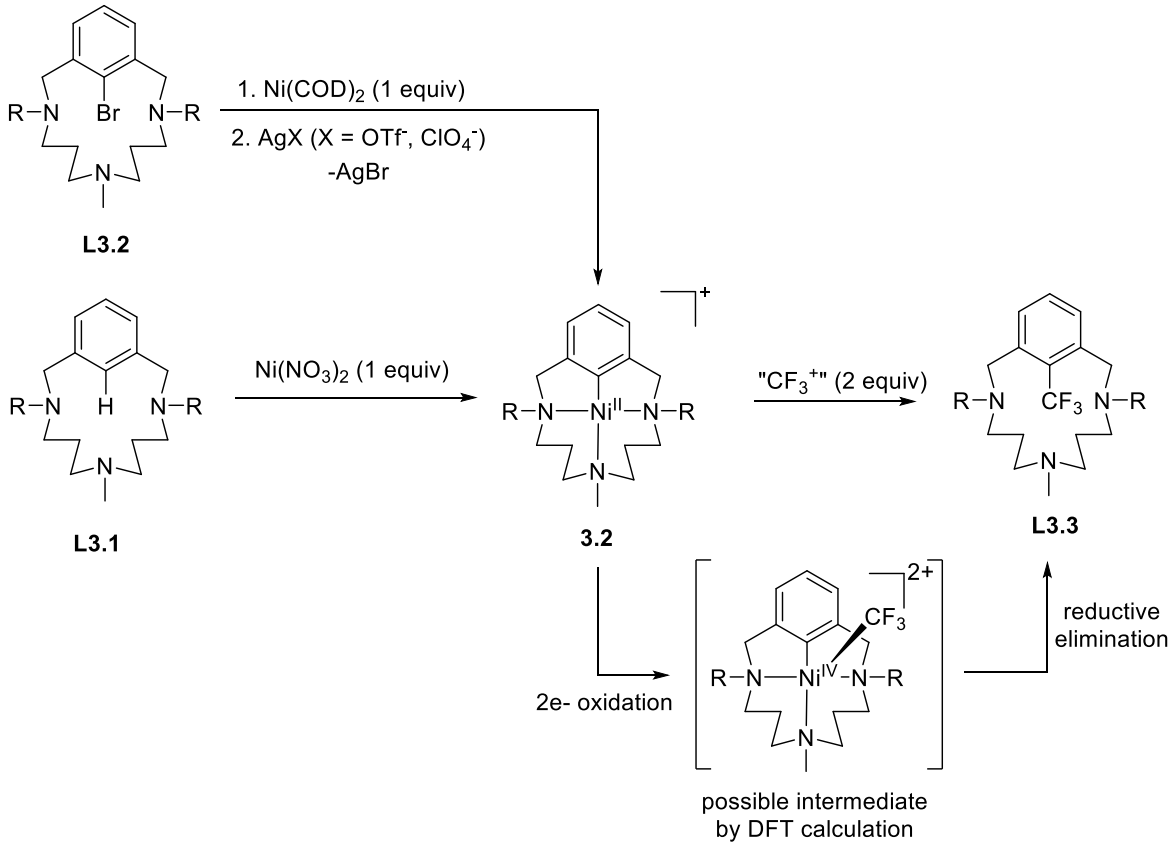

In 2017, the Ribas group utilized a similar triazamacrocyclic scaffold to synthesize the Ni^{II}-aryl complex **3.2** via oxidative addition of **L3.2** to $Ni(COD)_2$ in THF or C-H activation of **L3.1** with $Ni^{II}(NO_3)_2$ in MeCN.[104] Treating complex **3.2** with 2 equiv of electrophile CF_3 sources (Togni or Umemoto's reagent) led to the formation of aryl-CF_3 coupling product **L3.3**, likely through reductive elimination from a Ni^{IV} intermediate species. (**Scheme 3.2**)

Macrocyclic pyridinophane-based ligands are also utilized to study the mechanism of C-C or C-X bond formation mediated by first-row transition metals due to their coordination to stabilize unusual oxidation states or another type of reactive species.[47-49] For example, in 2015, Mirica and coworkers showed the synthesis of bis(acetonitrile) and bis(alkoxo) aryl-Ni^{III} complexes **3.3** and **3.4** supported by tetradentate pyridinophane ligands. [105] Treatment complex **3.3** with $PhI(PyOMe)_2(OTf)_2$ as an oxidant in the presence of an excess amount of

nucleophilic alkoxyl group OR^- resulted in the formation of Ar-OR elimination product, presumably due to the reductive elimination in Ni^{IV} intermediate. (**Scheme 3.3**)

Scheme 3.3. Synthesis of cyclometalated Ni^{III}-aryl complexes **3.3** and **3.4** and their C-OR reductive elimination.

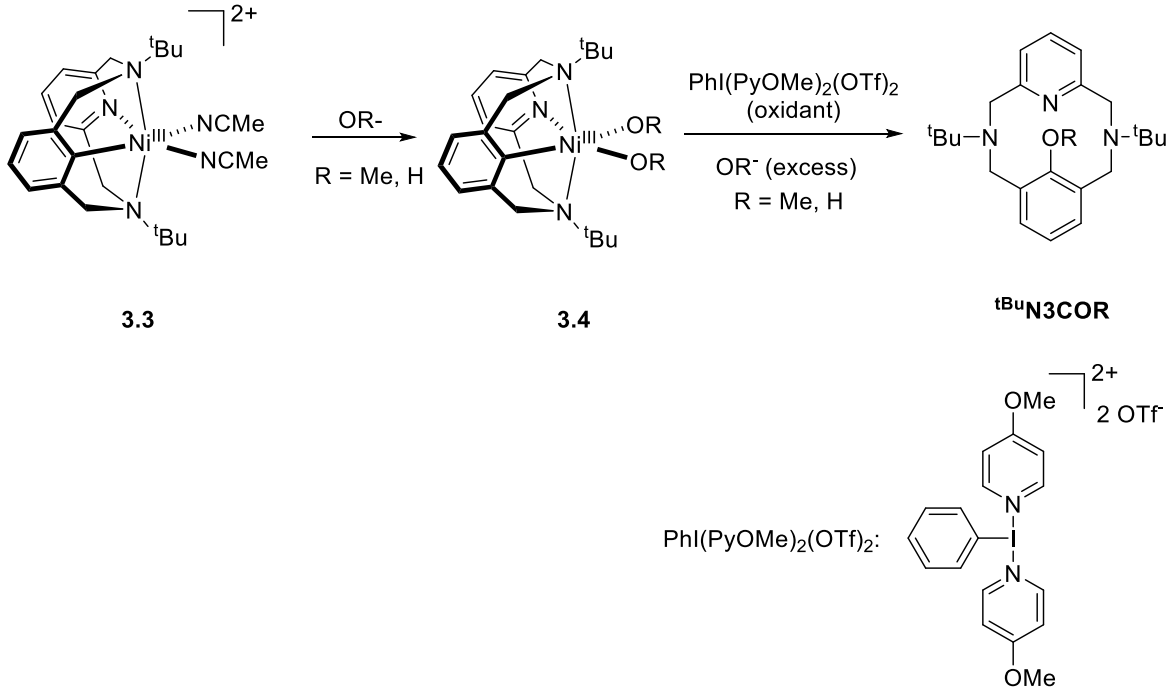

In 2016, the Mirica group reported the synthesis and reactivity of Ni^{III}-dimethyl complex **3.6** supported by macrocyclic pyridinophane ligands.[106] Treatment of $Ni^{II}(Me)_2$ complex **3.5** supported κ^2-coordinated pyridinophane-based ligand with 1 equiv. of $FcPF_6$ led to the formation of a high-valent nickel(III) dimethyl complex **3.6** with the ligand bound to the center in a tetradentate fashion. In the presence of a one-electron oxidant, complex **3.6** undergoes reductive elimination to yield ethane as a C-C coupling product and nickel(II) complex **3.7**, presumably via nickel(IV) intermediates.(**Scheme 3.4**)

Scheme 3.4. Synthesis of nickel(III) dimethyl complex supported by pyridinophane-based ligand and its reductive elimination promoted by one-electron oxidant.

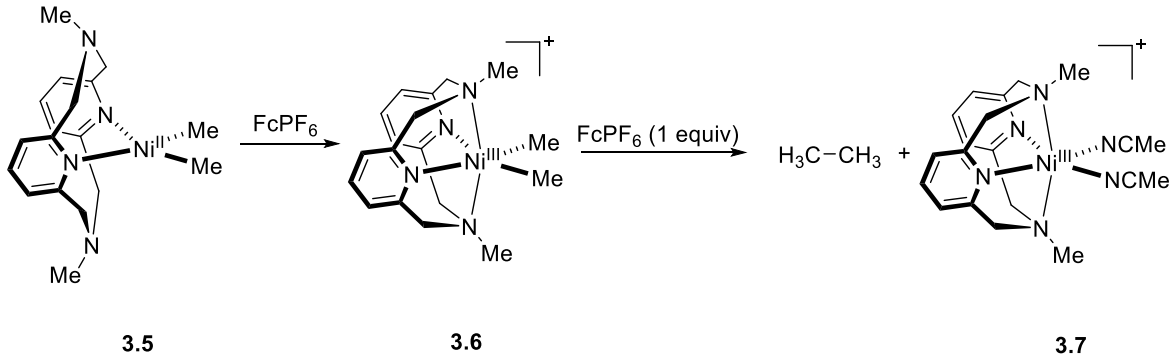

In 2016, to understand the mechanism of alkyne annulation catalyzed by cobalt complexes, Ribas and coworkers isolated cyclometalated cobalt(III) complex **3.8** obtained by C-H activation of **^{H}N3CH** ligand to $Co^{II}(OAc)_2$ under air.[107] Treatment of complex **3.8** with an alkyne led to the formation of an annulated product **L3.4** or **L3.5**, depending on the nature of the alkyne and the reaction temperature. This finding shed light on the mechanism of cobalt-mediated alkyne annulation, with solid evidence of Co^{III} species as an intermediate for the reaction.

Scheme 3.5. Synthesis of Co^{III} complex **3.8** and its reactivity in alkyne annulation.

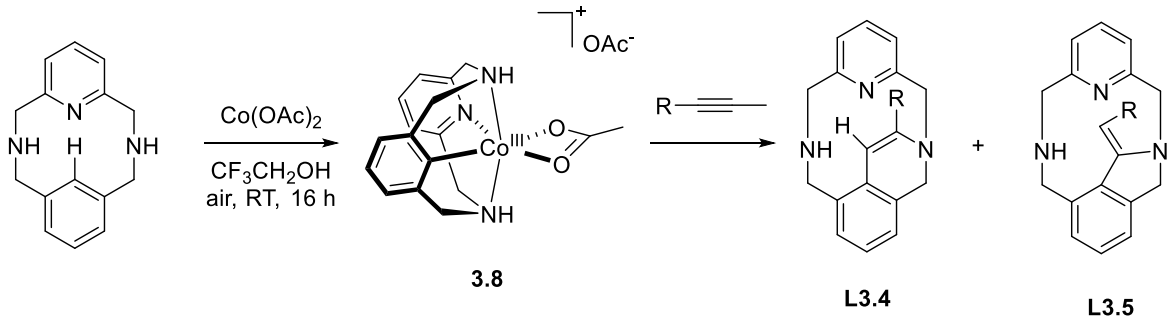

In 2021, Ribas and coworkers reported the synthesis of cyclometalated aryl-iron(II) complex **3.9** via oxidative addition of Ar-Br bond to $Fe^0(CO)_5$ precursor.[100] Treatment of the complex **3.9** with Grignard reagent PhMgBr followed by reacting with oxygen under air led to the formation of C-C bond formation product **^{Me}N3CCOPh**. Based on DFT calculations, the mechanism was proposed via the transmetalation of PhMgBr, followed by a carbonyl insertion to form intermediate **3.11**. In the presence of air, the Fe^{II} intermediate **3.11** is oxidized to form unstable Fe^{III} intermediate **3.12**, prone to reductive elimination to yield aryl-benzoyl product.

Scheme 3.6. Synthesis of Fe^{II} complex **3.9** and C-C aryl-benzoyl bond formation.

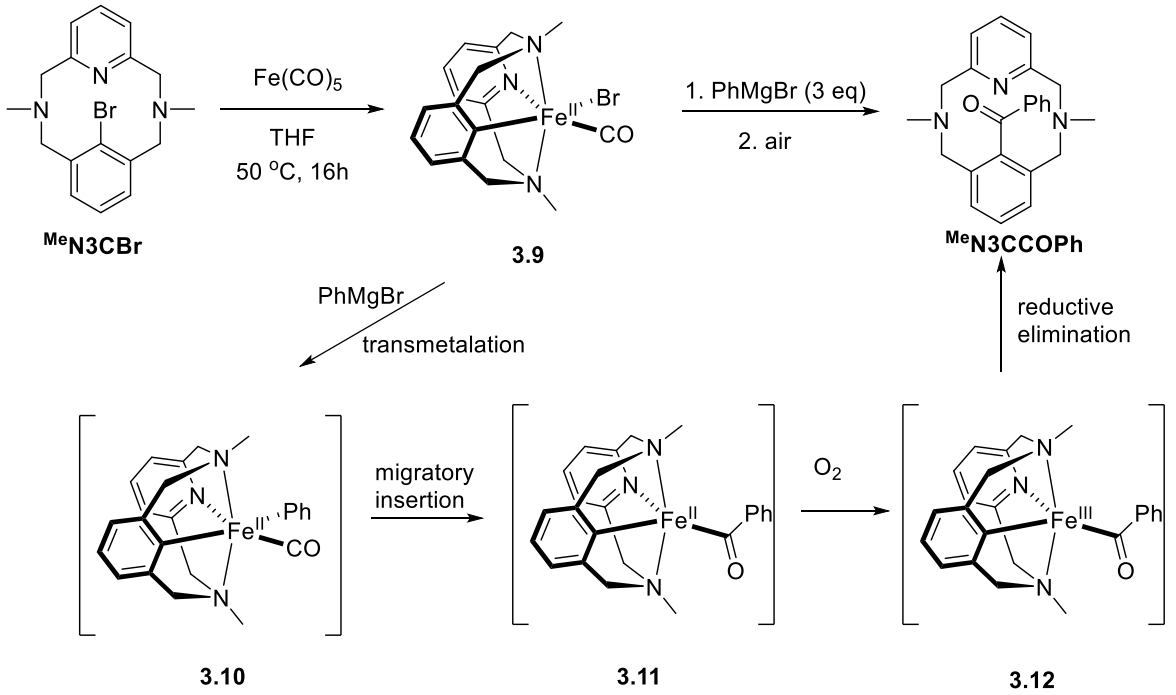

3.1.2 Synthesis of high-valent fluoro complexes

The incorporation of fluorine atom into bioactive compounds plays important roles in pharmaceuticals and agrochemicals, which can increase hydrophobicity, metabolic stability, binding selectivity, and membrane permeability.[108-109] In this regard, high-valent fluoro and perfluoroalkyl complexes of inexpensive, abundant first-row transition metals are of great interest as reagents and potential intermediates in various procedures of stoichiometric or catalytic fluorine incorporation.

However, synthesis of high-valent transition-metal fluoro complexes is challenging and most of the existing methodologies require expensive or highly reactive reagents. One of the common methods for fluoro complexes preparation is based on halogen exchange with silver

fluoride. For example, in 2012, the Groves group reported the synthesis of high-valent Mn^{IV} fluoride complex **3.14** by treating Mn^{IV} chloride complex **3.13** supported by substituted porphyrin ligand with an excess amount of AgF (**Scheme 3.7a**).[110] This complex **3.14** was proven as a key intermediate for oxidative C-H fluorination catalyzed by porphyrin-based manganese(III) complexes. In 2015, the Baker group showed the synthesis of perfluoroalkyl cobalt(III) fluoride complex **3.16** by treating perfluoroalkyl cobalt(III) iodide complex **3.15** with 3 equiv. of silver fluoride in dichloromethane (**Scheme 3.7b**).[111] Recently, Nebra and coworkers have reported the synthesis of Cu-F complex **3.18** by treating the anionic $[Cu(CF_3)_3Cl]^-$ **3.17** with an excess amount of AgF in acetonitrile at 0 °C (**Scheme 3.7c**).[112]

Scheme 3.7. Synthesis of high-valent fluoro complexes of first-row transition metal complex by reaction with silver fluoride.

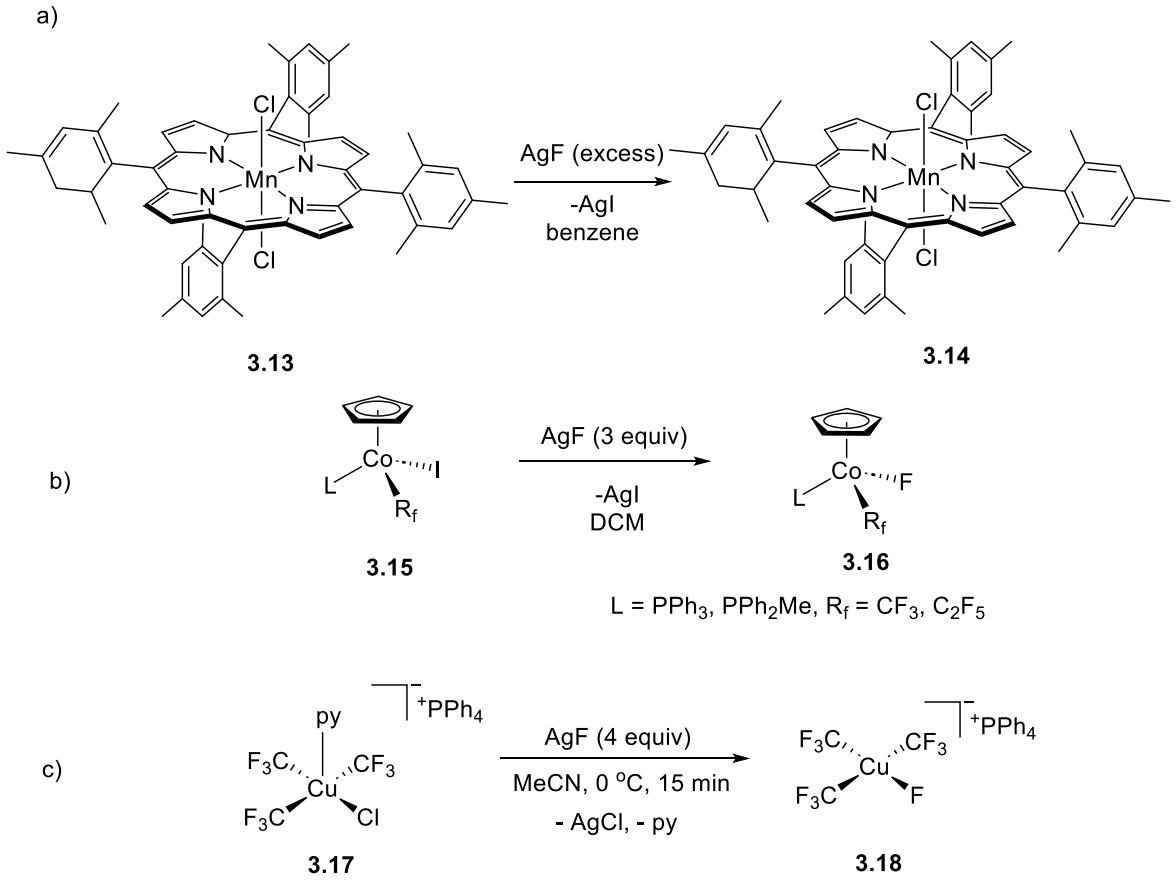

Another approach to obtain high-valent complexes is to oxidize low-valent complex by high-reactive xenon difluoride or Selectfluor reagent. For example, in 2017, the Nebra group obtained high-valent nickel(III) and nickel(IV) fluoro complexes via oxidation of $Ni^{II}(CF_3)_2(py)_2$ by XeF_2.[113] In detail, treatment of $Ni(CF_3)_2(py)_2$ with one equiv. of XeF_2 led to the formation of mono- and dimeric Ni^{III} complexes **3.19** and **3.20**. The addition of one more equiv. of XeF_2 resulted in the formation of Ni^{IV} complex **3.21**. The complex **3.21** can also be prepared by reacting $Ni(CF_3)_2(py)_2$ with 2 equiv. of XeF_2 at low temperatures (**Scheme 3.8a**). In the same year, Smith and coworkers reported the synthesis of pyridinophane $Mn^{III}F_2$ complexes **3.23** by treating Mn^{II} complexes **3.22** with XeF_2 in acetonitrile at room temperature (**Scheme 3.8b**).[114]

Scheme 3.8. Synthesis of high-valent fluoro complexes of first-row transition metal complex by reaction with XeF_2.

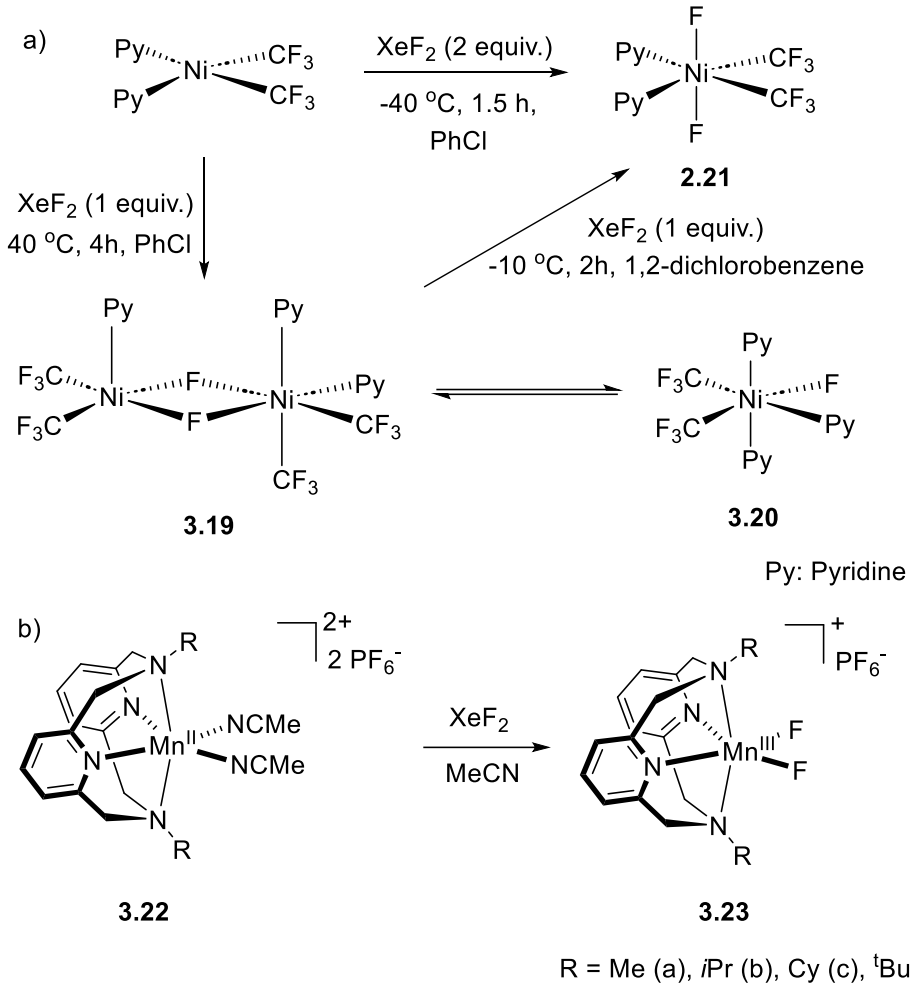

Scheme 3.9. Synthesis of nickel(IV) fluoride complex **3.13** via oxidation by Selectfluor reagent.

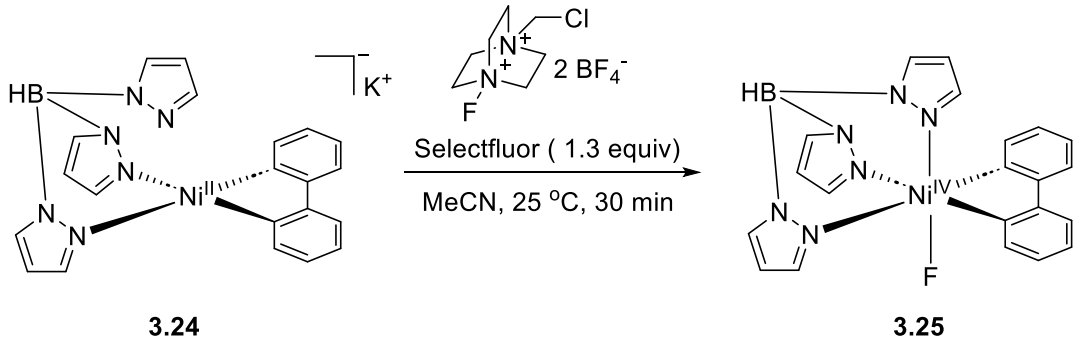

High-valent metal fluoride complexes could be prepared by using fluorinated metal precursors such as $Mn^{III}F_3$. For example, in 2003, Duboc-Toia and coworkers reported the synthesis of Mn^{III} complexes $Mn(bpea)F_3$ **3.26** (bpea = N,N-bis(2-pyridylmeth-yl)-ethylamine) and $Mn(terpy)F_3$ **3.27** (terpy = terpyridine) by simply mixing the suitable ligand with MnF_3 in methanol at room temperature (**Scheme 3.10a**).[115] Smith and coworkers showed an alternative approach to synthesize **3.23a** and **3.23b** by treating pyridinophane ligand ^{Me}**N4** or ^{iPr}**N4** with 1 equiv of MnF_3 in the presence of $NaPF_6$ (1 equiv) in methanol at 50 °C (**Scheme 3.10b**).[114]

Scheme 3.10. Synthesis of Mn^{III} fluoride complexes of first-row transition metal complex by complexation with MnF_3 precursor.

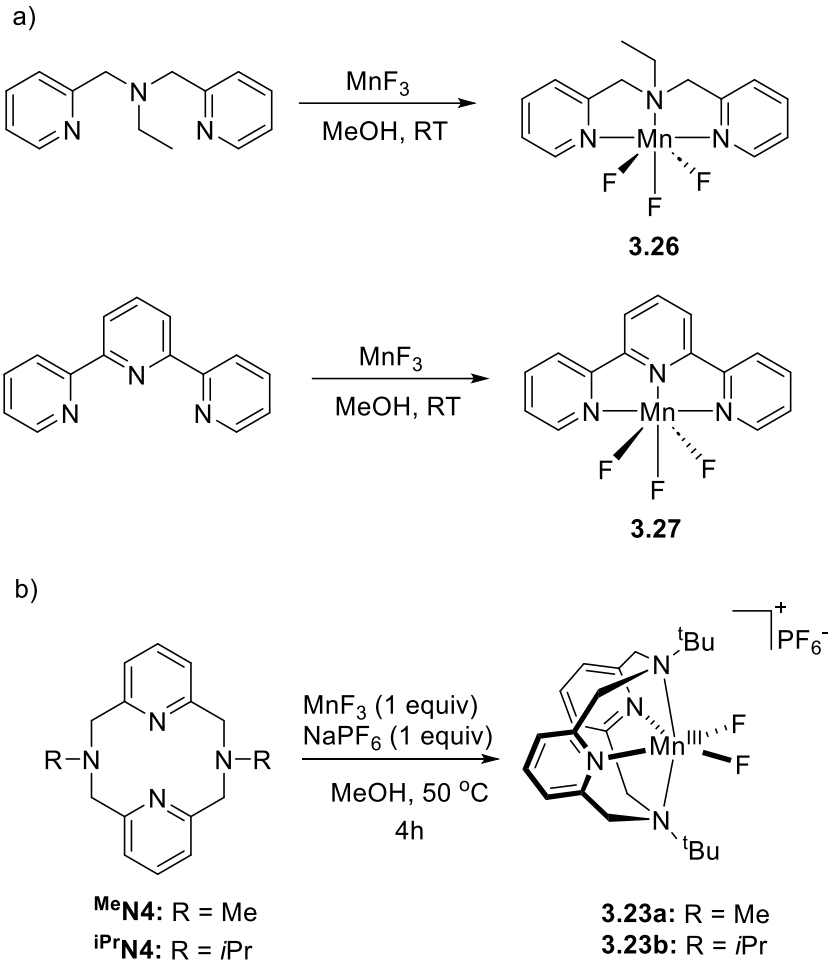

Considering that the macrocyclic pyridinophane-based ligand can stabilize unsual oxidation states or other types of reactive species, in this chapter, we reported the synthesis of cyclometalated aryl-Mn^{III} dibromide complexes supported by macrocyclic pyridinophane-based ^{tBu}**N3C**$^{-}$ ligand via oxidative addition of an aryl bromide to a manganese(I) precursor $Mn(CO)_5Br$. In the presence of one-electron oxidant, the complex underwent reductive elimination to form aryl bromide adduct and Mn^{II} species, presumably via Mn^{IV} intermediate. We also present the alternative synthesis of cyclometalated high-valent manganese(III) fluoro complexes using trifluoromethyl reagent via transmetalation followed by α-fluorine elimination, resulting in the release of a difluorocarbene. That facile generation of a difluorocarbene could be utilized in difluorocarbenation of alkenes and alkynes using Zn trifluoromethyl reagent at lower temperatures and shorter time as compared to manganese-free reaction.

3.2. Results and Discussion

3.2.1 Synthesis of aryl-Mn^{III} dibromide complexes supported by ^{tBu}N3C ligand

Scheme 3.11. Synthesis of Mn^{III} complex **3.28**

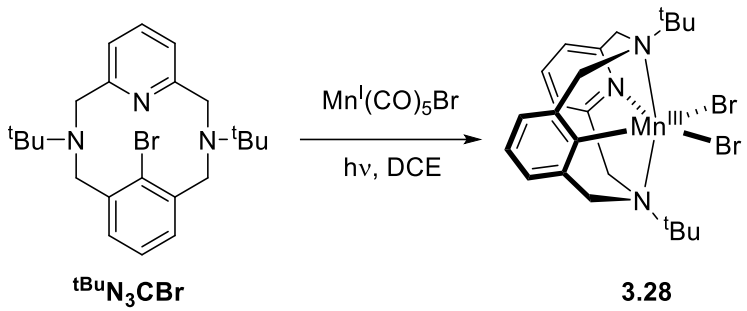

$^{tBu}N_3CBr$ **3.28**

As a strategy for preparation of manganese(III) organometallic complexes, we targeted oxidative addition of the macrocylic pyridinophane-based **^{tBu}N3CBr** to manganese(I) precursor, $Mn(CO)_5Br$. Considering that such oxidative addition would require removal of carbonyl ligands to allow for vacant coordination sites, we performed the reaction under UV light irradiation to facilitate CO dissociation. Irradiation of the solution containing equimolar amounts of **^{tBu}N3CBr** and $Mn(CO)_5Br$ in dichloroethane using a mercury lamp resulted in the formation of (**^{tBu}N3C**)$MnBr_2$ complex **3.28**, which was isolated as a deep-red crystalline solid in 58% yield. The complex was characterized by single crystal X-ray diffraction (SC-XRD), ^{1}H NMR spectroscopy, ultraviolet–visible (UV–vis), and Fourier transform infrared (FT-IR) spectroscopies, high-resolution mass spectrometry (HR-MS), and elemental analysis. According to SC-XRD, complex **3.28** has a distorted octahedral geometry around the metal center surrounded by $^{t\text{Bu}}$N3C$^-$ ligand coordinating in κ^4 coordination mode, and two bromide ligands. The $Mn–N_{amine}$ distances in **3.28** (2.474(2) Å and 2.445(2) Å) are elongated compared to $Mn–N_{pyridine}$ bond distance (2.063(11) Å). The $Mn–C_{ipso}$ bond distance is 2.027(14) Å, and the Mn-Br bond distances are 2.4623(4) and 2.4793(5) Å. The magnetic moment determined by the Evans method for a DCM solution of **3.28** was 4.98 μ_B, suggesting an S = 2 ground state corresponding to a high-spin d^4 configuration for the Mn^{III} center. ESI-HRMS analysis of **3.28** shows the presence of a peak at 484.1149 (z = 1), which was assigned to [**3.28** − Br]$^+$ fragment.

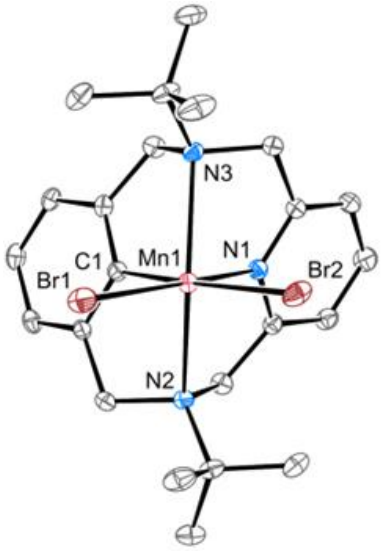

Figure 3.1. ORTEP of neutral complexes **3.28** (a) at 50 % probability level according to single crystal X-ray diffraction data. Hydrogen atoms and minor disordered components are omitted for clarity; equivalent atoms are labelled by the superscript *i* (–*x*+1, –*y*, –*z*+1). Selected interatomic distances [Å]: Br1–Mn1 2.4623(4), Br2–Mn1 2.4793(5), Mn1–C1 2.027(14), Mn1–N1 2.063(11), Mn1–N2 2.474(2), Mn1–N3 2.445(2).

Sine complex **3.28** was obtained by two-electron oxidative addition to a manganese(I) center, which could be via either non-radical or radical mechanism. To examine if the reaction involves a free radical formation, (2,2,6,6-tetramethylpiperidin-1-yl)oxyl (TEMPO) as a radical trap or 9,10-dihydroanthracene as an H-atom donor was added in the reaction. No TEMPO adducts or anthracene was detected in the reaction mixtures, ruling out free Ar radical formation hypothesis. To argue against the possibility of free Br radical or Br_2 formation after, the synthesis of **3.28** was carried out in the presence of 1-hexene or 1-decene. As expected, no brominated products were detected by GC-MS analysis. These results proved that the mechanism of the reaction is via non-radical oxidative addition, and the role of UV light irradiation in the reaction is likely to promote CO ligand dissociation.

3.2.2 Reductive elimination in aryl-Mn^{III} dibromide complexes

After having complex **3.28** in hand, we next examined if the complex could undergo reductive elimination. Heating the complex at 150 ºC with or without the presence of strong coordinated ligand like PPh_3 or CO did not lead to the formation of any reductive elimination products. These results suggested that reductive elimination could not be feasible in Mn^{III} oxidation state. This is not unexpected as the two-electron reductive elimination from Mn^{III} is expected to produce Mn^{I} complex, while our experiments showed that the reverse reaction, oxidative addition of aryl bromide to Mn^{I}, is favorable.

By analogous with literature that uses oxidant to increase the oxidation state in the metal center and promote reductive elimination,[116-119] we hypothesized that the aryl-Br reductive elimination can be achieved in the higher oxidation state of manganese. Therefore, we next studied the electrochemical properties of complex **3.28** by cyclic voltammetry to gain insight into the accessibility of other oxidation states. The anodic scan revealed a quasi-reversible oxidation wave at $E_{1/2}$ = 0.47 V vs Fc^{+}/Fc (ΔE_p = 290 mV), which was assigned tentatively as a Mn^{III}/Mn^{IV} oxidation, along with an irreversible oxidation at higher positive potentials ($E_{pa} \approx$ 1.12 V). This suggested that the $1e^{-}$-oxidized product can be accessible by using conventional chemical oxidants. [120]

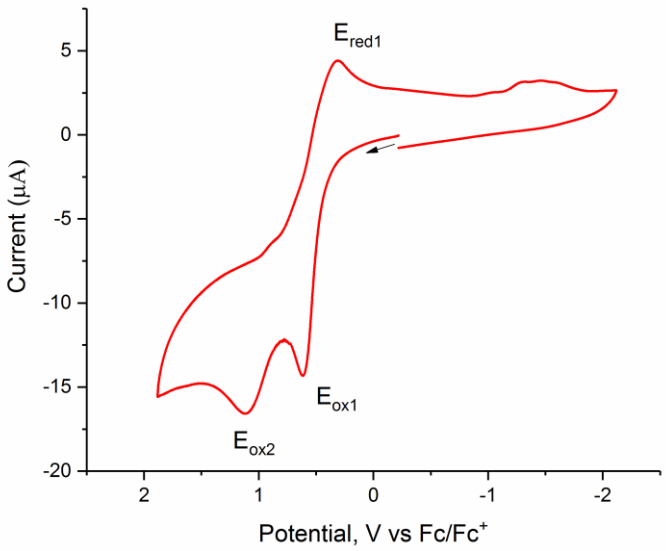

Figure 3.2. Cyclic voltammogram of **3.28** (2 mM) in 0.1 M $^{n}Bu_4NPF_6$/MeCN at 25 °C (scan rate 50 mV s^{-1}; 1.6 mm Pt disk working electrode; the arrow indicates the initial scan direction). E_{ox1} = 0.611 V; E_{red1} = 0.321 V (quasi-rev.); ΔE_p = 290 mV; $E_{1/2}$ = 0.466 mV; E_{ox2} = 1.120 mV (irrev.).

First, $NOBF_4$ was used as an oxidant to react with complex **3.28**. Treatment of complex **3.28** with 1.1 equiv of $NOBF_4$ in dichloromethane led to a gradual change of the initial red-colored solution to yellow within 2 h. The analogous reaction in acetonitrile resulted in a complete change of the solution color to yellow within a minute. ESI-HRMS analysis of the resulting solution showed a peak of m/z 430.1836, corresponding to a metal-free [$^{t\text{Bu}}$**N3CBr** + H]$^+$ species (calculated m/z 430.1852). Interestingly, when 2 equiv. of $NOBF_4$ was used, single crystals were obtained from acetonitrile solution showing a cocrystallized metal-free $^{t\text{Bu}}N_3CBr$ together with $[Mn(MeCN)_6]^{2+}$, NO^+, and BF_4^- counterions. Although the crystal disorder prevents an unambiguous assignment of charges and oxidation states for all components, this structure proves the formation of **$^{t\text{Bu}}$N3CBr**. The existence of excess NO^+ equivalents implies that less than 2 equivalents of the oxidant may be necessary.

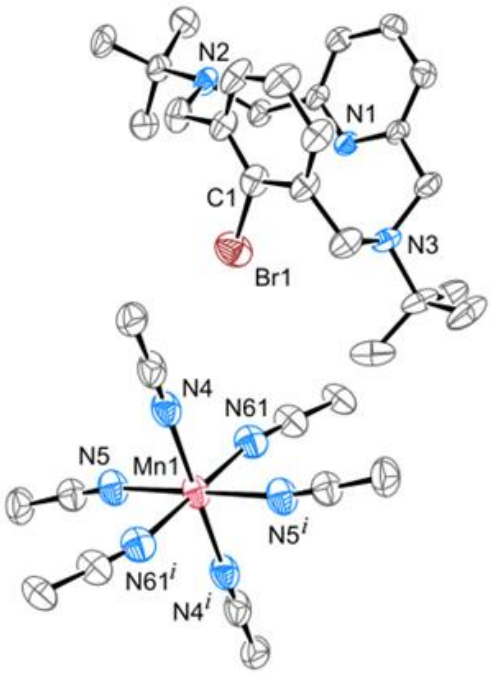

Figure 3.3. ORTEP of co-crystal of free ligand **$^{t\text{Bu}}$N3CBr** and hexakis(acetonitrile)manganese(II) complex at 50 % probability level according to single crystal X-ray diffraction data. Hydrogen atoms, minor disordered components, counterions and solvent molecules are omitted for clarity; equivalent atoms are labelled by the superscript *i* (–*x*+1, –*y*, –*z*+1).

NMR analysis of the crude product confirms the formation of free **$^{t\text{Bu}}$N3CBr** with 84% NMR yield based on internal standard. By using flash chromatography for purification, the free **$^{t\text{Bu}}$N3CBr** was isolated in 65% yield as an average of three trials. The byproduct of the reaction was identified as the protonated ligand **$^{t\text{Bu}}$N3CH**, formed in ca. 16–17% yield. The formation of the byproduct is likely due to the protonation of the ligand by protic impurities present in the oxidant or the solvent. Indeed, the formation of **$^{t\text{Bu}}$N3CH** was also observed when the reaction was carried out in CD_2Cl_2, CD_3CN, or in CD_2Cl_2/toluene-d_8, suggesting that **^{t}BuN$_3$CH** does not result from H-atom abstraction from the solvent or benzylic protons, as would be anticipated for the formation of free aryl radical.

Scheme 3.12. Oxidatively-Induced Reductive Elimination of Ar–Br Bonds

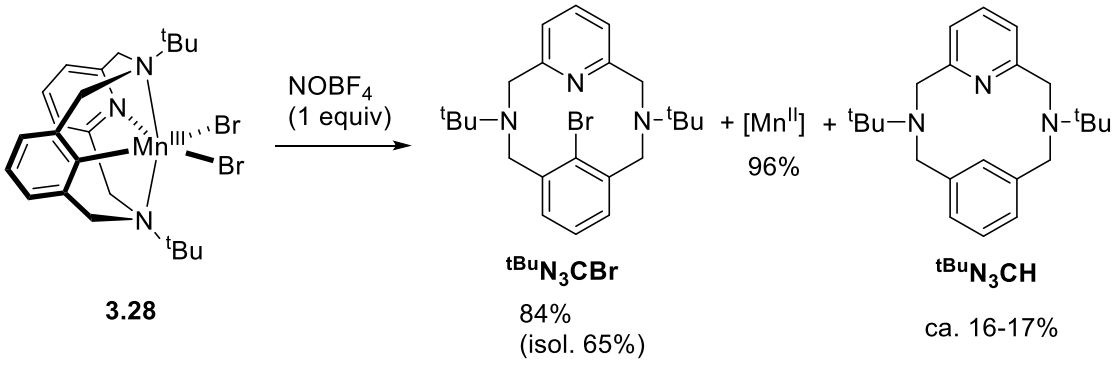

3.28

To examine the product containing Mn, the reaction mixture resulting from the treatment of **3.28** with 1.1 equivalents of $NOBF_4$ in MeCN solution was diluted with water and subjected to analysis using electron paramagnetic resonance (EPR) spectroscopy. The EPR spectrum recorded at 298 K exhibits a distinctive sextet at g = 2.01 (A = 95 G), which is characteristic of Mn^{2+} salts showing hyperfine splitting from ^{55}Mn (I = 5/2) (see **Figure 3.4**). This spectrum closely resembles that of $[Mn(H_2O)_6]^{2+}$ obtained by dissolving manganese(II) sulfate in water. By using spin integration against a standard solution of $MnSO_4$, we were able to estimate the yield of Mn^{2+} salt as 96% based on an average of two experimental runs.

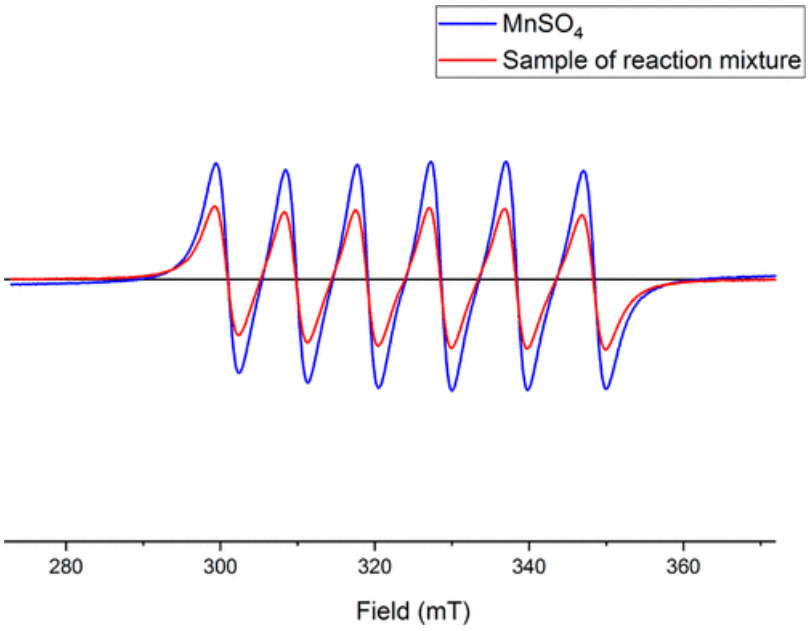

Figure 3.4. X-band EPR spectra of H_2O-diluted sample from oxidation of **3.16** with 1.1 equiv of $NOBF_4$ (red) and reference sample of $MnSO_4$ in H_2O (blue) at 298 K.

We next examined whether reductive elimination could proceed in the presence of other oxidants. Reaction of **3.28** with 1.1 equiv of arylaminium radical "Magic Blue" led to the formation of organic product $^{t\text{Bu}}$**N3CBr** in 56% yield after 12 h. The analogous reaction with H_2O_2 resulted in $^{t\text{Bu}}$**N3CBr** in 37% yield. Overall, these experiments suggest that the aryl-bromide elimination can be achieved by using different oxidants not specific to $NOBF_4$.

Next, to understand the mechanism of this reaction, we carried out the experiments in the presence of TEMPO that could trap carbon-based radicals. However, no TEMPO adduct was detected in NMR spectroscopy and GC-MS analysis, and the isolated yield of aryl-bromide elimination product was not changed significantly in 78-82% yield, suggesting that free Ar radical formation does not play a significant role. The aryl-bromide elimination in the

presence of 1-decene did not produce any products of bromination of 1-decene, proving no involvement of either Br_2 or free Br radical in the reaction. We then tried to detect proposed Mn^{IV} intermediates by a variable temperature UV-Vis spectroscopy at -78 to 20 °C in acetonitrile; however, no intermediates were detected.

3.2.3 Synthesis of aryl-Mn^{III} fluoro complexes

Next, we focused on synthesizing aryl-Mn^{III} fluoro complexes to study the possibility of C-F bond elimination mediated by manganese complexes. Based on the previous literature, our first efforts to obtain Mn^{III} aryl fluoro-complexes by reacting complex **3.28** with an excess amount of silver fluoride or other fluoride salts; however, none of the efforts led to the formation of the desired product and the starting complex **3.28** remained unreacted. Based on our previous study showing that complex **3.28** undergoes transmetalation using common organolithium, Grignard, and organozinc reagents and then reductive elimination to form C-C coupling product,[121] we then treated the complex **3.28** with a common bis(trifluoromethyl) zinc precursor $[Zn(CF_3)_2(DMPU)_2]$[122] supported by two DMPU ligands. Interestingly, instead of obtaining Mn^{III}-CF_3 complexes or aryl-CF_3 reductive elimination product, treating **3.28** with 2 equiv. of $[Zn(CF_3)_2(DMPU)_2]$ in methanol at room temperature for 16 hours resulted in the formation of difluoro Mn^{III} complex **3.29**, which was isolated as a purple crystalline solid in 74% yield. Complex **3.29** was characterized by single crystal X-ray diffraction (SC-XRD), UV-Vis and IR spectroscopy, electrospray ionization high-resolution mass spectrometry (ESI-HRMS) and elemental analysis. SC-XRD revealed that **3.28** is a bimetallic complex, where one fluoride acts as a bridging ligand between manganese and zinc atoms. The Mn atom showed a distorted octahedral geometry and was surrounded by a $^{t\text{Bu}}$N3C$^-$ ligand coordinating in a tetradentate fashion and two fluorides.

Similar to the structure of **3.28**, the Mn-$N_{pyridine}$ bond distance in **3.29** (2.0536(17) Å) are shortened compared to the Mn-N_{amine} distances (2.3932(18) and 2.3933(17) Å). The bond distance of manganese and a bridging fluoride ligand is 1.9645(12) Å), which is slightly longer than the bond distance of Mn and terminal fluoride (1.9125(13) Å). SC-XRD showed the distorted tetrahedral structure in Zn atom, which is surrounded by two bromides, one fluoride, and a methanol ligand. The presence of protonated methanol coordinating the Zn atom rather than a methoxyl group was confirmed by SC-XRD, with the hydrogen's position determined by the Fourier difference maps. The Zn-O bond distance is 2.0125(17) Å, which was consistent with typical tetrahedral Zn-methanol bond length (1.97-2.05 Å)[123-126], while the Zn-O distance in Zn-methoxide complex is significantly shorter (1.80-1.90 Å)[127-130]. According to SC-XRD, one methanol molecule was co-crystallized in the complexes which binds to the terminal [Mn−]F atom and the O atom of the methanol co-ligand through hydrogen bond. The magnetic moment measured by the Evans method of complex **3.29** in dichloromethane was 4.82 μB, suggesting an S = 2 ground state corresponding to a high-spin d^4 configuration for the Mn^{III} center.

Scheme 3.13. Synthesis of **3.29** and **3.30**. Isolated yields are shown in parentheses.

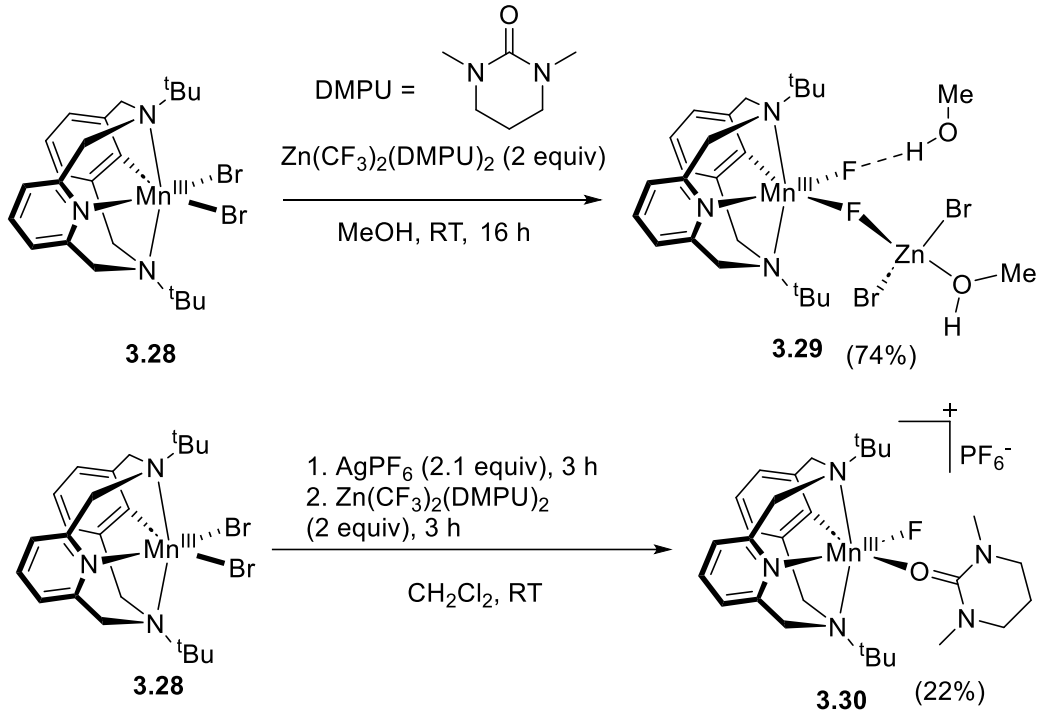

Next, complex **3.28** was treated with 2.1 equiv. of $AgPF_6$ in dichloromethane in order to remove the bromides, and then 2 equiv. of $[Zn(CF_3)_2(DMPU)_2]$ was added, which led to the formation of cationic monofluoride complex **3.30**. Complex **3.30** was isolated as a red crystalline solid in 22% yield and was characterized by SC-XRD, ESI-HRMS, elemental analysis and UV-Vis and IR spectroscopies. According to SC-XRD, complex **3.30** is a cationic complex with PF_6^- present as a counteranion. The X-ray structure of **3.30** reveals a distorted octahedral geometry around Mn^{III} center surrounded by three N-donors, an aryl, one fluoride and one DMPU ligand. Similar to complexes **3.28** and **3.29**, the Mn-Namine bond distances are 2.4081(13) and 2.4033(13) Å, which is longer than the Mn-$N_{pyridine}$ distance (2.049(13) Å), while the Mn-C_{ipso} bond length is 1.9990(15) Å. The Mn-F bond distance in complex **3.30** is 1.8578(9) Å, shorter than the Mn-F bonds in complex **3.29**, likely due to the cationic nature of the complex. Similar to complex **3.29**, complex **3.30** is paramagnetic with the effective magnetic moment measured by Evans method in dichloromethane solution is 4.71 μB, suggesting an $S = 2$ ground state and a high-spin d^4 configuration of the Mn^{III} center.

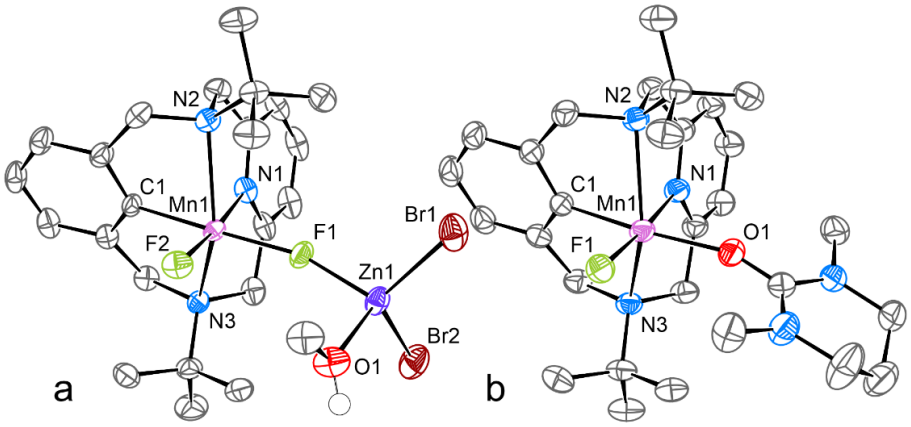

Figure 3.5. ORTEP of **3.29** (a) and **3.30** (b) at the 80% and 60% probability levels, respectively. The hydrogen atoms (except for [O]H), solvent molecules, and PF_6^- anion (for **3.30**) are omitted for clarity.

Table 3.1. Selected bond distances [Å] for complexes **3.29** and **3.30** in the crystals according to SC-XRD.

Complex	Mn1–N1	Mn1–N2	Mn1–N3	Mn1–C1	Mn1–F1	Mn1–F2	Mn1–O1
3.29	2.0536(17)	2.3932(18)	2.3933(17)	1.9933(19)	1.9645(12)	1.9125(13)	N/A
3.30	2.0490(13)	2.4081(13)	2.4033(13)	1.9990(15)	1.8578(9)	N/A	2.0197(12)

*N/A: not applicable.

After having full characterization of complexes **3.29** and **3.30**, we next examined if these complexes could undergo aryl-fluoride reductive elimination. However, our attempts to promote aryl-fluoride reductive elimination under heating, light irradiation or in the presence of oxidant did not lead to the formation of aryl-F bond elimination product; the starting compound remained unreacted or decomposed in all cases. On the other hand, the cyclic voltammograms of complex **3.29** and complex **3.30** showed that the oxidation potentials are comparable with the aryl-Mn^{III} dibromo complex **3.28**, suggesting that the aryl-fluoride elimination in these Mn^{III}-F complexes cannot be achieved likely due to its high-kinetic barrier but not the inaccessibility of oxidized species.

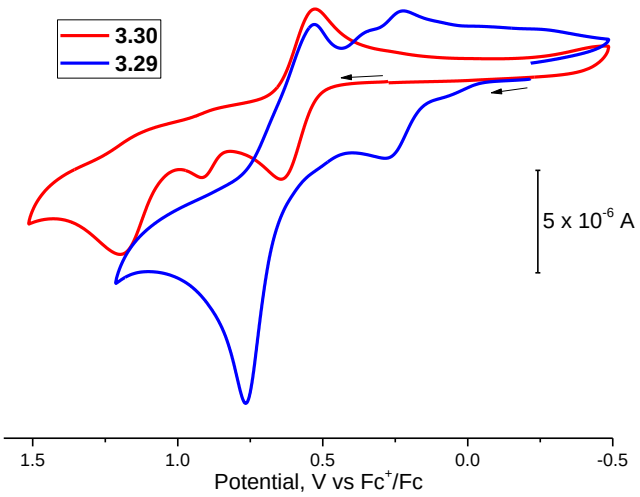

Figure 3.6. Cyclic voltammograms of **3.29** (blue) and **3.30** (red) in 0.1 M $^{n}Bu_4NPF_6$/MeCN at 25 °C (concentration 1 mM, scan rate 50 mV s^{-1}; 1.6 mm Pt disk working electrode; the arrow indicates the initial scan direction).

3.2.4 Difluorocarbene Trapping Experiments and Proposed Mechanism of Mn^{III} Fluoride Formation

Although we could not detect or organomanganese intermediates or fluoro-organic byproducts of Mn^{III} fluoride complex formation directly, the reaction of **3.28** with $[Zn(CF_3)_2(DMPU)_2]$ likely occur via initial transmetalation to form unstable Mn^{III} trifluoromethyl intermediate.[92, 94, 121, 131] The unstable intermediate undergoes to an α-F elimination to form manganese(III) fluoride complex and carbene generation, which is similar to the decomposition pathways in unstable trifluoromethyl or perfluoroalkyl of main group metals. For example, trifluoromethyl lithium or trifluoromethyl magnesium iodide was reported to decompose even at low temperatures to form tetrafluoroethylene, presumably via dimerization of difluorocarbene generated by α-F elimination. [132-133] Similarly, heptafluoropropyl lithium decomposes to form lithium fluoride and

hexafluoropropene.[133] When the temperature is above 5 °C, bis(trifluoromethyl)cadmium $Cd(CF_3)_2$ decomposes to CdF_2 and the release of difluorocarbene.[134] In 2020, the Finze group demonstrated the preparation of perfluoroethylaluminate complexes and their decomposition via α-F elimination with the loss of carbene $CF(CF_3)$.[135] The trifluoromethyl zinc precursor $[Zn(CF_3)_2(DMPU)_2]$ has been known to generate difluorocarbene, although heating condition is required.[136] To the best of our knowledge, α-F elimination reactivity has not been previously reported for organomanganese complexes.

By analogy with previous literature, we hypothesized that the α-F elimination occurred at Mn-CF_3 intermediate would lead to the generation of difluorocarbene. To test our hypothesis, the synthesis of complex **3.29** was carried out in the presence of 4 equiv of 1,1-diphenylethylene as a difluorocarbene trap for 16 h at RT, led to the formation of 2,2-difluoro-1-phenylcyclopropyl)benzene in 22% yield, which was confirmed by ^{19}F NMR and GC-MS analysis (**Scheme 3.14**a). This experiment confirms the difluorocarbene generation during the preparation of **3.29**. At the same time, the control experiment using $[Zn(CF_3)_2(DMPU)_2]$ without the presence of Mn complex **3.29** resulted in only 4% yield of (2,2-difluoro-1-phenylcyclopropyl)benzenes, indicating that the background reactivity of zinc reagent only has a minor contribution for the generation of difluorocarbene. On the other hand, treating manganese salts like $Mn^{III}(OAc)_3$ or $Mn^{III}(acac)_3$ (acac=acetylacetonate) with 2 equiv. of $[Zn(CF_3)_2(DMPU)_2]$ in the presence of 1,1-diphenylethylene under similar conditions did not result in the formation of difluorocyclopropanation product after 16 hours, suggesting the important role of ^{tBu}**N3C**$^-$ pyridinophane ligand to promote α-F elimination and difluorocarbene generation.

In order to eliminate the possibility of CF_3 radical generation from Mn-C bond homolysis, we tried to trap CF_3 radical by performing the synthesis of **3.29** in the presence of 2 equiv. of (2,2,6,6-tetramethylpiperidin-1-yl)oxyl (TEMPO) radical trap in 24 hours; however no TEMPO-CF_3 adduct was detected by ^{19}F NMR spectroscopy, arguing against the CF_3 radical formation (**Scheme 3.14b**)

Scheme 3.14. a. Difluorocarbene trapping by 1,1-diphenylethylene. b. Attempted radical trapping with TEMPO.

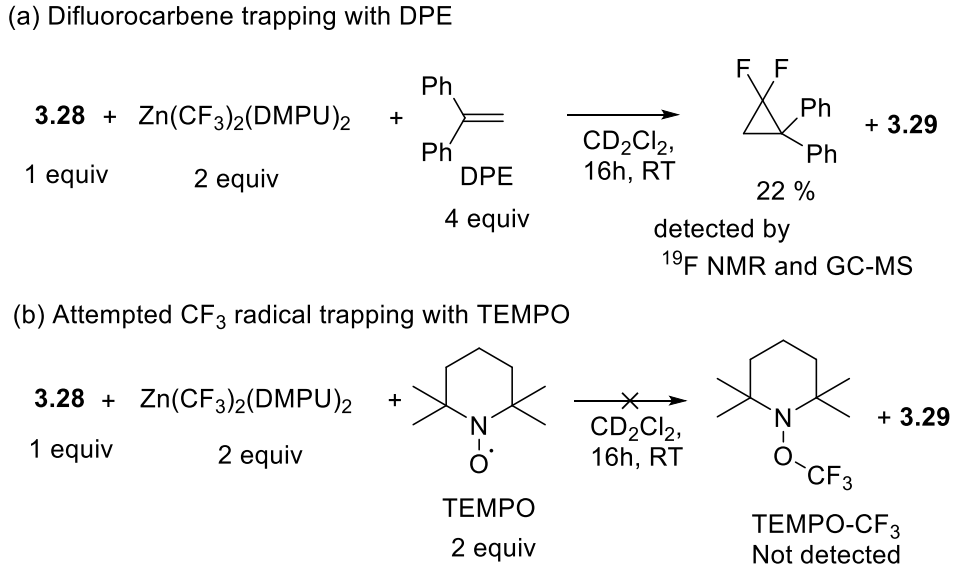

Based on these experiments, the mechanism of Mn^{III}–F in complexes **3.29** and **3.30** formation is proposed via the transmetalation from Zn-CF_3 precursor to form an unstable Mn^{III}-CF_3 intermediate, followed by α–F elimination to generate Mn^{III} fluoride and difluorocarbene (**Scheme 3.15**). While the production of **3.30** needs the transmetalation of

only one Mn^{III}-Br bond, the second bromide is eliminated by $AgPF_6$; the formation of **3.29** most likely requires two transmetalation steps to replace both Mn^{III}-Br bonds.

Scheme 3.15. Proposed mechanism of the formation of **3.29.**

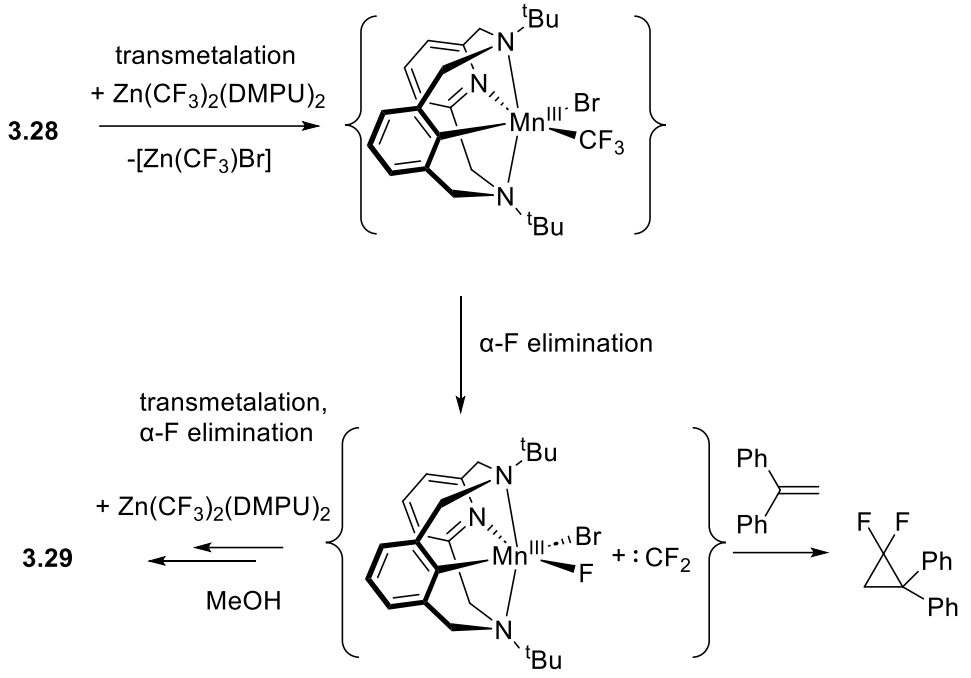

3.2.5 The Effect of Mn^{III} On Difluorocyclopropanation and Cyclopropenation of Alkenes and Alkynes

Considering that the synthesis of **3.29** and **3.30** generated difluorocarbene under mild condition without any additives, we next tried to take advantage of this reactivity in difluorocyclopropanation and difluorocyclopropenation of alkenes and alkynes.

Based on our experiments which trapped difluorocarbene by 1,1-diphenylethylene at room temperature in the presence of Mn^{III} complex **3.28**, we anticipated that transmetalation to Mn^{III} from Zn could promote more facile difluorocarbene formation as compared to the zinc reagent $[Zn(CF_3)_2(DMPU)_2]$ alone and then accelerate difluorocyclopropanation of alkene with $[Zn(CF_3)_2(DMPU)_2]$ under milder conditions. To test that hypothesis, α-methylstyrene was chosen as a model substrate to react with $[Zn(CF_3)_2(DMPU)_2]$ as a trifluoromethyl group source in the presence or absence of $(^{tBu}N3C)Mn^{III}Br_2$ complex **3.28** at room temperature or at mild-heating condition. The reaction of α-methylstyrene with 2 equiv. of $[Zn(CF_3)_2(DMPU)_2]$ in the presence of 1 equiv. of **3.28** at room temperature for 12 hours resulted in the formation of difluorocyclopropanated product **3.Ib** in low yield (14%, entry 1, **Table 3.2**), whereas no reactivity was observed in the absence of **3.28** at the analogous conditions. Heating α-methylstyrene with 2 equiv of $[Zn(CF_3)_2(DMPU)_2]$ in the presence of 1 equiv of **3.28** in toluene at 60 ºC for 4 h yield difluorocyclopropanation product **3.Ib** in 84% yield (entry). For comparison, the analogous reaction in the absence of **3.28** at 60 ºC for 4 h gave **3.Ib** in only 8% (entry 4). On the other hand, the reaction with the presence of 1 equiv of **3.28** at 60 ºC for shorter time (2 h) yields only 66% of the product (entry 5). Only low yields of **3.Ib** were obtained when MeCN, THF or dichloromethane was used as a solvent instead of toluene, while using strongly coordinating solvents (DMF, DMSO) failed to give any product.

Table 3.2. Optimization for difluorocyclopropanation mediated by complex **3.28**.

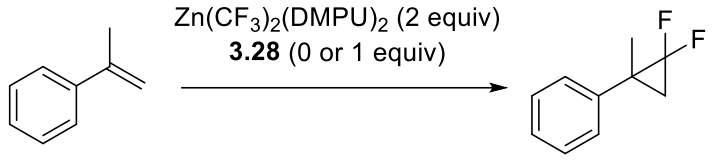

3.Ia **3.Ib**

Entry	Solvent	T (ºC)	Amount of **1** (equiv)	Time (h)	Yield of **3.Ib** (%)[a]
1	Toluene	RT	1	12	14
2	Toluene	RT	0	12	0
3	Toluene	60	1	4	84
4	Toluene	60	0	4	8
5	Toluene	60	1	2	66
6	Toluene	60	0	2	6

[a]Yield was determined by NMR integration using fluorobenzene as an internal standard. Typical conditions: α-methylstyrene (0.01 mmol), [$Zn(CF_3)_2(DMPU)_2$] (0.02 mmol), **1** (0.01 mmol), toluene (0.5 mL) in a sealed reaction tube.

After getting an optimal condition, we then tested the reactivity with other substrates like alkenes or terminal alkynes in a standard condition using a **substrate** : **2** : **1** molar ratio of 1 : 2 : 1 in toluene at 60 °C for 4 hours. In all cases, the yields were compared for the reaction in the presence and absence of **3.28**. The highest yields were observed in the cases of electron-rich substrates, giving 84-67% for **3.Ib** – **3.IVb**. as compared to 23-50% in the absence of **3.28**, showing moderate yield enhancement in the presence of **3.28**. At the same time, when electron-deficient halogenated substrates **3.Vb** – **3.VIIIb** were used, only trace amount of cyclopropanated product was obtained in the absence of **3.28**. More pronounced difference in reactivity was observed in the presence of **3.28**, although at the sacrifice of synthetic yield. The yield could not be further improved at longer reaction time. On the other hand, no cyclopropanated product was obtained when unactive alkyne such as cyclohexene was used both with or without the presence of **3.28** under standard conditions.

In summary, this study indicates that a Mn^{III} complex **3.28** shows moderate enhancement in difluorocyclopropanation of alkenes and alkynes when using $Zn(CF_3)_2(DPMU)_2$ complex, increasing the yield at least two-fold compared to the similar condition in the absence of Mn. While the practical utility of Mn^{III} in difluorocyclopropanation catalysis may be limited, these findings suggest the potential of Mn^{III} perfluoroalkyl compounds as reactive species in carbene transfer reactivity.

Scheme 3.16. Scope of difluorocarbenation mediated by **3.28**. Yield in the bracket is the yield of the control experiment without the presence of **3.28**. [a] reaction was conducted at 80 °C for 4 h.

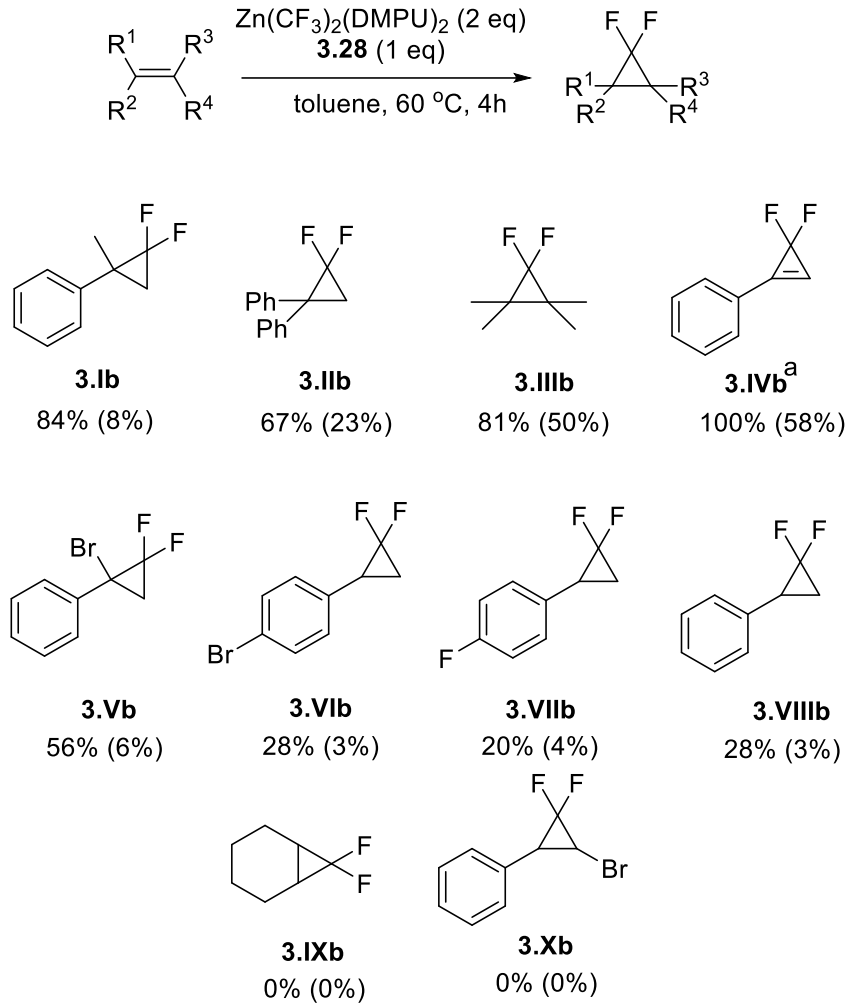

3.3. Conclusion

In conclusion, we reported a stable monoaryl Mn^{III} bromo complexes synthesized via oxidative addition of Ar-Br bond to a Mn^{I} precursor $Mn(CO)_5Br$. In the presence of one-electron oxidation, the complex undergoes facile non-radical reductive elimination, resulting in Ar-Br bond formation and the release of Mn^{II} species. These studies therefore provided the first example of observation of Ar-X oxidative addition to Mn^{I} followed by oxidatively-induced Ar-X reductive elimination. Although these steps could not be connected to a catalytic cycle due to lack of accessible pathways to recycle Mn^{II} product into reactive Mn^{I} species, it provided clear evidence that these elementary steps may be observed at the single Mn center.

Driven by the initial intent to obtain Mn^{III} trifluoromethyl complexes to study C-C reductive elimination, we unexpectedly uncovered a new way of preparation of high-valent manganese(III) neutral difluoro and cationic monofluoro complexes using trifluoromethyl zinc reagent under mild conditions. Compared to the trifluoromethyl zinc complex, the proposed trifluoromethyl manganese(III) intermediated are more reactive and undergo more facile α-fluoride elimination to yield Mn^{III} fluorides and release difluorocarbene, which was detected by a trapping experiment.

Such more facile difluorocarbene generation from Mn^{III} results in moderate enhancement of difluorocyclopropanation and difluorocyclopropenation of alkenes and alkynes using

trifluoromethyl zinc reagent at lower temperature (20 – 60 °C) and shorter reaction time (4 h), suggesting potential application of perfluoroalkyl manganese(III) complexes as reactive agents for carbene transfer reactivity.

3.4. Experimental section

Below experimental data is reported in the following publications:

1. Sarbajna, A.; He, Y.-T.; Dinh, M. H.; Gladkovskaya, O.; Rahaman, S. M. W.; Karimata, A.; Khaskin, E.; Lapointe, S.; Fayzullin, R. R.; Khusnutdinova, J. R., Aryl–X Bond-Forming Reductive Elimination from High-Valent Mn–Aryl Complexes. *Organometallics* **2019**, *38*, 4409-4419.

2. Dinh, M. H.; He, Y.-T.; Fayzullin, R. R.; Vasylevskyi, S.; Khaskin, E.; Khusnutdinova, J. R. Synthesis of Aryl-Manganese(III) Fluoride Complexes via α-Fluorine Elimination from CF3 and Difluorocarbene Generation. *Eur. J. Inorg. Chem.* **2023***, 26* (32)*,* e202300460.

General considerations

All reactions were performed using standard Schlenk or glovebox techniques under a dry argon or nitrogen atmosphere if not indicated otherwise. Unless noted otherwise, all chemicals were purchased from major commercial suppliers (TCI, Sigma-Aldrich, and Nacalai-Tesque) and used without further purification. Anhydrous solvents were dispensed from an MBRAUN solvent purification system and degassed prior to use. Anhydrous deuterated solvents were purchased from Eurisotop and stored over 4 Å molecular sieves. **^{tBu}N3CBr** ligand was synthesized according to previously reported procedure with some modifications.[105] Complex $[Zn(CF_3)_2(DMPU)_2]$[122] were prepared according to the literature procedures. NMR spectra were recorded on a JEOL ECS400S 400 MHz and JEOL ECZ600R 600 MHz. The following abbreviations are used for describing NMR spectra: s (singlet), d (doublet), t (triplet). A typical Evans method magnetic moment measurement was done in a coaxial tube containing the solvent and the internal standard. Electrospray ionization high-resolution mass spectrometry (ESI-HRMS) measurements were performed on a Thermo Scientific ETD apparatus using MeOH or MeCN as a solvent for injection. Gas chromatography/mass spectrometry (GC-MS) analysis was performed using a Shimadzu GCMS-QP2010 equipped with a Shimadzu SH-Rxi-1 ms 30-meter column. Elemental analyses were performed using an Exeter Analytical CE440 instrument. Solid-state FT-IR spectra were recorded using an Agilent Cary 630 with an ATR module in an argon-filled glovebox. UV-vis spectra were recorded on an Agilent Cary 60 spectrophotometer. The X-ray diffraction data for single crystals **3.28**–**3.30** was recorded on a Rigaku Xtalab Pro diffractometer or a Bruker D8 Venture diffractometer.

Synthesis of ^{tBu}N3CBr

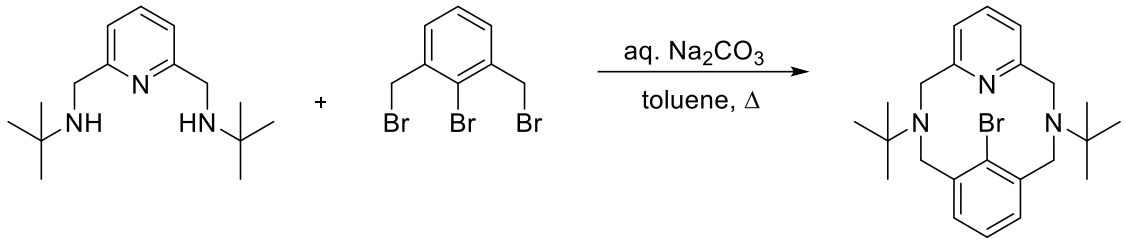

^{tBu}N3CBr

A single neck round bottomed flask was charged with mixture of 100 mL of toluene, 40 mL of 10% (w/w) Na_2CO_3 solution and 2,6-bis(tert-butylaminomethyl)pyridine (2.18 g, 8.74 mmol, 1 equiv). The flask was supplemented with 2-neck extension; one neck was connected to reflux condenser, and the other one with an additional funnel. The reaction mixture is heated up to 80 °C under nitrogen atmosphere. A solution of 2-bromo-1,3-bis(bromomethyl)benzene (2.70 g, 7.88 mmol, 0.9 equiv) in 100 mL of toluene was added dropwise through the addition funnel to the reaction mixture over the course of 3 hours. Afterwards, the temperature was adjusted to 90 °C and the reaction was left to stir for 20 hours. After completion, the reaction was cooled down and transferred to separation funnel. The aqueous layer was discarded and the pale-yellow toluene layer was washed 3 times with saturated K_2CO_3 and dried over anhydrous $MgSO_4$ for 10 min. The solvent was removed under vacuum and the solid residue was washed with a minimal amount of methanol and filtered off. The insoluble part was collected and dried to give a pure product, typical yield 1.45 g (3.34 mmol, 43%). NMR spectra were consistent with those reported in the literature.[105]

^{1}H NMR (400 MHz, $CDCl_3$), δ: 7.13 (t, J = 7.5 Hz, 1H, ArH), 6.79 (d, J = 7.5 Hz, 2H, ArH), 6.74 (d, J = 7.5 Hz, 2H, ArH), 6.60 (t, J = 7.5 Hz, 1H, ArH), 4.20-4.10 (m, 4H, two CH_2 groups), 4.04 (d, J = 12.8 Hz, 2H, CH_2), 3.57 (d, J = 13.2 Hz, 2H, CH_2), 1.32 (s, 18H, *t*Bu).

^{1}H NMR (400 MHz, C_6D_6), δ: 6.96 (t, J = 7.5 Hz, 1H, ArH), 6.88 (d, J = 7.5 Hz, 2H, ArH), 6.70 (d, J = 7.5 Hz, 2H, ArH), 6.61 (t, J = 7.5 Hz, 1H, ArH), 4.38 (d, J = 12.7 Hz, 2H, CH_2), 4.02 (d, J = 13.4 Hz, 2H, CH_2), 3.95 (d, J = 12.7 Hz, 2H, CH_2), 3.85 (d, J = 13.4 Hz, 2H, CH_2), 1.12 (s, 18H, *t*Bu).

Synthesis of ($^{t\text{Bu}}$N3C)$Mn^{III}Br_2$ (3.28)

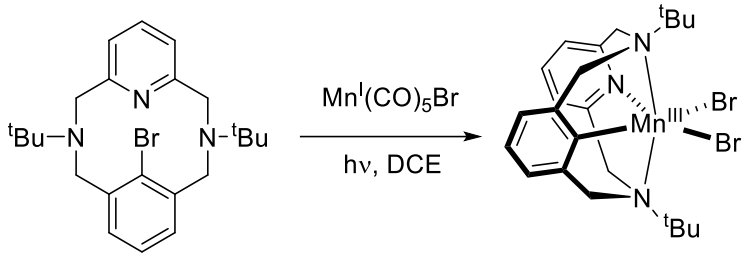

$^{t\text{Bu}}N_3CBr$ **3.28**

First, 410 mg of $^{t\text{Bu}}$**N3CBr** ligand (0.952 mmol) and 261.4 mg of $Mn(CO)_5Br$ (0.951 mmol) were combined in a flame-dried Schlenk flask inside a glovebox, and 20 mL of dichloroethane was added to give a yellow suspension. The flask was taken outside the glovebox and stirred in a water bath in front of a mercury lamp. The reaction vessel was subjected to vacuum for 1 s every hour, then stirred under static vacuum, and after 3 h, the reaction was then stirred under a static vacuum overnight. After 13 h, the solution appeared wine-red, and all the solvent evaporated under reduced pressure. The solid obtained was redissolved in a minimal amount of dichloromethane and filtered through Celite. The filtrate obtained was evaporated under reduced pressure to yield a red solid which was washed three times with copious amounts of diethyl ether (≈ 15 mL) and then dried to yield **3.28**. Deep red crystals were grown by vapor diffusion of diethyl ether into a dichloromethane solution of the complex (about 6 mL of DCM). Yield of isolated product 310 mg (0.548 mmol), 58%. The product was recrystallized second time to give 260 mg of the crystalline product as large dark-red crystals (0.460 mmol).

UV–vis, λ, nm (ε, $M^{-1}\cdot cm^{-1}$), CH_2Cl_2: 547 (560), 430 (620, sh), 383 (1720), 270 (10 200).

μ_{eff} = 4.98 μB (298 K, Evans method, CD_2Cl_2).

FT-IR (ATR, solid, cm^{-1}): ν 3049 (w), 2972 (w), 2008 (w), 1926 (w), 1598 (w), 1575 (w), 1457 (w), 1430 (w), 1267 (s), 1194 (w), 849 (w), 731 (s), 701 (m).

^{1}H NMR (CD_2Cl_2, 400 MHz, 25 °C), δ: 47.80 (br), 36.55 (br), 23.73 (br), 11.38, 3.73, 3.42, 1.29, 1.14, 0.87, 0.08, −20.49 (br), −105.21 (br), −154.97 (br).

ESI-HRMS in CH_3CN (*m*/*z*): calculated for $[C_{23}H_{32}BrN_3Mn]^+$, ($[M\text{-}Br]^+$, *z* = 1): 484.1155. Found: 484.1149.

Anal. Calcd for $Mn_1C_{23}H_{32}Br_2N_3$: C, 49.02; H, 5.72; N, 7.46. Found: C, 49.01; H, 5.75; N, 7.47.

Oxidation of 3.28 by 2 equiv of $NOBF_4$ in MeCN and Crystallization of the Co-Crystal of $^{t\text{Bu}}$N3CBr with $Mn(MeCN)_6^{2+}$ and NO^+ and BF_4^- Counterions

First, 56.3 mg (0.1 mmol) of **3.28** was weighed out in a scintillation vial inside a glovebox, and 5 mL of acetonitrile was added. To the red solution was added 1.1 equiv (for ESI-MS measurements) or 2 equiv (for crystallization) of $NOBF_4$ in one portion, and the mixture was allowed to stir for 2 h and analyzed by ESI-MS. The resulting yellow solution was concentrated to ca. 2 mL and filtered through a small pad of Celite, and crystals of the adduct were grown by vapor diffusion of ether into the filtrate.

Isolation of $^{t\text{Bu}}$N3CBr Product after Oxidation

First, 56.3 mg (0.1 mmol) of **3.28** was weighed out in a scintillation vial inside a glovebox, and 5 mL of dichloromethane was added. To the red solution was added 12.2 mg (0.11 mmol)

of $NOBF_4$ in one portion, and the mixture was allowed to stir for 2 h over which time period the color of the solution gradually changed to yellow and the reaction stopped. The solvent was then completely removed under vacuum, and the yellow solid was dried completely. The vial was then taken out of the glovebox, and 5 mL of a saturated solution of K_2CO_3 was added to it and vigorously stirred for 30 min. Initially, some effervescence is seen, and gradually a dark brown precipitate appears. The aqueous solution was extracted with dichloromethane, filtered, and then dried over anhydrous $MgSO_4$. The dichloromethane was completely evaporated by a rotavapor, and the solid left behind was identified to be $^{t\text{Bu}}$**N3CBr**. NMR yield was confirmed by adding 1,3,5-trimethoxybenzene (0.33 mmol) to the $CDCl_3$ solution. Analytically pure $^{t\text{Bu}}$**N3CBr** could be isolated by a short flash column chromatography in 3:97 methanol/dichloromethane mixture. *In situ* yield (before chromatography) was found to be 84% based upon internal standard, whereas isolated yields were averaged to be 65% based on average three runs.

Isolation of $^{t\text{Bu}}$**N3CBr** was performed after reaction in CH_2Cl_2 solution, since attempted isolation from CH_3CN even after evaporation of the solvent leads to partial transferring of the paramagnetic species (presumably solvated Mn^{2+} ion) into the organic layer even after treatment with a base, leading to broadening of NMR spectra. ^{1}H NMR (400 MHz, $CDCl_3$), δ: 7.13 (t, J = 7.6 Hz, 1H, ArH), 6.79 (d, J = 7.5 Hz, 2H, ArH), 6.74 (d, J = 7.6 Hz, 2H, ArH), 6.60 (t, J = 7.4 Hz, 1H, ArH), 4.19–4.10 (m, 4H, two CH_2 groups), 4.04 (d, J = 12.8 Hz, 2H, CH_2), 3.57 (d, J = 13.3 Hz, 2H, CH_2), 1.32 (s, 18H, *t*Bu). ^{13}C NMR (101 MHz, $CDCl_3$), δ: 160.05, 138.88, 135.04, 131.54, 131.08, 125.69, 121.38, 56.78, 55.94, 54.47, 27.85. ESI-(HR)MS (first most intense peak): *m*/*z* 430.1837 (calcd $[M + H]^+$, $C_{23}H_{33}N_3Br$, *m*/*z* 430.1852).

Quantitative Determination of a Mn^{2+} Product by Spin Integration

Standard 10.0 mM $MnSO_4$ solution in water was prepared for comparison of spin integration values. Measurements were performed in quartz precision capillary tubes (50 μL) at RT; microwave frequency 9114 MHz.

First, 14.1 mg (25 μmol) of **3.28** was dissolved in 4 mL of acetonitrile, and 3.2 mg (1.1 equiv) of $NOBF_4$ was added and stirred for 1 h. Next, a 1000 μL aliquot of this solution was taken and diluted to 10 mL by addition of 9 mL of water in a volumetric flask to give a final solution with a final expected concentration of Mn species of 0.625 mM.

EPR measurements were performed at RT in quartz thin capillary tubes. Spin integration was compared for the reaction mixture and the standard $MnSO_4$ solution. The measurements were performed two times, and the average of two runs was used. The concentration of Mn^{2+} in the final solution was calculated as 0.601 mM corresponding to the yield of 96% as an average of two trials.

The sextet corresponding to Mn^{2+} species obtained from the reaction mixture was observed at g = 2.01 and shows hyperfine splitting to ^{55}Mn (I = 5/2; A = 95 G). An identical signal was obtained by dissolving $MnSO_4$ in water (g = 2.01, A = 95 G).

Synthesis of 3.29

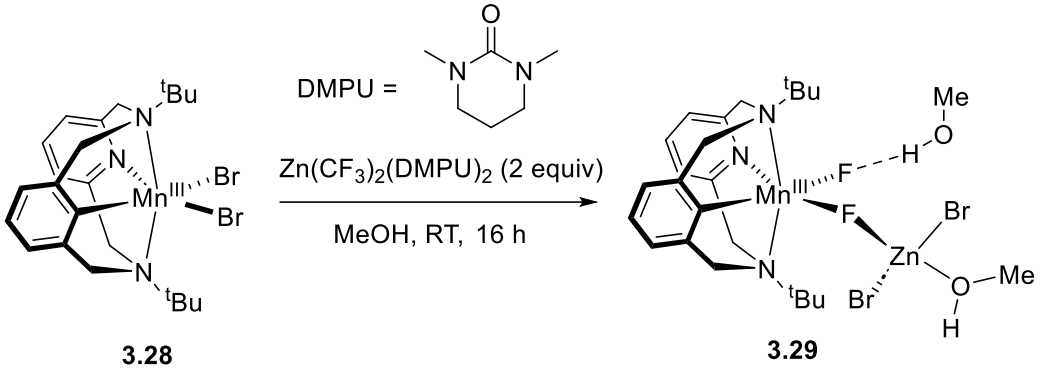

3.28 **3.29**

In the glove box, 56.3 mg of **3.28** (0.100 mmol) was dissolved in 4.0 mL methanol and stirred at room temperature for 10 minutes. 91.6 mg of $[Zn(CF_3)_2(DMPU)_2]$ (0.200 mmol – 2 equiv) was added to the mixture, and then the reaction was further stirred at room temperature for 16 hours. During this time, the solution color changed to purple from wine-red. The resulting mixture was filtered through a pad of celite. Purple crystals were grown by vapor diffusion of diethyl ether into the obtained solution to produce **3.29**. Yield: 54.0 mg (74%).

μ_{eff} = 4.82 μB (298 K, Evans method, CD_2Cl_2).

ESI-HRMS in MeOH (*m/z*): calculated for $[C_{23}H_{32}F_2N_3Mn]^+$, ($[M - F]^+$, z = 1): 424.1955; found: 424.1958.

EA found (calc.): $MnZnC_{24}H_{36}Br_2F_2N_3O$: C 40.88 (41.14), H 5.26 (5.18), N 5.76 (6.00).

UV-vis (CH_2Cl_2), λ, nm (ε, M^{-1} m^{-1}): 549 (340), 363 (1330), 234 (8071).

FT-IR (ATR, solid, cm^{-1}): ν 3070 (w), 2975 (w), 2787 (w), 1603 (w), 1464 (w), 1249 (s), 1015 (s), 910 (w), 853 (w), 726 (s).

Synthesis of [(^{tBu}N3C)Mn(DMPU)F]PF_6 3.30

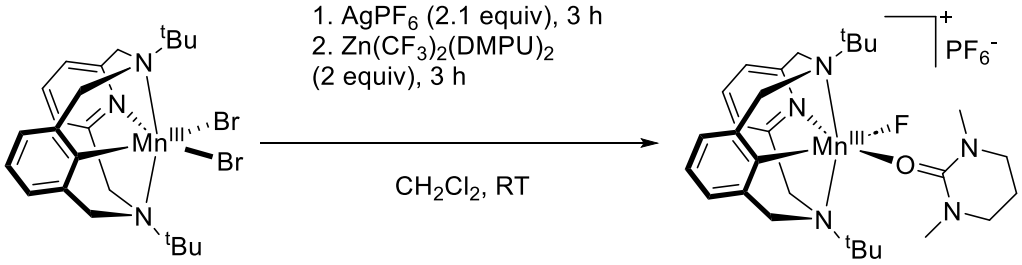

3.28 **3.30**

In the glove box, 56.5 mg (0.100 mmol) of **3.28** was dissolved in 10 mL of dichloromethane, and 53.0 mg (0.210 mmol, 2.1 equiv) of $AgPF_6$ was added and stirred for 3 hours in the dark. The AgBr salt was filtered off through a pad of celite to give a yellow-colored solution. To the obtained solution, 91.9 mg (0.200 mmol, 2.0 equiv) of $[Zn(CF_3)_2(DMPU)_2]$ was added. The resulting mixture was stirred for 3 hours and then filtered through a pad of celite to give a deep red solution. Red crystals were grown by vapor diffusion of ether into THF solution of the complex. The desired complex **3.30** was obtained in 22% yield (15 mg) after recrystallization.

μ_{eff} = 4.71 μB (294 K, Evans method, CD_2Cl_2).

ESI-HRMS (*m/z*), calculated for $[(^{tBu}N3C)MnF]^+$ ($C_{23}H_{32}F_1Mn_1N_3$): *m/z* observed (cald): 424.1980 (424.1955).

EA found (calc.): $C_{29}H_{44}F_7MnN_5O_1P$: C 49.34 (49.93), H 5.86 (6.36), N 9.65 (10.04).

UV-vis (CH_2Cl_2), λ, nm (ε, M^{-1} m^{-1}): 554 (1585), 363 (6185).

FT-IR (ATR, solid, cm^{-1}): 2960 (br), 2890 (br), 1578 (s), 1564 (s), 1480 (m), 1422 (m), 1323 (m), 1226 (m), 1194 (m), 1068 (m), 834 (s), 724 (s), 702 (m).

Observation of difluorocarbene formation

In the glove box, 7.1 mg of **3.28** (0.013 mmol), 11.5 mg of $[Zn(CF_3)_2(DMPU)_2]$ (0.025 mmol – 2 equiv), and 1,1-diphenylethylene (0.05 mmol – 4 equiv) were dissolved in 0.5 mL of CD_2Cl_2. To the solution, 4.7 μL of fluorobenzene (0.05 mmol – 4 equiv) was added as an internal standard. The resulting mixture was stirred for 24 hours. The formation of the product 1,1-difluoro-2,2-diphenyl cyclopropane was identified by GC-MS and comparison of NMR spectra with the literature reports. [137] The yield of 1,1-difluoro-2,2-diphenyl cyclopropane was determined by ^{19}F NMR integration against fluorobenzene as an internal standard.

Radical trap experiment

In the glove box, 7.1 mg of **3.28** (0.013 mmol), 11.5 mg of $[Zn(CF_3)_2(DMPU)_2]$ (0.025 mmol – 2 equiv), and 3.9 mg of (2,2,6,6-tetramethylpiperidin-1-yl)oxyl (TEMPO) (0.025 mmol – 2 equiv) were dissolved in 0.5 mL of CD_2Cl_2. To the solution, 4.7 μL of fluorobenzene (0.05 mmol – 4 equiv) was added as an internal standard. The resulting mixture was stirred for 24 hours and then analyzed by ^{19}F NMR spectroscopy. No TEMPO–CF_3 adduct was found.

Attempted difluorocarbene detection in the presence of $Mn^{III}(OAc)_3$ and $Mn^{III}(acac)_3$ (acac=acetylacetonate)

In the glovebox, 0.013 mmol of $Mn(OAc)_3$ or $Mn(acac)_3$, 11.5 mg of $[Zn(CF_3)_2(DMPU)_2]$ (0.025 mmol – 2 equiv), and 1,1-diphenylethylene (0.05 mmol – 4 equiv) were dissolved in 0.5 mL of CD_2Cl_2. To the solution, 4.7 μL of fluorobenzene (0.05 mmol – 4 equiv) was added as an internal standard. The resulting mixture was stirred at RT for 16 hours. 1,1-difluoro-2,2-diphenyl cyclopropane product was not detected in ^{19}F NMR spectroscopy or GC-MS.

Cyclodifluoropropanation mediated by 3.28, general procedure

In the glove box, 9.2 mg (0.02 mmol – 2 equiv) of $[Zn(CF_3)_2(DMPU)_2]$ and 5.7 mg of **1** (0.01 mmol – 1 equiv) were combined in an 11 mL screw-cap reaction tube. To the reaction tube, 0.01 mmol of alkene and 0.5 mL of toluene were added. The tube was then sealed by electric tape to avoid gas exchange and brought out of the glove box. The tube was heated at 60 °C for 4 hours. After the completion of the reaction, 1.9 μL of fluorobenzene (0.02 mmol – 2 equiv) was added to the mixture as an internal standard and the resulting mixture was analyzed by NMR and GC-MS spectroscopy. The formation of the difluorocyclopropanation product was identified by GC-MS and comparison of NMR spectra with earlier literature reports.[137] The yields were determined by ^{19}F NMR integration against fluorobenzene.

Chapter 4. Photoinduced Perfluoroalkylation Mediated by Cobalt Complexes Supported by Naphthyridine Ligands

The content described in this chapter is partially reported in the following publication:[138] Reprinted and adapted with permission from Dinh, M. H.; Govindarajan, R.; Deolka, S.; Fayzullin, R. R.; Vasylevskyi, S.; Khaskin, E.; Khusnutdinova, J. R. "Photoinduced Perfluoroalkylation Mediated by Cobalt Complexes Supported by Naphthyridine Ligands" *Organometallics*, **2023**, *42*, 2632-2643. Copyright 2023 American Chemical Society.

Declaration of Contribution: Prof. Julia R. Khusnutdinova guided the project. I (Hoan M. Dinh) synthesized and characterized all complexes, performed the reactivity and catalytic activity of cobalt complexes in photo-induced perfluoroethylation, as well as conducted the computational calculations. Dr. Ramadoss Govindarajan helped with ligand synthesis. Dr. Shubham Deolka synthesized the first complex. Dr. Eugene Khaskin performed X-ray data collection. Dr. Robert R. Fayzullin and Dr. Serhii Vasylevskyi finalized X-ray structural measurement to publication level.

All of the figure, table and scheme **4.24** – **4.30** in this chapter are from this publication.[138]

4.1. Introduction

In the previous chapter, we described the attempted synthesis of manganese(III) trifluoromethyl complexes via transmetalation, which instead results in difluorocarbene elimination likely due to intrinsic reactivity of manganese(III) perfluoroalkyl derivatives formed as intermediates. The lack of available coordination sites at Mn center supported by a tetradentate chelating ligand likely hindered its catalytic reactivity; however, it has shown the potential of using inexpensive and earth-abundant first-row metals as catalyst for the synthesis of fluorine-containing organic compounds. These results have further prompted us to study a wider range of first-row metal complexes with simple N-donor ligands as catalyst for the synthesis of fluorinated compounds, either via difluorocarbene transfer or fluoroalkyl group incorporation. For this purpose, we have stepped away from macrocyclic tetradentate ligands and examined the reactivity of first-row metal complexes with other types of N-heterocycle-based ligands, eventually leading to the development of photoinduced Co-catalyzed perfluoroalkylation described in this chapter.

4.1.1 Trifluoromethylation mediated by first-row transition metal

The incorporation of the fluoroalkyl group into bioactive compounds has a significant role in pharmaceuticals and agrochemicals, which can modulate the properties of the compounds such as lipophilicity, membrane permeability, binding selectivity, and avoid unwanted metabolic degradation.[139-141]

C-H trifluoromethylation mediated by first-row metal complexes, particularly with nickel and copper, as an alternative for precious metals has recently gained significant attention. For example, in 2015, Sanford and coworkers reported a bis(trifluoromethyl) nickel(IV) complex **4.3** supported by tris(pyrazolyl)borate (Tp) ligand.[142] The complex was synthesized via oxidation of Ni^{II}-CF_3 complex **4.1** using aryliodonium salts at -35 ^oC or oxidation of Ni^{II}-CF_3 complex **4.2** by Umemoto reagent at room temperature. At 55 ^oC, the complex undergoes reductive elimination to yield (trifluoromethyl)benzene and release Ni(II) complexes. (**Scheme 4.1**)

Scheme 4.1. Synthesis pathways of nickel(IV) complex **4.3** and its reductive elimination to form benzotrifluoride

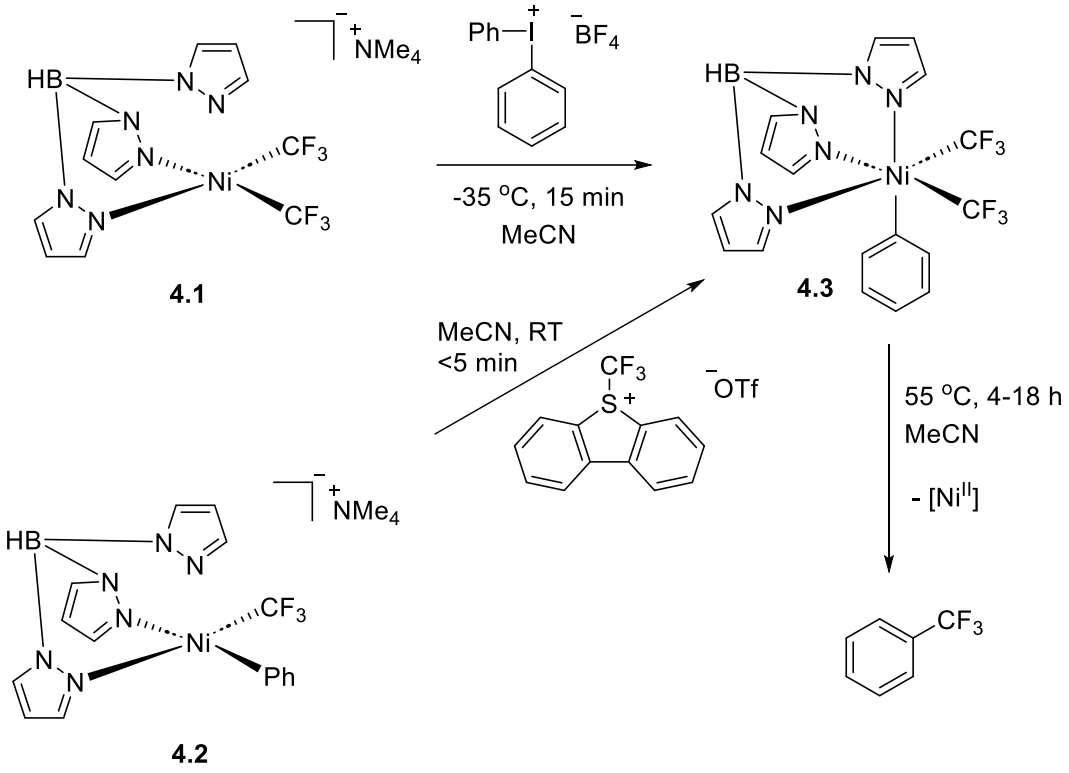

Later, the same group reported the synthesis of $TpNi^{III}$ complexes **4.4** with phenyl and trifluoromethyl group via one-electron oxidation of $TpNi^{II}$ complex **4.2**.[143] Upon heating to 80 °C for 5 min, the complex undergoes reductive elimination to form trifluoromethylated arene. (**Scheme 4.2**)

Scheme 4.2. Synthesis of nickel(III) complex **4.4** and its reductive elimination at 80 °C to from benzotrifluoride

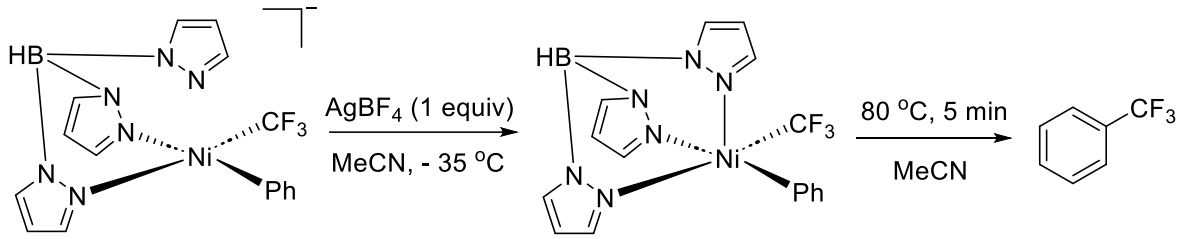

In 2017, Sanford and coworkers reported the synthesis of Ni^{IV}-CF_3 complex **4.6** by the reaction between Ni^{IV}-$OC(O)CF_3$ complex **4.5** in the presence of excess amount of tetramethylammonium fluoride.[143] Upon heating to 70 °C for 12 hours, the complex underwent aryl-CF_3 reductive elimination to form nickel(II) complex **4.7**. (**Scheme 4.3**)

Scheme 4.3. Synthesis of trifluoromethyl nickel(IV) complex **4.6** and its reductive elimination to functionalize co-ligand.

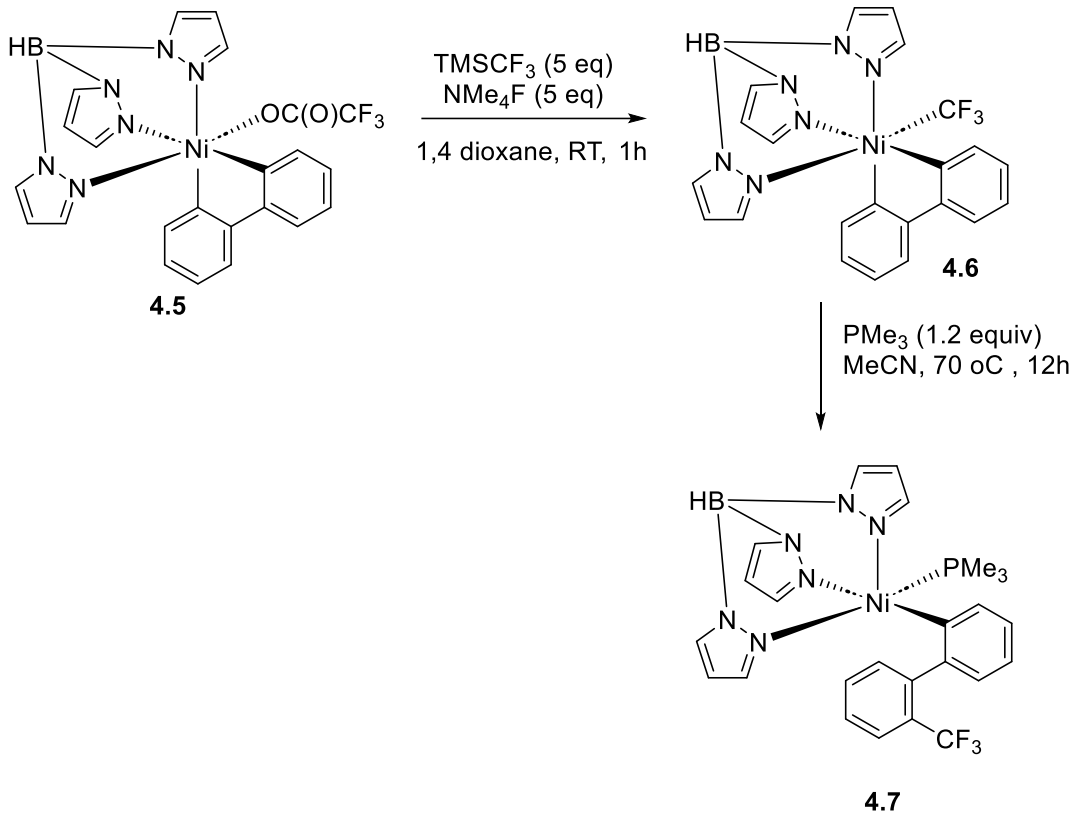

The same year, the Nebra group reported a preparation of Ni^{IV}-CF_3 complex supported by simple pyridine ligands and its application in stoichiometric trifluoromethylation.[113] Treatment of $Ni(CF_3)_2(py)_2$ with one equiv. of XeF_2 led to the formation of mono- and dimeric Ni^{III} complexes **4.9** and **4.8**. Addition of one more equiv. of XeF_2 resulted in the formation of Ni^{IV} complex **4.10**. The complex **4.10** can also be synthesized by reacting $Ni(CF_3)_2(py)_2$ with 2 equiv. of XeF_2 at low temperature. This complex **4.10** has shown C-H activation of 1,2-dichlorobenzene under room temperature in 3 days to form trifluoromethylated adducts with 94% yield. (**Scheme 4.4**)

Scheme 4.4. Synthesis of Ni^{III} and Ni^{IV} complex supported by monodentate pyridine ligands.

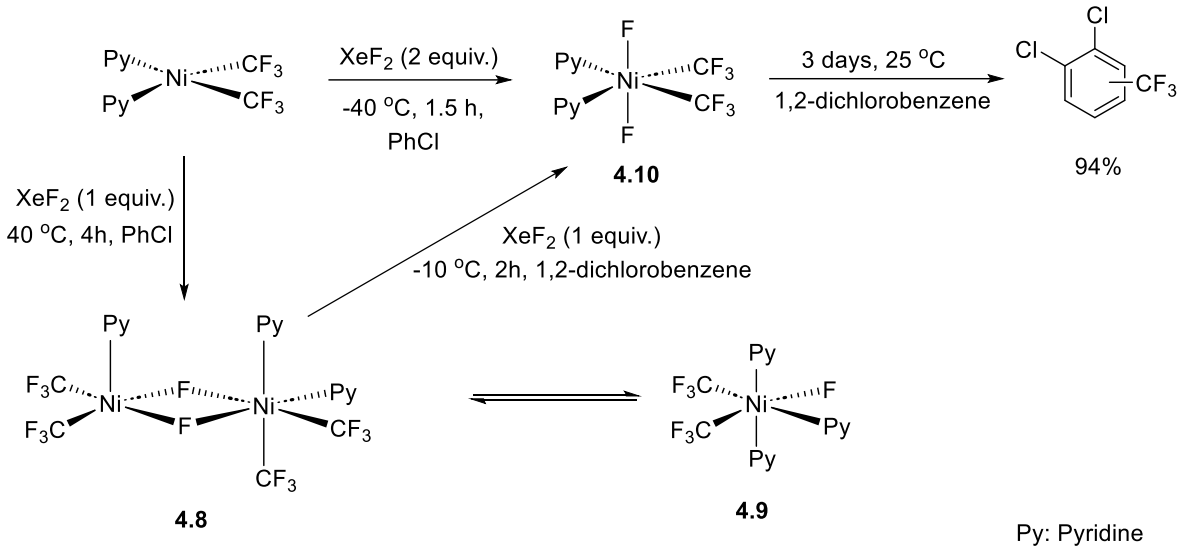

In 2019, the Sanford group demonstrated the first catalytic methodology for trifluoromethylation by high-valent nickel(IV) complexes.[144] By using 5 mol% of (Tp)Ni^{IV}-CF_3 complex **4.11** loading, the trifluoromethylation using Umemoto reagent II as an oxidant and trifluoromethyl group source was operated at room temperature in DMSO with the yield up to 99%. This protocol can be applied to late-stage trifluoromethylation of biologically active molecules such as melatonin, Boc-L-tryptophan, resorcinol, and tadalafil. The mechanism studies were carried out by both experiments and DFT calculations, and they supported the radical pathway with the involvement of Ni^{II}–CF_3, Ni^{III}–CF_3, and Ni^{IV}–CF_3 intermediates. (**Scheme 4.5**)[144]

Scheme 4.5. Trifluoromethylation of arenes using Umemoto's reagent catalyzed by Ni^{IV} complex **4.11**.

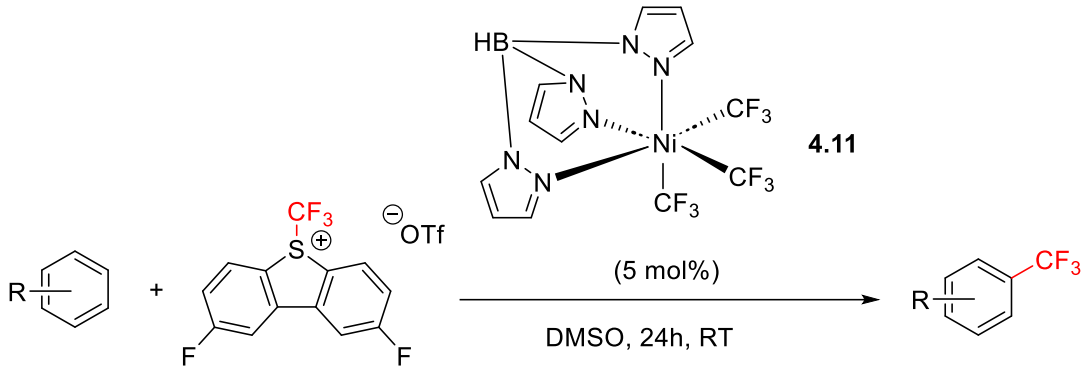

In 2020, the Vicic group reported the synthesis of anionic nickel(II) tris(trifluoromethyl) (**4.12**) and nickel(II) tetrakis(trifluoromethyl) (**4.13**). This was achieved through the reaction of $NiBr_2$(glyme) with an excess of in situ $AgCF_3$ in the presence of PPh_4Cl. The subsequent reaction of anionic nickel complex **4.12** with an aryl iodonium salt resulted in the formation of trifluoromethylated arene, likely facilitated by a high-valent oxidation state of nickel. The plausibility of the proposed intermediate was validated by reacting another anionic nickel precursor, **4.13**, with potassium persulfate as an oxidant, leading to the formation of a Ni^{IV} complex, **4.14**.[145]

Scheme 4.6. a. Synthesis of anionic tris(trifluoromethyl) and tetrakis(trifluoromethyl) nickel(II) complex **4.12** and **4.13**. b. Reaction of complex **4.12** with an aryl iodonium salt to form trifluoromethylated product. c. Synthesis of nickel(IV) complex **4.14**

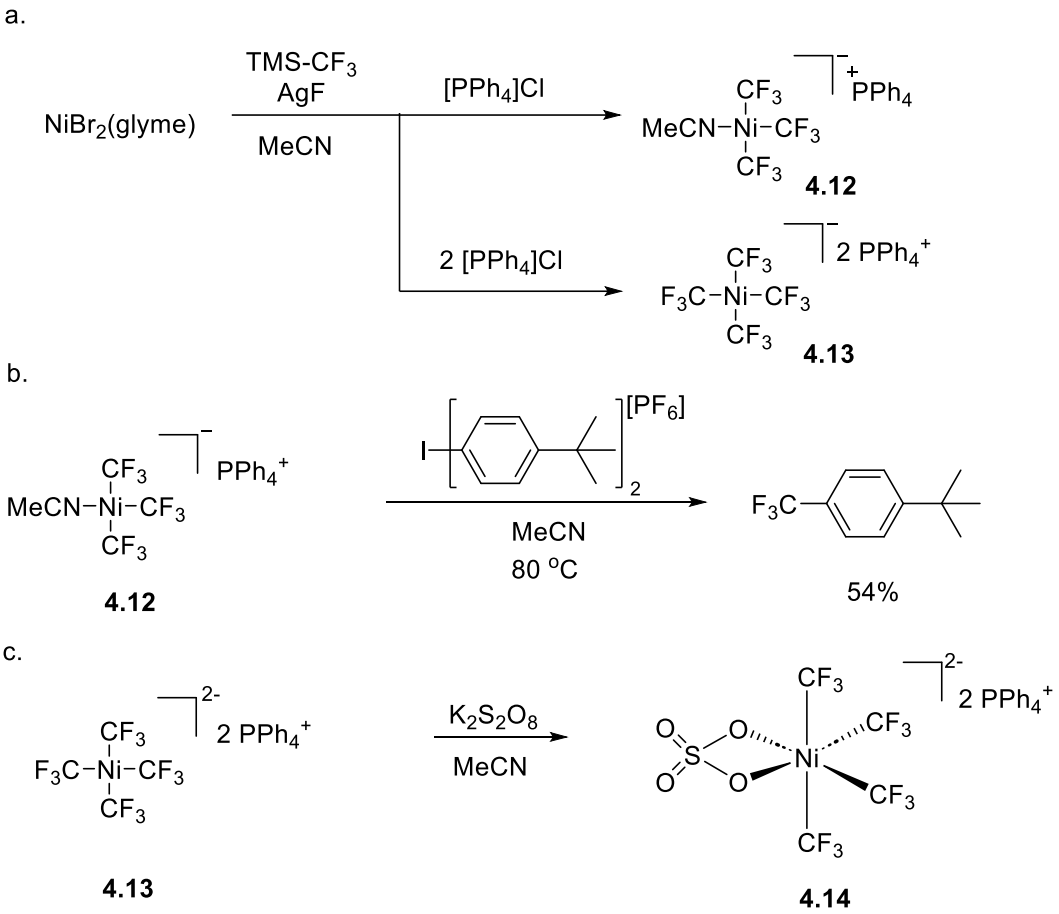

In 2021, Vicic and coworkers reported the preparation of high-valent tetrakis(trifluoromethyl)nickel(IV) complex **4.15** by reacting anionic nickel(II) complex **4.13** with "magic blue" as an oxidant. The authors also reported that the nickel(II) precursor **4.13** can play as a catalyst for trifluoromethylation of arenes and heteroarenes by Umemoto reagent II in good yield. The mechanism was proposed through a radical pathway with the involvement of Ni^{IV} intermediate.[146]

Scheme 4.7. a. Synthesis of solvated tetrakis(trifluoromethyl) nickel(IV) complex and b. Trifluoromethylation of arenes using Umemoto's reagent catalyzed by anionic Ni(II) complex **4.13**.

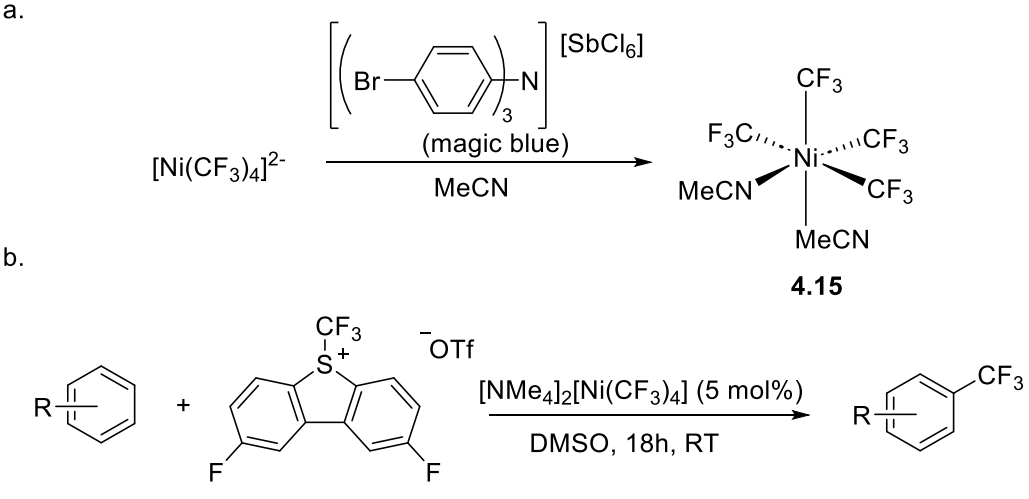

Copper has also shown much promise in trifluoromethylation. In the beginning, most of the examples of copper-mediated trifluoromethylation were carried out through the in-situ generation of "Cu^{I}-CF_3" species.[147-150] In 2008, the first example of a well-defined trifluoromethyl copper(I) complex was reported by the Vicic group.[151] Treatment of tert-butoxide copper complex supported by unsaturated NHC-carbene ligand with $TMSCF_3$ led to the formation of a mixture of two Cu^{I}-CF_3 complexes **4.16** and **4.16b**, where the silylated complex **4.16** is a major product. On the other hand, the analogous reaction of tert-butoxide copper dimer supported by saturated NHC-carbene ligands **4.17** with 2 equiv. of $TMSCF_3$ led to the exclusive formation of Cu^{I}-CF_3 complex **4.18** with 91% isolated yield. The authors also showed the application in trifluoromethylation of halogenated arenes mediated by complex **4.18** generated in situ in DMF at room temperature with the yield up to 99%. (**Scheme 4.8**)

Scheme 4.8. Synthesis of Cu^{I}-CF3 complex supported by NHC-carbene ligands

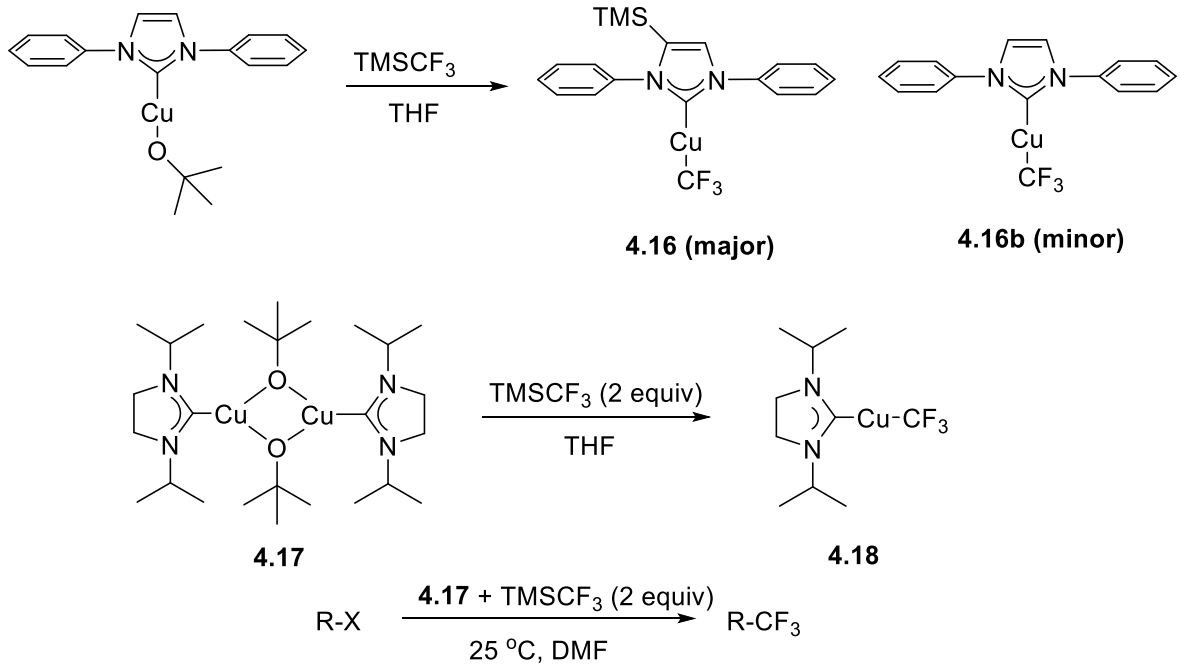

In 2011, Hartwig and coworkers disclosed the preparation of $Cu^{I}(CF_3)$(phen) complexes **4.19** (phen = 1,10-phenanthroline) by reaction of copper(I) tert-butoxide with 1,10-phenanthroline, followed by the addition of TMS-CF_3.[152] Heating complex **4.19** in the presence of halogenated arenes at 50 °C for 18 hours led to the formation of trifluoromethylated products. (**Scheme 4.9**)

Scheme 4.9. Stoichiometric trifluoromethylation of halogenated arenes mediated by (phen)Cu^{I}-CF_3 complexes **4.19**.

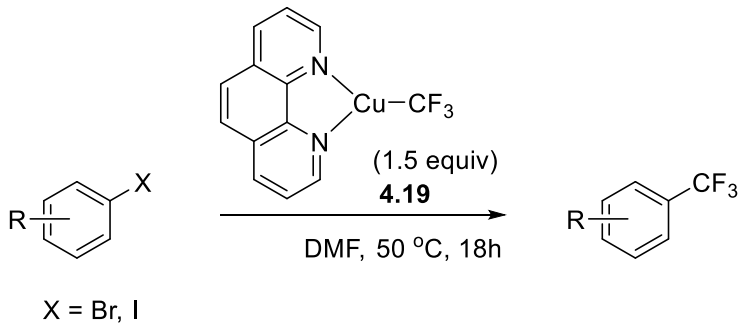

The same year, the Grushin group reported the synthesis of air-stable Cu^{I}-CF_3 complexes 4**.20** supported by triphenylphosphine ligands.[153] The complex was prepared by reaction of $CuF_2.3H_2O$ with triphenylphosphine in methanol, followed by the addition of $TMSCF_3$. The phosphine ligands are labile, which was proved by the ligand exchange reaction with 1,10-phenanthroline (phen) to yield Cu^{I} complex **4.21**. Both complexes **4.20** and **4.21** were proven as good trifluoromethylation reagents of aryl and heteroaryl iodides. (**scheme 4.10**)

Scheme 4.10. Synthesis of phosphine-stabilized copper(I)-CF3 complexes.

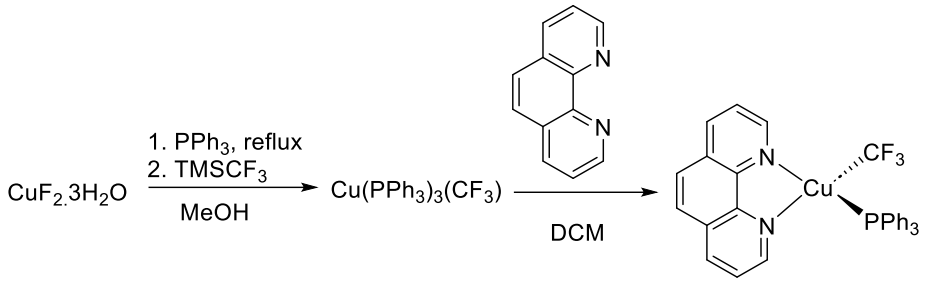

4.20 **4.21**

High-valent trifluoromethyl copper(III) complexes have also gained a lot of attention since they have frequently been proposed as key intermediates for reductive elimination in copper-catalyzed coupling reactions.[154-155] The first isolation and characterization of copper(III) complexes was reported by Burton and coworkers in 1989, where oxidation of anionic $[Cu^{I}(CF_3)_2]^-$ by thiuramdisulphide led to the formation of square-planar $Cu^{III}(CF_3)_2$(dithiocarbamate) complex.[156] This complex performed stoichiometric trifluoromethylation of halogenated arenes at 90-100 ºC. Later, by using halogen to oxidize in situ Cu^{I} trifluoromethyl complex, Naumann and coworkers reported the synthesis and characterization of anionic square planar $[Cu^{III}(CF_3)_4]^-$ complexes.[157] The synthesis of this complex was optimized by the Grushin group by treating CuCl with $TMSCF_3$ in the presence of KF under air as an oxidant.[158]

In 2016, Zhang and coworkers reported the synthesis and characterization of tris(trifluoromethyl) copper(III) complexes supported by bidentate phen or bpy ligand.[159] These complexes were obtained by treating copper(I) iodide with an excess amount of $TMSCF_3$ and AgF in the presence of the respective ligand. The authors demonstrated the reactivity of copper(III) complex **4.22** in stoichiometric trifluoromethylation of boronic acid derivatives mediated at room temperature. In contrast, the reaction of bipyridine-supported complex **4.23** with aryl boronic acids required heating conditions at 50 ºC. (**Scheme 4.11**)

Scheme 4.11. Synthesis of tris(trifluoromethyl) copper(III) complexes **4.22** and **4.23** and stoichiometric trifluoromethylation of boronic acid derivatives mediated by these complexes

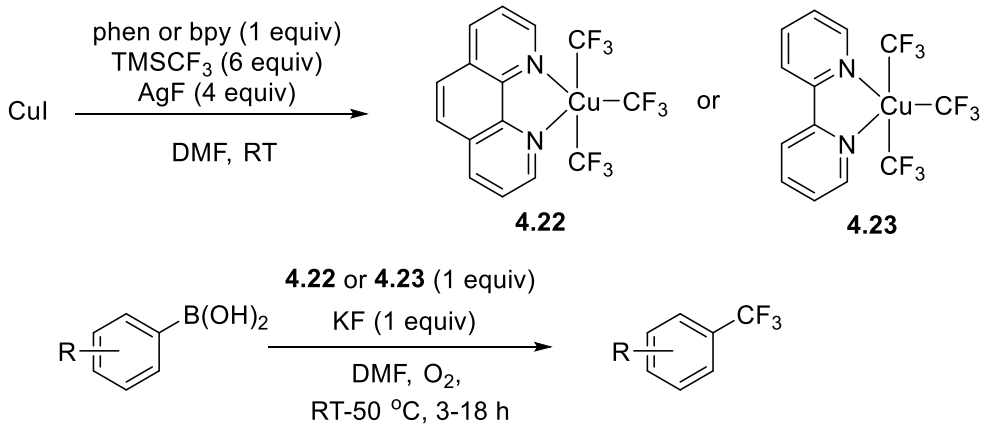

Scheme 4.12. a. structure of Cu^{III}-CF_3 complexes **4.24–4.27** supported by mono-, bi- and tridentate ligands. b. trifluoromethylation of boronic acid derivatives and terminal arylacetylenes mediated by copper(III) complexes. c. s*yn*-fluoro- and -oxy-trifluoromethylation of alkynes mediated by copper(III) complexes **4.24**.

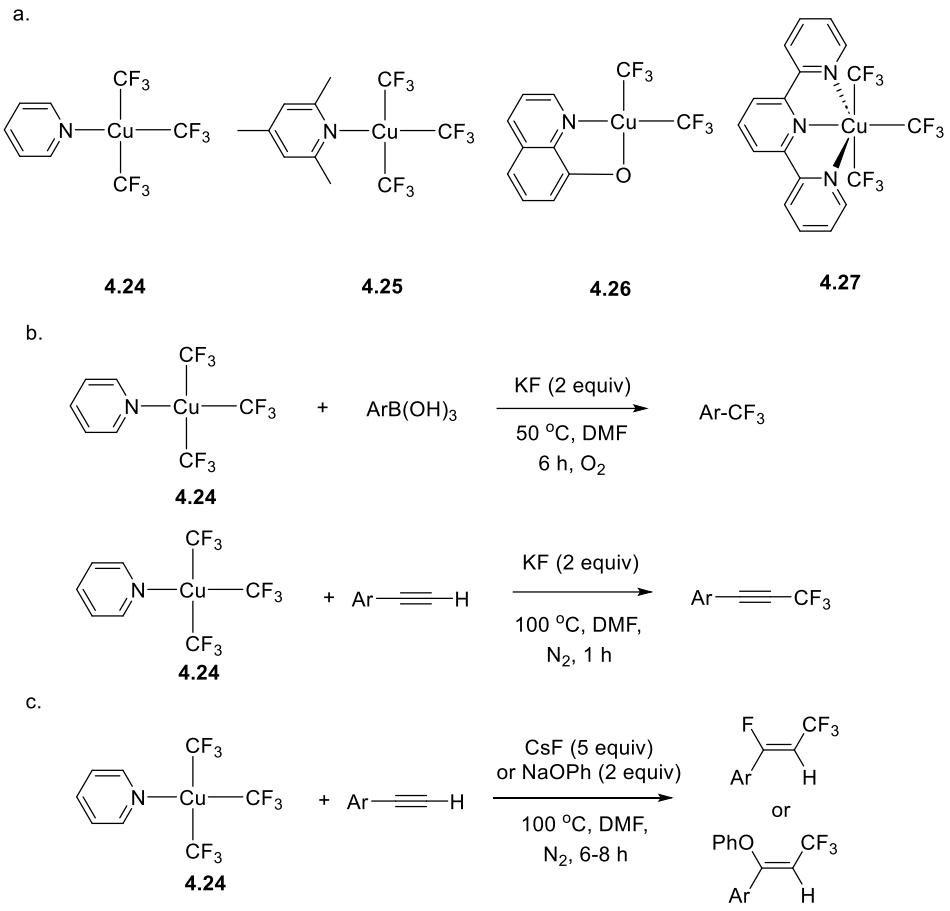

In 2018, Zhang and coworkers reported the synthesis of a new set of Cu^{III}-CF_3 complexes **4.24–4.27** supported by mono-, bi- and tridentate ligands.[160] These complexes showed good reactivity to trifluoromethylation of boronic acid derivatives or terminal arylacetylenes, as well as s*yn*-fluoro- and -oxy-trifluoromethylation of alkynes. (**Scheme 4.12**)

In 2019, the Liu group demonstrated the synthesis of [alkyl-Cu^{III}-$(CF_3)_3$]$^-$ complexes by reaction of $Cu^{III}(CF_3)_3$(py) (py = pyridine) with alkyl zinc reagent in acetonitrile at room temperature for 5 min.[161] Upon heating to 50 °C for 2 hours, these alkyl-$Cu^{III}(CF_3)_3$ undergoes alkyl-CF_3 reductive elimination to form trifluoromethylated adducts and Cu(I) species. The authors also demonstrated the application of these complexes in late stage trifluoromethylation of high functionalized organozinc reagents. (**Scheme 4.13**)

Scheme 4.13. Synthesis of [alkyl-Cu^{III}-$(CF_3)_3$]$^-$ complex **4.28** and its reductive elimination reaction.

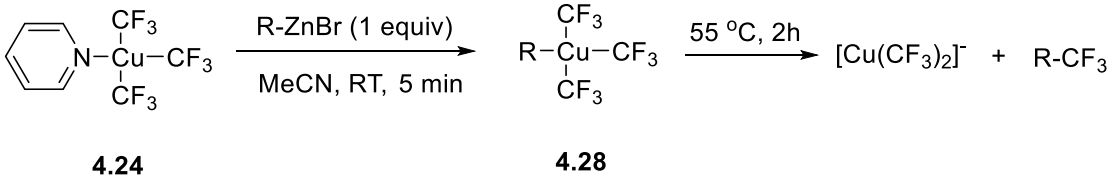

In the same year, Shen and coworkers reported the preparation of [aryl-Cu^{III}-$(CF_3)_3$]$^-$ complexes by treating $Cu(CF_3)_3$(bpy) **4.23** with aryl pinacolyl boronate in the presence of Cs_2CO_3 and $^nBu_4NBr$.[162] Heating the complex in dichloroethane at 95% for 4-12 hours, the complexes underwent C(sp^2)-CF_3 reductive elimination to generate trifluoromethylated

arene and Cu^{I} species. Mechanistic studies, including kinetic experiments and DFT calculations, revealed that the reductive elimination occurred via a three-membered ring transition state. (**Scheme 4.14**)

Scheme 4.14. Synthesis of [aryl-Cu^{III}-$(CF_3)_3$]$^-$ complex **4.29** and its reductive elimination.

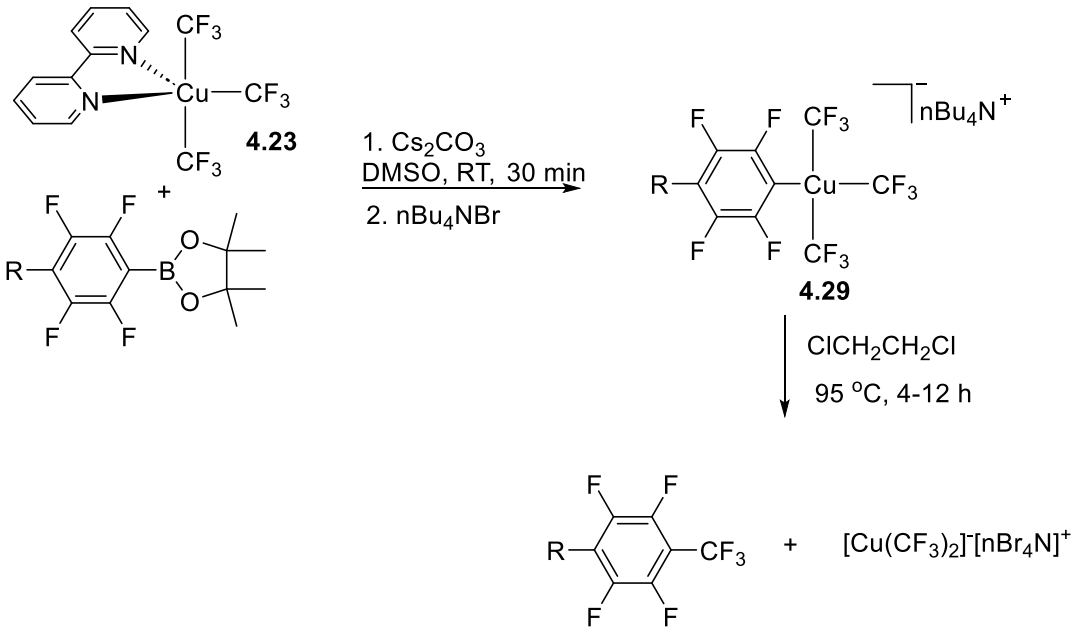

Scheme 4.15. Synthesis and reductive elimination reactivity of neutral of neutral five-coordinate organocopper(III) complex **4.30.**

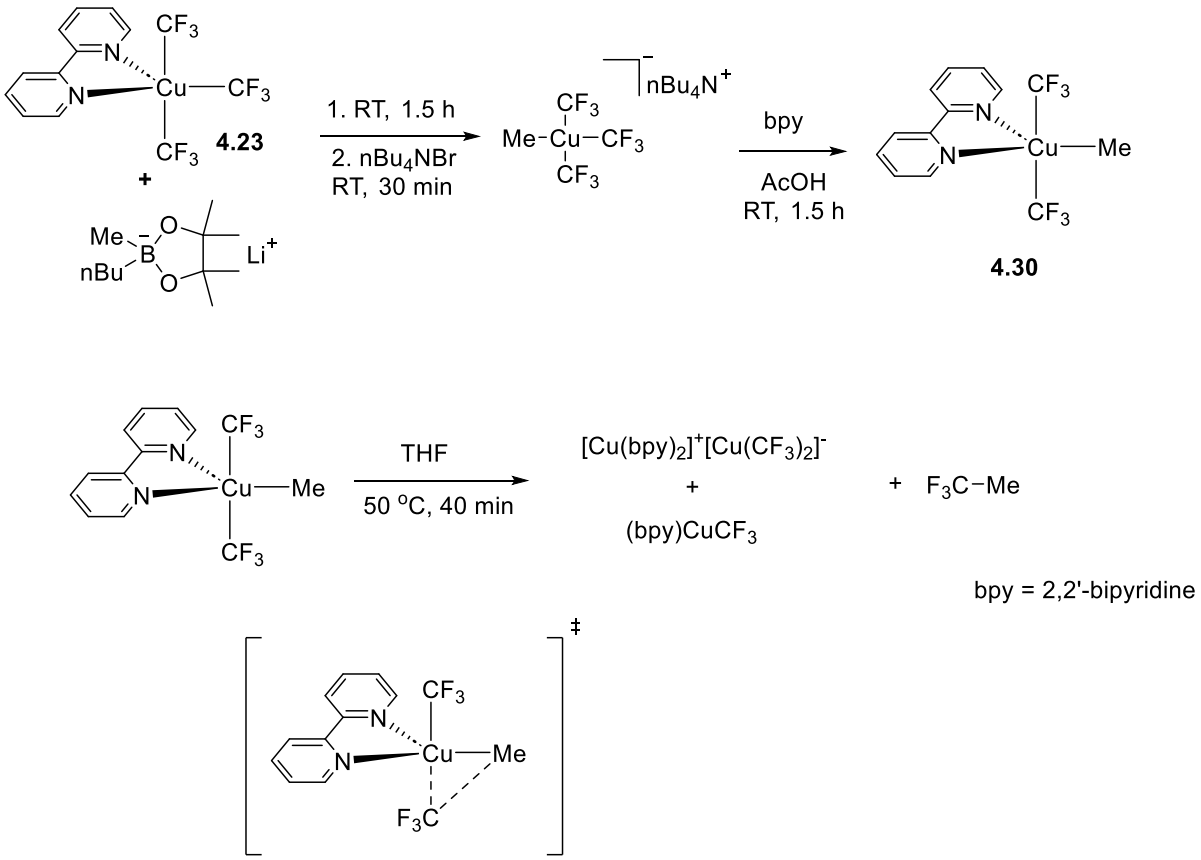

In 2020, Shen and coworkers reported the synthesis and characterization of neutral five-coordinate organocopper(III) complex Cu(Me)$(CF_3)_2$(bpy) (**4.30**) (bpy=2,2'-bipyridine).[163]

At 50 °C for 40 min, the complexes underwent C(sp3)-CF_3 reductive elimination to form CH_3-CF_3 and a mixture of $Cu^I(CF_3)(bpy)$ and $[Cu(bpy)_2]^+[Cu(CF_3)_2]^-$. The kinetic experiments and DFT calculations suggested that the mechanism of the CH_3-CF_3 reductive elimination occurs via three-membered ring transition state. (**Scheme 4.15**)

4.1.2 Longer-chain perfluoroalkylation mediated by first-row transition metals

While trifluomethylation has become a major focus, the incorporation of longer chain perfluoroalkyl has underexplored, although the presence of longer perfluoroalkyl groups may have a significant effect on pharmacokinetic properties of organic compounds as compared to trifluoromethyl groups. The addition of one or more CF_2 groups can significantly alter the physical properties, such as increasing the steric effect, electronegativity, and hydrophobicity.[164-165] Hence, longer-chain perfluoroalkylation is applied in some bioactive molecules, such as KC-515[166-167] (antihypertensive potassium (K^+) channel opener), DuP 532[168-169] (angiotensin II receptor antagonist) and Fulvestrant[170-171] (antibreast cancer drug).

Scheme 4.16. Representative longer-chain perfluoroalkyl groups in drug design.

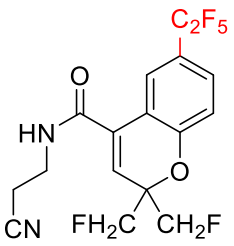

KC-515

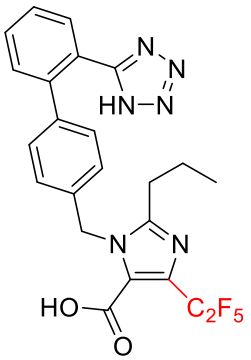

DuP 532

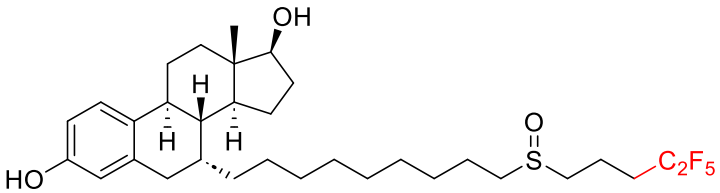

Fulvestrant

The common approach to incorporating longer-chain perfluoroalkyl group into organic compounds is typically cross-coupling of organohalides with appropriate perfluoroalkyl reagents mediated by transition metal.[172-175] The protocol might require the presence of expensive reagents/additives or in special conditions.[176-178] Meanwhile, examples for longer-chain perfluoroalkylation of arenes and heteroarenes catalyzed by inexpensive first-row transition-metal complexes are still scarce. For example, in 2021, the Vicic group described perfluoroalkylation of iodonium salts and diazonium salts mediated by solvated perfluoroalkyl nickel(II) complexes.[146] The authors also showed the catalytic activity of ligandless trifluoromethyl nickel(II) complexes in trifluoromethylation using Umemoto reagent II. Meanwhile, only stoichiometric reactivity was observed in longer-chain perfluoroethylation. (**Scheme 4.17**)

Scheme 4.17. Stoichiometric pentafluoroethylation of diazonium salts mediated by solvated $[Ni(C_2F_5)_3(MeCN)](NMe_4)$ complexes.

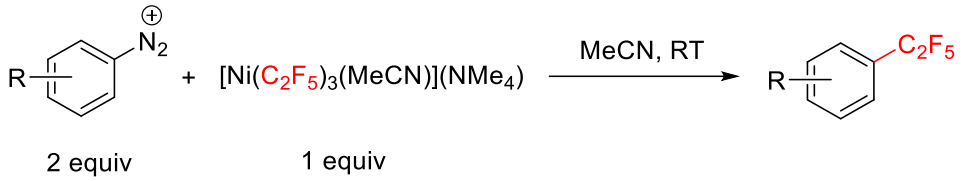

In 2022, our group reported a simple catalytic protocol for perfluoroalkylation of arenes and heteroarenes by using solvated nickel(II) bis(perfluoroalkyl) complexes in combination with commercially available Acid Togni reagents containing trifluoromethyl, perfluoroethyl or perfluoropropyl groups.[179] The protocol proceeds in mild conditions without the need for light or additives or photosensitizers. This protocol can be applied to late stage perfluoroethylation of natural products, drug molecules and peptides. The mechanistic investigations suggested the involvement of high-valent nickel intermediates and the catalysis proceeds through a radical mechanism. (**Scheme 4.18**)

Scheme 4.18. Perfluoroalkylation using Acidic Togni reagents catalyzed by solvated nickel(II) complexes.

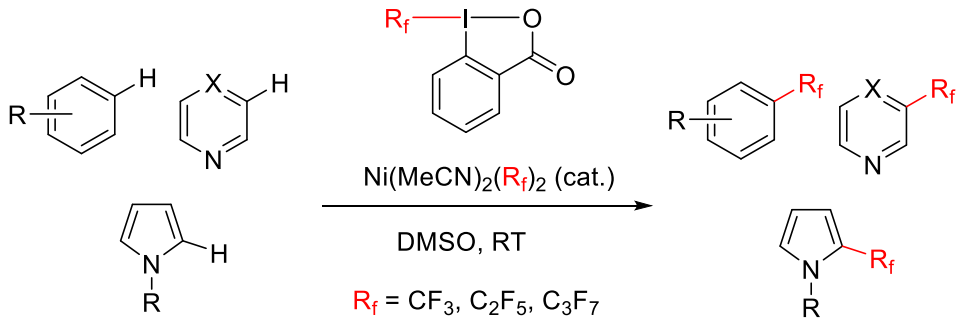

In a recent study, our research group demonstrated the utility of solvated cyclometalated nickel complex **4.31** as a catalyst for the perfluoroalkylation of arenes, heteroarenes, and peptides by using commercially available Acid Togni reagents under mild conditions, without the need for photosensitizers.[180] This approach represents a significant advancement over previous methodologies, which required the synthesis of suitable solvated nickel(II) bis(perfluoroalkyl) precursors for each perfluoroalkyl-chain incorporation. The new protocol simplifies the requirement for nickel catalysts and reduces the amount of Togni reagents needed, thereby lowering the operational costs associated with perfluoroalkyl incorporation reactions. Mechanistic insights were studied through a combination of experimental and computational analyses, which suggested the involvement of a high-valent Ni^{IV} intermediate in the generation of perfluoroalkyl radicals and Ni^{III} intermediates. Density functional theory (DFT) calculations further proposed that Togni reagents play a crucial role in stabilizing the Ni^{III} species and their adducts with the substrate.

Scheme 4.19. Perfluoroalkylation using Acidic Togni reagents catalyzed by solvated nickel(II) metallocycle complex **4.31**.

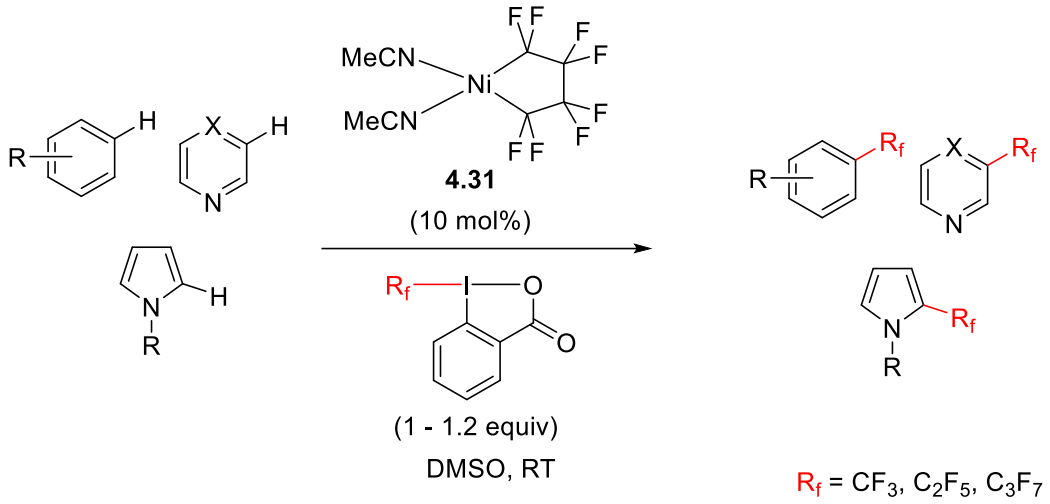

4.1.3 Synthesis and reactivity of cobalt perfluoroalkyl complexes

While nickel or copper have garnered significant attention in the field of trifluoromethylation and perfluoroalkylation, the utilization of cobalt complexes in these reactions remains relatively unexplored. Notably, there are limited examples of perfluoroalkylation mediated by cobalt complexes. For example, in 2018, the Hisaeda group reported on an approach involving a combined electrochemical/photochemical perfluoroalkylation of electron-rich arenes and heteroarenes, catalyzed by cobalamin derivatives containing ester-derivatized tetradentate corrin macrocyclic ligands (**4.32**).[181] The proposed mechanism involves the visible light-induced formation of perfluoroalkyl radicals from Co^{III}-R_f complexes. Initially, a cobalt(I) species is generated through the electroreduction of Co^{II} complexes. The Co^{I} species then reacts with perfluoroalkyl iodide to form the Co^{III}-R_f complex, which, upon light irradiation, rapidly releases the perfluoroalkyl radical.

Scheme 4.20. Perfluoroalkylation catalyzed by Co(II) complexes **4.32** supported by corrin-based ligand.

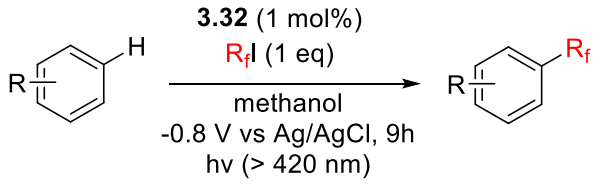

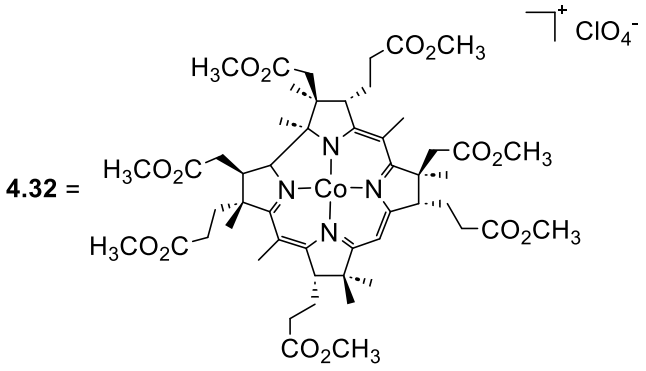

To confirm their proposed mechanism, this group later reported the synthesis of Co^{III}-CF_3 complex **4.33** supported by ester-derivatized tetradentate corrin macrocyclic ligand by reacting vitamin B_{12} derivative **4.32** with trifluoroiodomethane under the presence of $NaBH_4$

in the dark.[182] As expected, the complex **4.33** is unstable under visible light (hv > 420 nm), showing a Co-CF_3 bond homolysis and releasing CF_3 radical, which was proved by PBN trapping experiment(PBN = alpha-phenyl N-tertiary-butyl nitrone) (**Scheme 4.21**).

Scheme 4.21. Synthesis of Co^{III}-CF_3 complexes **4.33** supported by corrin-based ligand and its photo-induced Co-CF_3 bond homolysis.

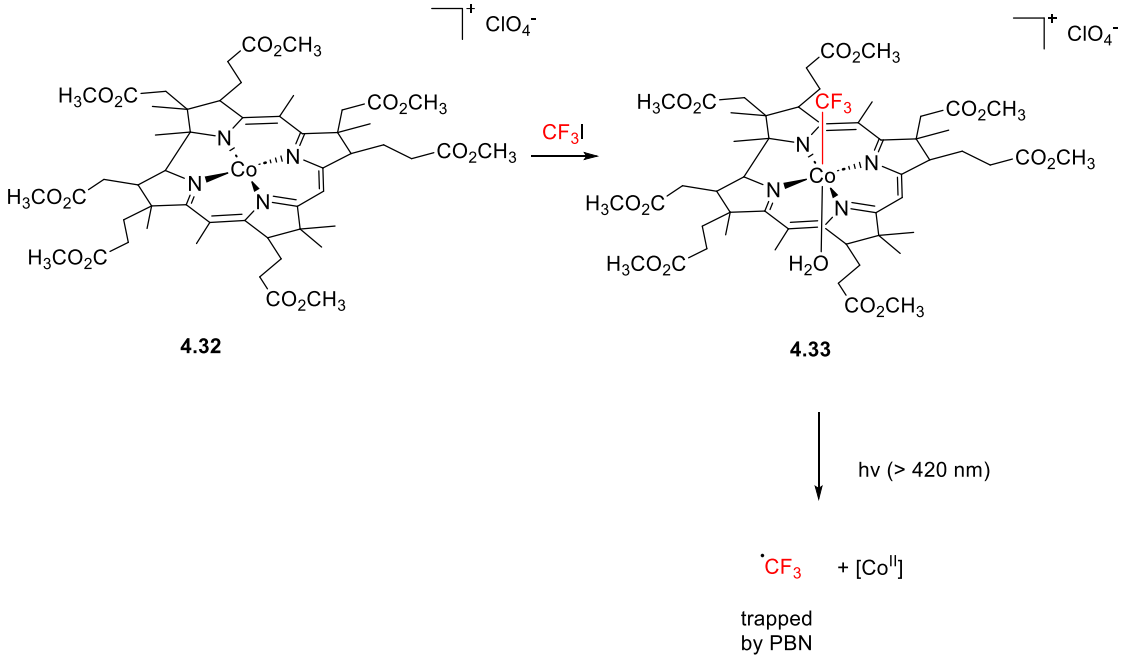

In 2018, the Soper group reported the preparation of Co^{III}-CF_3 complex **4.34** by treating Co^{II} complex supported by non-innocent OCO pincer ligand with AgF and TMS-CF_3. Exposure complex **4.34** under visible light resulted in the facile Co-CF_3 bond homolysis and the release of CF_3 radical, which was confirmed by TEMPO radical trap experiment. This complex has shown light-induced C-H functionalization of arenes and heteroarenes under room temperature in 3 days to yield trifluoromethylated adducts.(**Scheme 4.22**)[183]

Scheme 4.22. Photo-induced trifluoromethylation mediated by Co^{III}-CF_3 complexes supported by OCO pincer ligand.

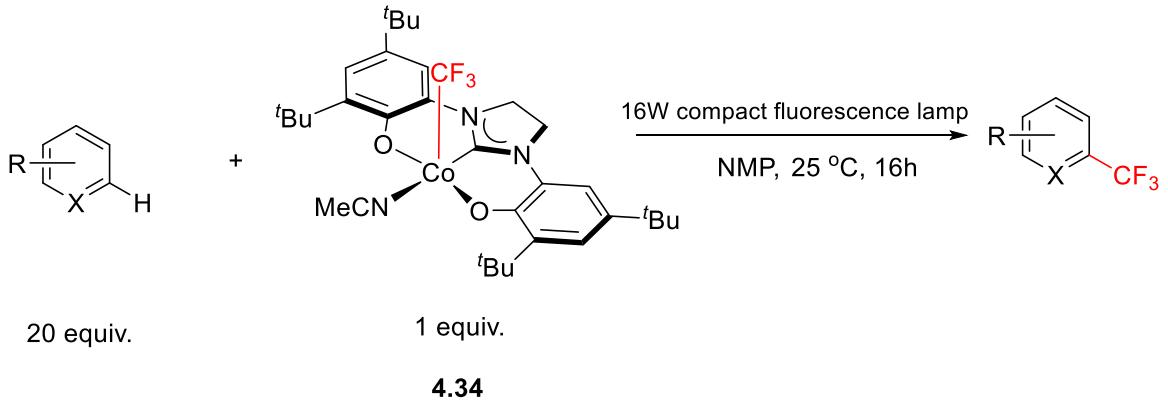

Vicic group has reported the synthesis and isolation of $Co(Rf)_3(MeCN)_3$ (Rf = CF_3, C_2F_5) by reacting $CoBr_2$ with the excess amount of AgF and $TMSR_f$. (**Scheme 4.22**)[184-185] While the preparation and isolation of $Co(CF_3)_3(MeCN)_3$ **4.35a** is tedious due to its insolubility and instability, $Co(C_2F_5)_3(MeCN)_3$ **4.35b** precursor was more convenient to obtain in good yield. Later, the Vicic group showed that $Co(CF_3)_3(MeCN)_3$ **4.35a** is less reactive compared to the

ligand-less trifluoromethyl nickel complexes as a catalyst for trifluoromethylation using the Umemoto reagent II.[146]

Scheme 4.23. Synthesis of acetonitrile-supported cobalt(III) perfluoroalkyl complexes

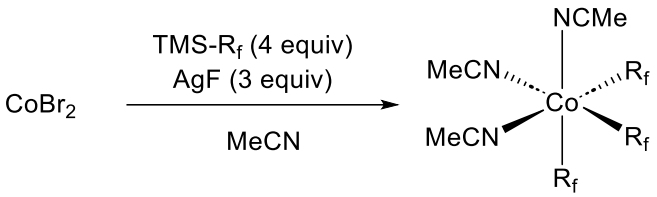

4.35a: $R_f = CF_3$
4.35b: $R_f = C_2F_5$

Overall, compared with nickel complexes, perfluoroalkylation mediated by cobalt complexes has received less attention due to their perceived lower activity.[146] Furthermore, the number of methodologies for longer-chain perfluoroalkylation is still limited despite the fact that the addition of one more CF_2 group can significantly alter the physical properties of the substrate.

Previously, our group reported a photo-induced trifluoromethylation catalyzed by nickel(III) complexes supported by simple naphthyridine-based ligands.[186] Based on the previous studies, our objective was to extend this reactivity to cobalt using simple naphthyridine ligands. Given that the longer-chain perfluoroethyl cobalt precursors are conveniently accessible, we aimed to obtain perfluoroethyl Co complexes supported by naphthyridines and study its reactivity in perfluoroalkylation, potentially via light irradiation.

Therefore, in this chapter, I focus on the synthesis of a new family of cobalt complexes with naphthyridine and perfluoroethyl ligands and studied their structure and electronic properties. These N-donor cobalt complexes could undergo Co-C_2F_5 bond homolysis under visible-light exposure without the need for a macrocyclic or redox-innocent ligand. Although limited to electron-rich substrates, preliminary investigations revealed that these complexes possess the ability to catalyze C(sp^2)–H perfluoroethylation using the commercially available perfluoroethyl Togni reagent.

4.2. Results and Discussion

4.2.1 Complex synthesis and characterization

4.2.1.1. Neutral cobalt(III) complexes

Our initial attempts to synthesize Co^{III} complexes supported by naphthyridine ligands were focused on the use of a common precursor, $Co^{III}(C_2F_5)_3(MeCN)_3$, as reported by Vicic and coworkers.[184] The treatment of $Co^{III}(C_2F_5)_3(MeCN)_3$ with 1 equiv. of 1,8-naphthyridine (**L1**) in tetrahydrofuran (THF) solution at room temperature (RT) for 16 hours resulted in the formation of a neutral complex Co(**L1**)(MeCN)$(C_2F_5)_3$ (**4.36**), which was isolated as a pale yellow crystalline solid in 65% yield (S**cheme 4.23**). Similarly, the treatment of monomethyl-substituted 2-methyl-1,8-naphthyridine ligand with 1 equiv. of $Co^{III}(C_2F_5)_3(MeCN)_3$ led to the formation of complex **4.37** with 68% isolated yield. Complexes **4.36** and **4.37** were fully characterized by NMR spectroscopy, ESI-HRMS, elemental analysis, UV-Vis and FT-IR spectroscopies, and single-crystal X-ray diffraction (SC-XRD). According to SC-XRD analysis, complexes **4.36** and **4.37** have a distorted octahedral geometry around the cobalt center, supported by bidentate-coordinated naphthyridine and one MeCN ligand (**Figure 4.1**, a-b). The Co–C bond distances of C_2F_5

trans to N-atoms of naphthyridine are ranging from 1.942(3)-1.987(2) Å, while this value of Co–C bond *trans* to MeCN is in the range of 1.976(6)-1.981(2) Å.

Scheme 4.24. Synthesis of neutral tris(perfluoroethyl) cobalt(III) complexes

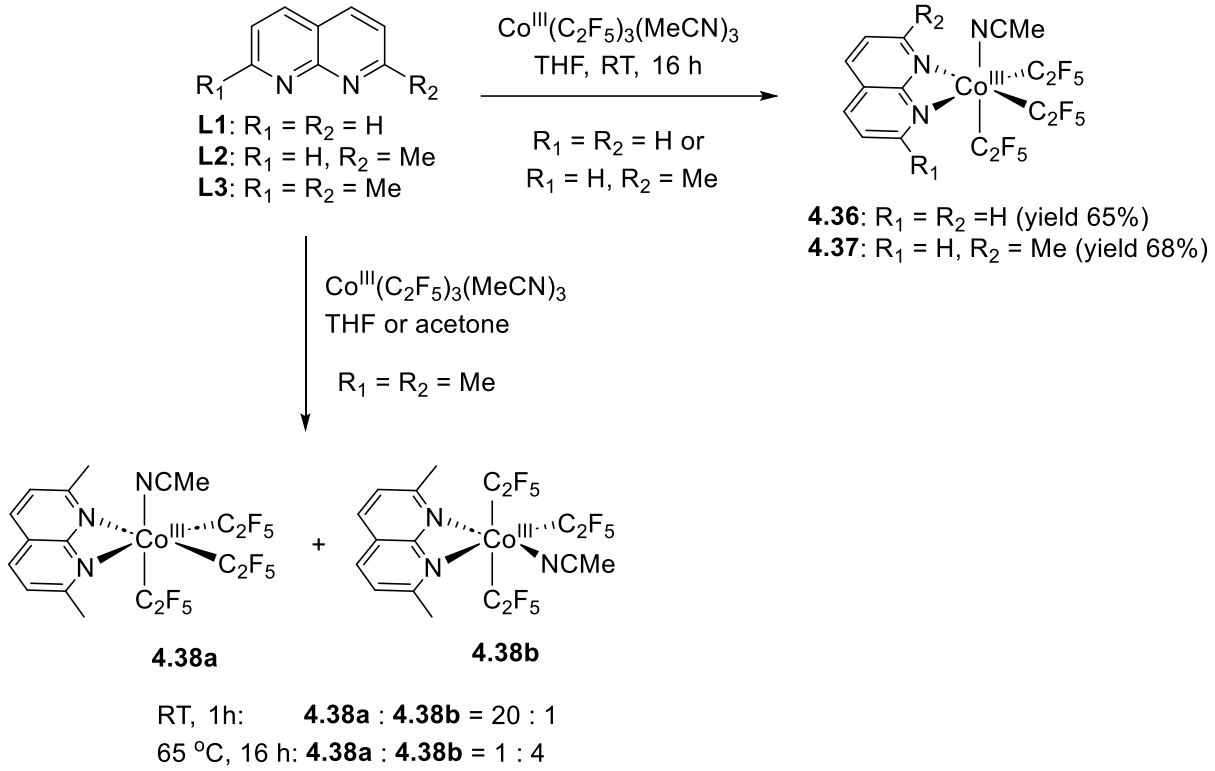

The ^{1}H NMR spectrum of **4.36** showed two multiplets in the aromatic region assigned to the **L1** ligand, which is consistent with the symmetry of the complex. The ^{19}F NMR spectrum of **4.36** showed two signals for CF_3 groups in 2 :1 ratio at –80.58 and –80.79 ppm, corresponding the two set of inequivalent C_2F_5 groups in *trans*- and *cis*-position to the N-atoms of naphthyridine ligand. On the other hand, the aromatic protons of complex **4.37** appeared as four sets of doublets and a doublet of doublets due to the unsymmetrical structure of **L2**. The ^{19}F NMR spectrum of **4.37** showed a set of three broad singlets corresponding for CF_2 groups and six doublets assigned for CF_3 groups due to the three inequivalent C_2F_5 ligands.

Interestingly, treatment of bulkier bis(methyl)-substituted 2,7-dimethyl-1,8-naphthyridine ligand (**L3**) with $Co^{III}(C_2F_5)_3(MeCN)_3$ precursor resulted in the formation of two isomers **4.38a** and **4.38b**. When the reaction was monitored by ^{1}H NMR spectroscopy in acetone-d_6, **L3** was almost consumed after 1 hour at room temperature, and a major product **4.38a** was appeared, accompanied by a minor product **4.38b** with a ratio **4.38a** : **4.38b** = 20 : 1. The aromatic protons of the major species **4.38a** appeared in ^{1}H NMR spectrum as two doublets at 8.53 and 7.71 ppm, where the proton signal of methyl groups showed as a singlet at 3.34 ppm, consistent with the presence of a plane of symmetry in *fac*-$(C_2F_5)_3Co^{III}$ isomeric structure. Yellow crystals are obtained from pentane/THF solution from the reaction mixture at -30 °C, which was confirmed as **4.38a** by SC-XRD analysis. According to SC-XRD, **4.38a** has a distorted octahedral geometry around cobalt center, with three C_2F_5 groups are present in *cis*-position to each other. The naphthyridine-based ligand **L3** binds to the cobalt center in bidentate fashion, and the MeCN ligand is at *cis*-position compared to an N-atom of **L3**.

Heating of the mixture at 65 °C for 16 hours led to the formation of a mixture of **4.38a : 4.38b** = 1 : 4, where the minor species **4.38b** becomes the predominant product. Orange

crystals were obtained from pentane/THF solution of the reaction mixture at. The orange crystal structure was confirmed by SC-XRD as **4.38b** in *mer*-$Co(C_2F_5)_3$ configuration, where the MeCN ligand is at the trans-position compared to an N-atom of **L3**. Due to the unsymmetrical environment around cobalt center, ^{1}H NMR spectrum showed a set of four doublets in a range of 8.51 – 7.53 ppm in the aromatic region and two singlets at 2.81 and 2.62 ppm corresponding to the two inequivalent methyl group of **L3**.

Further prolonged the reaction at 65 ºC for 2 days did not result to the formation of **4.38b** as the only product and the isomeric ratio of **4.38a : 4.38b** stayed unchanged, suggesting that the two isomers have similar kinetic stability, and *fac*-isomer **4.38a** is slightly less thermodynamically stable compared to *mer*-**4.38b**, likely due to the steric bulk caused by two ortho-Me groups in **L3** ligand. DFT calculations also confirmed the relative stability of two isomers by showing that **4.38b** is marginally more stable than **4.38a** by 0.26 kcal/mol, although this value is within the error expected from DFT calculations.

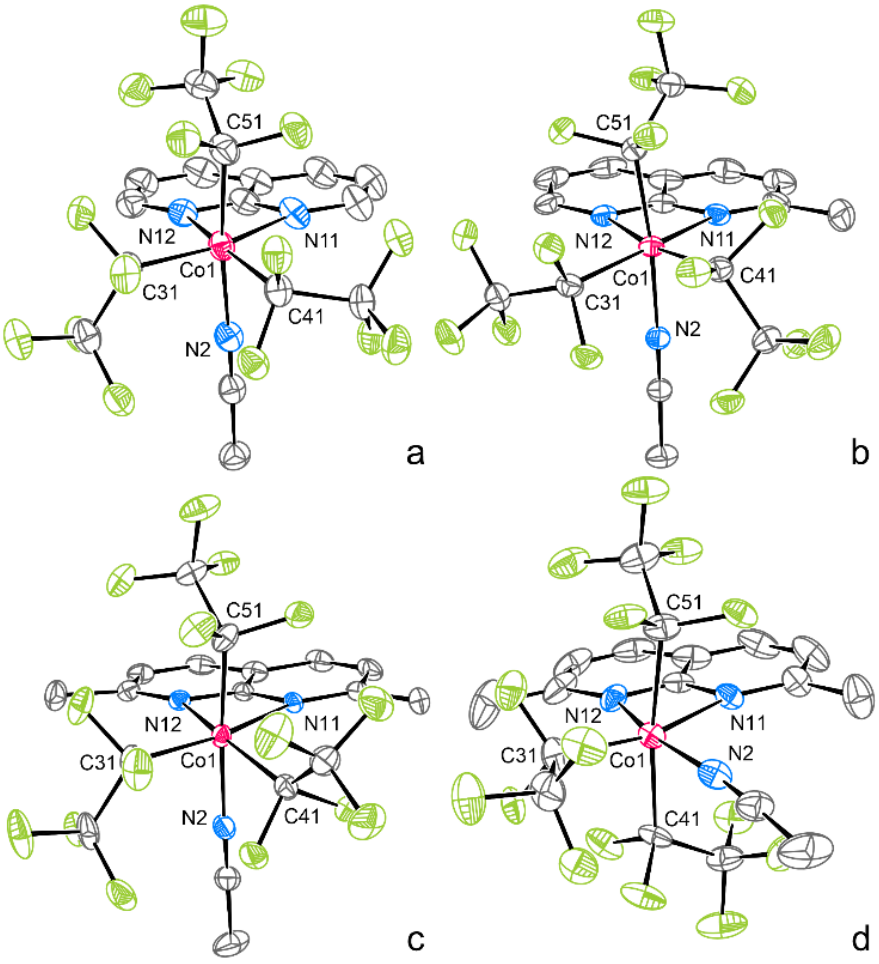

Figure 4.1. ORTEP of **4.36** (a), **4.37** (b), **4.38a** (c), and **4.38b** (d) at 50 % probability level according to single-crystal X-ray diffraction. Minor disorder components and hydrogen atoms are omitted for clarity.

Table 4.1. Selected internuclear distances [Å] for **4.36-4.38b** according to single-crystal X-ray diffraction. Data for the main disorder component is present. Atomic numbering scheme is given in **Figure 4.1**.

Bond	**4.36**	**4.37**	**4.38a**	**4.38b**
Co1–N11	2.082(4)	2.130(2)	2.082(3)	2.045(5)
Co1–N12	2.057(4)	2.073(2)	2.123(3)	1.996(6)
Co1–N2	1.959(4)	1.9645(17)	1.974(3)	1.881(6)
Co1–C31	1.963(6)	1.987(2)	1.965(3)	1.933(13)
Co1–C41	1.982(5)	1.942(3)	1.987(4)	2.047(6)
Co1–C51	1.976(6)	1.981(2)	1.963(4)	2.085(15)

4.2.1.2. Cationic cobalt(III) complexes

Scheme 4.25. Synthesis of monocationic cobalt(III) complexes

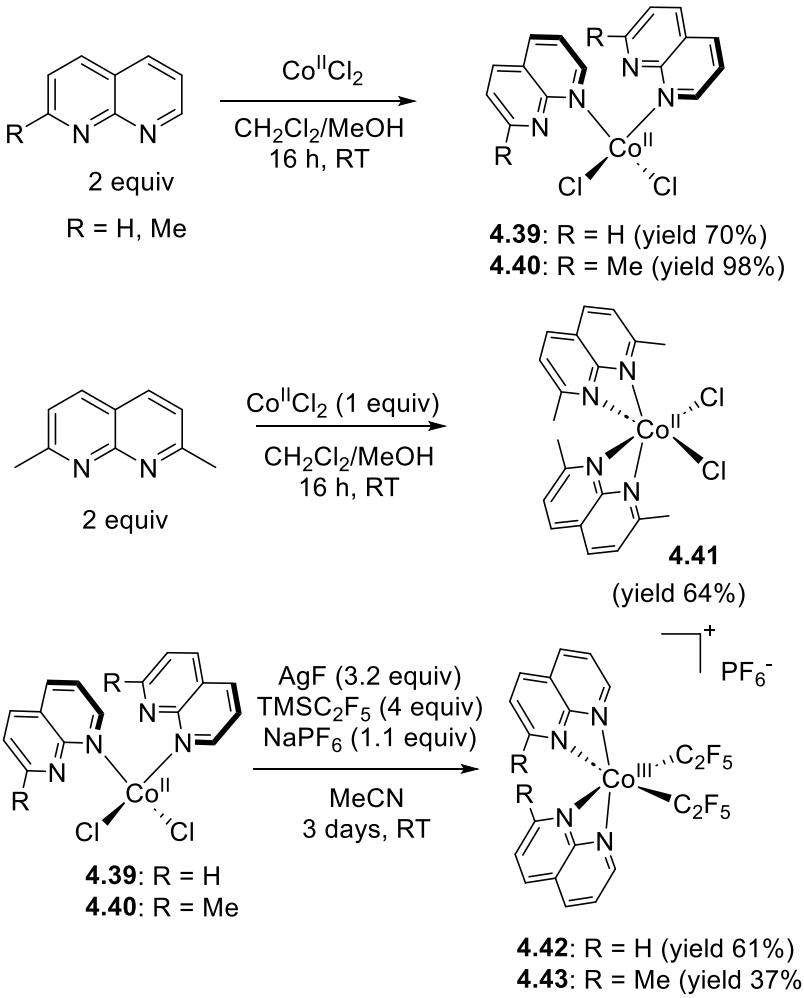

Based on our previous study which showed that cationic $[(\mathbf{L3})_2Ni^{III}(CF_3)_2]^+$ complexes supported by two naphthyridine-based ligands were active in photo-induced C(sp^2)-H trifluoromethylation, our next attempts were focused on obtaining the similar structure in cationic cobalt complexes with two C_2F_5 groups and two naphthyridine ligands. To obtain such complexes, we started with a different approach from the bis(naphthyridine)$Co^{II}Cl_2$ complexes. Treating 2 equiv. of **L1** or **L2** with 1 equiv. of anhydrous $CoCl_2$ in MeOH-DCM

solution at room temperature for 16 hours led to the formation of complexes Co(**L1**)$_2$Cl$_2$ **4.39** and Co(**L2**)$_2$Cl$_2$ **4.40**, which were isolated as blue crystals with 70 and 98% yield, respectively. The complexes **4.39** and **4.40** were characterized by UV-vis, FT-IR spectroscopy, ESI-HRMS, elemental analysis, and SC-XRD. SC-XRD analysis confirmed the distorted tetrahedral structure around cobalt center in complex **4.39** and **4.40**, where two naphthyridine-based ligands coordinate in a monodentate fashion. The analogous reaction of $CoCl_2$ to 2 equiv. of **L3** generated complex **4.41** in 64% isolated yield. In contrast with complexes **4.39** and **4.40**, SC-XRD analysis revealed a distorted octahedral geometry around the cobalt center in complex **4.41**, with two **L3** ligands coordinating in a bidentate mode (**Figure 4.2**, c). The magnetic moment measured by the Evans method in methanol-d_4 solutions of complex **4.39**, **4.40** and **4.41** were 4.65, 5.06 and 4.88 μ_B, respectively, suggesting the high-spin d^7 configuration (S=3/2) in the Co^{II}.

Table 4.2. Selected internuclear distances [Å] for **4.39-4.41** according to single-crystal X-ray diffraction. For **4.40**, data for one of three symmetry-independent molecules are present. Atomic numbering scheme is given in **Figure 4.2**.

Bond	**4.39**	**4.40**	**4.41**
Co1–N11	2.0381(17)	2.0267(19)	2.272(2)
Co1–N12	3.0177(18)	2.738(2)	2.188(2)
Co1–N21	2.0371(16)	2.040(2)	2.269(2)
Co1–N22	3.0860(17)	2.9134(19)	2.183(2)
Co1–Cl1	2.2770(5)	2.2747(7)	2.3748(7)
Co1–Cl2	2.2679(5)	2.2867(7)	2.3512(7)

Next, treatment of **4.39** with 4 equiv. of $TMSCF_3$ and 3.2 equiv. of AgF in the presence of 1 equiv. of $NaPF_6$ in acetonitrile resulted in the formation of Co^{III} complex **4.42** with 61% isolated yield as orange crystals (**Scheme 4.24**). Complex **4.42** was air-stable for months in solid form without any sign of decomposition. The analogous reaction of complex **4.40** with 3.2 equiv. of AgF, 4 equiv. $TMSC_2F_5$, and 1 equiv. of $NaPF_6$ in acetonitrile afforded complex **4.43** in 37% isolated yield as an orange crystalline solid. Complexes **4.42** and **4.43** were characterized by multinuclear NMR, UV-vis, IR spectroscopy, ESI-HRMS, elemental analysis, and SC-XRD (**Figure 4.2** and **Table 4.3**). In contrast, the analogous reaction with complex **4.41** resulted in the formation of a mixture of two unknown products that cannot be separated by crystallization or characterized by other methods.

SC-XRD analysis showed that complex **4.42** and **4.43** have a distorted octahedral structure around Co^{III} center with two C_2F_5 groups in *cis*-positions to each other and two naphthyridine-based ligands coordinating in a bidentate mode. The PF_6 group was also present as a counteranion, according to SC-XRD. The structure of complexes **4.42** and **4.43** were also confirmed by NMR spectroscopy. ^{19}F NMR spectrum of complex **4.42** showed two doublets of unresolved multiplets at -86.13 ppm and -94.08 ppm that correspond to the geminally coupled F-atoms of the CF_2 group and one triplet at -81.58 ppm (J_{FF} ~ 5 Hz) corresponding to the CF_3 group. The uncoordinated counteranionic PF_6^- group appeared at -72.81 ppm as a doublet. Similarly, the ^{19}F NMR spectrum of **4.43** showed two doublets at -84.24 ppm and -94.08 ppm corresponding to the geminally coupled CF_2 groups and one multiplet at -81.77 ppm corresponding to the CF_3 group, as well as a doublet at -72.78 ppm assigned to uncoordinated PF_6^- group.

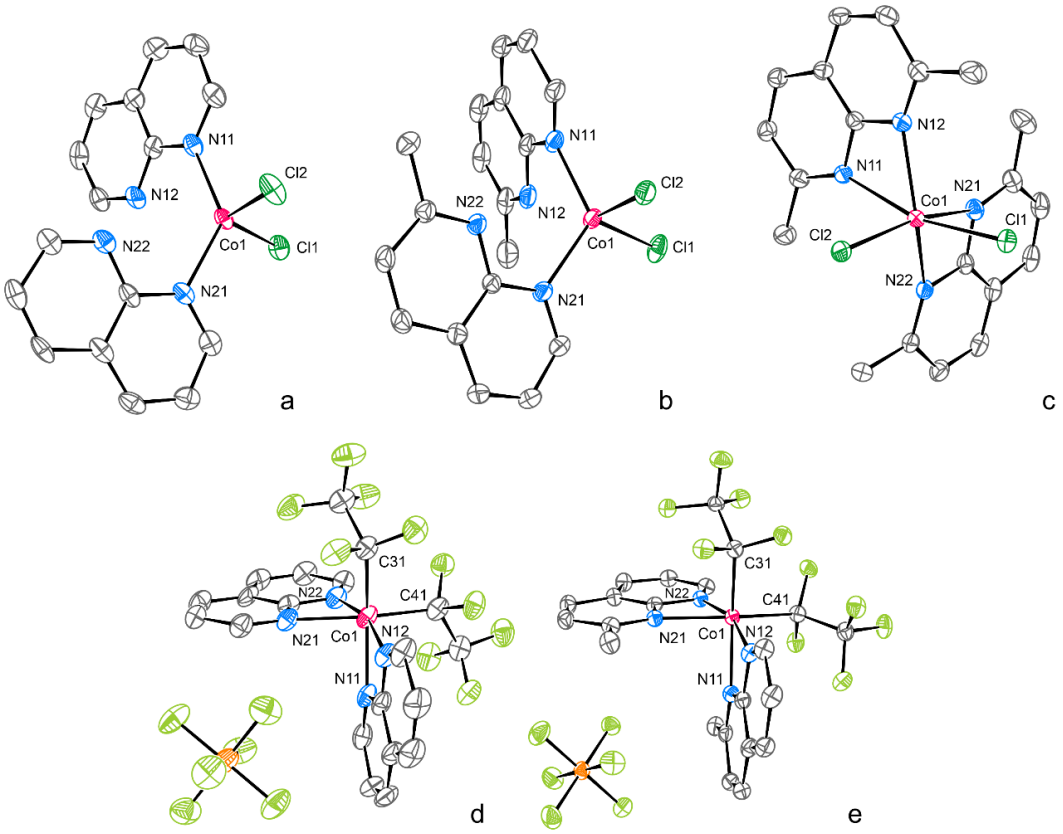

Figure 4.2. ORTEP of **4.39** (a), **4.40** (b), **4.41** (c), **4.42** (d), and **4.43** (e) at 80 % (**4.39**) or 50 % (**4.40-4.43**) probability level. Minor disorder components, solvent molecules, and hydrogen atoms are omitted for clarity. For **4.40**, one of three symmetry-independent molecules is shown.

4.2.1.3. Cyclic voltammetry of cobalt(III) complexes

After having the perfluoroethyl cobalt(III) complexes in hand, we next investigated the redox properties of these complexes by cyclic voltammetry to examine whether we can access to other oxidation states of Co-C_2F_5 complex. The anodic scan of neutral complexes **4.36-4.38** showed irreversible oxidation waves at high potentials (>1 V vs. Fc^+/Fc), while the cathodic scan revealed two irreversible reduction waves at highly negative potentials (ca. -1.6 V vs Fc^+/Fc for the first wave), suggesting that both higher and lower oxidation states are difficult to access or provide unstable products from the neutral complexes. On the other hand, the complexes **4.42** and **4.43** showed a quasireversible reduction wave in the cathodic scan at –0.76 V and –0.90 V vs. Fc^+/Fc, respectively, as well as two irreversible reduction peaks at highly negative potentials, suggesting that Co^{II}-C_2F_5 complex can be accessible and provide stable product from one electron reduction of cationic bis(perfluoroethyl) Co^{III} complexes.

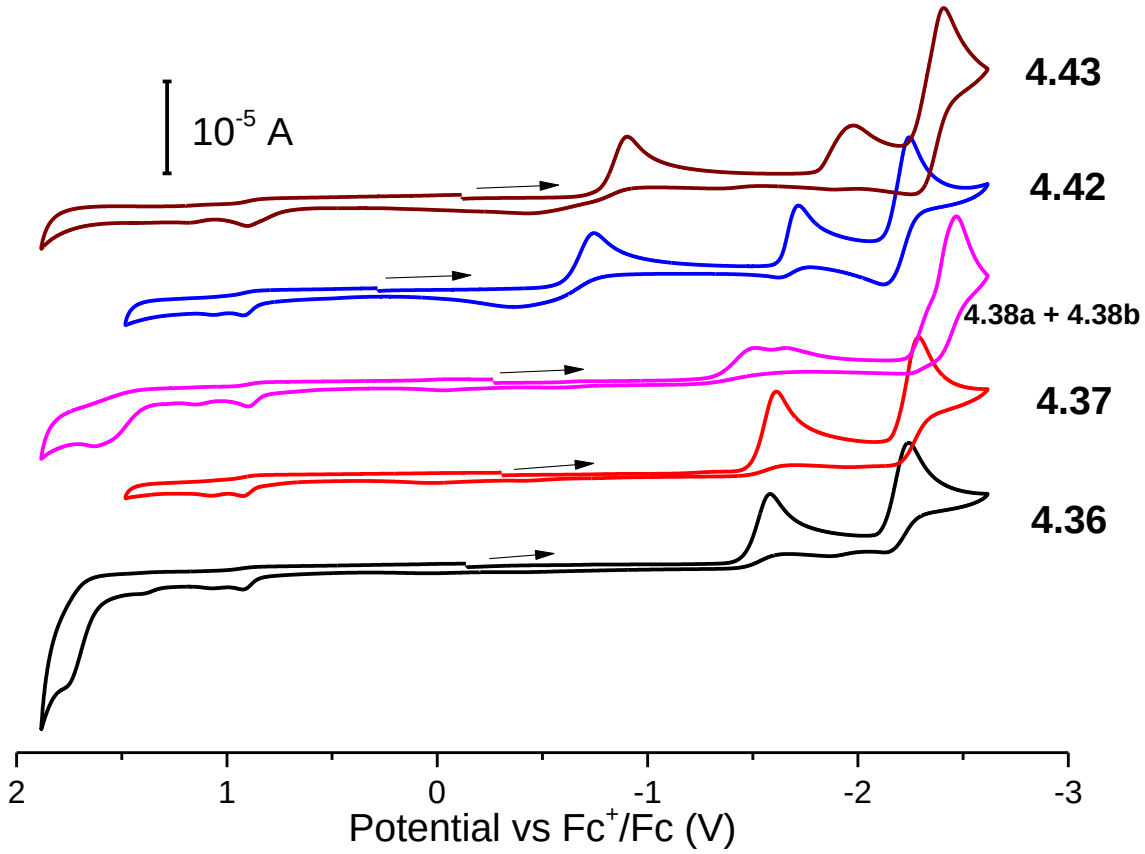

Figure 4.3. Cyclic voltammograms of complex **4.36**, **4.37**, **4.38a** + **4.38b** (**4.38a**:**4.38b** = 1:4), **4.42**, and **4.43** (2 mM) in 0.1 M $^{n}Bu_4NClO_4$/MeCN solution at 23 °C (scan rate 100 mV s^{-1}; 1.6 mm glassy carbon disk working electrode; the arrow indicates the initial scan direction).

As expected, treatment of complex **4.42** with 1 equiv. of potassium graphite (KC_8) as a reductant in THF led to the formation of a new Co^{II} complex **4.44** as a deep-red crystals with 52% isolated yield. The magnetic moment of **4.44** measured by the Evans method in acetone-d_6 was 1.85 μ_B, suggesting an S=1/2 ground state to a low-spin d^7 configuration for the Co^{II} center.

Scheme 4.26. Synthesis of perfluoroethyl cobalt(II) complexes

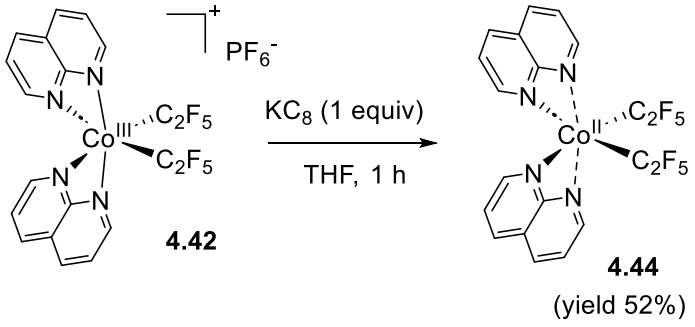

SC-XRD analysis confirmed that **4.44** is a neutral complex, where two C_2F_5 groups and two naphthyridine ligands bound to the cobalt center. The short Co–N11 (1.9918(16) Å) and Co1–N21 (1.9954(17) Å) are present in *trans*-position to the carbon atoms of C_2F_5 groups, while the significant longer Co-N12 and Co-N22 distance (2.5049(18) and 2.4053(17) Å) appear in *cis*-position to C_2F_5 groups. That such significant difference of Co-N distances and axially elongated octahedral geometry around cobalt center could be explained by the Jahn-

Teller distortion in d^7 configuration Co^{II} complexes, similar with the elongated octahedral structure in d^7 Ni^{III} complexes with **L3** ligand reported earlier.[186]

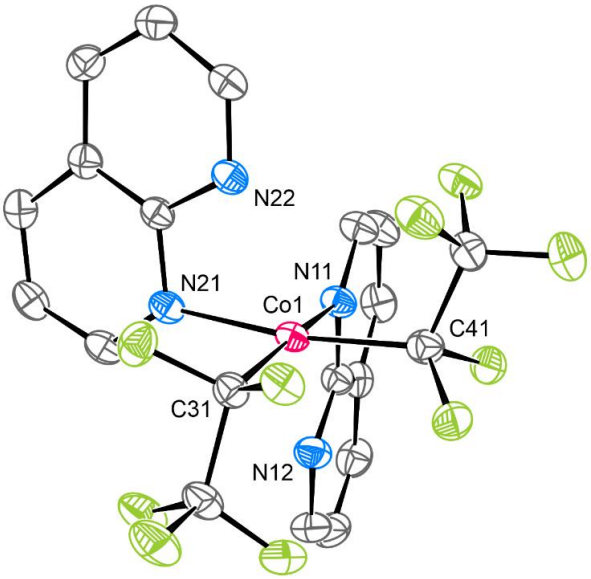

Figure 4.4. ORTEP of **4.44** at 50 % probability level. Minor disorder components, solvent molecules, and hydrogen atoms are omitted for clarity.

Table 4.3. Selected internuclear distances [Å] for **4.42-4.44** according to single-crystal X-ray diffraction. Atomic numbering scheme is given in **Figure 4.2**.

Bond	**4.42**	**4.43**	**4.44**
Co1–N11	2.074(5)	2.0778(17)	1.9918(16)
Co1–N12	1.926(4)	1.9429(17)	2.5049(18)
Co1–N21	2.073(5)	2.0765(16)	1.9954(17)
Co1–N22	1.942(4)	1.9354(16)	2.4053(17)
Co1–C31	1.948(6)	1.949(2)	1.9451(19)
Co1–C41	1.935(6)	1.9443(19)	1.957(2)

To further explain the structure of complex **4.44**, the quantum theory of atoms in molecules (QTAIM) was used to analyze the DFT-optimized structure of this complex. According to QTAIM, all interactions around atom Co1 in complex **4.44** are characterized by the small positive values of the electron density ρ_b and the Laplacian of electron density $\nabla^2\rho_b$ at the corresponding bond critical points (**Figure 4.5** and **table 4.4**), with the lower values of the electron density at the bond critical points located along axially elongated Co–N bonds.

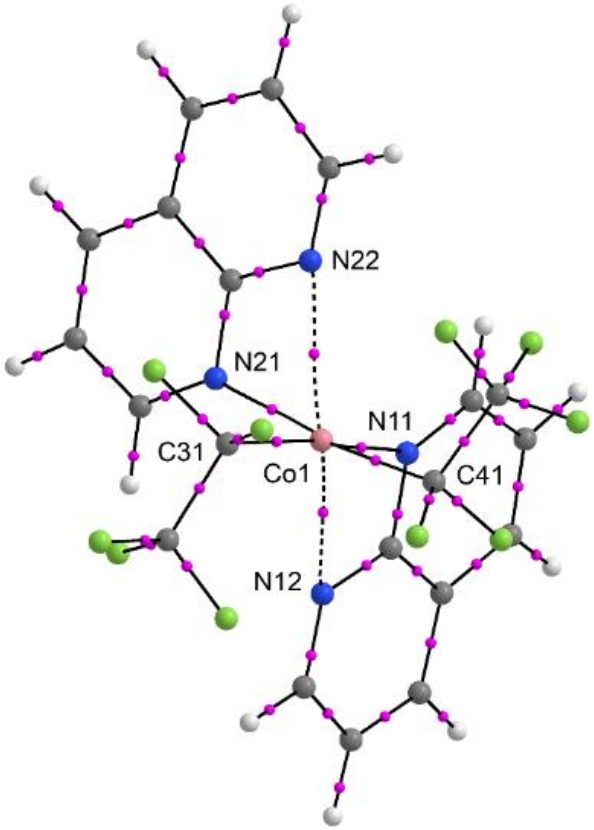

Figure 4.5. Molecular graph of gas-phase optimized complex **4.44**. Bond critical points and bond paths are shown as magenta spheres and black lines. These elements are omitted if the value of electron density at the bond critical point is less than 0.02 a.u. If the value of electron density at the bond critical point is less than 0.03 a.u., the corresponding bond paths are shown as dashed lines.

Table 4.4. Selected internuclear distances ($\boldsymbol{d}$, Å) as well as the values of the electron density ($\boldsymbol{\rho_b}$, a.u.), its Laplacian ($\boldsymbol{\nabla^2\rho_b}$, a.u.), and delocalization indices at the corresponding critical bond points for gas-phase optimized complex **4.44**.

Bond	d[a]	ρ_b[b]	$\nabla^2\rho_b$[c]	DI[d]
Co1–N11	2.03749	0.070901	0.430733	0.435116
Co1–N12	2.45412	0.029185	0.122357	0.192274
Co1–N21	2.03659	0.071073	0.431815	0.436411
Co1–N22	2.45659	0.029079	0.121303	0.190935
Co1–C31	1.97454	0.111561	0.294288	0.753186
Co1–C41	1.97537	0.111342	0.294331	0.752245

4.2.2 Photoinduced Co–C_2F_5 bond homolysis and C–H bond perfluoroethylation.

4.2.2.1. Co-C_2F_5 bond homolysis

Table 4.5. Photoinduced Co-C_2F_5 bond homolysis trapped by TEMPO.

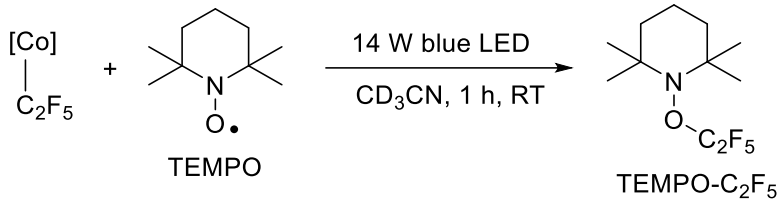

Entry	Complex	Modification of standard conditions	Yield of TEMPO-C_2F_5 (%)[a]
1	**4.36**	None	21
2	**4.37**	None	46
3	**4.38a+4.38b**	None	46
4	**4.42**	None	74
5	**4.43**	None	37
6	**4.44**	None	6
7	$Co(C_2F_5)_3(MeCN)_3$	None	18
8	**4.42**	No blue LED	Not detected

[a]Yields were determined by ^{19}F NMR integration against α,α,α-trifluorotoluene as an internal standard.

To evaluate the ability of the obtained Co-C_2F_5 complexes in Co-C bond homolysis, the complexes were subjected to blue LED irradiation (465 nm) in the presence of 2 equiv. of 2,2,6,6-tetramethyl-1-piperidinyloxyl (TEMPO) as the radical trap (refer to **Table 4.5**). Exposure of neutral complexes **4.36**, **4.37**, or an isomeric mixture complexes **4.38a** and **4.38b** (**4.38a**: **4.38b** = 1:4) to blue LED light for 1 hour at room temperature resulted in the generation of a TEMPO-C_2F_5 adduct, as confirmed by ^{19}F NMR spectroscopy (see **Table 4.5**). [187] The yield, determined by ^{19}F NMR integration against α,α,α-trifluorotoluene as an internal standard, showed moderate amounts of TEMPO-C_2F_5, ranging between 21% and 46% yield based on the quantity of Co complex. Similarly, irradiation of cationic complexes **4.42** and **4.43** under blue LED for 1 hour led to the formation of TEMPO-C_2F_5 adduct, with the highest yield observed in complex **4.42** supported by **L1** ligand as 74%. Treatment of complex **4.42** with 2 equiv. of TEMPO in the absence of light did not yield the desired TEMPO-C_2F_5 product. For comparison, exposure of a Co precursor $Co^{III}(C_2F_5)_3(MeCN)_3$ in the presence of TEMPO under analogous conditions only resulted in 18% NMR yield of TEMPO-C_2F_5. These results suggested that, akin to previously reported Ni^{III} complexes[186], visible light irradiation of Co^{III} complexes led to the formation of a C_2F_5 radical trapped by TEMPO, and this reactivity is enhanced in the presence of a naphthyridine ligand. Interestingly, subjecting a Co^{II} complex **4.44** with blue LED under similar conditions yielded only a small amount of TEMPO-C_2F_5 adduct, indicating potentially less efficient light-induced bond homolysis at the Co^{II} oxidation state.

Although the Co-containing product after irradiation could not be isolated in a pure form, ESI-MS analysis of the solution of **4.42** after blue LED irradiation in the absence of TEMPO revealed a peak of *m/z* 438.0344, corresponding to the cationic $[Co^{II}(\mathbf{L1})_2(C_2F_5)]^+$ fragment (calculated *m/z* 438.0309), resulting from the loss of one C_2F_5 group (see **Scheme 4.26**). Similarly, exposure of complex **4.43** under analogous conditions and analysis of the resulting reaction mixture by ESI-HRMS allowed the detection of the corresponding peak of $[Co^{II}(\mathbf{L2})_2(C_2F_5)]^+$ characterized by *m/z* 466.0659 (calculated *m/z* 466.0622).

Scheme 4.27. Photoinduced Co^{III}-C_2F_5 bond homolysis in complex **4.42**.

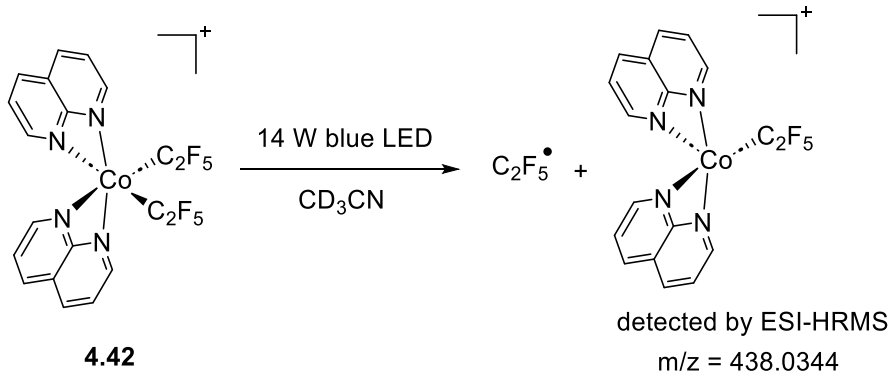

4.2.2.2. Stoichiometric C(sp2)-H pentafluoroethylation mediated by cobalt complexes

Next, we examined the reactivity of Co^{III} complexes in stoichiometric C(sp^2)-H perfluoroethylation. The cobalt perfluoroethyl complexes were reacted with 1 equiv. of an electron-rich substrate, either N-phenylpyrrole (**4.Ia**) or 1,3,5-trimethoxybenzene (**4.Ib**), in acetonitrile-*d*$_3$ for 24 hours at room temperature under blue LED light irradiation. The highest yields of mono-pentafluoroethylated products **4.IIa** and **4.IIb** were observed in the reaction with cationic bis-naphthyridine-based complexes **4.42** and **4.43**, while the analogous reaction with neutral complexes **4.36-4.38** received significantly lower yields. Co^{II} complex **4.44** yielded no detected amount of perfluoroethylated products in both cases, while only trace amount of pentafluorethylated product was obtained in the presence of cobalt(III) precursor $Co(C_2F_5)_3(MeCN)_3$. Without blue LED irradiation, no perfluoroethylated product was detected in the reaction of **4.Ia** or **4.Ib** with complex **4.42**.

In all cases, only mono-perfluoroethylation products were obtained in photo-induced perfluoroethylation. The double-perfluoroethylation products were not detected in both GC-MS analysis and NMR spectroscopy. ^{19}F NMR spectroscopy verified that pentafluoroethane (C_2F_5H) was always present as a byproduct with a yield ranging from 3 to 15% in both cases, while no other fluorine-containing byproducts were found.

Table 4.6. Stoichiometric C-H perfluoroethylation of **4.Ia** and **4.Ib** by cobalt complexes.[a]

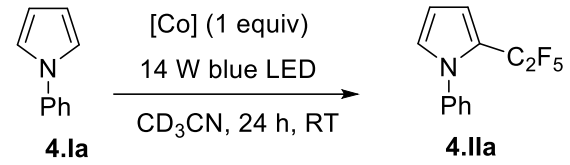

4.Ia **4.IIa**

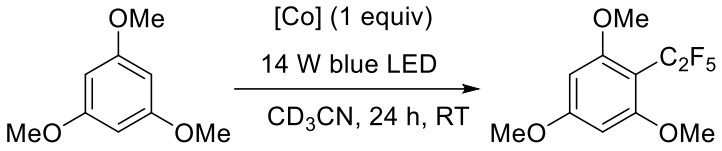

4.Ib **4.IIb**

Entry	Substrate	[Co] complex	Product	Yield (%)[b]
1	**4.Ia**	**4.36**	**4.IIa**	24
2	**4.Ia**	**4.37**	**4.IIa**	29
3	**4.Ia**	**4.38a+4.38b**	**4.IIa**	54
4	**4.Ia**	**4.42**	**4.IIa**	60
5	**4.Ia**	**4.43**	**4.IIa**	59
6	**4.Ia**	**4.44**	**4.IIa**	2
7	**4.Ia**	**4.42**[c]	**4.IIa**	n.d.
8	**4.Ia**	$Co(C_2F_5)_3(MeCN)_3$	**4.IIa**	3
9	**4.Ib**	**4.36**	**4.IIb**	11
10	**4.Ib**	**4.37**	**4.IIb**	24
11	**4.Ib**	**4.38a+4.38b**	**4.IIb**	15
12	**4.Ib**	**4.42**	**4.IIb**	58
13	**4.Ib**	**4.43**	**4.IIb**	43
14	**4.Ib**	**4.44**	**4.IIb**	n.d.
15	**4.Ib**	**4.42**[c]	**4.IIb**	n.d.
16	**4.Ib**	$Co(C_2F_5)_3(MeCN)_3$	**4.IIb**	10

[a]The reactions were performed under N_2 atmosphere for 24 hours using 1 equiv. of substrate and 1 equiv. of a complex in acetonitrile-d_3 at RT under blue light LED (465 nm) unless indicated otherwise [b]Yields were determined by ^{19}F NMR integration against α,α,α-trifluorotoluene as an internal standard. [c]Without 14W blue LED irradiation. n.d. – not detected.

Among these perfluoroethylated cobalt(III) complexes supported by naphthyridine ligands, cationic complexes **4.42** and **4.43** exhibit higher absorption in the visible region evidenced by the broad bands at 4.74 nm and 4.73 nm, respectively, showing better overlap with blue LED emission band (4.65 nm). On the other hand, neutral complexes **4.36-4.38** show less absorption in the range of blue LED emission, which also correlates with their less reactivity in photoinduced perfluoroethylation, compared with cationic complex **4.42** and **4.43** Additionally, the unreactive cobalt(II) complexes **4.44** exhibit a great visible absorption at 471 nm; however, its lack of reactivity could likely be attributed to the instability of the Co^{I}

product resulting from the Co^{II}-C_2F_5 bond homolysis due to poor stabilization of this low oxidation state by N-donor ligands.

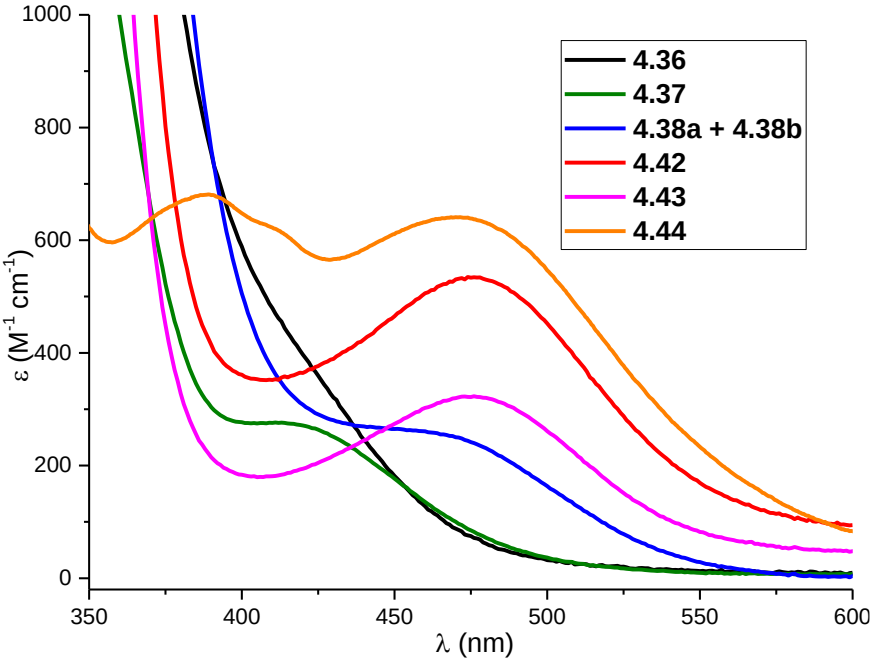

Figure 4.6. Overlay of UV-vis absorption spectra of complexes **4.36**, **4.37**, **4.38a** + **4.38b**, **4.42**, **4.43**, and **4.44** in MeCN.

Scheme 4.28. Reactivity of **4.42** with other substrates in stoichiometric perfluoroethylation.

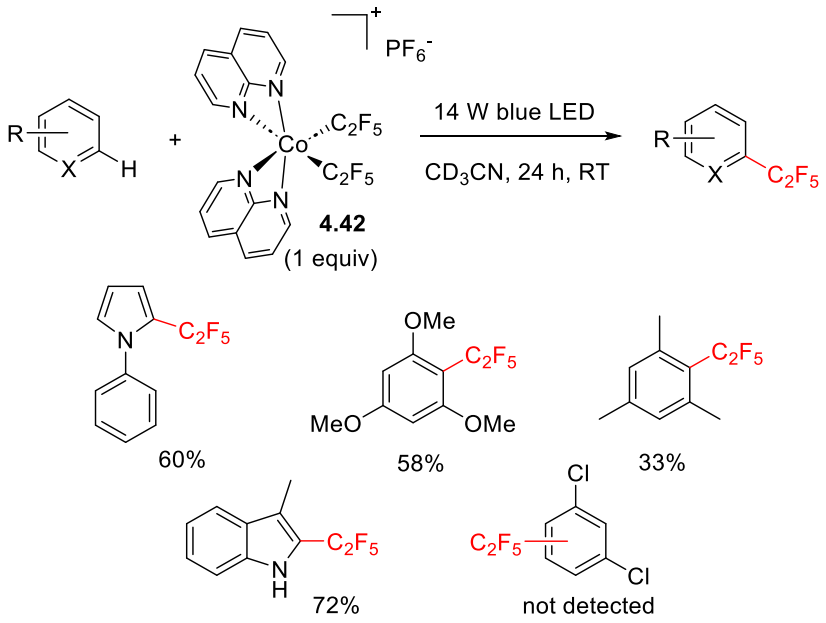

To evaluate the reactivity to other substrates, complex **4.42** underwent reactions with arenes and heteroarenes using standard conditions (**Scheme 4.27**), producing perfluoroethylated products in moderate yield (72%) with 3-methylindole and low yield (33%) with mesitylene. Notably, no reactivity was observed with electron-poor *meta*-dichlorobenzene. In all cases, only one equiv. of a substrate relative to the complex was used and resulted in only the formation of mono-perfluoroethylation, while most reported protocols for radical

trifluoromethylation used a large excess of a substrate, probably to prevent the side reactions such as double perfluoroalkylation.

Based on the radical trap experiment and previous literature, the mechanism for the reaction mediated by cationic complexes **4.42** and **4.43** is proposed in S**cheme 4.28**. A similar pathway might operate in the case of neutral complexes **4.36–4.38**. The formation of a perfluoroethyl-substituted arene in a stoichiometric reaction is likely to occur first through light-induced Co^{III}-C_2F_5 bond homolysis, followed by the C_2F_5 radical attack at the electron-rich arene to yield a radical **4.III**. Given that stoichiometric perfluoroethylation did not include the use of sacrificial reagents, the starting material (complex **4.42** or **4.43**) might act as a sacrificial oxidant to produce inactive **4.44** and release proton. The formation of byproduct C_2F_5H might occur due to the H-atom abstraction from radical **4.III**, which could limit the reaction yield to just 58–60% of perfluoroethylated arene in the best conditions shown in **Table 4.5**.

Scheme 4.29. Proposed mechanism for perfluoroethylated arene formation in the presence of cationic complexes **4.42** or **4.43**.

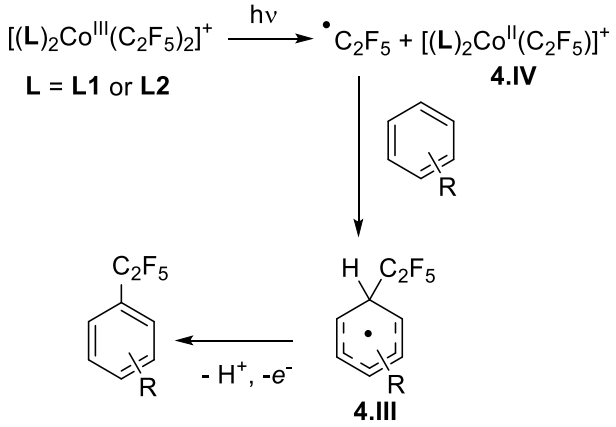

In order to study the effect of additives (base and oxidant) in the perfluoroethylation mediated by complex **4.42**, the reaction was first performed in the presence of 2 equiv. of free naphthyridine ligand or 2,6-di-*tert*-butyl-pyridine, which could potentially play as a proton acceptor during the reaction. However, slightly lower yields were obtained in both cases. In the presence of one equivalent of HBF_4, 68% of the complex remained stable after 24 hours at room temperature, suggesting that a minor amount of acid generated during the reaction might be tolerated in these conditions. On the other hand, the presence of 1 equiv. of copper(II) triflate or ferrocenium as one-electron oxidant improved the yield of perfluoroethylated product **4.IIa** (73 and 65%, respectively) compared to the control experiment under the same conditions (50-60%). Similarly, the addition of 1,4-benzoquinone, which can play as both proton and electron acceptors, also led to the increase of the yield (70%). Surprisingly, azobenzene had a negative impact, most likely due to its strong absorption in the visible spectrum and competing reactivity. Therefore, one possible explanation for the limited yield in stoichiometric perfluoroethylation by **4.42** could be its role as a sacrificial reagent via reduction to inactive **4.44** by **4.III** in the absence of external oxidants, or unproductive release of C_2F_5H via a H atom abstraction by the C_2F_5 radical.

Table 4.7. Stoichiometric C-H pentafluoroethylation of **4.Ia** mediated by **4.42** with the presence of additives.

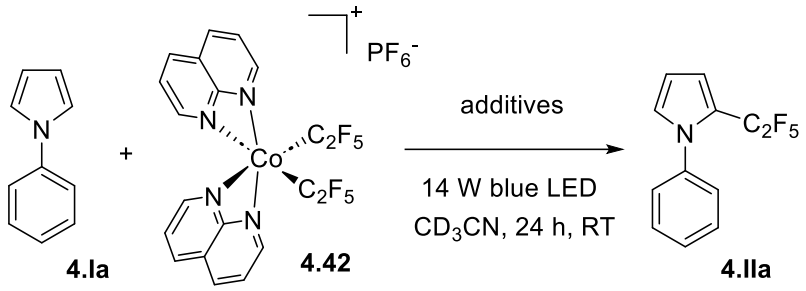

Entry	Additive	Equiv.	Yield of **4.IIa** (%)
1	1,8-naphthyridine	2	44
2	2,6-ditertbutylpyridine	2	41
3	$Cu(OTf)_2$	1	73
4	$Fc^+PF_6^-$	1	65
5	benzoquinone	1	70
6	azobenzene	1	43
7	none		50

4.2.2.3. Catalytic activity of cobalt complexes in perfluoroethylation

We next examined the possibility of cobalt perfluoroethyl complexes as a catalyst for photo-induced perfluoroethylation. While trifluoromethylation catalyzed by nickel or cobalt complexes is often performed with Umemoto or Langlois reagents, or trifluoromethanesulfonyl chloride, the analogous reagents containing perfluoroethyl group are not easy to access. We first attempted to test the catalytic activity of **4.42** using TMS-C_2F_5 in the presence of oxidant, however, no catalytic results were observed. Therefore, we continued to study the catalytic reactivity with a commercially available pentafluoroethyl-1,2-benziodoxol-3(1*H*)-one (Acid C_2F_5-Togni reagent, **4.V**) as a pentafluoroethylation reagent, which was previously used in Ni-catalyzed perfluoroalkylation reported by our group. [179]

1-phenylpyrrole was chosen as a model substrate to react with Acid C_2F_5-Togni reagent **4.V** in the presence of 10 mol% of complex **4.42** in DMSO-d_6 under blue LED irradiation for 24 in room temperature, resulting in the selective formation of mono-pentafluoroethylated product with 76% yield. Changing the solvent to acetonitrile-d_3 did not affect the reaction yield. A significantly lower yield of 32% was obtained in the absence of complex **4.42**, and only 14% of product **4.IIa** was formed in the absence of LED light.

Table 4.8. Perfluoroethylation of **4.Ia** using Acid C_2F_5-Togni reagent IV and complex **4.42**.

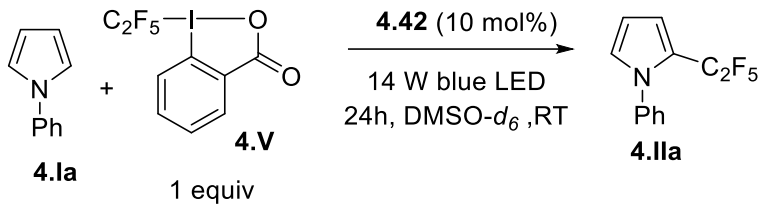

Entry	Modification of standard conditions	Yield (%)
1	None	76
2	CD_3CN instead of DMSO-d_6	76
3	No catalyst **4.42** present	32
4	No blue LED irradiation	14

After obtaining the optimal conditions, other arene and heteroarene substrates were tested, and the results indicated that only the electron-rich N-phenylpyrrole and 1,3,5-trimethoxybenzene exhibited significant reactivity, while mesitylene and meta-dichlorobenzene remained mostly unreacted. Low yield (33%) was obtained in the case of 3-methylindole (**Scheme 4.29**). These experiments showed that complex **4.42** can be a catalyst under these conditions, yet it is not as competitive compared to Ni-catalyzed perfluoroalkylation.[179-180]

Scheme 4.30. Scope of pentafluoroethylation catalyzed by **4.42**.

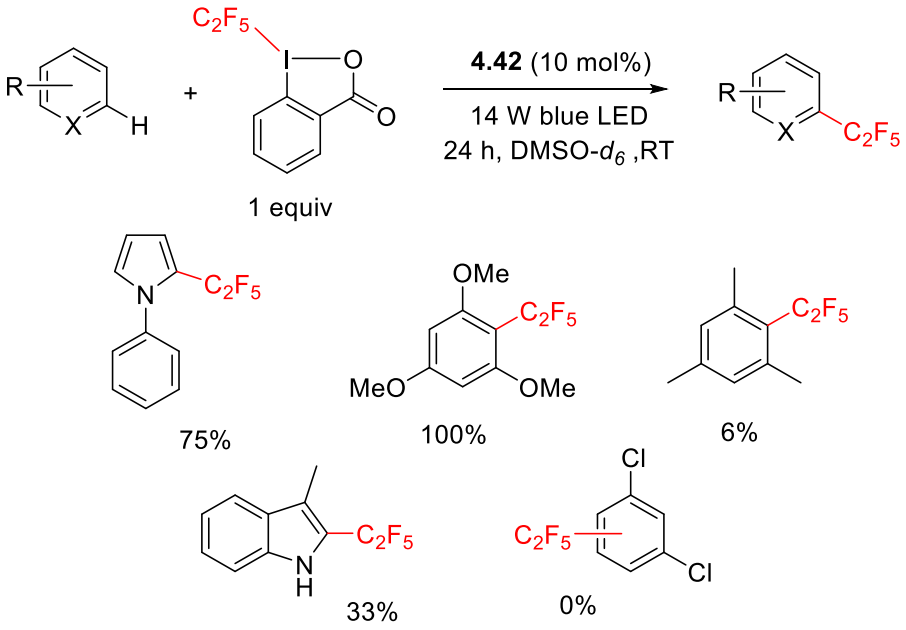

4.3. Conclusion

In this chapter, a new family of cobalt(III) and cobalt(II) perfluoroethyl complexes supported by 1,8-naphthyridine ligand or its mono- and dimethylsubstituted analogs were synthesized and characterized the structural and electronic properties. Under blue LED irradiation, these complexes undergo facile Co-C_2F_5 bond homolysis and release a C_2F_5 radical, which can be trapped by TEMPO radical trap. Selective, monoperfluoroethylation of arenes and heteroarenes mediated by cobalt(III) complexes was observed under blue light irradiation, while cobalt(II) complexes were unreactive. Catalytic C(sp^2)-H perfluoroethylation with

pentafluoroethyl-1,2-benziodoxol-3(1H)-one (Acid C_2F_5-Togni reagent) catalyzed by cobalt(III) complexes has also demonstrated the potential for catalytic applications, albeit moderate yields were observed and the reactivity was limited to electron-rich arenes. Although the catalytic reactivity is less competitive than the reported nickel complex, this study demonstrates the possibility of cobalt catalysts in perfluoroalkylation, perhaps with different ligand system.

4.4. Experimental section

Below experimental data is reported in the following publication:

Dinh, M. H.; Govindarajan, R.; Deolka, S.; Fayzullin, R. R.; Vasylevskyi, S.; Khaskin, E.; Khusnutdinova, J. R. "Photoinduced Perfluoroalkylation Mediated by Cobalt Complexes Supported by Naphthyridine Ligands" *Organometallics*, **2023**, 42, 2632-2643.

$Co(C_2F_5)_3(MeCN)_3$ was prepared according to the literature procedure. [184]

General Specifications

All reactions were performed using standard Schlenk or glovebox techniques under a dry nitrogen atmosphere if not indicated otherwise. Unless noted otherwise, all chemicals were purchased from major commercial suppliers (TCI, Sigma-Aldrich, and Nacalai-Tesque) and used without purification. Anhydrous solvents were dispensed from an MBRAUN solvent purification system and degassed prior to use. Anhydrous deuterated solvents were purchased from Eurisotop and stored over 4 Å molecular sieves. NMR spectra were recorded on a JEOL ECS400S 400 MHz and JEOL ECZ600R 600 MHz. The following abbreviations are used for describing NMR spectra: s (singlet), d (doublet), t (triplet), m (multiplet), dd (doublet of doublets), tt (triplet of triplets), tq (triplet of quartets), vd (virtual doublet), br (broad). A typical Evans method magnetic moment measurement was done in a coaxial tube containing the solvent and the internal standard. Electrospray ionization high-resolution mass spectrometry (ESI-HRMS) measurements were performed on a Thermo Scientific ETD apparatus using MeOH or MeCN as a solvent for injection. Elemental analyses were performed using an Exeter Analytical CE440 instrument. Solid-state FT-IR spectra were recorded using an Agilent Cary 630 with an ATR module in an argon-filled glovebox. The following abbreviations are used for describing FT-IR spectra: s (strong), m (medium), w (weak), and br (broad). UV–vis spectra were recorded on an Agilent Cary 60 spectrophotometer. The X-ray diffraction data for single crystals **1**–**9** was recorded on a Rigaku Xtalab Pro diffractometer or a Bruker D8 Venture diffractometer. Cyclic voltammetry experiments were performed on an ALS CHI 660E electrochemical workstation under N_2 atmosphere. Electrochemical grade tetrabutylammonium perchlorate (TBAP) from Sigma-Aldrich was used as the supporting electrolyte in anhydrous MeCN as a solvent. A glassy carbon disk electrode (d = 1.6 mm) was used as a working electrode. A nonaqueous Ag-wire reference electrode assembly was filled with 0.01 M $AgNO_3$ in 0.1 M TBAP/MeCN solution as a reference electrode. A Pt-wire was used as an auxiliary electrode. The reference electrode was calibrated against $FeCp_2$ (Fc), where the Fc/Fc^+ couple vs $Ag/AgNO_3$/MeCN. Blue LED light was purchased from Akiba LED, 14W, 465 nm.

Synthesis of 4.36:

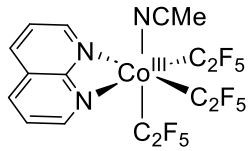

In a glove box, 50.0 mg (0.384 mmol) of 1,8-naphthyridine and 207.1 mg (0.384 mmol, 1 equiv.) of *fac*-$(MeCN)_3Co(C_2F_5)_3$ were dissolved in 5 mL of THF. The reaction mixture was stirred at room temperature for 16 hours. The yellow resulting solution was then crystallized by slow diffusion of pentane to yield **4.36** as yellow crystals. Yield: 146 mg (65%).

^{1}H NMR (600 MHz, –30 °C, acetone-d_6): δ 9.09 (vd, J_{HH} = 4.9 Hz, o-$\boldsymbol{H}_{Naph}$, 2H), 8.86 (dd, J_{HH} = 8.4, 1.6 Hz, p-$\boldsymbol{H}_{Naph}$, 2H), 8.03 (dd, J_{HH} = 8.4, 4.8 Hz, m-$\boldsymbol{H}_{Naph}$, 2H), 2.14 (s, C$\boldsymbol{H}_3$-CN, 3H).

^{19}F NMR (565 MHz, –30 °C, acetone-d_6) δ -80.58 (br s, C$\boldsymbol{F}_3$-CF_2, 6F), -80.79 (br s, C$\boldsymbol{F}_3$-CF_2, 3F), -94.88 - -96.67 (m, CF_3-C$\boldsymbol{F}_2$, 4F).

^{13}C{^{1}H} NMR (151 MHz, –30 °C, acetone-d_6) δ 159.42 (quat.-$\boldsymbol{C}_{Naph}$), 156.03 (o-$\boldsymbol{C}_{Naph}$), 139.80 (p-$\boldsymbol{C}_{Naph}$), 126.33 (m-$\boldsymbol{C}_{Naph}$), 125.45 ($\boldsymbol{C}F_3$-CF_2), 123.15, 121.35 (quat.-$\boldsymbol{C}_{Naph}$), 121.23, 119.31, 117.39 2.44 ($\boldsymbol{C}H_3$-CN). The carbon atom of the nitrile group could not be identified due to low intensity. Peaks at 123.15, 121.23, 119.31, and 117.39 ppm were not clearly identified due to splitting from F and low intensity.

ESI-HRMS (*m*/*z*): found (calcd.): $C_{14}H_9Co_1F_{10}N_3^+$: 467.9897 (467.9963).

Elemental analysis found (calcd.): $C_{16}H_9Co_1F_{15}N_3$: C 33.20 (32.73), H 1.53 (1.54), 6.96 (7.16).

UV-Vis (CH_3CN), λ, nm (ε, M^{-1} cm^{-1}): 425 (360), 357 (1880), 308 (9430).

FT-IR (ATR, solid): 3163 (br), 2999 (br), 2944 (br), 2291 (m), 2252 (s), 1434 (m), 1418 (br), 1374 (s), 1038 (s), 747 (s), 665 (m), 654 (m).

Synthesis of 4.37:

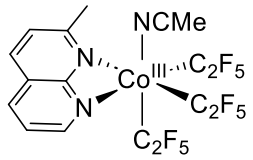

In a glove box, 27.0 mg (0.188 mmol) of 2-methyl-1,8-naphthyridine and 101.1 mg (0.188 mmol, 1 equiv.) of *fac*-$(MeCN)_3Co(C_2F_5)_3$ were dissolved in 3 mL of THF. The reaction mixture was stirred at room temperature for 16 hours. The yellow resulting solution was then crystallized by slow diffusion of pentane to yield **4.37** as yellow crystals. Yield: 76.5 mg (68%).

^{1}H NMR (600 MHz, –30 °C , acetone-d_6): δ 9.13 (d, $^3J_{HH}$ = 5.2 Hz, o-$\boldsymbol{H}_{Naph}$, 1H), 8.80 (d, $^3J_{HH}$ = 8.2 Hz, p-$\boldsymbol{H}_{Naph}$, 1H), 8.68 (d, $^3J_{HH}$ = 8.5 Hz, p-$\boldsymbol{H}_{Naph}$, 1H), 7.97 (dd, J_{HH} = 8.3, 5.0 Hz, m-$\boldsymbol{H}_{Naph}$, 1H), 7.83 (d, $^3J_{HH}$ = 8.4 Hz, m-$\boldsymbol{H}_{Naph}$, 1H), 2.76 (s, $\boldsymbol{H}_{Me}$, 3H), 2.23 (s, C$\boldsymbol{H}_3$CN, 3H).

^{19}F NMR (565 MHz, –30 °C , acetone-d_6) δ -78.86 (br s, C$\boldsymbol{F}_3$-CF_2, 3F), -79.89 (br s, C$\boldsymbol{F}_3$-CF_2, 3F), -81.01 (d, $^2J_{FF}$ = 256.8 Hz, CF_3-C$\boldsymbol{F}_2$, 1F), -81.09 (br s, C$\boldsymbol{F}_3$-CF_2, 3F), -88.26 (d, J = 237.9 Hz, CF_3-C$\boldsymbol{F}_2$, 1F), -91.83 (d, $^2J_{FF}$ = 258.9 Hz, CF_3-C$\boldsymbol{F}_2$, 1F), -97.36 (d, $^2J_{FF}$ = 238.1 Hz, CF_3-C$\boldsymbol{F}_2$, 1F), -98.45 (d, $^2J_{FF}$ = 259.2 Hz, CF_3-C$\boldsymbol{F}_2$, 1F), -100.39 (d, $^2J_{FF}$ = 259.0 Hz, CF_3-C$\boldsymbol{F}_2$, 1F).

^{13}C{^{1}H} NMR (151 MHz, –30 °C, acetone-d_6) δ 210.13 (CH_3-$\boldsymbol{C}$N), 168.66 (quat.-$\boldsymbol{C}_{Naph}$), 159.63 (quat.-$\boldsymbol{C}_{Naph}$), 155.20 (o-$\boldsymbol{C}_{Naph}$), 139.62 (p-$\boldsymbol{C}_{Naph}$), 138.99 (p-$\boldsymbol{C}_{Naph}$), 128.62 (m-$\boldsymbol{C}_{Naph}$), 126.09 ($\boldsymbol{C}F_3$-CF_2), 125.14 (m-$\boldsymbol{C}_{Naph}$), 119.81 (quat.-$\boldsymbol{C}_{Naph}$), 22.91 ($\boldsymbol{C}_{Me}$), 2.53 ($\boldsymbol{C}H_3$-CN). The carbon atoms of C_2F_5 could not be identified due to splitting from F and low intensity.

ESI-HRMS (*m/z*): found (calcd): $C_{15}H_{11}Co_1F_{10}N_3^+$: 482.0055 (482.0120).

Elemental analysis found (calcd): $C_{17}H_{11}Co_1F_{15}N_3$: 34.15 (33.96), 1.61 (1.84), 7.03 (6.91).

UV-Vis (CH_3CN), λ, nm (ε, M^{-1} cm^{-1}): 425 (260), 311 (9097), 267 (9867).

FT-IR (ATR, solid): cm^{-1} 3162 (br), 3002 (br), 2943 (br), 2292 (m), 2251 (s), 1441 (s), 1428 (m), 1374 (s), 1038 (s), 917 (s), 747 (s).

Synthesis of 4.38a + 4.38b:

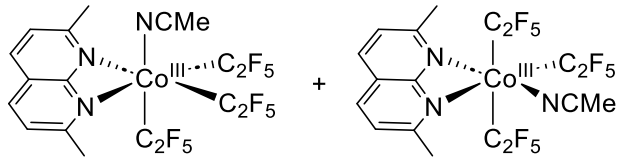

3a **3b**

In a glove box, 31.6 mg (0.2 mmol) of 2,7-bis(methyl)-1,8-naphthyridine (**L3**) and 107.8 mg (0.2 mmol, 1 equiv.) of *fac*-$(MeCN)_3Co(C_2F_5)_3$ were dissolved in 5 mL of THF. The mixture was then transferred to a 25 mL Schlenk flask and brought out of the glove box. The reaction was heated at 65 °C for 16 hours to yield a mixture **4.38a : 4.38b** = 1 : 4 . The resulting orange solution was then crystallized by slow diffusion of pentane to yield **4.38a : 4.38b** = 1:4 as orange crystals. Yield: 76.5 mg (68%).

ESI-HRMS (*m/z*): found (calcd): $C_{16}H_{13}Co_1F_{10}N_3^+$: 496.0214 (496.0274).

EA found (cald): $C_{18}H_{13}Co_1F_{15}N_3$: C 35.14 (35.14), H 1.71 (2.13), N 6.72 (6.83). UV-Vis (CH_3CN), λ, nm (ε, M^{-1} cm^{-1}): 450 (265), 311 (16142).

FT-IR (ATR, solid, cm^{-1}): 3163 (br), 3003 (br), 2943 (br), 2291 (s), 2251 (s), 1779 (br), 1694 (br), 1440 (s), 1429 (br), 1374 (s), 1037 (s), 917 (s), 748 (s), 674 (s).

^{1}H NMR for **4.38a** (600 MHz, 23 °C, acetone-*d*$_6$): δ 8.53 (d, $^3J_{HH}$ = 8.3 Hz, ***H***$_{naph}$, 2H), 7.71 (d, $^3J_{HH}$ = 8.3 Hz, ***H***$_{naph}$, 2H), 2.79 (s, C***H***$_3$, 6H).

^{1}H NMR for **4.38b** (600 MHz, 23 °C, acetone-*d*$_6$): δ 8.51 (d, $^3J_{HH}$ = 8.5 Hz, ***H***$_{naph}$, 1H), 8.47 (d, $^3J_{HH}$ = 8.4 Hz, ***H***$_{naph}$, 1H), 7.74 (d, $^3J_{HH}$ = 8.5 Hz, ***H***$_{naph}$, 1H), 7.53 (d, $^3J_{HH}$ = 8.4 Hz, 1H), 2.81 (s, C***H***$_3$, 3H), 2.65 (s, C***H***$_3$-CN, 3H), 2.62 (s, C***H***$_3$, 3H).

^{19}F peaks of **4.38a** are broadened in ^{19}F NMR spectrum and could not be fully resolved even at low temperature. In ^{19}F NMR spectrum obtained for **4.38a : 4.38b** = 1 :4 mixture, only peaks of **4.38b** could be clearly assigned (eq = equatorial C_2F_5 in-plane with naphthyridine; ap – apical C_2F_5 groups perpendicular to naphthyridine place): ^{19}F NMR of **4.38b** (565 MHz, 23 °C, acetone-*d*$_6$): δ -75.68 (br m, CF_3-C***F***$_2$ eq, 2F), -79.24 (tt, $^5J_{FF}$ = 9.2, 25 Hz, C***F***$_3$-CF_2 eq, 3F), -81.75 (t, $^3J_{FF}$ = 7.8 Hz, C***F***$_3$-CF_2 ap, 6F), -96.82 (dq, $^2J_{FF}$ = 283 Hz, $^5J_{FF}$ = 8.5 Hz,CF_3-C***F***F ap, 2F), -103.11 (dm, $^2J_{FF}$ = 284 Hz, CF_3-CF***F*** ap, 2F).

^{13}C{^{1}H} NMR of **4.38a : 4.38b** = 1 : 4 (151 MHz, 23 °C, acetone-*d*$_6$) δ 210.03, 170.44, 168.24, 167.40, 159.27, 138.79, 138.69, 138.04, 133.43, 129.14, 127.97, 127.83, 127.51, 124.44, 124.23, 124.01, 122.52, 122.31, 122.10, 120.79, 120.57, 120.39, 118.86, 118.64, 118.15, 116.29, 69.20, 68.04, 66.10, 54.95, 54.78, 54.66, 54.53, 22.25, 22.20, 22.15, 21.42.

Observation of the 4.38a+4.38b (**4.38a** : **4.38b** = 20 : 1) **formation at RT:** In a glove box, 2.9 mg (0.18 mmol) of **L3** and 10.0 mg (0.18 mmol, 1 equiv.) of *fac*-$(MeCN)_3Co(C_2F_5)_3$ were dissolved in 1 mL of acetone-*d*$_6$. The reaction mixture was stirred at room temperature for 1 hour, and then was analyzed by ^{1}H NMR, showing the formation of a mixture **4.38a : 4.38b** = 20 : 1. Single crystals of **4.38a** could be obtained by diffusing pentane to the solution at –30 °C.

Synthesis of 4.39:

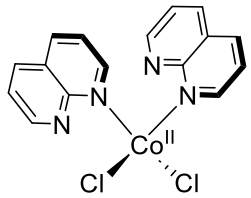

200.0 mg of **L1** (1.537 mmol, 2 equiv.) and 41.0 mg of $CoCl_2$ (0.768 mmol, 1 equiv.) were dissolved in 10 mL of 2:1 DCM-MeOH mixture. The dark blue solution was then stirred vigorously at room temperature for 16 h, then recrystallized by diffusing ether to the mother solution to yield **4.39** as blue crystals. Yield: 210 mg (70%).

EA found (calcd) : $C_{16}H_{12}Co_1Cl_2N_4$: C 48.45 (49.26), H 2.84 (3.10), N 13.89 (14.36).

ESI-HRMS (*m/z*): found (calcd): $C_{16}H_{12}Co_1Cl_1N_4^+$: 354.0080 (354.0077).

UV-Vis (CH_3OH), λ, nm (ε, M^{-1} cm^{-1}): 530 (11), 301 (15024).

FT-IR (ATR, solid): 3047 (br), 1595 (s), 1498 (s), 1391 (m), 1293 (m), 1235 (m), 1197 (m), 1143 (s), 1128 (s), 1062 (s), 1034 (m), 956 (m), 841 (s), 800 (s). 782 (s).

μ_{eff} = 4.65 μB (298 K, Evans method, methanol-d_4).

Synthesis of 4.40:

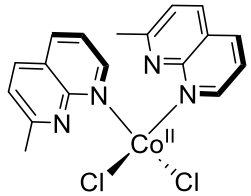

200.0 mg of **L2** (1.387 mmol, 2 equiv.) and 89.6 mg of $CoCl_2$ (0.694 mmol, 1 equiv.) were dissolved in 15 mL of 2:1 DCM-MeOH mixture. The dark blue solution was then stirred vigorously at room temperature for 16 h and recrystallized by diffusing ether to the mother solution to yield **4.40** as blue crystals. Yield: 284.2 mg (98%).

ESI-HRMS (*m/z*): found (calcd): $C_{18}H_{16}Co_1Cl_1N_4^+$: 382.0386 (382.0390).

EA found (calcd) : $C_{18}H_{16}Co_1Cl_2N_4$: C 51.23 (51.70), H 3.75 (3.86), N 12.78 (13.40).

UV-Vis (CH_3OH), λ, nm (ε, M^{-1} cm^{-1}): 315 (7535), 298 (8472), 7262 (257), 224 (7484).

FT-IR (ATR, solid): 3048 (br), 1613 (s), 1566 (s), 1493 (s), 1421 (m), 1376 (s), 1300 (s), 1286 (s), 1218 (m), 1138 (s), 1132 (m), 1063 (m), 1035 (m), 909 (m), 847 (s), 798 (s), 708 (m), 656 (s).

μ_{eff} = 5.06 μB (298 K, Evans method, methanol-d_4).

Synthesis of 4.41:

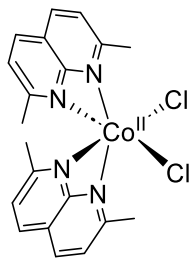

100.0 mg of **L3** (0.632 mmol, 2 equiv.) and 41.0 mg of $CoCl_2$ (0.316 mmol, 1 equiv.) were dissolved in 10 mL of 2:1 DCM-MeOH mixture. The dark blue solution was then stirred vigorously at room temperature for 16 h, then recrystallized by diffusing ether to the mother solution to yield **4.41** as blue crystals. Yield: 90 mg (64%).

ESI-HRMS (*m/z*) found (calcd): $C_{20}H_{20}Co_1Cl_1N_4$+: 410.0692 (410.0703).

UV-Vis (CH_3OH), λ, nm (ε, M^{-1} cm^{-1}): 316 (18660), 310 (15600), 253 (6900). 217 (27000).

FT-IR (ATR, solid): 3061 (br), 3007 (br), 1609 (s), 1566 (m), 1509 (s), 1439 (s), 1377 (s), 1313 (s), 1252 (s), 1215 (m), 1141 (s), 1035 (m), 998 (m), 853 (s), 800 (s), 789 (br).

μ_{eff} = 4.88 μB (298 K, Evans method, methanol-d_4).

Synthesis of 4.42:

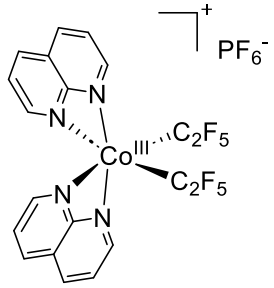

In a glovebox, 100.0 mg of AgF (0.820 mmol, 3.2 equiv.) and 180 μL of $TMSC_2F_5$ (1.03 mmol, 4 equiv.) were mixed in 10 mL of acetonitrile. The reaction mixture was stirred in a dark for 2 hours, then the mixture was transferred to a 20-mL vial containing 100.0 mg of **4.39** (0.256 mmol, 1 equiv.) and 47.4 mg of $NaPF_6$ (0.282 mmol, 1.1 equiv.). The mixture was stirred vigorously in the dark for 3 days. The resulting yellow-brown slurry was filtered over celite, and the solvent was removed under vacuum to yield an orange-red precipitate, which was washed by pentane. Orange single crystals were grown by slow diffusion of pentane to the THF solution of **4.42**. Yield: 109 mg (61%).

^{1}H NMR (400 MHz, 23 °C, CD_3CN) δ 8.80 (dd, $^3J_{HH}$ = 8.5, 1.4 Hz, $\boldsymbol{H}_{Naph}$, 2H), 8.77 (dd, J_{HH} = 5.2, 1.4 Hz, $\boldsymbol{H}_{Naph}$, 2H), 8.73 (dd, J_{HH} = 8.6, 1.5 Hz, $\boldsymbol{H}_{Naph}$, 2H), 8.68 (dd, J_{HH} = 4.8, 1.5 Hz, $\boldsymbol{H}_{Naph}$, 2H), 7.90 (dd, J_{HH} = 8.5, 5.2 Hz, $\boldsymbol{H}_{Naph}$, 2H), 7.82 (dd, $^3J_{HH}$ = 8.5, 4.8 Hz, $\boldsymbol{H}_{Naph}$, 2H).

^{19}F NMR (564 MHz, 23 °C, CD_3CN): δ -72.81 (d, $^1J_{PF}$ = 706.4 Hz, P$\boldsymbol{F}_6$, 6 H), -81.58 (t, J ~ 5 Hz, C$\boldsymbol{F}_3$-CF_2, 6H), -86.13 (vd, $^2J_{FF}$ = 228.5 Hz, CF_3-C$\boldsymbol{F}_2$, 2H), -94.08 (vd, $^2J_{FF}$ = 227.5 Hz, CF_3-C$\boldsymbol{F}_2$, 2H).

^{13}C{^{1}H} NMR (101 MHz, 23 °C, CD_3CN): δ 159.11 (quat.-$\boldsymbol{C}_{Naph}$), 158.76 (*o*-$\boldsymbol{C}_{,Naph}$), 155.53 (*p*-$\boldsymbol{C}_{Naph}$), 141.69 (*o*-$\boldsymbol{C}_{Naph}$), 140.60 (*p*-$\boldsymbol{C}_{Naph}$), 127.60 (*m*-$\boldsymbol{C}_{Naph}$), 127.43 (*o*-$\boldsymbol{C}_{Naph}$), 121.43 (quat.-C_{Naph}). The carbon atoms of C_2F_5 could not be identified due to splitting from F and low intensity.

ESI-HRMS (*m/z*): found (calcd): $C_{20}H_{12}Co_1F_{10}N_4^+$: 557.0245 (557.0229).

EA found (calculated) $C_{20}H_{12}Co_1F_{16}N_4P_1$: C 33.81 (34.21), H 1.33 (1.72), N 7.93 (7.98). UV-Vis (CH_3CN), λ, nm (ε, M^{-1} cm^{-1}): 474 (534), 302 (22000).

FT-IR (ATR, solid) 3162 (br), 3002 (br), 2943 (br), 2626 (br), 2405 (br), 2291 (s), 2251 (s), 1738 (m), 1442 (m), 1420 (br), 1374 (s), 1038 (s), 918 (s), 748 (s), 667 (m).

Synthesis of 4.43:

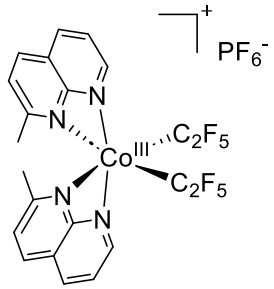

In a glovebox, 97.1 mg of AgF (0.765 mmol, 3.2 equiv.) and 168 μL of $TMSC_2F_5$ (0.96 mmol, 4 equiv.) were mixed in 10 mL of acetonitrile. The reaction mixture was stirred in a dark for 2 hours, then the mixture was transferred to a 20-mL vial containing 100.0 mg of **4.40** (0.239 mmol, 1 equiv.) and 44.1 mg of $NaPF_6$ (0.263 mmol, 1.1 equiv.). The mixture was stirred vigorously in the dark for 3 days. The resulting yellow-brown slurry was filtered over celite, and the solvent was removed under vacuum to yield an orange-red precipitate, which was washed by pentane. Orange single crystals can be recrystallized by slow diffusion of pentane to the THF solution of **4.43**. Yield 64.2 mg (37%).

^{1}H NMR (400 MHz, 23 ºC, CD_3CN) δ 8.80 (d, $^3J_{HH}$ = 5.1 Hz, o-$\boldsymbol{H}_{Naph}$, 2H), 8.75 (dd, J_{HH} = 8.3, 1.2 Hz, p-$\boldsymbol{H}_{Naph}$, 2H), 8.54 (d, $^3J_{HH}$ = 8.7 Hz, p-$\boldsymbol{H}_{Naph}$, 2H), 7.85 (dd, J_{HH} = 8.5, 5.1 Hz, m-$\boldsymbol{H}_{Naph}$, 2H), 7.64 (d, $^3J_{HH}$ = 8.7 Hz, m-$\boldsymbol{H}_{Naph}$, 2H), 1.77 (s, C$\boldsymbol{H}_3$, 6H).

^{19}F NMR (564 MHz, 23 ºC, CD_3CN) δ -72.78 (d, $^1J_{PF}$ = 706.3 Hz, P$\boldsymbol{F}_6$, 6F), -81.77 (m, CF_3-C$\boldsymbol{F}_2$, 6H), -84.27 (vd, $^2J_{FF}$ = 226.2 Hz, CF_3-C$\boldsymbol{F}_2$, 2F), -93.13 (vd, $^2J_{FF}$ = 219.8 Hz, CF_3-C$\boldsymbol{F}_2$, 2F).

^{13}C{^{1}H} NMR (101 MHz, 23 ºC, CD_3CN): δ 168.25 (quat.-$\boldsymbol{C}_{Naph}$), 159.19 (quat.-$\boldsymbol{C}_{Naph}$), 157.95 (o-$\boldsymbol{C}_{Naph}$), 141.74 (p-$\boldsymbol{C}_{Naph}$), 139.54 (p-$\boldsymbol{C}_{Naph}$), 129.49 (m-$\boldsymbol{C}_{Naph}$), 126.72 (m-$\boldsymbol{C}_{Naph}$), 119.24 (quat.-$\boldsymbol{C}_{Naph}$), 21.42 ($\boldsymbol{C}_{Me}$). The carbon atoms of C_2F_5 could not be identified due to splitting from F and low intensity.

ESI-HRMS (*m/z*): found (calcd): $C_{22}H_{16}Co_1F_{10}N_4^+$: 585.0559 (585.0542).

EA found (cald): 36.77 (36.18), 1.99 (2.21), 7.08 (7.67).

UV-Vis (CH_3CN), λ, nm (ε, M^{-1} cm^{-1}): 473 (322), 304 (17130).

FT-IR (ATR, solid): cm^{-1} 3162 (br), 3001 (br), 2943 (br), 2628 (br), 2405 (br), 2291 (s), 2251 (s), 1738 (m), 1442 (m), 1417 (br), 1374 (s), 1217 (br), 1038 (s), 917 (s), 747 (s), 667 (br).

Synthesis of 4.44:

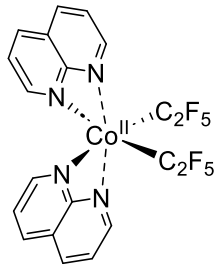

In a glove box, 100.0 mg (0.142 mmol) of complex **4.42** was dissolved in 5 mL of THF. The orange solution was then transferred to a 20-mL vial containing 19.3 mg (0.142 mmol, 1 equiv.) of potassium graphite and the reaction mixture was stirred for 3 hours. The mixture was filtered through celite to remove any precipitate, and the solvent was removed under a vacuum to yield a red-wine powder, which was washed with a copious amount of pentane.

Red wine single crystals were recrystallized by slow diffusion of pentane to the THF solution of **4.44**. Yield: 41 mg (52%).

μ_{eff} = 1.85 μB (298 K, Evans method, acetone-d_6).

ESI-HRMS (*m/z*): found (calcd): $C_{18}H_{12}Co_1F_5N_4^+$: 438.0335 (438.0309).

EA found (cald): $C_{20}H_{12}Co_1F_{10}N_4$: C 41.17 (43.11), H 1.85 (2.17), N 9.55 (10.05).

UV-Vis (MeCN), λ, nm (ε, M^{-1} cm^{-1}): 471 (641), 389 (681), 296 (13250).

FT-IR (ATR, solid) : 2972 (m), 2857 (m), 1459 (br), 1176 (br), 1067 (s), 907 (s).

Radical trap by TEMPO experiments: In a glove box, a specified cobalt complex (0.01 mmol) and 3.1 mg of TEMPO (0.02 mmol, 2 equiv.) were dissolved in 0.7 mL of acetonitrile-d_3. To the solution, 1.2 μL of α,α,α-trifluorotoluene (0.01 mmol, 1 equiv.) was added as an internal standard. The resulting solution was then transferred to a young NMR tube and was placed 2-3 cm far away from a 14 W blue LED light equipped with a fan. The reaction was irradiated under the blue LED for one hour. The yield of the reaction was determined by ^{19}F NMR integration against α,α,α-trifluorotoluene as an internal standard.

ESI-HRMS analysis of the reaction mixture containing cobalt(III) complexes after irradiation: In a glove box, 0.01 mmol of a Co^{III} complex (**4.42** or **4.43**) was dissolved in 1 mL of acetonitrile. The resulting solution was transferred to a J. Young NMR tube, which was then placed 2-3 cm far away from 14 W blue LED light equipped with a fan and irradiated for 30 minutes. The reaction mixture was immediately analyzed by ESI-HRMS. The HRMS analysis shows the appearance of a new peak, which was not present in the solution of the starting complexes before irradiation.

After irradiation of complex **4.42**, a new peak is assigned to $[Co(\mathbf{L1})_2(C_2F_5)]^+$ ($C_{18}H_{12}Co_1F_5N_4$): *m/z* observed (cald): 438.0344 (438.0309).

After irradiation of complex **4.43**, a new peak is assigned to $[Co(\mathbf{L2})_2(C_2F_5)]^+$ ($C_{20}H_{16}Co_1F_5N_4$): *m/z* observed (cald): 466.0659 (466.0622).

General procedure for stoichiometric C-H perfluoroethylation: In a glove box, an arene or heteroarene substrate (0.01 mmol) and cobalt complex (0.01 mmol, 1 equiv.) were dissolved in 1 mL of acetonitrile-d_3. The solution was transferred to a J. Young NMR tube, which was then placed 2-3 cm far away from a 14 W blue LED light and irradiated for 24 hours. The reaction setup was equipped with a fan to avoid heating from irradiation. After the completion of the reaction, α,α,α-trifluorotoluene (0.01 mmol, 1 equiv.) was added to the reaction mixture. The yields were determined by ^{19}F NMR integration against α,α,α-trifluorotoluene as an internal standard. The formation of C_2F_5H is established by NMR spectroscopy by comparison with the literature reports[188-189] and the yield are shown for individual reaction mixtures in the Supporting Information.

A similar procedure was used for perfluoroethylation of N-phenylpyrrole in the presence of additives.

General procedure for perfluoroethylation in the presence of catalytic amount of 4.42 and Acid C_2F_5-Togni reagent: In a glove box, an arene or heteroarene substrate (0.05 mmol), complex **4.42** (3.5 mg, 0.005 mmol, 10 mol%) and 1-pentafluoroethyl-1,2-benziodoxol-3(1*H*)-one (18.3 mg, 0.05 mmol, 1 equiv.) were dissolved in 1 mL of DMSO-d_6 or different solvent. The mixture was then transferred to an 11 mL screw-cap reaction tube and sealed with electric tape to avoid gas exchange. The tube was placed 2-3 cm far away from a 14 W blue LED light and irradiated for 24 hours. The reaction setup was equipped with a fan to avoid heating from irradiation. After the completion of the reaction, 6.1 μL of

α,α,α -trifluorotoluene (0.01 mmol, 1 equiv.) were added to the reaction mixture as internal standard and the resulting mixture was analyzed by NMR and GS-MS spectroscopy. The yields were determined by ^{19}F NMR integration against α,α,α-trifluorotoluene as an internal standard.

Computational details. All DFT calculations were implemented in the Gaussian 16 program. [53] Geometries were optimized without symmetry restrictions using M06L functional[190] and SDD[55] (for Co)/6-31++g(d,p) [56-63] (for other elements) basis set; ground state corresponded to the absence of imaginary frequencies. For comparison of relative stabilities of **4.38a** and **4.38b**, the structures were optimized taking into account the solvent (acetone) effect via the SMD model. [64] The quantum-topological analysis of the calculated electron density for "gas-phase" and solution (acetone) optimized structures was performed within the quantum topological theory of atoms in molecules by means of the AIMAll package (v 19.10.12).[191]

Conclusion and Future Outlook

This thesis presents a study of the synthesis and reactivity of metal complexes supported by non-phosphine ligands, with a particular focus on metal-ligand cooperation and fluoroalkyl incorporation. The new family of manganese(I) and ruthenium(II) complexes supported by N,S-donor macrocyclic pyridinophane ligand showed reversible single and double deprotonation of the CH_2S arms, leading to the formation of single and double dearomatization of the pyridine rings.

The main conclusion followed from my initial studies of the reactivity of tetradentate **N2S2**-pyridinophane Mn and Ru complexes is that the macrocyclic ligand framework allows to some extent to stabilize singly and even doubly deprotonated and dearomatized species, making them more accessible as compared to sulfur-containing tridentate pincer ligands. This allowed for their direct structural and spectroscopic comparison. However, the application of these complexes in catalytic and stoichiometric bond activation was limited by two factors: (1) lack of vacant coordination sites and (2) irreversible rearrangement of the sulfur-containing macrocycle (in the case of a Ru complex). Even when relatively more labile acetonitrile ligand was employed at the Ru center, no catalytic activity could be observed. Therefore, more robust ligand framework that at the same time allows for the presence of vacant coordination sites is required to obtain potentially catalytically active transition metal complexes supported by non-phosphine, N,S-donor ligands.

The macrocylic pyridinophane ligand was then utilized to stabilize high-valent aryl-Mn^{III} dibromide complex via oxidative addition of Ar-Br bond to manganese(I) precursor. Upon one-electron oxidation, the complex underwent reductive elimination, likely via Mn^{IV} intermediate, to form Ar-Br coupling product and Mn^{II} species. This result suggested that tetradentate N,C-donor pyridinophane ligand scaffolds offer a unique possibility to stabilize organometallic Mn^{III} derivatives and enable studying oxidative addition/reductive elimination processes at the first-row metal center, especially in paramagnetic high-valent complexes. At the same time, catalytic activity was prevented in this case due to multidentate nature of the ligand and lack of accessible pathway to recycle paramagnetic Mn^{II} product into reactive Mn^{I} species. However, these studies showed that aryl-heteroatom reductive elimination was not possible at the Mn^{III} center and required its further chemical oxidation, presumably to Mn^{IV}.

Unexpectedly, my further studies into developing similar **N3C**-pyridinophane Mn^{III} complexes for C-C bond elimination yielded in uncovering an unexpected synthetic approach to prepare high-valent manganese(III) fluoro complexes via transmetalation followed by α-fluorine elimination, resulting in the release of a difluorocarbene. That more facile generation of a difluorocarbene was then employed in difluorocyclopropanation and difluorocyclopropenation of alkene and alkynes using trifluoromethyl zinc reagent, under milder conditions (lower temperature and shorter time) as compared to manganese-free reaction.

Following these results that led me to the topic of fluorine incorporation into organic molecules, I then further simplified the ligand scaffold and utilized a simple, bidentate N-donor ligand, naphthyridine and its methyl-substituted derivatives. This led to the isolation of a a new series of Co^{II} and Co^{III} perfluoroethyl complexes. These complexes exhibited Co-C_2F_5 bond homolysis under visible-light irradiation and could serve as catalysts for arene perfluoroalkylation using the Togni reagent.

Overall, through the course of my studies, I have been able to study the reactivity of a range of first-row metal complexes (except Ru) with non-phosphine-donor ligands, progressing from macrocyclic, tetradentate N,S-donor ligands to N,C-donor pyridinophanes and eventually simple N-donor ligands, which ultimately lead to the development of catalytic C-H bond perfluoroalkylation under visible light. These studies show that among various ligand scaffolds utilized in this work, tetradentate macrocyclic pyridinophane ligands are convenient tools to study elementary reaction steps in organometallic chemistry such as oxidative addition, reductive elimination, α-fluorine elimination; however, catalytic activity is generally hindered due to overstabilization of otherwise inaccessible species. At the same, using simple but non-trivial naphthyridine ligands, photocatalytically active complexes could be eventually obtained, by contrast to previous literature where sophisticated multidentate ligand design was employed.

In the future, I expect that further studies will be needed to clarify the role of the naphthyridine ligand in first-row transition metal complexes and its electronic and steric differences with other commonly employed N-heterocycles, such as bipyridine-based ligands.

Reference List

1. Tsuji, J., *Transition metal reagents and catalysts: innovations in organic synthesis*. John Wiley & Sons: 2002.
2. Van Leeuwen, P. W., *Homogeneous catalysis: understanding the art*. Springer Science & Business Media: 2006.
3. Brandsma, L.; Vasilevsky, S. F.; Verkruijsse, H. D., *Application of transition metal catalysts in organic synthesis*. Springer Science & Business Media: 2012.
4. Crawley, M. L.; Trost, B. M., *Applications of transition metal catalysis in drug discovery and development: an industrial perspective*. Wiley Online Library: 2012.
5. Hartwig, J. F., *Organotransition Metal Chemistry: From Bonding to Catalysis*. University Science Books: 2010.
6. Crabtree, R. H., *The Organometallic Chemistry of the Transition Metals*. Wiley: 2005.
7. Lorent, C.; Katz, S.; Duan, J.; Kulka, C. J.; Caserta, G.; Teutloff, C.; Yadav, S.; Apfel, U.-P.; Winkler, M.; Happe, T.; Horch, M.; Zebger, I., Shedding Light on Proton and Electron Dynamics in [FeFe] Hydrogenases. *Journal of the American Chemical Society* **2020,** *142* (12), 5493-5497.
8. Artz, J. H.; Zadvornyy, O. A.; Mulder, D. W.; Keable, S. M.; Cohen, A. E.; Ratzloff, M. W.; Williams, S. G.; Ginovska, B.; Kumar, N.; Song, J.; McPhillips, S. E.; Davidson, C. M.; Lyubimov, A. Y.; Pence, N.; Schut, G. J.; Jones, A. K.; Soltis, S. M.; Adams, M. W. W.; Raugei, S.; King, P. W.; Peters, J. W., Tuning Catalytic Bias of Hydrogen Gas Producing Hydrogenases. *Journal of the American Chemical Society* **2020,** *142* (3), 1227-1235.
9. Ogata, H.; Lubitz, W.; Higuchi, Y., [NiFe] hydrogenases: structural and spectroscopic studies of the reaction mechanism. *Dalton Transactions* **2009,** (37), 7577-7587.
10. Elsby, M. R.; Baker, R. T., Strategies and mechanisms of metal–ligand cooperativity in first-row transition metal complex catalysts. *Chemical Society Reviews* **2020,** *49* (24), 8933-8987.
11. Moulton, C. J.; Shaw, B. L., Transition metal–carbon bonds. Part XLII. Complexes of nickel, palladium, platinum, rhodium and iridium with the tridentate ligand 2,6-bis[(di-t-butylphosphino)methyl]phenyl. *Journal of the Chemical Society, Dalton Transactions* **1976,** (11), 1020-1024.
12. van Koten, G.; Timmer, K.; Noltes, J. G.; Spek, A. L., A novel type of Pt–C interaction and a model for the final stage in reductive elimination processes involving C–C coupling at Pt; synthesis and molecular geometry of [1,N,N′ -η -2,6-bis{(dimethylamino)methyl}-toluene]iodoplatinum(II) tetrafluoroborate. *Journal of the Chemical Society, Chemical Communications* **1978,** (6), 250-252.
13. van Koten, G.; Jastrzebski, J. T. B. H.; Noltes, J. G.; Spek, A. L.; Schoone, J. C., Triorganotin cations stabilized by intramolecular Sn-N coordination; synthesis and characterization of {C,N,N′ -2,6-bis[(dimethylamino)methyl]phenyl}-diorganotin bromides. *Journal of Organometallic Chemistry* **1978,** *148* (3), 233-245.
14. Ben-Ari, E.; Leitus, G.; Shimon, L. J. W.; Milstein, D., Metal−Ligand Cooperation in C−H and H2 Activation by an Electron-Rich PNP Ir(I) System: Facile Ligand Dearomatization−Aromatization as Key Steps. *Journal of the American Chemical Society* **2006,** *128* (48), 15390-15391.

15. Milstein, D., Discovery of Environmentally Benign Catalytic Reactions of Alcohols Catalyzed by Pyridine-Based Pincer Ru Complexes, Based on Metal–Ligand Cooperation. *Topics in Catalysis* **2010,** *53* (13), 915-923.
16. Gunanathan, C.; Milstein, D., Bond Activation by Metal-Ligand Cooperation: Design of "Green" Catalytic Reactions Based on Aromatization-Dearomatization of Pincer Complexes. In *Bifunctional Molecular Catalysis*, Ikariya, T.; Shibasaki, M., Eds. Springer Berlin Heidelberg: Berlin, Heidelberg, 2011; pp 55-84.
17. Gunanathan, C.; Milstein, D., Bond Activation and Catalysis by Ruthenium Pincer Complexes. *Chemical Reviews* **2014,** *114* (24), 12024-12087.
18. Khusnutdinova, J. R.; Milstein, D., Metal–Ligand Cooperation. *Angewandte Chemie International Edition* **2015,** *54* (42), 12236-12273.
19. Zell, T.; Milstein, D., Hydrogenation and Dehydrogenation Iron Pincer Catalysts Capable of Metal–Ligand Cooperation by Aromatization/Dearomatization. *Accounts of Chemical Research* **2015,** *48* (7), 1979-1994.
20. Zhang, J.; Leitus, G.; Ben-David, Y.; Milstein, D., Efficient Homogeneous Catalytic Hydrogenation of Esters to Alcohols. *Angewandte Chemie International Edition* **2006,** *45* (7), 1113-1115.
21. Zhang, J.; Leitus, G.; Ben-David, Y.; Milstein, D., Facile Conversion of Alcohols into Esters and Dihydrogen Catalyzed by New Ruthenium Complexes. *Journal of the American Chemical Society* **2005,** *127* (31), 10840-10841.
22. Gunanathan, C.; Ben-David, Y.; Milstein, D., Direct Synthesis of Amides from Alcohols and Amines with Liberation of H2. *Science* **2007,** *317* (5839), 790-792.
23. Balaraman, E.; Gunanathan, C.; Zhang, J.; Shimon, L. J. W.; Milstein, D., Efficient hydrogenation of organic carbonates, carbamates and formates indicates alternative routes to methanol based on CO2 and CO. *Nature Chemistry* **2011,** *3* (8), 609-614.
24. Balaraman, E.; Ben-David, Y.; Milstein, D., Unprecedented Catalytic Hydrogenation of Urea Derivatives to Amines and Methanol. *Angewandte Chemie International Edition* **2011,** *50* (49), 11702-11705.
25. Khusnutdinova, J. R.; Garg, J. A.; Milstein, D., Combining Low-Pressure CO2 Capture and Hydrogenation To Form Methanol. *ACS Catalysis* **2015,** *5* (4), 2416-2422.
26. Montag, M.; Zhang, J.; Milstein, D., Aldehyde Binding through Reversible C–C Coupling with the Pincer Ligand upon Alcohol Dehydrogenation by a PNP–Ruthenium Catalyst. *Journal of the American Chemical Society* **2012,** *134* (25), 10325-10328.
27. Huff, C. A.; Kampf, J. W.; Sanford, M. S., Reversible carbon–carbon bond formation between carbonyl compounds and a ruthenium pincer complex. *Chemical Communications* **2013,** *49* (64), 7147-7149.
28. Vogt, M.; Gargir, M.; Iron, M. A.; Diskin-Posner, Y.; Ben-David, Y.; Milstein, D., A New Mode of Activation of CO2 by Metal–Ligand Cooperation with Reversible C-C and M-O Bond Formation at Ambient Temperature. *Chemistry – A European Journal* **2012,** *18* (30), 9194-9197.
29. Huff, C. A.; Kampf, J. W.; Sanford, M. S., Role of a Noninnocent Pincer Ligand in the Activation of CO2 at (PNN)Ru(H)(CO). *Organometallics* **2012,** *31* (13), 4643-4645.
30. Anaby, A.; Butschke, B.; Ben-David, Y.; Shimon, L. J. W.; Leitus, G.; Feller, M.; Milstein, D., B–H Bond Cleavage via Metal–Ligand Cooperation by Dearomatized Ruthenium Pincer Complexes. *Organometallics* **2014,** *33* (14), 3716-3726.

31. Mukherjee, A.; Nerush, A.; Leitus, G.; Shimon, L. J. W.; Ben David, Y.; Espinosa Jalapa, N. A.; Milstein, D., Manganese-Catalyzed Environmentally Benign Dehydrogenative Coupling of Alcohols and Amines to Form Aldimines and H2: A Catalytic and Mechanistic Study. *Journal of the American Chemical Society* **2016,** *138* (13), 4298-4301.
32. Zou, Y.-Q.; Chakraborty, S.; Nerush, A.; Oren, D.; Diskin-Posner, Y.; Ben-David, Y.; Milstein, D., Highly Selective, Efficient Deoxygenative Hydrogenation of Amides Catalyzed by a Manganese Pincer Complex via Metal–Ligand Cooperation. *ACS Catalysis* **2018,** *8* (9), 8014-8019.
33. Das, U. K.; Ben-David, Y.; Leitus, G.; Diskin-Posner, Y.; Milstein, D., Dehydrogenative Cross-Coupling of Primary Alcohols To Form Cross-Esters Catalyzed by a Manganese Pincer Complex. *ACS Catalysis* **2019,** *9* (1), 479-484.
34. Das, U. K.; Kumar, A.; Ben-David, Y.; Iron, M. A.; Milstein, D., Manganese Catalyzed Hydrogenation of Carbamates and Urea Derivatives. *Journal of the American Chemical Society* **2019,** *141* (33), 12962-12966.
35. Kumar, A.; Daw, P.; Espinosa-Jalapa, N. A.; Leitus, G.; Shimon, L. J. W.; Ben-David, Y.; Milstein, D., CO2 activation by manganese pincer complexes through different modes of metal–ligand cooperation. *Dalton Transactions* **2019,** *48* (39), 14580-14584.
36. Spasyuk, D.; Smith, S.; Gusev, D. G., Replacing Phosphorus with Sulfur for the Efficient Hydrogenation of Esters. *Angewandte Chemie International Edition* **2013,** *52* (9), 2538-2542.
37. Puylaert, P.; van Heck, R.; Fan, Y.; Spannenberg, A.; Baumann, W.; Beller, M.; Medlock, J.; Bonrath, W.; Lefort, L.; Hinze, S.; de Vries, J. G., Selective Hydrogenation of α,β-Unsaturated Aldehydes and Ketones by Air-Stable Ruthenium NNS Complexes. *Chemistry – A European Journal* **2017,** *23* (35), 8473-8481.
38. Midya, S. P.; Landge, V. G.; Sahoo, M. K.; Rana, J.; Balaraman, E., Cobalt-catalyzed acceptorless dehydrogenative coupling of aminoalcohols with alcohols: direct access to pyrrole, pyridine and pyrazine derivatives. *Chemical Communications* **2018,** *54* (1), 90-93.
39. Das, K.; Mondal, A.; Pal, D.; Srivastava, H. K.; Srimani, D., Phosphine-Free Well-Defined Mn(I) Complex-Catalyzed Synthesis of Amine, Imine, and 2,3-Dihydro-1H-perimidine via Hydrogen Autotransfer or Acceptorless Dehydrogenative Coupling of Amine and Alcohol. *Organometallics* **2019,** *38* (8), 1815-1825.
40. Das, K.; Mondal, A.; Pal, D.; Srimani, D., Sustainable Synthesis of Quinazoline and 2-Aminoquinoline via Dehydrogenative Coupling of 2-Aminobenzyl Alcohol and Nitrile Catalyzed by Phosphine-Free Manganese Pincer Complex. *Organic Letters* **2019,** *21* (9), 3223-3227.
41. Dinh, H. M.; Gridneva, T.; Karimata, A.; Garcia-Roca, A.; Pruchyathamkorn, J.; Patil, P. H.; Petrov, A.; Sarbajna, A.; Lapointe, S.; Khaskin, E.; Fayzullin, R. R.; Khusnutdinova, J. R., Single and Double Deprotonation/Dearomatization of the N,S-Donor Pyridinophane Ligand in Ruthenium Complexes. *Dalton Transactions* **2022,** *51* (38), 14734-14746.
42. Sarbajna, A.; Patil, P. H.; Dinh, M. H.; Gladkovskaya, O.; Fayzullin, R. R.; Lapointe, S.; Khaskin, E.; Khusnutdinova, J. R., Facile and Reversible Double Dearomatization of Pyridines in Non-Phosphine Mn^{I} Complexes with N,S-Donor Pyridinophane Ligand. *Chemical Communications* **2019,** *55* (22), 3282-3285.
43. Gargir, M.; Ben-David, Y.; Leitus, G.; Diskin-Posner, Y.; Shimon, L. J. W.; Milstein, D., PNS-Type Ruthenium Pincer Complexes. *Organometallics* **2012,** *31* (17), 6207-6214.

44. Schaub, T.; Radius, U.; Diskin-Posner, Y.; Leitus, G.; Shimon, L. J. W.; Milstein, D., Pyridine-Based Sulfoxide Pincer Complexes of Rhodium and Iridium. *Organometallics* **2008,** *27* (8), 1892-1901.
45. Meneghetti, S. P.; Lutz, P. J.; Kress, J., Neutral and Cationic Palladium(II) Complexes of a Diazapyridinophane. Structure, Fluxionality, and Reactivity toward Ethylene. *Organometallics* **2001,** *20* (24), 5050-5055.
46. Khusnutdinova, J. R.; Rath, N. P.; Mirica, L. M., The Conformational Flexibility of the Tetradentate Ligand tBuN4 is Essential for the Stabilization of (tBuN4)PdIII Complexes. *Inorganic Chemistry* **2014,** *53* (24), 13112-13129.
47. Luo, J.; Rath, N. P.; Mirica, L. M., Oxidative Reactivity of (N2S2)PdRX Complexes (R = Me, Cl; X = Me, Cl, Br): Involvement of Palladium(III) and Palladium(IV) Intermediates. *Organometallics* **2013,** *32* (11), 3343-3353.
48. Luo, J.; Tran, G. N.; Rath, N. P.; Mirica, L. M., Detection and Characterization of Mononuclear Pd(I) Complexes Supported by N2S2 and N4 Tetradentate Ligands. *Inorganic Chemistry* **2020,** *59* (21), 15659-15669.
49. Sinha, S.; Tran, G. N.; Na, H.; Mirica, L. M., Electrocatalytic H2 evolution promoted by a bioinspired (N2S2)Ni(ii) complex. *Chemical Communications* **2022,** *58* (8), 1143-1146.
50. Deolka, S.; Tarannam, N.; Fayzullin, R. R.; Kozuch, S.; Khaskin, E., Unusual rearrangement of modified PNP ligand based Ru complexes relevant to alcohol dehydrogenation catalysis. *Chemical Communications* **2019,** *55* (76), 11350-11353.
51. Feller, M.; Ben-Ari, E.; Iron, M. A.; Diskin-Posner, Y.; Leitus, G.; Shimon, L. J. W.; Konstantinovski, L.; Milstein, D., Cationic, Neutral, and Anionic PNP PdII and PtII Complexes: Dearomatization by Deprotonation and Double-Deprotonation of Pincer Systems. *Inorganic Chemistry* **2010,** *49* (4), 1615-1625.
52. Moriguchi, T.; Kitamura, S.; Sakata, K.; Tsuge, A., Syntheses and structures of dichloropalladium(II)(dithia[3.3]metadipyridinophane) and dichloroplatinum(II)(dithia[3.3]metadipyridinophane) complexes. *Polyhedron* **2001,** *20* (18), 2315-2320.
53. Frisch, M. J.; Trucks, G. W.; Schlegel, H. B.; Scuseria, G. E.; Robb, M. A.; Cheeseman, J. R.; Scalmani, G.; Barone, V.; Petersson, G. A.; Nakatsuji, H.; Li, X.; Caricato, M.; Marenich, A. V.; Bloino, J.; Janesko, B. G.; Gomperts, R.; Mennucci, B.; Hratchian, H. P.; Ortiz, J. V.; Izmaylov, A. F.; Sonnenberg, J. L.; Williams; Ding, F.; Lipparini, F.; Egidi, F.; Goings, J.; Peng, B.; Petrone, A.; Henderson, T.; Ranasinghe, D.; Zakrzewski, V. G.; Gao, J.; Rega, N.; Zheng, G.; Liang, W.; Hada, M.; Ehara, M.; Toyota, K.; Fukuda, R.; Hasegawa, J.; Ishida, M.; Nakajima, T.; Honda, Y.; Kitao, O.; Nakai, H.; Vreven, T.; Throssell, K.; Montgomery Jr., J. A.; Peralta, J. E.; Ogliaro, F.; Bearpark, M. J.; Heyd, J. J.; Brothers, E. N.; Kudin, K. N.; Staroverov, V. N.; Keith, T. A.; Kobayashi, R.; Normand, J.; Raghavachari, K.; Rendell, A. P.; Burant, J. C.; Iyengar, S. S.; Tomasi, J.; Cossi, M.; Millam, J. M.; Klene, M.; Adamo, C.; Cammi, R.; Ochterski, J. W.; Martin, R. L.; Morokuma, K.; Farkas, O.; Foresman, J. B.; Fox, D. J. *Gaussian 16 Rev. C.01*, Wallingford, CT, 2016.
54. Zhao, Y.; Truhlar, D. G., The M06 suite of density functionals for main group thermochemistry, thermochemical kinetics, noncovalent interactions, excited states, and transition elements: two new functionals and systematic testing of four M06-class functionals and 12 other functionals. *Theoretical Chemistry Accounts* **2008,** *120* (1), 215-241.
55. Andrae, D.; Häußermann, U.; Dolg, M.; Stoll, H.; Preuß, H., Energy-adjustedab initio pseudopotentials for the second and third row transition elements. *Theoretica chimica acta* **1990,** *77* (2), 123-141.

56. Krishnan, R.; Binkley, J. S.; Seeger, R.; Pople, J. A., Self‐consistent molecular orbital methods. XX. A basis set for correlated wave functions. *The Journal of Chemical Physics* **1980,** *72* (1), 650-654.
57. McLean, A. D.; Chandler, G. S., Contracted Gaussian basis sets for molecular calculations. I. Second row atoms, Z=11–18. *The Journal of Chemical Physics* **1980,** *72* (10), 5639-5648.
58. Francl, M. M.; Pietro, W. J.; Hehre, W. J.; Binkley, J. S.; Gordon, M. S.; DeFrees, D. J.; Pople, J. A., Self‐consistent molecular orbital methods. XXIII. A polarization‐type basis set for second‐row elements. *The Journal of Chemical Physics* **1982,** *77* (7), 3654-3665.
59. Clark, T.; Chandrasekhar, J.; Spitznagel, G. W.; Schleyer, P. V. R., Efficient diffuse function-augmented basis sets for anion calculations. III. The 3-21+G basis set for first-row elements, Li–F. *Journal of Computational Chemistry* **1983,** *4* (3), 294-301.
60. Spitznagel, G. W.; Clark, T.; von Ragué Schleyer, P.; Hehre, W. J., An evaluation of the performance of diffuse function-augmented basis sets for second row elements, Na-Cl. *Journal of Computational Chemistry* **1987,** *8* (8), 1109-1116.
61. Feller, D., The role of databases in support of computational chemistry calculations. *Journal of Computational Chemistry* **1996,** *17* (13), 1571-1586.
62. Schuchardt, K. L.; Didier, B. T.; Elsethagen, T.; Sun, L.; Gurumoorthi, V.; Chase, J.; Li, J.; Windus, T. L., Basis Set Exchange: A Community Database for Computational Sciences. *Journal of Chemical Information and Modeling* **2007,** *47* (3), 1045-1052.
63. Pritchard, B. P.; Altarawy, D.; Didier, B.; Gibson, T. D.; Windus, T. L., New Basis Set Exchange: An Open, Up-to-Date Resource for the Molecular Sciences Community. *Journal of Chemical Information and Modeling* **2019,** *59* (11), 4814-4820.
64. Marenich, A. V.; Cramer, C. J.; Truhlar, D. G., Universal Solvation Model Based on Solute Electron Density and on a Continuum Model of the Solvent Defined by the Bulk Dielectric Constant and Atomic Surface Tensions. *The Journal of Physical Chemistry B* **2009,** *113* (18), 6378-6396.
65. Lu, T.; Chen, F., Multiwfn: A multifunctional wavefunction analyzer. *Journal of Computational Chemistry* **2012,** *33* (5), 580-592.
66. Dinh, H. M.; He, Y.-T.; Fayzullin, R. R.; Vasylevskyi, S.; Khaskin, E.; Khusnutdinova, J. R., Synthesis of Aryl-Manganese(III) Fluoride Complexes via α-Fluorine Elimination from CF_3 and Difluorocarbene Generation. *European Journal of Inorganic Chemistry* **2023,** *26* (32), e202300460.
67. Sarbajna, A.; He, Y.-T.; Dinh, M. H.; Gladkovskaya, O.; Rahaman, S. M. W.; Karimata, A.; Khaskin, E.; Lapointe, S.; Fayzullin, R. R.; Khusnutdinova, J. R., Aryl–X Bond-Forming Reductive Elimination from High-Valent Mn–Aryl Complexes. *Organometallics* **2019,** *38* (22), 4409-4419.
68. Labinger, J. A., Tutorial on Oxidative Addition. *Organometallics* **2015,** *34* (20), 4784-4795.
69. Lyons, T. W.; Sanford, M. S., Palladium-Catalyzed Ligand-Directed C−H Functionalization Reactions. *Chemical Reviews* **2010,** *110* (2), 1147-1169.
70. Engle, K. M.; Mei, T.-S.; Wasa, M.; Yu, J.-Q., Weak Coordination as a Powerful Means for Developing Broadly Useful C–H Functionalization Reactions. *Accounts of Chemical Research* **2012,** *45* (6), 788-802.

71. He, J.; Wasa, M.; Chan, K. S. L.; Shao, Q.; Yu, J.-Q., Palladium-Catalyzed Transformations of Alkyl C–H Bonds. *Chemical Reviews* **2017,** *117* (13), 8754-8786.
72. Rej, S.; Chatani, N., Rhodium-Catalyzed C(sp2)- or C(sp3)−H Bond Functionalization Assisted by Removable Directing Groups. *Angewandte Chemie International Edition* **2019,** *58* (25), 8304-8329.
73. Brown, M. P.; Puddephatt, R. J.; Upton, C. E. E., Mechanism of reductive elimination of ethane from some halogenotrimethylbis(tertiary phosphine)platinum(IV) complexes. *Journal of the Chemical Society, Dalton Transactions* **1974,** (22), 2457-2465.
74. Williams, B. S.; Holland, A. W.; Goldberg, K. I., Direct Observation of C−O Reductive Elimination from Pt(IV). *Journal of the American Chemical Society* **1999,** *121* (1), 252-253.
75. Roy, A. H.; Hartwig, J. F., Directly Observed Reductive Elimination of Aryl Halides from Monomeric Arylpalladium(II) Halide Complexes. *Journal of the American Chemical Society* **2003,** *125* (46), 13944-13945.
76. Yahav-Levi, A.; Goldberg, I.; Vigalok, A., Aryl-Halide versus Aryl−Aryl Reductive Elimination in Pt(IV)−Phosphine Complexes. *Journal of the American Chemical Society* **2006,** *128* (27), 8710-8711.
77. Oloo, W.; Zavalij, P. Y.; Zhang, J.; Khaskin, E.; Vedernikov, A. N., Preparation and C−X Reductive Elimination Reactivity of Monoaryl PdIV−X Complexes in Water (X = OH, OH2, Cl, Br). *Journal of the American Chemical Society* **2010,** *132* (41), 14400-14402.
78. Powers, D. C.; Benitez, D.; Tkatchouk, E.; Goddard, W. A., III; Ritter, T., Bimetallic Reductive Elimination from Dinuclear Pd(III) Complexes. *Journal of the American Chemical Society* **2010,** *132* (40), 14092-14103.
79. Vigalok, A., Electrophilic Halogenation–Reductive Elimination Chemistry of Organopalladium and -Platinum Complexes. *Accounts of Chemical Research* **2015,** *48* (2), 238-247.
80. Winston, M. S.; Wolf, W. J.; Toste, F. D., Halide-Dependent Mechanisms of Reductive Elimination from Gold(III). *Journal of the American Chemical Society* **2015,** *137* (24), 7921-7928.
81. Zeineddine, A.; Estévez, L.; Mallet-Ladeira, S.; Miqueu, K.; Amgoune, A.; Bourissou, D., Rational development of catalytic Au(I)/Au(III) arylation involving mild oxidative addition of aryl halides. *Nature Communications* **2017,** *8* (1), 565.
82. Kuninobu, Y.; Nishina, Y.; Takeuchi, T.; Takai, K., Manganese-Catalyzed Insertion of Aldehydes into a C-H Bond. *Angewandte Chemie International Edition* **2007,** *46* (34), 6518-6520.
83. Zhou, B.; Chen, H.; Wang, C., Mn-Catalyzed Aromatic C–H Alkenylation with Terminal Alkynes. *Journal of the American Chemical Society* **2013,** *135* (4), 1264-1267.
84. Liu, W.; Bang, J.; Zhang, Y.; Ackermann, L., Manganese(I)-Catalyzed C–H Aminocarbonylation of Heteroarenes. *Angewandte Chemie International Edition* **2015,** *54* (47), 14137-14140.
85. Liu, W.; Zell, D.; John, M.; Ackermann, L., Manganese-Catalyzed Synthesis of cis-β-Amino Acid Esters through Organometallic C-H Activation of Ketimines. *Angewandte Chemie International Edition* **2015,** *54* (13), 4092-4096.
86. Shi, L.; Zhong, X.; She, H.; Lei, Z.; Li, F., Manganese catalyzed C–H functionalization of indoles with alkynes to synthesize bis/trisubstituted indolylalkenes and carbazoles: the acid is the key to control selectivity. *Chemical Communications* **2015,** *51* (33), 7136-7139.

87. Zhou, B.; Hu, Y.; Wang, C., Manganese-Catalyzed Direct Nucleophilic C(sp2)-H Addition to Aldehydes and Nitriles. *Angewandte Chemie International Edition* **2015,** *54* (46), 13659-13663.
88. Carney, J. R.; Dillon, B. R.; Thomas, S. P., Recent Advances of Manganese Catalysis for Organic Synthesis. *European Journal of Organic Chemistry* **2016,** *2016* (23), 3912-3929.
89. Liu, W.; Ackermann, L., Manganese-Catalyzed C–H Activation. *ACS Catalysis* **2016,** *6* (6), 3743-3752.
90. Hammarback, L. A.; Robinson, A.; Lynam, J. M.; Fairlamb, I. J. S., Mechanistic Insight into Catalytic Redox-Neutral C–H Bond Activation Involving Manganese(I) Carbonyls: Catalyst Activation, Turnover, and Deactivation Pathways Reveal an Intricate Network of Steps. *Journal of the American Chemical Society* **2019,** *141* (6), 2316-2328.
91. Cahiez, G.; Moyeux, A.; Buendia, J.; Duplais, C., Manganese- or Iron-Catalyzed Homocoupling of Grignard Reagents Using Atmospheric Oxygen as an Oxidant. *Journal of the American Chemical Society* **2007,** *129* (45), 13788-13789.
92. Sato, T.; Yoshida, T.; Al Mamari, H. H.; Ilies, L.; Nakamura, E., Manganese-Catalyzed Directed Methylation of C(sp2)–H Bonds at 25 °C with High Catalytic Turnover. *Organic Letters* **2017,** *19* (19), 5458-5461.
93. Dakarapu, R.; Falck, J. R., Stereospecific Stille Cross-Couplings Using Mn(II)Cl2. *The Journal of Organic Chemistry* **2018,** *83* (3), 1241-1251.
94. Zhu, C.; Oliveira, J. C. A.; Shen, Z.; Huang, H.; Ackermann, L., Manganese(II/III/I)-Catalyzed C–H Arylations in Continuous Flow. *ACS Catalysis* **2018,** *8* (5), 4402-4407.
95. Layfield, R. A., Manganese(ii): the black sheep of the organometallic family. *Chemical Society Reviews* **2008,** *37* (6), 1098-1107.
96. Cahiez, G.; Duplais, C.; Buendia, J., Chemistry of Organomanganese(II) Compounds. *Chemical Reviews* **2009,** *109* (3), 1434-1476.
97. Lefèvre, G.; Taillefer, M.; Adamo, C.; Ciofini, I.; Jutand, A., First Evidence of the Oxidative Addition of Fe0(N,N)2 to Aryl Halides: This Precondition Is Not a Guarantee of Efficient Iron-Catalysed C–N Cross-Coupling Reactions. *European Journal of Organic Chemistry* **2011,** *2011* (20-21), 3768-3780.
98. Lefèvre, G.; Jutand, A., Activation of Aryl and Heteroaryl Halides by an Iron(I) Complex Generated in the Reduction of [Fe(acac)3] by PhMgBr: Electron Transfer versus Oxidative Addition. *Chemistry – A European Journal* **2014,** *20* (16), 4796-4805.
99. Carpenter, S. H.; Baker, T. M.; Muñoz, S. B.; Brennessel, W. W.; Neidig, M. L., Multinuclear iron–phenyl species in reactions of simple iron salts with PhMgBr: identification of Fe4(μ-Ph)6(THF)4 as a key reactive species for cross-coupling catalysis. *Chemical Science* **2018,** *9* (41), 7931-7939.
100. Magallón, C.; Planas, O.; Roldán-Gómez, S.; Luis, J. M.; Company, A.; Ribas, X., Well-Defined Aryl-FeII Complexes in Cross-Coupling and C–H Activation Processes. *Organometallics* **2021,** *40* (9), 1195-1200.
101. Smith, A. L.; Hardcastle, K. I.; Soper, J. D., Redox-Active Ligand-Mediated Oxidative Addition and Reductive Elimination at Square Planar Cobalt(III): Multielectron Reactions for Cross-Coupling. *Journal of the American Chemical Society* **2010,** *132* (41), 14358-14360.
102. Rummelt, S. M.; Zhong, H.; Léonard, N. G.; Semproni, S. P.; Chirik, P. J., Oxidative Addition of Dihydrogen, Boron Compounds, and Aryl Halides to a

Cobalt(I) Cation Supported by a Strong-Field Pincer Ligand. *Organometallics* **2019,** *38* (5), 1081-1090.
103. Casitas, A.; King, A. E.; Parella, T.; Costas, M.; Stahl, S. S.; Ribas, X., Direct observation of CuI/CuIII redox steps relevant to Ullmann-type coupling reactions. *Chemical Science* **2010,** *1* (3), 326-330.
104. Rovira, M.; Roldán-Gómez, S.; Martin-Diaconescu, V.; Whiteoak, C. J.; Company, A.; Luis, J. M.; Ribas, X., Trifluoromethylation of a Well-Defined Square-Planar Aryl-NiII Complex involving NiIII/CF3. and NiIV−CF3 Intermediate Species. *Chemistry – A European Journal* **2017,** *23* (48), 11662-11668.
105. Zhou, W.; Schultz, J. W.; Rath, N. P.; Mirica, L. M., Aromatic Methoxylation and Hydroxylation by Organometallic High-Valent Nickel Complexes. *Journal of the American Chemical Society* **2015,** *137* (24), 7604-7607.
106. Schultz, J. W.; Fuchigami, K.; Zheng, B.; Rath, N. P.; Mirica, L. M., Isolated Organometallic Nickel(III) and Nickel(IV) Complexes Relevant to Carbon–Carbon Bond Formation Reactions. *Journal of the American Chemical Society* **2016,** *138* (39), 12928-12934.
107. Planas, O.; Whiteoak, C. J.; Martin-Diaconescu, V.; Gamba, I.; Luis, J. M.; Parella, T.; Company, A.; Ribas, X., Isolation of Key Organometallic Aryl-Co(III) Intermediates in Cobalt-Catalyzed C(sp2)–H Functionalizations and New Insights into Alkyne Annulation Reaction Mechanisms. *Journal of the American Chemical Society* **2016,** *138* (43), 14388-14397.
108. Furuya, T.; Kamlet, A. S.; Ritter, T., Catalysis for fluorination and trifluoromethylation. *Nature* **2011,** *473* (7348), 470-477.
109. Gillis, E. P.; Eastman, K. J.; Hill, M. D.; Donnelly, D. J.; Meanwell, N. A., Applications of Fluorine in Medicinal Chemistry. *Journal of Medicinal Chemistry* **2015,** *58* (21), 8315-8359.
110. Liu, W.; Huang, X.; Cheng, M.-J.; Nielsen, R. J.; Goddard, W. A.; Groves, J. T., Oxidative Aliphatic C-H Fluorination with Fluoride Ion Catalyzed by a Manganese Porphyrin. *Science* **2012,** *337* (6100), 1322-1325.
111. Leclerc, M. C.; Bayne, J. M.; Lee, G. M.; Gorelsky, S. I.; Vasiliu, M.; Korobkov, I.; Harrison, D. J.; Dixon, D. A.; Baker, R. T., Perfluoroalkyl Cobalt(III) Fluoride and Bis(perfluoroalkyl) Complexes: Catalytic Fluorination and Selective Difluorocarbene Formation. *Journal of the American Chemical Society* **2015,** *137* (51), 16064-16073.
112. Joven-Sancho, D.; Echeverri, A.; Saffon-Merceron, N.; Contreras-García, J.; Nebra, N., An Organocopper(III) Fluoride Triggering C−CF3 Bond Formation. *Angewandte Chemie International Edition* **2023,** *n/a* (n/a), e202319412.
113. D'Accriscio, F.; Borja, P.; Saffon-Merceron, N.; Fustier-Boutignon, M.; Mézailles, N.; Nebra, N., C−H Bond Trifluoromethylation of Arenes Enabled by a Robust, High-Valent Nickel(IV) Complex. *Angewandte Chemie International Edition* **2017,** *56* (42), 12898-12902.
114. Xu, S.; Bucinsky, L.; Breza, M.; Krzystek, J.; Chen, C.-H.; Pink, M.; Telser, J.; Smith, J. M., Ligand Substituent Effects in Manganese Pyridinophane Complexes: Implications for Oxygen-Evolving Catalysis. *Inorganic Chemistry* **2017,** *56* (22), 14315-14325.
115. Mantel, C.; Hassan, A. K.; Pécaut, J.; Deronzier, A.; Collomb, M.-N.; Duboc-Toia, C., A High-Frequency and High-Field EPR Study of New Azide and Fluoride Mononuclear Mn(III) Complexes. *Journal of the American Chemical Society* **2003,** *125* (40), 12337-12344.

116. Higgs, A. T.; Zinn, P. J.; Simmons, S. J.; Sanford, M. S., Oxidatively Induced Carbon−Halogen Bond-Forming Reactions at Nickel. *Organometallics* **2009,** *28* (21), 6142-6144.
117. Lanci, M. P.; Remy, M. S.; Kaminsky, W.; Mayer, J. M.; Sanford, M. S., Oxidatively Induced Reductive Elimination from (tBu2bpy)Pd(Me)2: Palladium(IV) Intermediates in a One-Electron Oxidation Reaction. *Journal of the American Chemical Society* **2009,** *131* (43), 15618-15620.
118. Shin, K.; Park, Y.; Baik, M.-H.; Chang, S., Iridium-catalysed arylation of C–H bonds enabled by oxidatively induced reductive elimination. *Nature Chemistry* **2018,** *10* (2), 218-224.
119. Kim, J.; Shin, K.; Jin, S.; Kim, D.; Chang, S., Oxidatively Induced Reductive Elimination: Exploring the Scope and Catalyst Systems with Ir, Rh, and Ru Complexes. *Journal of the American Chemical Society* **2019,** *141* (9), 4137-4146.
120. Connelly, N. G.; Geiger, W. E., Chemical Redox Agents for Organometallic Chemistry. *Chemical Reviews* **1996,** *96* (2), 877-910.
121. He, Y.-T.; Karimata, A.; Gladkovskaya, O.; Khaskin, E.; Fayzullin, R. R.; Sarbajna, A.; Khusnutdinova, J. R., C–C Bond Elimination from High-Valent Mn Aryl Complexes. *Organometallics* **2021,** *40* (14), 2320-2331.
122. Aikawa, K.; Nakamura, Y.; Yokota, Y.; Toya, W.; Mikami, K., Stable but Reactive Perfluoroalkylzinc Reagents: Application in Ligand-Free Copper-Catalyzed Perfluoroalkylation of Aryl Iodides. *Chemistry – A European Journal* **2015,** *21* (1), 96-100.
123. Xie, Y.; Wei, P.; Li, X.; Hong, T.; Zhang, K.; Furuta, H., Macrocycle Contraction and Expansion of a Dihydrosapphyrin Isomer. *Journal of the American Chemical Society* **2013,** *135* (51), 19119-19122.
124. Seebacher, J.; Shu, M.; Vahrenkamp, H., The best structural model of ADH so far: a pyrazolylbis(thioimidazolyl)borate zinc ethanol complex. *Chemical Communications* **2001,** (11), 1026-1027.
125. Kimblin, C.; M. Bridgewater, B.; G. Churchill, D.; Parkin, G., Mononuclear tris(2-mercapto-1-arylimidazolyl)hydroborato complexes of zinc, [TmAr]ZnX: structural evidence that a sulfur rich coordination environment promotes the formation of a tetrahedral alcohol complex in a synthetic analogue of LADH. *Chemical Communications* **1999,** (22), 2301-2302.
126. Dance, I. G., Formation, crystal structure, and reactions of catena-(.mu.-SPh)[(.mu.-SPh)6Zn4(CH3OH)(SPh)], a model for zinc thiolate metalloenzymes. *Journal of the American Chemical Society* **1980,** *102* (10), 3445-3451.
127. Brombacher, H.; Vahrenkamp, H., Pyrazolylborate−Zinc Alkoxide Complexes. 1. Basic Properties, Methylations, and Heterocumulene Insertions. *Inorganic Chemistry* **2004,** *43* (19), 6042-6049.
128. Cronin, L.; Walton, P. H., Synthesis and structure of [Zn(OMe)(L)]·[Zn(OH)(L)]·2(BPh4), L = cis,cis-1,3,5-tris[(E,E)-3-(2-furyl)acrylideneamino]cyclohexane: structural models of carbonic anhydrase and liver alcohol dehydrogenase. *Chemical Communications* **2003,** (13), 1572-1573.
129. Bergquist, C.; Parkin, G., Modeling the Catalytic Cycle of Liver Alcohol Dehydrogenase: Synthesis and Structural Characterization of a Four-Coordinate Zinc Ethoxide Complex and Determination of Relative Zn−OR versus Zn−OH Bond Energies. *Inorganic Chemistry* **1999,** *38* (3), 422-423.
130. Purdy, A. P.; George, C. F., Synthesis and structure of tri-tert-butoxyzincates. *Polyhedron* **1994,** *13* (5), 709-712.

131. Uzelac, M.; Mastropierro, P.; de Tullio, M.; Borilovic, I.; Tarrés, M.; Kennedy, A. R.; Aromí, G.; Hevia, E., Tandem Mn–I Exchange and Homocoupling Processes Mediated by a Synergistically Operative Lithium Manganate. *Angewandte Chemie International Edition* **2021,** *60* (6), 3247-3253.
132. Haszeldine, R., Perfluoroalkyl Grignard Reaction. Part IV. Trifluoromethylmagnesium Iodide. *J Chem Soc* **1954**, 1273-1279.
133. Pierce, O.; McBee, E.; Judd, G., Preparation and Reactions of Perfluoroalkyllithiums1. *Journal of the American Chemical Society* **1954,** *76* (2), 474-478.
134. Eujen, R.; Hoge, B., Donor-free bis (trifluoromethyl) cadmium,(CF3) 2Cd: a readily available low-temperature difluorocarbene source. *Journal of organometallic chemistry* **1995,** *503* (2), C51-C54.
135. Bischoff, L. A.; Riefer, J.; Wirthensohn, R.; Bischof, T.; Bertermann, R.; Ignat'ev, N. V.; Finze, M., Pentafluoroethylaluminates: A Combined Synthetic, Spectroscopic, and Structural Study. *Chemistry – A European Journal* **2020,** *26* (60), 13615-13620.
136. Aikawa, K.; Toya, W.; Nakamura, Y.; Mikami, K., Development of (Trifluoromethyl)zinc Reagent as Trifluoromethyl Anion and Difluorocarbene Sources. *Organic Letters* **2015,** *17* (20), 4996-4999.
137. Wang, F.; Luo, T.; Hu, J.; Wang, Y.; Krishnan, H. S.; Jog, P. V.; Ganesh, S. K.; Prakash, G. K. S.; Olah, G. A., Synthesis of gem-Difluorinated Cyclopropanes and Cyclopropenes: Trifluoromethyltrimethylsilane as a Difluorocarbene Source. *Angewandte Chemie International Edition* **2011,** *50* (31), 7153-7157.
138. Dinh, H. M.; Govindarajan, R.; Deolka, S.; Fayzullin, R. R.; Vasylevskyi, S.; Khaskin, E.; Khusnutdinova, J. R., Photoinduced Perfluoroalkylation Mediated by Cobalt Complexes Supported by Naphthyridine Ligands. *Organometallics* **2023,** *42* (18), 2632-2643.
139. Müller, K.; Faeh, C.; Diederich, F., Fluorine in Pharmaceuticals: Looking Beyond Intuition. *Science* **2007,** *317* (5846), 1881-1886.
140. Hagmann, W. K., The Many Roles for Fluorine in Medicinal Chemistry. *Journal of Medicinal Chemistry* **2008,** *51* (15), 4359-4369.
141. Purser, S.; Moore, P. R.; Swallow, S.; Gouverneur, V., Fluorine in medicinal chemistry. *Chemical Society Reviews* **2008,** *37* (2), 320-330.
142. Bour, J. R.; Camasso, N. M.; Sanford, M. S., Oxidation of Ni(II) to Ni(IV) with Aryl Electrophiles Enables Ni-Mediated Aryl–CF3 Coupling. *Journal of the American Chemical Society* **2015,** *137* (25), 8034-8037.
143. Bour, J. R.; Camasso, N. M.; Meucci, E. A.; Kampf, J. W.; Canty, A. J.; Sanford, M. S., Carbon–Carbon Bond-Forming Reductive Elimination from Isolated Nickel(III) Complexes. *Journal of the American Chemical Society* **2016,** *138* (49), 16105-16111.
144. Meucci, E. A.; Nguyen, S. N.; Camasso, N. M.; Chong, E.; Ariafard, A.; Canty, A. J.; Sanford, M. S., Nickel(IV)-Catalyzed C–H Trifluoromethylation of (Hetero)arenes. *Journal of the American Chemical Society* **2019,** *141* (32), 12872-12879.
145. Shreiber, S. T.; DiMucci, I. M.; Khrizanforov, M. N.; Titus, C. J.; Nordlund, D.; Dudkina, Y.; Cramer, R. E.; Budnikova, Y.; Lancaster, K. M.; Vicic, D. A., [(MeCN)Ni(CF3)3]− and [Ni(CF3)4]2–: Foundations toward the Development of Trifluoromethylations at Unsupported Nickel. *Inorganic Chemistry* **2020,** *59* (13), 9143-9151.

146. Shreiber, S. T.; Vicic, D. A., Solvated Nickel Complexes as Stoichiometric and Catalytic Perfluoroalkylation Agents**. *Angewandte Chemie International Edition* **2021,** *60* (33), 18162-18167.
147. Mudarra, Á. L.; Martínez de Salinas, S.; Pérez-Temprano, M. H., Nucleophilic Trifluoromethylation Reactions Involving Copper(I) Species: From Organometallic Insights to Scope. *Synthesis* **2019,** *51* (14), 2809-2820.
148. Urata, H.; Fuchikami, T., A novel and convenient method for trifluoromethylation of organic halides using CF3SiR'3/KF/Cu(I) system. *Tetrahedron Letters* **1991,** *32* (1), 91-94.
149. Folléas, B. t.; Marek, I.; Normant, J.-F.; Saint-Jalmes, L., Fluoroform: an Efficient Precursor for the Trifluoromethylation of Aldehydes. *Tetrahedron* **2000,** *56* (2), 275-283.
150. Knauber, T.; Arikan, F.; Röschenthaler, G.-V.; Gooßen, L. J., Copper-Catalyzed Trifluoromethylation of Aryl Iodides with Potassium (Trifluoromethyl)trimethoxyborate. *Chemistry – A European Journal* **2011,** *17* (9), 2689-2697.
151. Dubinina, G. G.; Furutachi, H.; Vicic, D. A., Active Trifluoromethylating Agents from Well-Defined Copper(I)−CF3 Complexes. *Journal of the American Chemical Society* **2008,** *130* (27), 8600-8601.
152. Morimoto, H.; Tsubogo, T.; Litvinas, N. D.; Hartwig, J. F., A Broadly Applicable Copper Reagent for Trifluoromethylations and Perfluoroalkylations of Aryl Iodides and Bromides. *Angewandte Chemie International Edition* **2011,** *50* (16), 3793-3798.
153. Tomashenko, O. A.; Escudero-Adán, E. C.; Martínez Belmonte, M.; Grushin, V. V., Simple, Stable, and Easily Accessible Well-Defined CuCF3 Aromatic Trifluoromethylating Agents. *Angewandte Chemie International Edition* **2011,** *50* (33), 7655-7659.
154. Casitas, A.; Ribas, X., The role of organometallic copper(iii) complexes in homogeneous catalysis. *Chemical Science* **2013,** *4* (6), 2301-2318.
155. Hickman, A. J.; Sanford, M. S., High-valent organometallic copper and palladium in catalysis. *Nature* **2012,** *484* (7393), 177-185.
156. Willert-Porada, M. A.; Burton, D. J.; Baenziger, N. C., Synthesis and X-ray structure of bis(trifluoromethyl)(N,N-diethyldithiocarbamato)-copper; a remarkably stable perfluoroalkylcopper(III) complex. *Journal of the Chemical Society, Chemical Communications* **1989,** (21), 1633-1634.
157. Naumann, D.; Roy, T.; Tebbe, K.-F.; Crump, W., Synthesis and Structure of Surprisingly Stable Tetrakis(trifluoromethyl)cuprate(III) Salts. *Angewandte Chemie International Edition in English* **1993,** *32* (10), 1482-1483.
158. Romine, A. M.; Nebra, N.; Konovalov, A. I.; Martin, E.; Benet-Buchholz, J.; Grushin, V. V., Easy Access to the Copper(III) Anion [Cu(CF3)4]−. *Angewandte Chemie International Edition* **2015,** *54* (9), 2745-2749.
159. Zhang, S.-L.; Bie, W.-F., Isolation and characterization of copper(iii) trifluoromethyl complexes and reactivity studies of aerobic trifluoromethylation of arylboronic acids. *RSC Advances* **2016,** *6* (75), 70902-70906.
160. Zhang, S.-L.; Xiao, C.; Wan, H.-X., Diverse copper(iii) trifluoromethyl complexes with mono-, bi- and tridentate ligands and their versatile reactivity. *Dalton Transactions* **2018,** *47* (14), 4779-4784.
161. Paeth, M.; Tyndall, S. B.; Chen, L.-Y.; Hong, J.-C.; Carson, W. P.; Liu, X.; Sun, X.; Liu, J.; Yang, K.; Hale, E. M.; Tierney, D. L.; Liu, B.; Cao, Z.; Cheng, M.-J.; Goddard, W. A., III; Liu, W., Csp3–Csp3 Bond-Forming Reductive Elimination

from Well-Defined Copper(III) Complexes. *Journal of the American Chemical Society* **2019,** *141* (7), 3153-3159.
162. Lu, Z.; Liu, H.; Liu, S.; Leng, X.; Lan, Y.; Shen, Q., A Key Intermediate in Copper-Mediated Arene Trifluoromethylation, [nBu4N][Cu(Ar)(CF3)3]: Synthesis, Characterization, and C(sp2)−CF3 Reductive Elimination. *Angewandte Chemie International Edition* **2019,** *58* (25), 8510-8514.
163. Liu, S.; Liu, H.; Liu, S.; Lu, Z.; Lu, C.; Leng, X.; Lan, Y.; Shen, Q., C(sp3)-CF3 Reductive Elimination from a Five-Coordinate Neutral Copper(III) Complex. *Journal of the American Chemical Society* **2020,** *142* (21), 9785-9791.
164. Fujiwara, T.; O'Hagan, D., Successful fluorine-containing herbicide agrochemicals. *Journal of Fluorine Chemistry* **2014,** *167*, 16-29.
165. Prchalová, E.; Štěpánek, O.; Smrček, S.; Kotora, M., Medicinal applications of perfluoroalkylated chain-containing compounds. *Future Medicinal Chemistry* **2014,** *6* (10), 1201-1229.
166. Carmody, M.; Byrne, B.; Murphy, B.; Breen, C.; Lynch, S.; Flood, E.; Finnan, S.; Caffrey, P., Analysis and manipulation of amphotericin biosynthetic genes by means of modified phage KC515 transduction techniques. *Gene* **2004,** *343* (1), 107-115.
167. Taka, N.; Koga, H.; Sato, H.; Ishizawa, T.; Takahashi, T.; Imagawa, J.-i., 6-Substituted 2,2-Bis(fluoromethyl)-benzopyran-4-carboxamide K+ channel openers. *Bioorganic & Medicinal Chemistry* **2000,** *8* (6), 1393-1405.
168. Pierce, M. E.; Carini, D. J.; Huhn, G. F.; Wells, G. J.; Arnett, J. F., Practical synthesis and regioselective alkylation of methyl 4(5)-(pentafluoroethyl)-2-propylimidazole-5(4)-carboxylate to give DuP 532, a potent angiotensin II antagonist. *The Journal of Organic Chemistry* **1993,** *58* (17), 4642-4645.
169. Chiu, A. T.; Carini, D. J.; Duncia, J. V.; Leung, K. H.; McCall, D. E.; Price, W. A.; Wong, P. C.; Smith, R. D.; Wexler, R. R.; Timmermans, P. B. M. W. M.; Chang, R. S. L.; Lotti, V. J., DuP 532: A second generation of nonpeptide angiotensin II receptor antagonists. *Biochemical and Biophysical Research Communications* **1991,** *177* (1), 209-217.
170. Vergote, I.; Abram, P., Fulvestrant, a new treatment option for advanced breast cancer: tolerability versus existing agents. *Annals of Oncology* **2006,** *17* (2), 200-204.
171. Curran, M.; Wiseman, L., Fulvestrant. *Drugs* **2001,** *61* (6), 807-813.
172. Tomashenko, O. A.; Grushin, V. V., Aromatic Trifluoromethylation with Metal Complexes. *Chemical Reviews* **2011,** *111* (8), 4475-4521.
173. Alonso, C.; Martínez de Marigorta, E.; Rubiales, G.; Palacios, F., Carbon Trifluoromethylation Reactions of Hydrocarbon Derivatives and Heteroarenes. *Chemical Reviews* **2015,** *115* (4), 1847-1935.
174. Liang, T.; Neumann, C. N.; Ritter, T., Introduction of Fluorine and Fluorine-Containing Functional Groups. *Angewandte Chemie International Edition* **2013,** *52* (32), 8214-8264.
175. Chen, P.; Liu, G., Recent Advances in Transition-Metal-Catalyzed Trifluoromethylation and Related Transformations. *Synthesis* **2013,** *45* (21), 2919-2939.
176. Zhang, S.; Rotta-Loria, N.; Weniger, F.; Rabeah, J.; Neumann, H.; Taeschler, C.; Beller, M., A general and practical Ni-catalyzed C–H perfluoroalkylation of (hetero)arenes. *Chemical Communications* **2019,** *55* (47), 6723-6726.
177. Zhao, X.; MacMillan, D. W. C., Metallaphotoredox Perfluoroalkylation of Organobromides. *Journal of the American Chemical Society* **2020,** *142* (46), 19480-19486.

178. Zhang, S.; Weniger, F.; Ye, F.; Rabeah, J.; Ellinger, S.; Zaragoza, F.; Taeschler, C.; Neumann, H.; Brückner, A.; Beller, M., Selective nickel-catalyzed fluoroalkylations of olefins. *Chemical Communications* **2020,** *56* (96), 15157-15160.
179. Deolka, S.; Govindarajan, R.; Vasylevskyi, S.; Roy, M. C.; Khusnutdinova, J. R.; Khaskin, E., Ligand-free nickel catalyzed perfluoroalkylation of arenes and heteroarenes. *Chemical Science* **2022,** *13* (44), 12971-12979.
180. Deolka, S.; Govindarajan, R.; Gridneva, T.; Roy, M. C.; Vasylevskyi, S.; Vardhanapu, P. K.; Khusnutdinova, J. R.; Khaskin, E., General High-Valent Nickel Metallocycle Catalyst for the Perfluoroalkylation of Heteroarenes and Peptides. *ACS Catalysis* **2023,** *13* (19), 13127-13139.
181. Hossain, M. J.; Ono, T.; Wakiya, K.; Hisaeda, Y., A vitamin B12 derivative catalyzed electrochemical trifluoromethylation and perfluoroalkylation of arenes and heteroarenes in organic media. *Chemical Communications* **2017,** *53* (79), 10878-10881.
182. Ono, T.; Wakiya, K.; Hossain, M. J.; Shimakoshi, H.; Hisaeda, Y., Synthesis of Trifluoromethylated B12 Derivative and Photolysis of Cobalt(III)–Trifluoromethyl Bond. *Chemistry Letters* **2018,** *47* (8), 979-981.
183. Harris, C. F.; Kuehner, C. S.; Bacsa, J.; Soper, J. D., Photoinduced Cobalt(III)−Trifluoromethyl Bond Activation Enables Arene C−H Trifluoromethylation. *Angewandte Chemie International Edition* **2018,** *57* (5), 1311-1315.
184. Shreiber, S. T.; Scudder, J. J.; Vicic, D. A., [(MeCN)3Co(C2F5)3]: A Versatile Precursor to Cobalt(III) Perfluoroethyl Complexes. *Organometallics* **2019,** *38* (16), 3169-3173.
185. Xue, T.; Vicic, D. A., Routes to Acetonitrile-Supported Trifluoromethyl and Perfluorometallacyclopentane Complexes of Cobalt. *Organometallics* **2020,** *39* (20), 3715-3720.
186. Deolka, S.; Govindarajan, R.; Khaskin, E.; Fayzullin, R. R.; Roy, M. C.; Khusnutdinova, J. R., Photoinduced Trifluoromethylation of Arenes and Heteroarenes Catalyzed by High-Valent Nickel Complexes. *Angewandte Chemie International Edition* **2021,** *60* (46), 24620-24629.
187. Xu, J.; Qiao, L.; Ying, B.; Zhu, X.; Shen, C.; Zhang, P., Transition-metal-free direct perfluoroalkylation of quinoline amides at C5 position through radical cross-coupling under mild conditions. *Organic Chemistry Frontiers* **2017,** *4* (6), 1116-1120.
188. Elleman, D. D.; Brown, L. C.; Williams, D., The nuclear magnetic resonance spectra of fluorocarbons: Part I. Halogenated ethanes. *Journal of Molecular Spectroscopy* **1961,** *7* (1), 307-321.
189. Foris, A., 19F and 1H NMR spectra of halocarbons. *Magnetic Resonance in Chemistry* **2004,** *42* (6), 534-555.
190. Zhao, Y.; Truhlar, D. G., A new local density functional for main-group thermochemistry, transition metal bonding, thermochemical kinetics, and noncovalent interactions. *The Journal of Chemical Physics* **2006,** *125* (19), 194101.
191. Keith, T. A., AIMAll (Version 19.10. 12). *TK Gristmill Software: Overland Park, KS, USA* **2019**.